International Journal of Advanced Research in Engineering and Technology (IJARET)
Volume 11, Issue 10, October 2020, pp.28-35, Article ID: IJARET_11_10_003
Available online at http://iaeme.com/Home/issue/IJARET?Volume=11&Issue=10
ISSN Print: 0976-6480 and ISSN Online: 0976-6499
DOI: 10.34218/IJARET.11.10.2020.003

FUZZY REGULAR SUBSEMIGROUPS OF PARTIALLY ORDERED Γ- SEMIGROUPS

Srinivas Telikepalli*
Dept. of Mathematics, QIS INSTITUTE OF TECHNOLOGY, Ongole, India

A. Gangadhara Rao
Dept. of Mathematics, V.S.R. & N.V.R. College, Tenali, India

K.V. Naga Lakshmi
Dept. of Mathematics, SRR & CVR Govt Degree College, Vijayawada, India

A. Anjaneyulu
Dept. of Mathematics, V.S.R. & N.V.R. College, Tenali, India

Corresponding Authors*

ABSTRACT

In this paper, the terms Fuzzy regular Γ-Subsemigroup, λ-Cut, Fuzzy left and right regular Γ-Subsemigroup, Fuzzy intra regular Γ-Subsemigroup, Fuzzy completely Regular Γ-subsemigroup, ideal generated by the ordered fuzzy point a_λ, fuzzy semi simple in a PO Gamma semigroup are introduced. It is proved that (1) If f is fuzzy regular Γ-subsemigroup of S then f is fuzzy Idempotent,(2) If f is fuzzy completely regular then f is regular, left regular and right regular, (3) If a_λ is fuzzy regular then a_λ is fuzzy semi simple, (4) If an orderd fuzzy point a_λ of S is left(right) regular Γ-semigroup then a_λ is fuzzy semi simple, (5) If a_λ is fuzzy intra regular Gamma semigroup then $a_\lambda$is fuzzy semi simple.

Mathematical Subject Classification (2010): 20M12; 20M17; 20N25.

Keywords: Fuzzy regular Γ-subsemigroup, fuzzy completely regular Γ-subsemigroup, fuzzy intra regular Γ -sub semigroup, fuzzy semisimple

Cite this Article: Srinivas Telikepalli, A. Gangadhara Rao, K.V. Naga Lakshmi and A. Anjaneyulu, Fuzzy Regular Subsemigroups of Partially Ordered Γ- Semigroups, *International Journal of Advanced Research in Engineering and Technology (IJARET),* 11(10), 2020, pp.28-35,
http://iaeme.com/Home/issue/IJARET?Volume=11&Issue=10

1. INTRODUCTION

The algebraic theory of semigroups has been extensively studied by CLIFFORD [2],[3],PETRICH [5] and LJAPIN [4]. *Anjaneyulu* [1] puts forward the ideal theory in general semigroups. In this article, we introduce the concepts of fuzzy regular elements, fuzzy completely regular elements and fuzzy intra regular elements in Po-Γ-semigroup. *Lzadeh* proposes the concept of fuzzy subset in 1965. Since then, a series of studies on fuzzy sets results fuzzy logic, fuzzy set theory, fuzzy algebra, etc. we Introduced fuzzy regular Γ-subsemigroup, fuzzy completely regular Γ-subsemigroup, Fuzzy intra regular semigroups and fuzzy semisimple concepts.

2. PRELIMINARIES

Definition 2.1: A **Γ -** semigroup S with an ordered relation $\leq$ is said to be po - **Γ-** semigroup if S is a partially ordered set such that $a \leq b \Rightarrow a\gamma c \leq b\gamma c$ and $c\gamma a \leq c\gamma b$ for all a, b, c ∈ S and ∀ γ ∈ Γ .

DEFINITION 2.2: A function f from S to the closed interval [0,1] is called a ***fuzzy subset*** of S. The po- **Γ**-semigroup S itself is a fuzzy subset of S such that S(x)=1, $\forall x \in S$. It is denoted by S or 1.

DEFINITION 2.3: Let A be a non-empty subset of S. We denote f_A, ***the characteristic mapping*** **of A**. i.e., The mapping of S into [0,1] defined by

$f_A(x)=\begin{cases}1 \; if \; x \in A \\ 0 \; if \; x \notin A\end{cases}$ **then f_A is fuzzy subset of S**

DEFINITION 2.4: Let f and g be two fuzzy subsets of po semigroup S. Then ***the inclusion relation*** f⊆g is defined by f(x)≤g(x),∀x∈ S and $f \cup g$, $f \cap g$ are defined by

$(f \cup g)(x) = max\{f(x), g(x)\} = f(x) \vee g(x), \forall x \in S$,

$(f \cap g)(x) = min\{f(x), g(x)\} = f(x) \wedge g(x), \forall x \in S.$

DEFINITION 2.5: ([13]) Let (S, ≤) be a po- Γ- semigroup and f,g be two fuzzy subsets of S. For $x \in S$ **the product** $f \Gamma g$ is defined by $(f \Gamma g)(x) = \begin{cases} V_{x \leq y\gamma z} \; f(y) \wedge g(z), & if \; x \leq y\gamma z \\ 0 & otherwise \end{cases}$

DEFINITION 2.6: Let S be a po- **Γ-** semigroup. For H⊆ S

we define **(H]**={t∈S / t≤ h for some h∈H}. For H={a} we write (a]= ({a}] = { t∈S / t ≤a}

DEFINITION 2.7: ([14]) **A** fuzzy subset f of a po- **Γ-** semigroup S is called

fuzzy Γ-subsemigroup of S if $f(x\gamma y) \geq f(x) \wedge f(y)$, ∀x, y ∈ S and $\gamma \in \Gamma$.

PROPOSITION 2.8: ([15]) **A fuzzy subset f of a** po- **Γ-** semigroup **S is fuzzy**

Γ-**subsemigroup of S⇔** $f\Gamma f \subseteq f$.

DEFINITION 2.9: A fuzzy subset f of a po- Γ- semigroup S is called ***fuzzy po*** Γ-***subsemigroup*** of S if (i) $x \leq y$ then $f(x) \geq f(y)$ (ii) $f(x\gamma y) \geq f(x) \wedge f(y)$, $\forall x, y \in S, \forall \gamma \in \Gamma$.

DEFINITION 2.10:[16]Let S be a po- Γ- semigroup . A fuzzy subset f of S is called a ***fuzzy left ideal*** of S if (i) $x \leq y$ *then* $f(x) \geq f(y)$ (ii) $f(x\gamma y) \geq f(y), \forall x, y \in S, \forall \gamma \in \Gamma$.

LEMMA 2.11: [16] Let S be a po- Γ- semigroup and f be a fuzzy subset of S. Then f is a fuzzy left ideal of S if and only if f satisfies that (i) x ≤ y then f(x) ≥ f(y) ∀ x,y∈S (ii) S**Γ**f ⊆ f.

DEFINITION 2.12: [16] Let S be a po- Γ- semigroup. A fuzzy subset f of S is called a f***uzzy right ideal*** of S if (i) x≤y then f(x)≥f(y) (ii) f(xγy) ≥ f(x), ∀ x,y∈S,∀$\gamma \in \Gamma$.

LEMMA 2.13: [16] Let S be a po- Γ- semigroup and f be a fuzzy subset of S. Then f is a fuzzy right ideal of S if and only if f satisfies that (i) $x \leq y$ **then** $f(x) \geq f(y)$ ∀ $x,y \in S$ **(ii)** f

$\Gamma s \subseteq f$. **DEFINITION 2.14:** [16]Let S be a po- Γ- semigroup . A fuzzy subset f of S is called a ***fuzzy ideal*** of S if (i) $x \leq y$ *then* $f(x) \geq f(y)$ (ii) $f(x\gamma y) \geq f(y)$, $f(x\gamma y) \geq f(x)$, $\forall\, x,y \in S, \forall \gamma \in \mathbf{\Gamma}$.

Example 1. Let S be the set of all non positive integers without zero and **Γ**

be the set of all non positive even integers without zero. Then S is a **Γ** -semigroup

if aγb denotes the usual multiplication of integers a, γ , b where a, b ∈ S and $\gamma \in \mathbf{\Gamma}$. Again with respect to usual ≤ of Z, S becomes a po- **Γ** -semigroup. Let f be a fuzzy subset of S, defined as follows

$$f(x) = \begin{cases} 0.1 & if\ x = -1 \\ 0.3 & if\ x = -2 \\ 0.5 & if\ x < -2 \end{cases}$$ Then f becomes a fuzzy ideal of S".

LEMMA 2.15: [16] Let S be a po- Γ- semigroup and f be a fuzzy subset of S. Then f is a fuzzy ideal of S if and only if f satisfies that (i) $x \leq y$ *then* $f(x) \geq f(y)$ $\forall\, x,y \in S$

(ii) $f\,\Gamma s \subseteq f$ *and* $s\,\Gamma f \subseteq f$.

DEFINITION 2.16: Let S be a po- Γ- semigroup . A fuzzy ideal f of S is called ***idempotent*** if

$f^2 = f\Gamma\, f\, = f$.

3. SPECIAL ELEMENTS IN FUZZY REGULAR SUBSEMIGROUP OF PO –Γ- SEMIGROUP:

DEFINITION 3.1: An element 'a' of a po- Γ- semigroup S is said to be ***regular*** if there exist

$x \in$S such that a≤ a$\alpha x\beta$a for some $x \in$A and α,β∈Γ.

DEFINITION 3.2: A po- Γ- semigroup S is said to be ***regular semigroup*** provided every element is regular.

DEFINITION 3.3: Let S be a po- Γ- semigroup and $x \in$S, α, β∈Γ. Define

$R_x = \{x'/x' \in s, x \leq x\alpha x'\beta x\}$. Let f be a fuzzy Γ- subsemigroup of S if $\forall\, x \in S$ there exist

$x' \in R_x$ such that $f\ (x) \leq f\ (x')$ provided $f(x) \neq 0$ then f is called ***fuzzy regular*** Γ-***subsemigroup*** of S.

THEOREM 3.4: Let A be a non-empty subset of po- Γ- semigroup S . A is regular

Γ**-subsemigroup of S if and only if** f_A**, the characteristic function of A is a fuzzy regular Γ-subsemigroup of S.**

***Proof*:** Suppose A is regular Γ- subsemigroup of S . Let x,y∈A and γ ∈ Γ ⇒ xγy∈A. Therefore$f_A\ (x\gamma y) \geq f_A\ (x) \wedge f_A\ (y)$.

Let x∈A ⇒ $f_A\ (x) = 1$. Then from the regularity of A there exists $x^1 \in R_x$ such that $x^1 \in A$ and $f_A\ (x') = 1$. ⇒ $f_A\,(x) \leq f_A\ (x')$. Therefore f_A is a fuzzy regular Γ-subsemigroup of S.

Conversely suppose that f_A is a fuzzy regular Γ - subsemigroup of S. Let $\gamma \in \Gamma$ and x,y ∈A ⇒ $f_A\ (x) = f_A\,(y) = 1$ and f_A is fuzzy regular-subsemigroup of S.

⇒ $f_A(x\gamma y) \geq f_A(x) \wedge f_A(y) = 1 \Rightarrow f_A(x\gamma y) = 1 \Rightarrow x\gamma y \in A \Rightarrow$ A is a Γ-subsemigroup of S.

Let x∈A ⇒ $f_A\ (x) = 1$. Since f_A is a fuzzy regular, there exists$x^1 \in R_x$such that

$f_A\,(x) \leq f_A\,(x')$. ⇒ $f_A\ (x') \geq 1 \Rightarrow x^1 \in A$

Therefore A is regular Γ –subsemigroup of S.

DEFINITION 3.5: Let f be a fuzzy subset of a po- Γ- semigroup S. Let $\lambda \in [0,1]$. Define

$f_\lambda = \{x \in S/f\ (x) \geq \lambda\}$ is the ***λ-cut of f.***

THEOREM 3.6: Let S be a po- Γ- semigroup. f is fuzzy Γ- subsemigroup of S if and only if $\forall\ \boldsymbol{\lambda} \in [\mathbf{0}, \mathbf{1}]$, $\boldsymbol{f_\lambda}$ is a Γ-subsemigroup of S.

***Proof*:** Assume that f is a fuzzy Γ-subsemigroup of S.

Let $\gamma \in \Gamma$ *and* $a, b \in f_\lambda \Rightarrow f(a) \geq \lambda, f(b) \geq \lambda$

Since $f(a\gamma b) \geq f(a) \wedge f(b) \geq \lambda \wedge \lambda = \lambda \Rightarrow f(a\gamma b) \geq \lambda \Rightarrow a\gamma b \in f_\lambda$

$\Rightarrow f_\lambda$ is Γ- subsemigroup of S.

Conversely suppose that f_λ is a Γ-subsemigroup of S.

Suppose there exists one $x_1, y_1 \in f_\lambda$ *and* $\gamma \in \boldsymbol{\Gamma}$ **s**uchthat

$f(x_1\gamma y_1) < f(x_1) \wedge f(y_1) < f(x_1) \Rightarrow f(x_1\gamma y_1) < f(x_1)$

Define $\lambda = \frac{1}{2}[f(x_1) - f(x_1\gamma y_1)]$ then $\lambda \in (0,1]$

and $0 \leq f(x_1\gamma y_1) < \lambda \leq 1$, $0 < \lambda < f(x_1) \leq 1$so that $x_1 \in f_\lambda$, similarly $y_1 \in f_\lambda \Rightarrow x_1\gamma y_1 \in f_\lambda \Rightarrow f(x_1\gamma y_1) \geq \lambda$

But $f(x_1\gamma y_1) < \lambda$ which is a contradiction.

Therefore $f(x\gamma y) \geq f(x) \wedge f(y), \forall x, y \in S, \gamma \in \boldsymbol{\Gamma} \Rightarrow f_\lambda$ is Γ- subsemigroup of S.

THEOREM 3.7: Let f be a fuzzy subset of a po- Γ- semigroup S. f is a fuzzy regular Γ-subsemigroup of S if and only if $\forall\ \boldsymbol{\lambda} \in (\mathbf{0}, \mathbf{1}]$, $\boldsymbol{f_\lambda}$ is a regular Γ-subsemigroup of S provided $\boldsymbol{f_\lambda} \neq \emptyset$.

***Proof*:** Assume that f is fuzzy regular Γ-subsemigroup of S. From theorem 3.6, f_λ is Γ-subsemigroup of S.

Let $x \in f_\lambda$ since f is fuzzy regular $\exists\ x' \in R_x$ such that $f(x) \leq f(x') \Rightarrow f(x') \geq \lambda$

$\Rightarrow x' \in f_\lambda$.

Therefore $\forall x \in f_\lambda \exists\ x' \in f_\lambda$and α, β∈**Γ** such that $x \leq x\alpha x'\beta x \Rightarrow f_\lambda$is a regular Γ-subsemigroup of S.

Conversely, suppose that f_λ is a regular **Γ**-subsemigroup of S provided $f_\lambda \neq \emptyset$

Assume that f is not fuzzy regular ⇒ there exists $x \in S$ such that f(x)≠ 0 and$\forall\ x' \in R_x$,

$f(x) > f(x')$. Set $\lambda = f(x)$, clearly $x \in f_\lambda$ and $\forall\ x' \in R_x \Rightarrow \lambda = f(x) > f(x') \Rightarrow x' \notin f_\lambda$

Which is a contradiction, since f_λ is regular. Therefore *f* is fuzzy regular Γ -subsemigroup of S.

THEOREM 3.8: Let S be a po- Γ- semigroup. If *f is* fuzzy regular Γ-subsemigroup of S then $\boldsymbol{f\Gamma f = f}$.

Proof: Let f be a fuzzy subset of S .

From [2.8] If f is a fuzzy Γ-subsemigroup of S if and only if $f\Gamma f \subseteq f$.

Let $x \in S$ if f(x) =0 then $(f\Gamma f)(x) \leq f(x) \Rightarrow (f\Gamma f)(x) = f(x) = 0$

if $f(x) \neq 0$ then $\exists\ x' \in R_x$ such that $f(x) \leq f(x')$,since f is fuzzy regular

Now$(f\ \boldsymbol{\Gamma} f)(x) =$

$= \underset{x \leq y\gamma z}{V} [f(y) \wedge f(z)] \qquad = \underset{x \leq x\ \alpha x'\ \beta x}{V} [f(x) \wedge f(x'\beta x)] \geq f(x) \wedge f(x') \wedge f(x)$

$= f(x), \forall x \in S$

$f \subseteq f\Gamma f.$

Therefore $f\ \Gamma f = f$ if f is fuzzy regular.

COROLLARY 3.9: Let S be a po- Γ- semigroup and f is fuzzy ideal of S. If f is fuzzy regular Γ-subsemigroup of S then f is fuzzy idempotent.

DEFINITION 3.10: [9] Let f be a fuzzy subset of a po- Γ- semigroup S. We define $(f]$ by $(f](x) = \bigvee_{x \le y} f(y), \forall x \in S$

NOTE 3.11: Clearly $f \subseteq (f]$.

DEFINITION 3.12: [9]Let S be a po- Γ- semigroup , $a \in S$ and $\lambda \in [0,1]$. An ***ordered fuzzy point a***

: $S \to [0,1]$ defined by

$$a_\lambda(x) = \begin{cases} \lambda & if\ x \in (a] \\ 0 & if\ x \notin (a] \end{cases}$$

clearly a_λ is a fuzzy subset of S.

LEMMA 3.13: [9] If a_λ is an ordered fuzzy point of S then $a_\lambda = (a_\lambda]$.

NOTE 3.14: Let f be a fuzzy subset of a po- Γ- semigroup S then $(f] = \bigcup_{y_\lambda \in (f]} y_\lambda$

DEFINITION 3.15: Let f be a fuzzy subset of a po- Γ- semigroup S. Then $\forall x \in S$, **the fuzzy**

Subset $(x\alpha f\beta x)$ of S is defined by $\forall y \in S$, $(x\alpha f\beta x](y) = \begin{cases} \bigvee_{y \le x\alpha s\beta x} f(s) & if\ \exists y \le x\alpha s\beta x \\ 0 & otherwise \end{cases}$

THEOREM 3.16: If f is a fuzzy Γ- subsemigroup of po- Γ- semigroup S. Then f is fuzzy regular if and only if $\forall x \in S$, $(x\alpha f\beta x](x) \ge f(x)$ provided $f(x) \ne 0$

Proof: Suppose f is fuzzy regular.

Consider $(x\alpha f\beta x](x) = \bigvee_{x \le x\alpha s\beta x} f(s) = \bigvee_{x \le x\alpha x^1\beta x} f(x') \ge f(x') \ge f(x)$,

Since f is fuzzy regular $\Rightarrow (x\alpha f\beta x)(x) \ge f(x)\ \forall x \in S$.

Conversely assume that $\forall x \in S$, $(x\alpha f\beta x)(x) \ge f(x)$.

Since $f(x) \le (x\alpha f\beta x](x) = \bigvee_{x \le x\alpha x^1\beta x} f(x') = \bigvee_{x \le x\alpha x^1\beta x} f(x')\ provided\ f(x) \ne 0$

That is $\forall x \in S\ \exists$ at least one x' such that $x \le x\alpha x'\beta x\ and\ f(x) \le f(x')\ since\ f(x) \ne 0$

$\Rightarrow f$ is fuzzy regular.

COROLLARY 3.17: If an ordered fuzzy point a_λ of a po- Γ- semigroup S is regular if and only if $\forall x \in S$, $(x\alpha a_\lambda\beta x](x) \ge a_\lambda(x)$ provided $a_\lambda(x) \ne 0$.

***Proof*:** Proof follows from the Theorem 3.14.

DEFINITION 3.18: Let S be a po- Γ- semigroup and $x \in S$, $\alpha, \beta \in \Gamma$.

Define $LR_x = \{x' \in S / x \le x\alpha x\beta x'\}$.

Let f be a fuzzy Γ-subsemigroup of S. For every $\alpha, \beta \in \Gamma$, $x \in S$, $\exists\ x' \in LR_x \ni f(x) \le f(x')$ provided f(x)≠ 0 then f is called ***fuzzy left regular*** Γ- ***subsemigroup*** of S.

DEFINITION 3.19: Let S be a po- Γ- semigroup and $x \in S$, $\alpha, \beta \in \Gamma$. Define $RR_x = \{x' \in S / x \le x'\alpha x\beta x\}$. Let f be a fuzzy Γ-subsemigroup of S.

For every $x \in Sand, \alpha, \beta \in \Gamma\ \exists\ x' \in RRx \ni f(x) \leq f(x')$ provided f(x)≠ 0 then f is called ***fuzzy right regular*** Γ-***subsemigroup***of S.

DEFINITION 3.20: Let S be a po- Γ- semigroup and $\alpha, \beta, \gamma \in \Gamma, x \in S$,

define$IR_x = \{x' \in S / x \leq x_1 \alpha a \beta a \gamma x_2\}$. Let f *be* a fuzzy Γ-subsemigroup of S. For every

$x \in S\ \exists\ (x1, x2) \in IRx \ni f(x) \leq f(x1) \wedge f(x2)$ provided f(x) ≠ 0 then f is called fuzzy Intraregular Γ-subsemigroupof S.

DEFINITION 3.21: Let S be a po- Γ- semigroup and $x \in S$, α,β∈Γ.

Define $R_x = \{x'/x' \in s, x \leq x\alpha x'\beta x\}$and $C_x = \{x' \in S/x\alpha x' = x'\beta x\}$.Let f be a fuzzy Γ-subsemigroup of S and for every $x \in S\ \exists x' \in R_x \cap C_x$

$\ni f(x) \leq f(x')$ provided f(x)≠ 0 then f is called fuzzy completely regular Γ-subsemigroup of S.

THEOREM3.22: Let S be a po- Γ- semigroup and f is a fuzzy Γ-subsemigroup of S. If f is fuzzy completely regular then f is regular, left regular and right regular.

***Proof*:** Suppose that f is completely regular.

Then for every α, β ∈ Γ, $x \in S\ \exists x' \in Rx \cap Cx \ni f(x) \leq f(x')$ provided f(x)≠ 0 . Since $x' \in Rx \Rightarrow x \leq x\alpha x'\beta x$ and $f(x) \leq f(x')$, f(x)≠ 0

⇒ f is fuzzy regular.

Now for every $x \in S\ \exists x' \in Rx \cap Cx \ni f(x) \leq f(x')$ provided f(x)≠ 0 .

$\Rightarrow x \leq x\alpha x'\beta x$ and $x\alpha x' = x'\beta x$.

Consider $x \leq x\alpha x'\beta x = x\alpha x\alpha x' = (x\alpha)^2 x' \Rightarrow x \leq (x\alpha)^2 x'$and $f(x) \leq f(x')$

⇒ f is fuzzy left regular.

Also $x \leq x\alpha x'\beta x = x'\beta x\beta x = x'(x\beta)^2$. Therefore f is fuzzy right regular.

DEFINITION 3.23: Let$a \in S, \lambda \in (0,1]$. Define ***ideal generated by the ordered fuzzy point*** a_λ

of S by $< a_\lambda >(x) = \begin{cases} \lambda, & \text{if } x \in (a) = (a \cup a\Gamma S \cup S\Gamma a \cup S\Gamma a\Gamma S] = (s'as') \\ 0, & \text{othewise} \end{cases}$

DEFINITION 3.24: An ordered fuzzy element a_λ of a po- Γ- semigroup S is said to be ***fuzzy semisimple*** if $a_\lambda \subseteq < a_\lambda >^2$**.**

NOTE 3.25: Clearly $a_\lambda \subseteq < a_\lambda >$

THEOREM 3.26: Let S be a po- Γ- Semi group and a_λ is a fuzzy Γ- subsemigroup of S. If a_λ is fuzzy regular then a_λ is fuzzy semisimple.

Proof: Suppose a_λ is fuzzy regular.

Consider $< a_\lambda >^2(x) = \bigvee_{x \leq yyz} [< a_\lambda > (y) \wedge < a_\lambda > (z)]$

$$\geq < a_\lambda > (y) \wedge < a_\lambda > (z)$$
$$\geq < a_\lambda > (x\alpha x') \wedge < a_\lambda > (x)$$
$$\geq a_\lambda(x\alpha x') \wedge a_\lambda(x) \geq a_\lambda(x) \wedge a_\lambda(x') \wedge a_\lambda(x)$$
$$\geq a_\lambda(x) \wedge a_\lambda(x) \wedge a_\lambda(x) = a_\lambda(x) \forall x \in S$$

$\Rightarrow a_\lambda \subseteq < a_\lambda >^2$

Therefore a_λ is fuzzy semisimple.

THEOREM 3.27: Let S be a po- Γ- Semi group. If an ordered fuzzy point $a_\lambda$of S is left(right) regular semigroup then a_λ is fuzzy semisimple.

***Proof*:** Suppose $a^{\lambda}$is fuzzy left regular. Then ∀ x∈S $\exists x^{'} \in LR^{x}$ such that
$a_\lambda(x) \leq a_\lambda(x^{'})$ provided $a_\lambda(x) \neq 0$.

Consider $< a_\lambda >^2 (x) = \bigvee_{x \leq y\gamma z}[< a_\lambda > (y) \wedge < a_\lambda > (z)]$

$\geq < a_\lambda > (y) \wedge < a_\lambda > (z)$

$\geq < a_\lambda > (x\alpha x) \wedge < a_\lambda > (x^{'})$

$\geq a_\lambda(x) \wedge a_\lambda(x) \wedge a_\lambda(x^{'})$

$\geq a_\lambda(x) \wedge a_\lambda(x^{'}) = a_\lambda(x)$

$\Rightarrow a_\lambda \subseteq < a_\lambda >^2$

Therefore a_λ is fuzzy semisimple.

Similarly if a_λ is fuzzy right regular semigroup then a_λ is fuzzy semisimple.

THEOREM 3.28: Let $\boldsymbol{a_\lambda}$ be an ordered fuzzy point of a po - Γ- semigroup S. If $\boldsymbol{a_\lambda}$ is fuzzy intra regular semigroup then $\boldsymbol{a_\lambda}$ is fuzzy semisimple.

***Proof*:** Let $a_\lambda$is fuzzy intra regular.

∀ x∈S ∃ $(x_1, x_2) \in IR_x \ni a_\lambda(x) \leq a_\lambda(x_1) \wedge a_\lambda(x_2)$ provided $a_\lambda(x) \neq 0$.

Consider $< a_\lambda >^2$(x) = $(< a_\lambda > o < a_\lambda >)(x)$

$$= \bigvee_{x \leq y\gamma z} |< a_\lambda > (y) \wedge < a_\lambda(z)|$$

$$\geq < a_\lambda > (y) \wedge < a_\lambda > (z)$$

$$\geq < a_\lambda > (x_1) \wedge < a_\lambda > (x\beta x\gamma x_2)$$

$$\geq a_\lambda(x_1) \wedge a_\lambda(x) \wedge a_\lambda(x\gamma x_2)$$

$$\geq a_\lambda(x_1) \wedge a_\lambda(x) \wedge a_\lambda(x_2)$$

$$\geq a_\lambda(x) \wedge a_\lambda(x) \wedge a_\lambda(x) = a_\lambda(x), \forall x \in S$$

$$\Rightarrow a_\lambda \subseteq < a_\lambda >^2$$

Therefore a_λ is fuzzy semi simple.

5. CONCLUSION

The objective of this paper is describing fuzzy completely regular and fuzzy regular and also establish the relation between them. The ordered fuzzy points of an ordered gamma semigroup S are key tools to describe the algebraic subsystems of S .we established the relation between fuzzy regular and fuzzy semi simple also fuzzy intra regular and fuzzy semi simple. We hope that the research along this direction can be continued, and in fact, some results in this paper have already constituted a platform for further discussion concerning the future development of ordered gamma semi groups. Hopefully, some new results in these topics can be obtained in the forthcoming paper.

ACKNOWLEDGEMENTS

The authors wish to express their sincere thanks to the referees for the valuable suggestions which lead to an improvement of this paper.

REFERENCES

[1] ANJANEYULU A., Structure and ideal theory of semigroups – Thesis, ANU (1980).

[2] Clifford A.H and Preston G.B., The algebroic theory of semigroups ,vol – I American Math. Society, Province (1961).

[3] Clifford A.H and Preston G.B., The algebroic theory of semigroups ,vol – II American Math. Society, Province (1967).

[4] LJAPIN E. S., Semigroups, American Mathematical Society, Providence, RhodeIsland (1974).

[5] Petrch.M. Introduction to semigroups ,Merril publishing company, Columbus Ohio(1973)

[6] W.M.Wu, Normal fuzzy subsemigroups, Fuzzy Math1(1).21-30(1981)

[7] T.M.G. Ahsanullah and F.A. AI-Thukair, Conditions on a semigroup to be a fuzzy neighborhood group, Fuzzy Sets and Systems, 55(1993), 333-340.

[8] J. N. Mordeson, D. S. Malik, N. Kuroki, Fuzzy Semigroups Springer-Verlag Berlin Heidelberg GmbH ISBN 978-3-642-05706-9 ISBN 978-3-540-37125-0 (eBook)

[9] DOI 10.1007/978-3-540-37125-0

[10] Xiang-Yun Xie,, Jian Tang, Fuzzy radicals and prime fuzzy ideals of ordered semigroups, Information Sciences 178 (2008), 4357–4374.

[11] N.Kehayopulu,M.Tsingelis, Fuzzy sets in ordered groupoids, Semigroup Forum 65(2002), 128-132

[12] Jizhongshen,On fuzzy Regular Subsemigroups of a semigroup, Information Sciences 51,111-120(1990)

[13] T.K. Dutta, N.C. Adhikari, on partially ordered Γ -semigroup, South East Asian Bull. Math., 28, No. 6 (2004), 1021-1028.

[14] S. K. Mujemder and S. K. Sardar, On properties of fuzzy ideals in PO-G-Semigroups, Armenian Journal of Mathematics. Vol. 2(2)(2009), 65.72.

[15] W. J. Lie, Fuzzy invariant subgroups and fuzzy ideals, Fuzzy sets syst. 8 (1982), 130.139.

[16] T.Nagaiah ,K.Vijay kumara Study of fuzzy ideals in PO-Gamma semigroupsPalestine Journal of Marhematics,Vol.6(2)(2017),591-597

[17] A. Iampan, Characterizing fuzzy sets in ordered G-Semigroups, Journal of Matematics Research,2(4)(2010), 52.60.

[18] Sen, M.K., Seth, A.: On po- Γ-semigroups. Bull. Calcutta Math. Soc. 85, 445–450 (1993)

IJPSR (2020), Volume 11, Issue 9 (Research Article)

INTERNATIONAL JOURNAL OF PHARMACEUTICAL SCIENCES AND RESEARCH

Received on 02 October 2019; received in revised form, 21 March 2020; accepted, 23 March 2020; published 01 September 2020

A VALIDATED LCMS METHOD FOR THE ANALYSIS OF ISOPROTERENOL – A β ADRENORECEPTOR AGONIST IN SPIKED HUMAN PLASMA

V. S. Singh Gaddala [*1], R. S. Reddy Dachuru [2] and E. Divakar Tella [3]

Department of Chemistry [1], SRR & CVR Government Degree College (A), Vijayawada - 520004, Andhra Pradesh, India.
Department of Chemistry [2], Krishna University, Machilipatnam - 521001, Andhra Pradesh, India.
Department of Chemistry [3], Noble College (A), Machilipatnam - 521001, Andhra Pradesh, India.

Keywords:

Isoproterenol, LCMS Analysis, Plasma extraction, Stability studies

Correspondence to Author:
Vijaya Swaroop Singh Gaddala

Lecturer,
Department of Chemistry, SRR & CVR Government Degree College (A), Vijayawada - 520004, Andhra Pradesh, India.

E-mail: vijayssgaddala@gmail.com

ABSTRACT: A simple, sensitive, and rapid Liquid Chromatography-Mass Spectroscopy method was developed and validated for the quantification of Isoproterenol in human plasma using Dobutamine as an internal standard. The method utilized simple liquid-liquid extraction using a mixture of diethyl ether and dichloromethane for the sample preparation involved prior to LCMS analysis. The analytes were chromatographed on Prontosil ODS C18 Column with isocratic elution using methanol, Acetonitrile and Tri ethyl-amine in the ratio of 60:25:15 (v/v) at pH 6.3 as the mobile phase at a flow rate of 0.9 mL/min and the UV detector response of the column eluents were recorded at a wavelength of 248 nm. Quantification was performed in multiple-reaction-monitoring mode with the ion transitions m/z 212.19 → 135.21 for Isoproterenol, m/z 302.19 → 107.05 for Dobutamine. Good linearity was obtained in the range of 0.50–300 ng/mL (r^2 = 0.999). The method was fully validated with accuracy, precision, matrix effects, recovery and stability. The results of the stability study confirm that the method was found to be stable. The validated data have met the acceptance criteria in FDA guidelines. This study could be readily applied in therapeutic drug monitoring of Isoproterenol in patients receiving such drug combinations.

INTRODUCTION: Isoproterenol (IPTN) is a non-selective β-adrenoreceptor agonist [1] prescribed for the treatment of slow heart rate (bradycardia), heart block and rarely for asthma. IPTN increases the heart rate and cardiac output by affecting the β1 adrenergic receptors in the myocardium. IPTN causes smooth muscle relaxation by affecting the β2 adrenergic receptors in bronchiolar and vascular smooth muscle [2, 3].

QUICK RESPONSE CODE

DOI: 10.13040/IJPSR.0975-8232.11(9).4567-74

This article can be accessed online on www.ijpsr.com

DOI link: http://dx.doi.org/10.13040/IJPSR.0975-8232.11(9).4567-74

IPTN has unwanted side effects on cardiac and metabolic functions, central nervous system, and motility of the gastrointestinal tract [4]. Limited experience with isoprenaline (Isoproterenol) does not show adverse effects on embryonic and fetal development [5].

The drug IPTN is available as several brands in the market and is widely used for the treatment of bradycardia and heart block. But in the literature, only one analytical HPLC method for the estimation of IPTN in pharmaceutical formulations [6], one HPLC method for the synthesis and characterization of IPTN and its process impurities [7] were reported. Hence, the present work is aimed to develop a validated HPLC tandem mass spectrophotometer method for the quantification of

IPTN in spiked human plasma. In the analysis of IPTN **Fig. 1A** in spiked plasma, a similar class of drug Dobutamine **Fig. 1B** was used as an internal standard (IS).

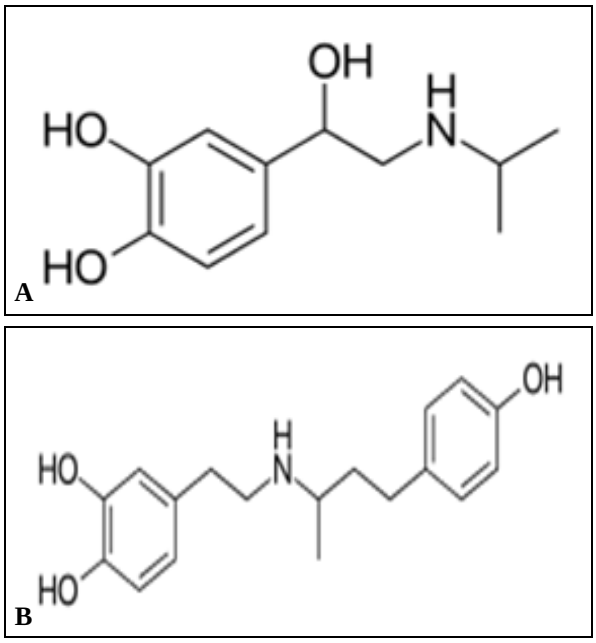

FIG. 1: MOLECULAR STRUCTURE OF STANDARD IPTN (1A) AND IS (1B)

MATERIALS AND METHODS:

Instrumentation: Agilent 1100 series HPLC with Quaternary G1311 A pump, COLCOM G1316A thermostat column temperature control, Thermo-static autosampler G 1329A with a sample volume of 0.1 - 1500 µL and variable programmable UV detector G 1314 A was used. The instrument was operated and integrated with Agilent chem. station LC software.

The HPLC system was coupled with Waters ZQ Mass Detector (model LAA 1369) with Waters Empower software. The mass spectra were taken in ESI (Turbo Ion Spray) positive mode in the mass range of 40-1000 amu and analyzed in the triple quadrupole analyzer. The nitrogen gas (300Psi) was used as a carrier gas in mass spectral analysis with fixed MS tune (3.0 kV capillary, 40V cone, 3V extractor)

Chemicals and Materials: Reference standards of IPTN (99.21%) and IS (99.17%) were obtained from Samarth Pharma Private Limited. (Mumbai, India). HPLC-grade methanol and acetonitrile were procured from Merck chemicals, Mumbai. Water used in the study was prepared from a Milli-Q water purification system from Millipore (Bangalore, India). Blank human plasma in K_3EDTA was obtained from a local diagnostic center, Guntur, and was stored at -20 °C until use.

Extraction of Drug from Plasma: A simple liquid-liquid extraction was used for the extraction of IS and IPTN from the plasma matrix. Prior to the analysis, the freeze and thaw plasma matrix were stored at -20 °C. In the liquid-liquid extraction process, 100 µl of plasma, 100 µl aliquot of working standard solution of IPTN and IS was added in polypropylene centrifuge tubes and then 600 µl of Diethyl ether and 400 µl of dichloromethane were added. Then tubes were centrifuged for 10 min at 3000 rpm. The clear supernatant layer was transferred into another conical glass tube, and the organic layer was completely evaporated at room temperature. Then it was reconstructed using the mobile phase. The solution was used for the analytical method development and validation study.

Preparation of Calibration Solutions: 10 mg each of standard drug IPTN and IS were weighed and dissolved in 10 mL of methanol separately in a 10 ml volumetric flask. A standard stock solution of 1000 µg/mL was obtained. Required calibration concentrations of IPTN and 100 µg/mL of IS were prepared separately.

0.5 - 300 ng/mL calibration curve standards of IPTN and 100 ng/mL of IS were spiked to human plasma and were extracted using liquid-liquid extraction. In the calibration range, a concentration of 25 ng/mL, 100 ng/mL, and 300 ng/mL were considered as low-quality control (LQC), middle-quality control (MQC) and high-quality control (HQC) standards respectively.

Method Development: Different compositions of the mobile phase, with different organic and pH modifiers, were studied for the separation and analysis of IPTN and IS. The separation was carried on different configurations of stationary phases, and eluents were recorded using a UV detector coupled with a mass spectrophotometer. The conditions that produce valid system suitability were studied for validation.

Method Validation: Method validation for the analysis of IPTN in the presence of IS in human plasma was done following the USFDA guidelines

[8]. The method was validated for selectivity, interference check, carryover, linearity, precision and accuracy, reinjection reproducibility, recovery, ion suppression/enhancement, matrix effect, stability, dilution integrity, and ruggedness.

Test for selectivity was carried out in 10 different batches of blank human plasma, including haemolysed & lipemic plasma collected with K_3EDTA as an anticoagulant. From each of the batch, two replicates each of 100 µL was spiked with 100 µL of methanol and deionized water (50:50, v/v). In the first set, the blank human plasma was directly injected after extraction (without analyte and IS), while the other set was spiked with only IS before. Further, one system suitability sample at PSCC - 10 concentration and two replicates of LLOQ concentration (PSCC-1) were prepared by spiking 100 µL blank human plasma with 100 µL of aqueous standards of IPTN and IS, respectively. The acceptance criterion requires that at least 90% of selectivity samples should be free from any interference at the retention time of analyte and IS.

The linearity of the method was determined by an analysis of ten calibration curves containing ten non-zero concentrations. The area ratio response for IPTN/IS obtained from multiple reaction monitoring was used for regression analysis. The calibration curve was analyzed individually by using the least square weighted ($1/x^2$) linear regression. The lowest standard on the calibration curve was accepted as the LLOQ, if the analyte response was at least ten times more than that of drug-free (blank) extracted plasma.

For determining the accuracy and precision, replicate analysis of plasma samples of analytes was performed on the same day for intraday and three different days for inter-day precision and accuracy. The run consisted of a calibration curve and six replicates of LQC, MQC and HQC samples. The deviation at each concentration level from the nominal concentration was expected to be within ±15%.

The relative recovery and matrix effect were assessed at HQC, MQC, and LQC levels in six replicates. Relative recovery was calculated by comparing the mean area response of pre-spiked samples (spiked before extraction) to that of extracts with post-spiked samples (spiked after extraction) at each QC level. The % recovery and the % RSD of the recovery were calculated.

The stability of the bioanalytical method developed was evaluated by measuring the area response of stability samples against freshly prepared comparison standards at LQC, MQC, and HQC levels. Stock solutions of IPTN and IS were checked for short term stability at room temperature (25 °C) and long term (benchtop) stability at 2-8 °C. Freeze-thaw stability was studied after three freeze, and thaw cycles of plasma matrix spiked with IPTN and IS at LQC, MQC and HQC levels. The CV (%) and accuracy (%) should be within ±15 %, and also, at least 2/3 quality control samples should meet the criteria of ±15% of nominal concentration is the acceptance criteria for the stability studies.

RESULTS AND DISCUSSION:

LCMS Analysis of IPTN: In the LCMS analysis of IPTN in the spiked human plasma, the mass spectra of column eluents were recorded in both positive and negative ion modes in electrospray ionization (ESI) detector.

The standard drug IPTN is having polar groups in the molecular structure that gives good mass spectrometric response in the negative mode. The molecule IPTN contains one basic and three acidic functional groups in the molecular structure with pKa of 9.81 (Strongly Acidic) and 8.96 (Strongly Basic). During the method development stage, the mass spectra of IPTN and IS was analyzed in ESI, and APCI (Atmospheric Pressure Chemical Ionization) by direct infusion of 50ng/mL solution of the analytes and the results confirm that ESI provided better ionization efficiency than APCI for both the analytes and hence further study was carried in ESI mode.

The observed mass spectra in the positive ion mode showed predominant protonated molecular ions [M-H]- at m/z 212.19 for IPTN and 312.19 for IS. The collision-induced dissociation of [M-H]- ions gave intense fragment/product ion at m/z of 194.57, 170.10, 135.21, and 72.09 for IPTN **Fig. 2A** and 284.25, 258.03, 137.48, and 107.05 for IS **Fig. 2B** respectively.

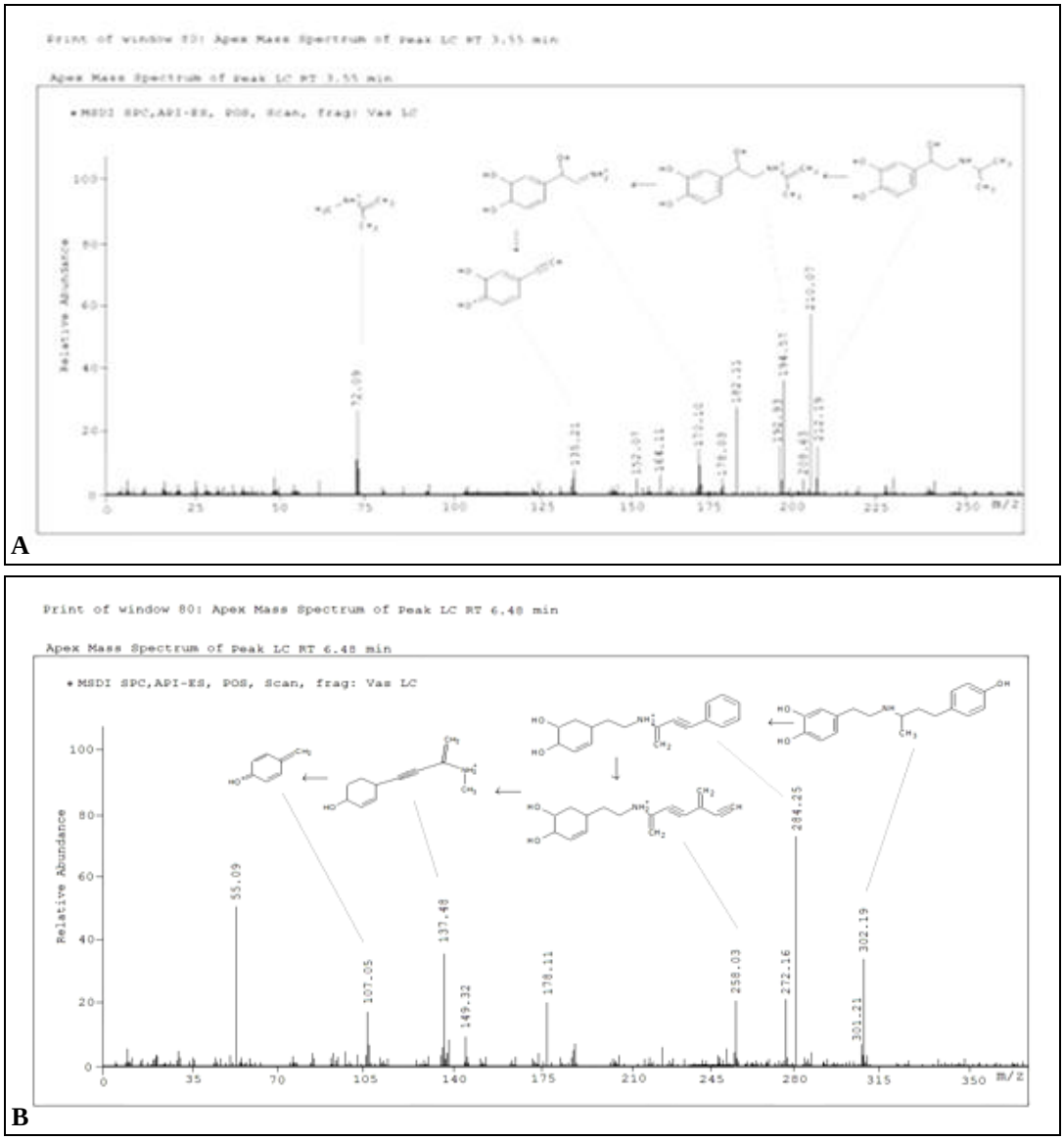

FIG. 2: ESI ION-CHROMATOGRAMS OF BLANK PLASMA SPIKED WITH IPTN AND IS. A) MASS SPECTRA OF IPTN AT THE RETENTION TIME OF 3.55 min. B) MASS SPECTRA OF IS AT THE RETENTION TIME OF 6.48 min

HPLC Optimized Conditions: In the optimization of LC conditions for the analysis of IPTN in spiked plasma samples, several reversed-phase columns with different configurations like Hypersil Gold C18 (50/100 mm × 3.0 mm, 5 µm), Gemini C18 (50/100 mm × 4.6 mm, 5.0 µm) and Prontosil ODS C18 Column (250 × 4.6 mm, 5 µm) were tested. For chromatographic separation of IPTN and IS from the plasma matrix, various combinations of methanol, acetonitrile in combination with different buffers in different pH ranges (3.5-6.5) were studied in order to obtain symmetrical peak shapes, suitable retention and adequate signal-to-noise ratio leading to lower limits of quantization. Compared to individual solvent mixtures, the combination of methanol and acetonitrile helped in providing higher sensitivity and sharp peaks shapes.

Another important observation was that a higher proportion (>75%) of organic diluents was necessary for the optimum resolution of the drugs. Both the peaks observed for IPTN and IS were satisfactorily resolved (Resolution factor ≥2) on all columns studied using Methanol, Acetonitrile and Triethylamine in the ratio of 60:25:15 (v/v) at pH 6.3 as the mobile phase at a flow rate of 0.9 mL/min and the UV detector response of the column eluents were recorded at a wavelength of 248 nm. The peak area response was not adequate on Hypersil Gold C18, and the peak shapes were not acceptable with Gemini C18 column. Nevertheless, the best chromatographic conditions were achieved on Prontosil ODS C18 Column (250 × 4.6 mm, 5µm) with an adequate response, resolution (Resolution factor ≥2), symmetric peak

shape, baseline separation within 2.0 min **Fig. 3**. The retention time of IPTN and IS were found to be 3.5 and 4.6 min, respectively. The use of labeled internal standards that had identical chromatographic behavior helped to achieve acceptable method performance.

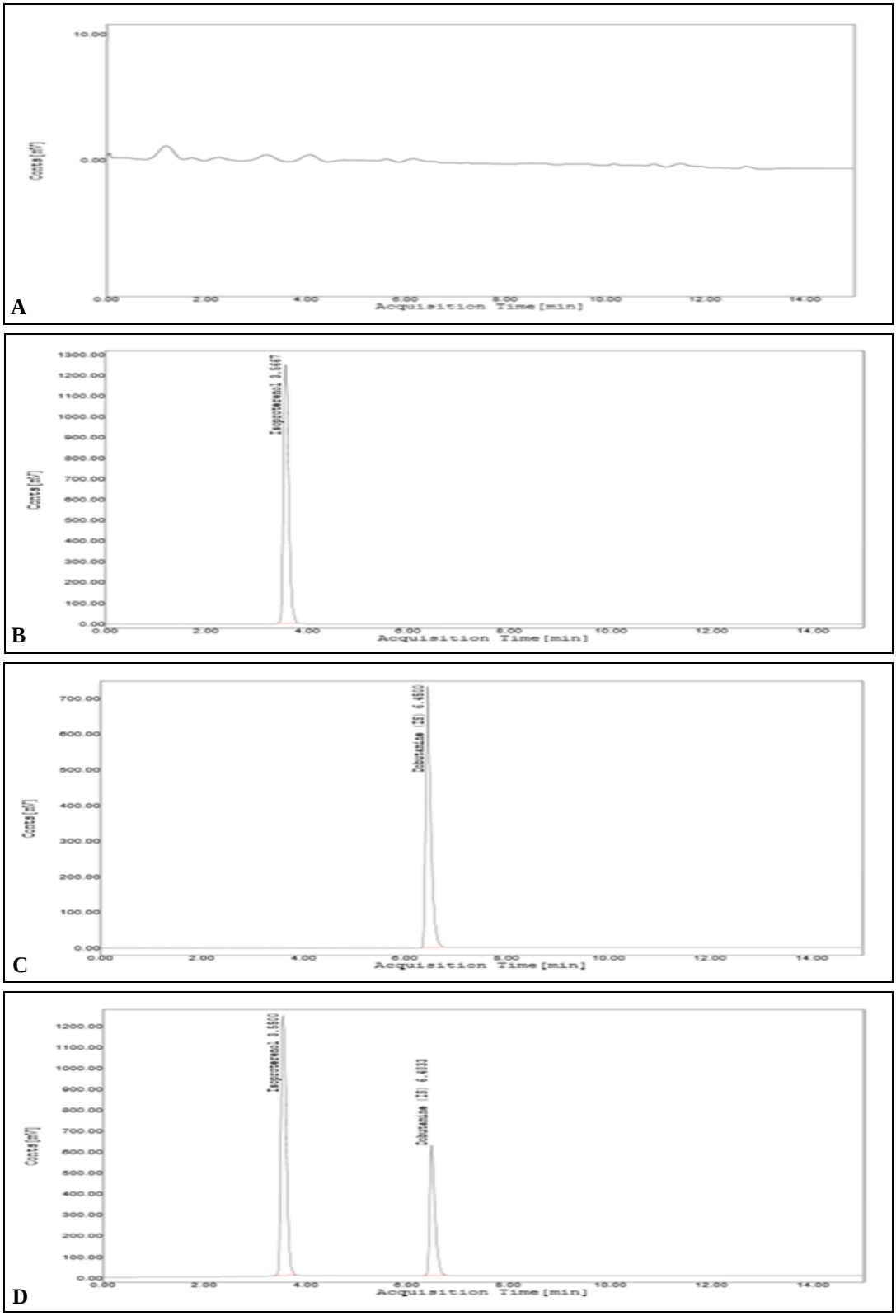

FIG. 3: SYSTEM SUITABILITY CHROMATOGRAM OF IPTN IN THE DEVELOPED METHOD. A) PLASMA SPIKED BLANK CHROMATOGRAM. B) CHROMATOGRAM OF BLANK PLASMA MATRIX SPIKED WITH IPTN. C) CHROMATOGRAM OF BLANK PLASMA MATRIX SPIKED WITH IS. D) STANDARD CHROMATOGRAM OF PLASMA SPIKED IPTN AND IS

The plasma spiked calibration curve for peak area ratio of IPTN and IS against the IPTN concentration prepared showed a linear relationship over a concentration range of 0.5-300 ng/mL. The regression equation for IPTN in the developed method was found to be y = 0.010x + 0.085, with a correlation coefficient (r^2) of 0.999 indicates the good linearity of the method. The results of the linearity study of IPTN in the developed method were given in **Table 1,** and the calibration curve was shown in **Fig. 4**.

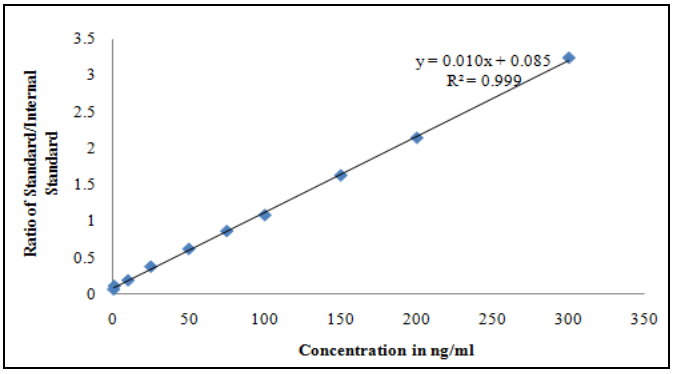

FIG. 4: CALIBRATION CURVE OF IPTN

TABLE 1: CALIBRATION CURVE RESULTS OF IPTN IN THE DEVELOPED METHOD

S. no.	Sample Id	Concentration in ng/ml	Peak Area observed for		Ratio of Standard/IS
			Isoproterenol - Standard	Dobutamine - IS	
1	PSCC 1	0.5	10143	150469	0.067
2	PSCC 2	1	17486	151171	0.116
3	PSCC 3	10	28947	150964	0.192
4	PSCC 4	25	57601	151769	0.380
5	PSCC 5	50	94295	151528	0.622
6	PSCC 6	75	130240	150361	0.866
7	PSCC 7	100	164963	151958	1.086
8	PSCC 8	150	247491	151822	1.630
9	PSCC 9	200	323884	151036	2.144
10	PSCC 10	300	491746	151739	3.241

The precision and accuracy of the method developed for IPTN were analyzed in three independent occasions in the calibration curve. The intra-assay coefficient of variation was found to be 0.143%, 0.828%, and 0.119% for HQC, MQC, and LQC, respectively, and trueness ranged from 98.665 to 99.913%. The inter-assay coefficients of variation ranged from 0.089% 0.837% and 0.119 for HQC, MQC, and LQC, respectively, and trueness ranged from 98.066% to 100.058% indicating that the assay method was sufficiently reliable and reproducible within the required analytical range. The results indicated that the matrix component in human plasma did not significantly affect response, and the method was found to be precise. **Table 2** shows the precision and accuracy results of the method developed for IPTN.

TABLE 2: PRECISION AND ACCURACY RESULTS

S. no.	Parameter	Intra-assay (n = 6)			Inter-assay (n = 6)		
		HQC	MQC	LQC	HQC	MQC	LQC
1	Concentration studied (ng/mL)	300 ng/ml	100 ng/ml	25 ng/ml	300 ng/ml	100 ng/ml	25 ng/ml
2	Concentration observed (ng/mL)	299.740	98.665	24.951	300.173	98.066	24.951
3	Peak Area	491320	162563	57487	492030	161576	57487
4	%CV	0.143	0.828	0.119	0.089	0.837	0.119
5	Trueness (%)	99.913	98.665	99.803	100.058	98.066	99.803
6	RE (%)	0.087	1.335	0.197	0.058	1.934	0.197

* CV = Coefficient of Variation; RE = Relative Error

Recovery and Matrix Effect: The absolute recovery IPTN and IS in the developed method was determined by comparing the peak area responses of QC samples (LQC, MQC, and HQC, n = 6) extracted in spiked plasma with corresponding standard concentrations prepared in reconstitution solvents. The % recovery was found to be 89.082, 93.431, and 84.80 for HQC, MQC, and LQC, respectively. The high recovery observed for both standard and IS and the % recovery of more than 85% and less than

115% observed confirms that the matrix effect was not observed. The result of the recovery study **Table 3** confirms that the method was found to be acceptable.

TABLE 3: RECOVERY RESULTS

S. no.	Parameter	HQC	MQC	LQC
1	Concentration studied (ng/mL)	300	100	25
2	Concentration observed (ng/mL)	267.25	93.431	21.20
3	Peak Area	542331	178446	67396
4	%CV	0.058	0.169	0.386
5	Recovery (%)	89.082	93.431	84.801
6	RE (%)	10.918	6.569	15.199

* n=6; CV = coefficient of variation; RE = relative error

The stability of both analyte and internal standard in the developed method was evaluated by short term stability, long term stability, and freeze-thaw stability. The % stability in all the stability studies was found to be 99.907, 97.555, and 87.461 for short term stability, 96.351, 93.362, and 87.461 for long term stability and 98.128, 96.126 and 88.919 for freeze-thaw stability in HQC, MQC and LQC respectively.

The results of the three stability studies **Table 4** confirms that the method was found to be stable and is suitable for the analysis of IPTN in biological samples.

TABLE 4: RECOVERY RESULTS

S. no	Parameter	HQC	MQC	LQC
	Short Term Stability			
1	Concentration studied (ng/mL)	300 ng/ml	100 ng/ml	25 ng/ml
2	Concentration observed (ng/mL)	299.721	97.555	21.865
3	Peak Area	491289	160734	50378
4	%CV	0.182	0.406	0.324
5	Stability (%)	99.907	97.555	87.461
6	RE (%)	0.093	2.445	12.539
	Long Term Stability			
7	Concentration studied (ng/mL)	300 ng/ml	100 ng/ml	25 ng/ml
8	Concentration observed (ng/mL)	289.053	93.362	21.865
9	Peak Area	473802	153825	50378
10	%CV	0.720	1.141	0.324
11	Stability (%)	96.351	93.362	87.461
12	RE (%)	3.649	6.638	12.539
	Freeze Thaw Stability			
13	Concentration studied (ng/mL)	300 ng/ml	100 ng/ml	25 ng/ml
14	Concentration observed (ng/mL)	294.384	96.126	22.229
15	Peak Area	482540	158381	51218
16	%CV	0.491	0.214	0.392
17	Stability (%)	98.128	96.126	88.919
18	RE (%)	1.872	3.874	11.081

* n=6; CV = coefficient of variation; RE = relative error

CONCLUSION: A simple and novel LCMS method was developed for the identification and quantification of IPTN in spiked human plasma samples. The method is applicable for the high throughput bio-analysis of IPTN owing to a run time of 15 min per sample.

The assay performance studies like linearity, accuracy, precision, and recovery were satisfactory for routine pharmacokinetic applications. Hence, the current LCMS method provides a valuable tool to improve the efficacy and safety of IPTN therapy.

ACKNOWLEDGEMENT: I am thankful for my authorities concerned for the permission accorded and coauthors for their valuable suggestions and guidance in carrying out this work.

CONFLICTS OF INTEREST: I declare that to the best of my knowledge and belief, neither my coauthors nor I have any interests which might conflict.

REFERENCES:

1. Osborn DA: Hemodynamics and Cardiology: Neonatology Questions and Controversies, Elsevier Academic Press, Cambridge, Massachusetts 2008: 229-65.
2. Arbuthnott G and Munoz MG: Companion to Psychiatric Studies Elsevier Academic Press, Cambridge, Massachusetts Edition 8, 2010: 45-76.
3. Mozayani A and Raymon L: Handbook of Drug Interactions: A Clinical and Forensic Guide. Springer Science & Business Media 2003: 541-42.
4. Jalba MS: Three Generations of Ongoing Controversies Concerning the Use of Short Acting Beta-Agonist Therapy in Asthma: A Review. Journal of Asthma 2008; 45(1): 9-18.

5. Garbis H: Drugs During Pregnancy and Lactation Elsevier Academic Press, Cambridge, Massachusetts: Elsevier Academic Press, Second Edition 2007: 63-77.
6. Muneer S, Hindustan AA and Chandrasekhar KB: Stability Indicating method development and validation for the quantification of Isoproterenol HCl in bulk and its formulation by RP-HPLC using PDA detection, Journal of Pharmaceutical and Scientific Innov 2018; 7(5): 183-87.
7. Kumar N, Rao DS, Reddy GP, Dubey SK and Kumar P: Synthesis, isolation, identification and characterization of new process-related impurity in isoproterenol hydrochloride by HPLC, LC/ESI-MS and NMR. Journal of Pharmaceutical Analysis 2017; 7(6): 394-400.
8. Guidance for Industry, Bioanalytical Method Validation, U. S. Department of Health and Human Services, Food and Drug Administration, Centre for Drug Evaluation and Research (CDER), Centre for Veterinary Medicine (CVM), 2001.

How to cite this article:
Gaddala VSS, Dachuru RSR and Tella ED: A validated LCMS method for the analysis of isoproterenol – A β adrenoreceptor agonist in spiked human plasma. Int J Pharm Sci & Res 2020; 11(9): 4567-74. doi: 10.13040/IJPSR.0975-8232.11(9).4567-74.

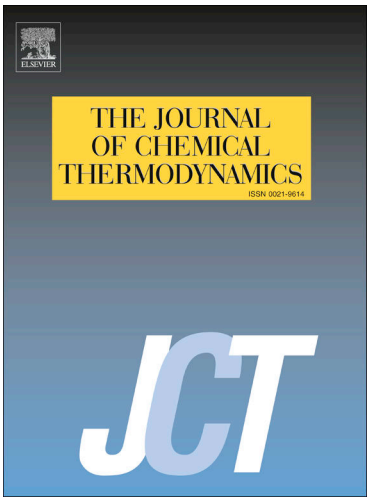

A molecular interactions study between 1-butyl-3-methylimidazolium hexafluorophosphate ([Bmim][PF_6]) and N-methylpyrrolidone

Sowjanya Prathipati, Srinivasa Rao Vipparla, Srinivasa Reddy Munnangi, Md Nayeem Sk, Hari Babu Bollikolla

PII: S0021-9614(20)30593-0
DOI: https://doi.org/10.1016/j.jct.2020.106330
Reference: YJCHT 106330

To appear in: *J. Chem. Thermodynamics*

Received Date: 20 May 2020
Revised Date: 21 October 2020
Accepted Date: 23 October 2020

Please cite this article as: S. Prathipati, S. Rao Vipparla, S. Reddy Munnangi, M. Nayeem Sk, H. Babu Bollikolla, A molecular interactions study between 1-butyl-3-methylimidazolium hexafluorophosphate ([Bmim][PF_6]) and N-methylpyrrolidone, *J. Chem. Thermodynamics* (2020), doi: https://doi.org/10.1016/j.jct.2020.106330

A molecular interactions study between 1-butyl-3-methylimidazolium hexafluorophosphate ([Bmim][PF_6]) and N-methylpyrrolidone

Sowjanya Prathipati[a], Srinivasa Rao Vipparla[a,b], Srinivasa Reddy Munnangi[c], Md Nayeem Sk[d], Hari Babu Bollikolla[a*]

[a]*Department of Chemistry, Acharya Nagarjuna University, Nagarjunanagar–522 510, A.P., India*

[b]*Department of Chemistry, Govt. Degree College , Avanigadda-521 121, A.P., India.*

[c]*Department of Chemistry, TRR Govt. Degree College, Kandukur-523 105, A.P., India.*

[d]*Department of Physics, KRK Govt. Degree College, Addanki-523 201, A.P., India.*

ABSTRACT:

The work entitled results from initial determination of physical parameters, density (ρ), speed of sound (u), refractive index of [Bmim][PF_6]/ N-methylpyrrolidone and their binaries at all compositions at atmospheric pressure and at task temperatures ranging from (303.15 - 323.15) K. The experimental results were utilized for computation of molar volumes (V_m^E)/partial molar volumes ($\overline{V}_m^E$)/ partial molar volumes at infinite dilution ($\overline{V}_m^{E,\infty}$)/isentropic compressibility (κ_s^E)/ free length (L_f^E)/ speeds of sound (u^E) and isobaric thermal expansion coefficient (α_P^E) of the binary system. Further, the binary coefficients and the standard deviations were deduced by fitting the excess properties in Redlich-Kister equation. A fortitude of these parameters indicated strong intermolecular interactions and likewise increases with increase of temperature. Furthermore, molecular properties were also evaluated using Sehgal's relation on non-linear parameters of Hartmann-Balizar and Ballou semiempirical relations at all temperatures. Moreover, the activity coefficients were calculated by Margules/Porter/Wilson/NRTL relations at temperature 308.15 K. The results of Prigogine–Flory–Patterson (PFP) theory of excess molar volume and IR spectra were supported the deduced strong interactions.

Key words: [Bmim][PF_6]; N-methylpyrrolidone; PFP theory; speed of sound; IR spectra; thermodynamic parameters.

* Corresponding Author:dr.b.haribabu@gmail.com

Phone: +91-8500338866

1. Introduction

Today Ionic Liquids (ILs) have attracted significant consideration for the reason of their distinctive properties, *viz.* thermal stability, non-volatility and reuse [1,2]. ILs can be selected to have various cations and anions, in order to shape Ionic Liquids with preferred properties. Besides, ILs have been recognized for quite a while, yet their wide utility as solvents in catalysis and processes design for chemical synthesis in recent times happen to be noteworthy. ILs have potential applications in many areas but real applications must be investigated further. However, the much cost of the ILs and more viscous nature than conventional organic solvents restricted their use in multiple applications.

Researchers are becoming more interested in IL mixtures with molecular organic solvents, as the resulting liquid mixtures provide many advantages than individual IL and organic solvent. The properties of such mixtures are dependent on the proportion of mixing. Mixing of IL with organic molecular solvents is one of the alternatives for reducing the use of costly ILs and also save the time in preparing new ILs of wanted properties [3], fortunately the mixtures also have reduced viscosity without loss in their advantages as green solvents. Meticulously, the mixing of co-solvents with polar nature may have a significant effect on physical and chemical properties of the IL's[4]. Recently it has been shown that specific (IL + molecular organic solvent) binary systems have better performance than pure ILs. These were also found to be useful in various advanced applications, *viz.* in super capacitors, bio-catalysed processes, as a medium for the solvation of biopolymers, *etc.* [5 17]. In recent years, therefore, the thermo-physical study of IL + molecular solvents has received increased attention. In view of the fact that these data are important for industrial applications, the prospective of the new systems can be exploited by examining their physicochemical properties.

The selection of the studied IL 1-butyl-3-methylimidazolium hexafluorophosphate, ([Bmim] [PF_6]) is based on its ability as a green plasticizer for poly (L-lactide) [18], in Tussah silk dyeing [19], RP HPLC [20], in organic synthesis [21], in separatión technology [22] and also used in enzymatic catalysis [23]. On the other hand, NMP (N-methylpyrrolidone) solvent is unique in its properties with low volatility compared to most of the organic liquids, and high polarity. Its commercial uses are in petrochemical and plastic industries, taking advantage of its

non-volatility and their capability to dissolve various materials[24]. Further, NMP is also used in drugs formulation and in the manufacture of lithium ion batteries.

Physico-chemical properties between [Bmim] [PF_6] with organic solvents such as dimethyl formamide [37], methyl methacrylate [25], butanol, acetone [38], THF, DMSO, methanol, acetonitrile [39], ethanol, benzene [40], 2-propoxyethanol [30], 2, 2, 2-trifluoroethanol [41], 2-Pyrrolidone [42], N-vinyl-2-pyrrolidinone [43], N-Methylaniline [26] and ethyl acetate [44] were found so far in literature. Feng *etal* [45] has reported density only at (298.15 - 313.15) K for the binary mixture under study. So, in this article, the authors made an attempt to fortitude the molecular interactions between ([Bmim][PF_6]) and N-methylpyrrolidone binary system using a comprehensive study on volumetric, acoustic, optical and their derived parameters at temperatures (303.15 - 323.15) K along with spectral studies.

On the basis of our initial experiments, the selected IL in all proportions completely miscible with NMP. Therefore, in this analysis, we propose to calculate the density, speed of sound and refractive index of [Bmim][PF_6] binary mixtures with NMP between 303.15 K - 323.15 K temperatures across all compositions and at atmospheric pressure. We calculated the deviation / excess properties based on the measured values, and these properties were fitted using Redlich-Kister polynomial equation for their possible application in industrial processes. Additionally, IR spectroscopy sought to understand the contact behavior between the two liquids in the mixture. Finally, the experimental excess molar volume data was contrasted with the theory of Prigogine-Flory-Patterson (PFP).

2. Experimental

2.1. Materials and methods

The [Bmim] [PF_6] (CAS 174501-64-5) with a mass fraction purity of 0.99 was bought from Iolitec GmBH (Germany); Sigma Aldrich supplied the NMP (CAS 872-50-4), with a mass fraction purity of 0.995. The chemicals used in this work were well purified using known methods [46,47]. Karl Fisher titrator was used to determine the water content in IL and NMP (Metrohm, 890 Titrando). All samples were dried under reduced pressure (0.1 bar) at moderate temperature for at least 72 h before taking each measurement (starting at room temperature and

gradually rising to 333 K). The water content of all samples was further checked, and was found less than 170 ppm, a much lower value than the pre-evacuation analysis, which showed values of around 210 ppm. The NMP solvent was further purified by distillation and [Bmim] [PF_6] was used without further purification (See Table S1, **SI** for other procedures and equipment). Further, the purities were checked by comparing measured density, speed of sound and refractive index with the literature values given in **Table 1**.

Measurement of density and speed of sound

Densities and speed of sound are measured with an Anton Paar DSA-5000M vibrating tube density and sound velocity meter. The density meter is calibrated with doubly distilled degassed water, and with dry air at atmospheric pressure. The temperature of the apparatus is controlled to within ±0.01 K by a built-in Peltier device. Measured density and speed of sound values (at frequency approximately 3 MHz) are precise to $5x10^{-3}$ $kg.m^{-3}$and $5x10^{-1}m.s^{-1}$respectively. The standard uncertainties associated with the measurements of temperature, density and speed of sound are estimated to be ±0.01 K, 1.0 kg m^{-3} and ±0.5 m s^{-1} respectively.

Measurement of refractive index

The refractive indices are determined using an automatic refractometer (Anton Paar Dr Krenchen Abbemat (WR-HT)) which has also a temperature controller that keeps the samples at working temperature. The uncertainties in the temperature and refractive index values are ±0.01K and $±5x10^{-4}$ respectively. The apparatus is calibrated by measuring the refractive index of Millipore quality water and tetrachloroethylene (supplied by the company) before each series of measurements according to manual instructions. The calibration is checked with pure liquids by known refractive index.

Measurement of infrared spectra

Infrared transmittance is measured by using Shimadzu Fourier transform infrared (FT-IR) spectrometer (IRAffinity-1S**)** equipped with attenuated total reflectance (ATR) accessories. The spectral region is (650-4000) cm^{-1} with resolution of 2 cm^{-1} and 100 scans. At least five repeated measurements are performed for each sample.

3. Results and discussion

Experimental density (ρ), speed of sound (u), refractive index (n_D), for binary mixtures of [Bmim] [PF_6] with NMP with respect to the mole fraction (x_1), of [Bmim][PF_6] at scrutinizing

temperatures were given in **Table 2**. The densities of the mixtures of this work have been graphically compared (**Figure 1**) with those of Feng *et al.* [45]. There are clear deviations of densities of pure solvents. This might be due to that Feng *et al.* [45] used NMP with mass fraction purity of 0.99 and didn't mention the purity of [Bmim][PF_6]. In this work, we not only used the solvents with high purity but also more sophisticated equipment for accuracy.Both [Bmim][PF_6] and N-methyl pyrrolidine are considered polar, which contributes to the full miscibility of themselves in all proportions and at temperatures. A close look density in **Table 2** clearly demonstrates a linear decrease when temperature rises due to expansiveness of volume. The thermal expansion coefficient (α_p) is a measure of the fluid expansion or contraction with temperature in all directions. The resulting values of [Bmim][PF_6] were smaller than NMP, which means that the IL expands or contracts less than NMP at a predetermined temperature.

From the above experimental data the authors computed the excess properties, molar volume (V_m^E), isentropic compressibility (κ_s^E), free length (L_f^E), velocity of sound (u^E) and isobaric thermal expansion coefficient (α_p^E) using thermodynamic equations (**S1-S11; SI**). The Plots of excess molar volume (V_m^E) against mole fraction of IL in the mixture with NMP at studied temperatures **(**303.15 to 323.15) K were shown in **Figure 2**. Excess molar volumes at all investigated temperatures were found negative for the mixtures and the more negative value was found to be -0.79x10^{-6}m^{3}mol^{-1} at x_1 = 0.1894 and T= 303.15 K. At upper temperatures the minimum of V_m^E further decreased (more negative) and changes were marginally to higher mole fraction of IL. Imidazolium ILs can also form hydrogen bonds at suitable conditions, as these act as both donor and acceptor of protons. So, the H-bonds between the [Bmim][PF_6] and NMP can therefore be assumed to be responsible for a significant contraction of the mixture volume. Moreover, the complimentary fitting of smaller NMP solvent molecules (at T=303.15 K, V_m= 96.94x10^{-6} m^{3}mol^{-1}) into cavities formed by larger [Bmim][PF_6] molecules (at T=303.15 K, V_m= 208.26x10-6 m^{3}mol^{-1}) is also considerable for these tough interactions. For other temperatures a similar pattern may also be observed and the effect is more predominant at upper temperature. This is owing to the reason that smaller NMP molecules are more favourably fitted into the cavities produced by larger [Bmim][PF_6] molecules, thus sinking the volume of the mixture to a greater degree, ensuing in more negative values with increasing temperature. In terms of

temperature, the order of interaction forces is (323.15>318.15>313.15>308.15>303.15) K. The polynomial coefficients of the Redlich-Kister and the corresponding standard deviations were given in **Table 3**.

The molecular interactions that occur in the system reflect well on the properties of partial molar volumes ($\overline{V}_m^E$). The ($\overline{V}_m^E$) of component 1 ([Bmim][PF_6]) and 2 (NMP) in the mixtures were calculated using equations **S12-S17 (**See **SI**) and the values were given in **Table 4**. From this table it can be found that the $\overline{V}_{m,1}$ values for [Bmim][PF_6] in the mixtures were almost lower than their individual molar volumes in their pure states, suggesting that the volume contraction occurs by combining [Bmim][PF_6] and NMP under any temperature. The **Figures 3** and **4** shows the discrepancy of excess partial molar volumes of ([Bmim][PF_6]) and (NMP) in the binary system at T = (303.15, 308.15, 313.15, 318.15 and 323.15) K respectively. The negative pattern of these properties found at all temperatures also supports the resultant negative excess molar volumes. A scrutiny of this data not only shows the presence of strong interactions between the different molecules but also supports conclusions drawn from excess molar volumes.

The partial molar volumes [Bmim][PF_6] and NMP denoted as $\overline{V}_{m,1}^{\infty}, \overline{V}_{m,2}^{\infty}$ and excess partial molar volumes at infinite dilution $\overline{V}_{m,1}^{E,\infty}, \overline{V}_{m,2}^{E,\infty}$ were computed from the known equations (**S18** and **S19** of **SI**). The computed values at all investigated temperatures of $\overline{V}_{m,1}^{\infty}, \overline{V}_{m,2}^{\infty}$ and $\overline{V}_{m,1}^{E,\infty}, \overline{V}_{m,2}^{E,\infty}$ were given in **Table 5.** The values of $\overline{V}_{m,1}^{E,\infty}$ were found negative and also become more negative with increased temperatures. This signify that the molecular association effect is larger than the dissociation for [Bmim][PF_6] IL system. On the other side the excess partial molar volumes at infinite dilution for NMP ($\overline{V}_{m,2}^{E,\infty}$) are positive at all temperatures determined. This is for the reason that of ion solvation process and extinction of ion-ion interactions in [Bmim][PF_6] [48]. This is observed in the case of V_m^E values which reproduce well from the computed parameters of partial molar volumes at infinite dilution at all temperatures calculated.

For [Bmim][PF_6] + NMP system, the excess isoentropic compressibility (κ_s^E) behavior is very likely to the $V_{\mathrm{m}}^{\mathrm{E}}$ that was shown in the **Figure 5**. It was also found negative in the entire

region of investigated temperatures and composition ratios and becomes more negative with rise in temperature. The negative values of κ_s^E mean that the mixtures are more compressible than the respective ideal mixtures [49]. Therefore, it is assumed that the decrease in free volume is making the mixture more compressible than the ideal mixture, which eventually results in negative values for excess isoentropic compressibility. The disparity of excess free length (L_f^E) against mole fraction of IL is shown in **Figure 6**. The negative values of excess free length suggested the presence of specific interactions between different molecules as well as structural adjustments in the liquid mixture leading to closer molecular packaging.

At all investigated temperatures the clearly **Figure 7** illustrates that the speeds of sound (u^E) values were positive for the current binary system over the whole compositions. The positive deviations are a sign of increase interactions between the component molecules of the binary liquid mixtures [50]. The deviations in refractive index ($\Delta_\phi n_D$) against mole fraction were plotted in **Figure 8** and the values were found positive in the studied composition ratios of the binary mixture. This further supported the existence of strong interaction forces among the component molecules [51]. **Figure 9** indicates negative values of α_P^E for the binary mixture over the entire composition and at all investigated temperatures. This further supported the presence of tough interactions between the component molecules [52].

3.1. Infrared spectral studies

The observed interactions from the above inferences of excess parameters in the system were well supported by the IR spectral data. The unique nature of imidazolium cations is demonstrated well by their electronic structure (**Figure 10**). Because of the less electron density on the C=N bond, the hydrogen in C_2-H has more acidic nature than C_4-H, and C_5-H. These hydrogens' resulting acidity is important for understanding the properties of the current ILs. The 'H' on the C_2 carbon (C_2–H) was shown to be normally associate with solvent molecules [53].

The infrared absorbance was recorded between 650 cm^{-1} to 4000 cm^{-1} wavelength (**Figure 11** and **Table 6**) to know the outcome of molecular interactions. For [Bmim][PF_6], signals can be divided into two different parts, the signals between 3000 cm^{-1} and 3200 cm^{-1} may be endorsed mainly to the C-H vibrational modes of aromatic imidazolium ring [54]. Further, the

signals from 2800 cm^{-1} to 3000 cm^{-1} are mainly due to aliphatic C-H stretchings in the methyl and butyl moieties [55–57]. Since for its stronger acidic character, the C_2-H vibrational frequency (3124.3 cm^{-1}) was found to be moved to a lower frequency by around 44.9 cm^{-1} compared to C_4-H and C_5-H stretchings (3169.2 cm^{-1}). The C_2-H and $C_{4,5}$-H stretching frequencies of the IL cation were examined (**Figure 12**) along with C=O stretching area of NMP (**Figure 13**). It was also found that the red shift is very predominant in C_2-H frequencies compared to $C_{4,5}$-H stretching frequencies, implying that more acidic C_2-H plays a most important role in the formation of H-bond with carbonyl oxygen of NMP (**Figure 13**). At the same time, a strong red shift is observed for C=O Sym Stretch frequencies in NMP, as the mole fraction of IL increases. This evidently demonstrated the formation of intermolecular hydrogen bonds between the 'H'-atoms of aromatic imidazolium ring and NMP carbonyl oxygen.

ATR-FTIR studies suggested the key role of hydrogen in miscibility and stability of the binary system. Hence it can be assumed that the hydrogen bonds in the system are also accountable for the existing tough interactions and contractions in the mixtures volumes.

3.2. Prigogine-Flory-Patterson statistical theory for excess molar volume V_m^E

The Prigogine-Flory-Patterson (PFP) theory was used to check and compare experimental excess molar volumes of binary mixtures [58–62]. At T = (303.15-323.15) K, we compared 'V_m^E' of the titled binary mixture utilizing the PFP theory over the whole mole fractions range. The calculation of various parameters of this theory is based on relevant equations reported in literature [63–67]. The parameters of pure components for the PFP theory were listed in **Table 7**. In the absence of experimental excess molar enthalpy (H_m^E), the Flory contact interaction parameter χ_{12}, the only adjustable parameter required in the PFP theory, was obtained from experimentally determined values of V_m^E. It was found that for all the investigated temperatures, the Flory contact interaction parameter χ_{12} was found negative. The values of said 3 contributions, V_{int}^E,$V_{fv}^E and V_{P^*}^E$, to V_m^E(PFP) at equimolar composition were given in **Table 8.** The first term V_{int}^E is negative, indicating the tough interactions occur in the mixture. For all measured temperatures the connecting forces contributions were observed negative. The second term V_{fv}^E was also found to be negative as V_{fv}^E is proportional to $-(\tilde{V}_1 - \tilde{V}_2)^2$ [59,68]. The degree of negative values of V_{fv}^E depends on difference in Flory's reduced volumes of the

components. Negative values in the magnitude of V_{fv}^{E} increase further with rise in temperature as more free volume becomes available in [Bmim][PF_6] to accommodate the smaller NMP molecules which resulted in more negative V_{m}^{E}. The third term, i.e. characteristic pressure V_{P*}^{E}, was found positive at investigated temperatures, the *P** effect which depends on the relative cohesive energy of the expanded and less expanded component. Further, it is proportional to $(\tilde{V}_1 - \tilde{V}_2)(P_1^* - P_2^*)$ and can have both the negative and positive sign depending upon the magnitude of P_i^* and $\widetilde{V_i^*}$ of unlike components [59,68]. For the system [Bmim][PF_6] + NMP, V_{P*}^{E} was found positive which was related to the structure-braking consequence of the solvent NMP on the electrostatic interactions between [Bmim][PF_6] ions and so the NMP molecules can be placed around the $[Bmim]^+$ and $[PF_6]^-$ ions[68]. V_{int}^{E} and V_{fv}^{E} were found to be negative in the present system while V_{P*}^{E} were found to be positive which indicates that the interaction and free volume contributions are responsible for the strong interactions between solute and solvent particles. We may summarize that the volumetric behavior of the binary mixture of {[Bmim][PF_6] + NMP} can be explained very effectively through the application of this PFP theory.

4. Conclusions

Density, speed of sound and refractive index for binary liquid mixtures of [Bmim][PF_6] with NMP were experimentally determined at atmospheric pressure and at temperatures 303.15 K, 308.15 K, 313.15 K, 318.15 K and 323.15 K over the whole compositions. From the experimental results the excess properties, V_m^E, κ_S^E, L_f^E, u^E, α_P^E and $\Delta_\phi n_D$ were calculated. The excess and deviation parameters were fitted to the Redlich-Kister polynomial, and the corresponding standard deviations were also determined. The observed excess values in the current binary liquid system [Bmim][PF_6] and NMP clearly indicated the predominance of strong attractive forces. Using Sehgal 's relationship on Hartmann-Balizar and Ballou semiempirical relations, molecular properties were determined at all temperatures. Activity coefficients determined by the NRTL relation showed low standard deviation at 308.15 K compared to other models. The inferences from excess properties were also supported by the IR spectral study. With reasonable success the PFP theory was applied to well explain the volumetric behavior of the studied system.

Acknowledgements

The first author thank DST for providing an INSPIRE fellowship (F.No-DST/INSPIRE Fellowship/2018/IF180782, dated 25.09.2019) and all the authors thank KTSS Raju, Dept. of Chemistry, A. L. College, Vijayawada, for help in instrumental support.

References:

[1] T.L. Greaves, C.J. Drummond, Chem. Rev. 115 (2015) 11379–11448.

[2] F. Guo, S. Zhang, J. Wang, B. Teng, T. Zhang, M. Fan, Curr. Org. Chem. 19 (2015) 455–468.

[3] A.A. Shamsuri, R. Daik, Rev. Adv. Mater. Sci 40 (2015) 45–59.

[4] C. Comminges, R. Barhdadi, M. Laurent, M. Troupel, J. Chem. Eng. Data 51 (2006) 680–685.

[5] M.D. Bhatt, C. O'Dwyer, Phys. Chem. Chem. Phys. 17 (2015) 4799–4844.

[6] C.J. Allen, S. Mukerjee, E.J. Plichta, M.A. Hendrickson, K.M. Abraham, J. Phys. Chem. Lett. 2 (2011) 2420–2424.

[7] S. Park, R.J. Kazlauskas, Curr. Opin. Biotechnol. 14 (2003) 432–437.

[8] M. Sureshkumar, C.-K. Lee, J. Mol. Catal. B Enzym. 60 (2009) 1–12.

[9] M. Moniruzzaman, K. Nakashima, N. Kamiya, M. Goto, Biochem. Eng. J. 48 (2010) 295–314.

[10] J. V Rodrigues, D. Ruivo, A. Rodríguez, F.J. Deive, J.M.S.S. Esperança, I.M. Marrucho, C.M. Gomes, L.P.N. Rebelo, Green Chem. 16 (2014) 4520–4523.

[11] M. da Graça Nascimento, J.M.R. da Silva, J.C. da Silva, M.M. Alves, J. Mol. Catal. B Enzym. 112 (2015) 1–8.

[12] P. Lozano, T. de Diego, D. Carrié, M. Vaultier, J.L. Iborra, Chem. Commun. (2002) 692–693.

[13] M.B. Turner, S.K. Spear, J.D. Holbrey, D.T. Daly, R.D. Rogers, Biomacromolecules 6 (2005) 2497–2502.

[14] M.B. Turner, S.K. Spear, J.D. Holbrey, R.D. Rogers, Biomacromolecules 5 (2004) 1379–1384.

[15] S.S.Y. Tan, D.R. MacFarlane, J. Upfal, L.A. Edye, W.O.S. Doherty, A.F. Patti, J.M. Pringle, J.L. Scott, Green Chem. 11 (2009) 339–345.

[16] M. Gericke, T. Liebert, T. Heinze, Macromol. Biosci. 9 (2009) 343–353.

[17] M. Gericke, J. Schaller, T. Liebert, P. Fardim, F. Meister, T. Heinze, Carbohydr. Polym. 89 (2012) 526–536.

[18] P. Zhang, L. Peng, W. Li, E-Polymers 8 (2008).

[19] J. Lin, Y. Teng, Y. Lu, S. Lu, X. Hao, D. Cheng, CLEAN–Soil, Air, Water 42 (2014) 799–803.

[20] J. Flieger, Anal. Lett. 42 (2009) 1632–1649.

[21] H. Zhao, S. V Malhotra, Aldrichimica Acta. 35 (2002) 75-83.

[22] D. Han, K.H. Row, Molecules 15 (2010) 2405–2426.

[23] M. Erbeldinger, A.J. Mesiano, A.J. Russell, Biotechnol. Prog. 16 (2000) 1129–1131.

[24] A.L. Harreus, R. Backes, J.O. Eichler, R. Feuerhake, C. Jäkel, U. Mahn, R. Pinkos, R. Vogelsang, Pyrrole 30 (2000) 615–618.

[25] W. Fan, Q. Zhou, J. Sun, S. Zhang, J. Chem. Eng. Data 54 (2009) 2307–2311.

[26] B. Goddu, M.M. Tadavarthi, V.K. Tadekoru, J.N. Guntupalli, J. Chem. Eng. Data 64 (2019) 2303–2319.

[27] M.A.A. Rocha, F.M.S. Ribeiro, A.I.M.C.L. Ferreira, J.A.P. Coutinho, L.M. Santos, J. Mol. Liq. 188 (2013) 196–202.

[28] M.G. Montalbán, C.L. Bolívar, F.G. Diaz Banos, G. Víllora, J. Chem. Eng. Data 60 (2015) 1986–1996.

[29] A.B. Pereiro, J.L. Legido, A. Rodrı, J. Chem. Thermodyn. 39 (2007) 1168–1175.

[30] T.S. Krishna, K. Raju, M. Gowrisankar, A.K. Nain, B. Munibhadrayya, J. Mol. Liq. 216 (2016) 484–495.

[31] J. Troncoso, C.A. Cerdeiriña, Y.A. Sanmamed, L. Romaní, L.P.N. Rebelo, J. Chem. Eng. Data 51 (2006) 1856–1859.

[32] T.S. Krishna, K. Narendra, M.G. Sankar, A.K. Nain, B. Munibhadrayya, J. Chem. Thermodyn. 98 (2016) 262–271.

[33] A. García-Abuín, D. Gomez-Diaz, M.D. La Rubia, J.M. Navaza, J. Chem. Eng. Data 56 (2011) 646–651.

[34] N. V Živković, S.S. Šerbanović, M.L. Kijevčanin, E.M. Zivkovic, J. Chem. Eng. Data 58 (2013) 3332–3341.

[35] J.-Y. Wu, Y.-P. Chen, C.-S. Su, J. Solution Chem. 44 (2015) 395–412.

[36] M. Mundhwa, S. Elmahmudi, Y. Maham, A. Henni, J. Chem. Eng. Data 54 (2009) 2895–2901.

[37] G. Yanfang, W. Tengfang, Y.U. Dahong, P. Changjun, L.I.U. Honglai, H.U. Ying, Chinese J. Chem. Eng. 16 (2008) 256–262.

[38] A. Zhu, J. Wang, L. Han, M. Fan, Chem. Eng. J. 147 (2009) 27–35.

[39] M.T. Zafarani-Moattar, R. Majdan-Cegincara, J. Chem. Eng. Data 52 (2007) 2359–2364.

[40] Y. Qiao, F. Yan, S. Xia, S. Yin, P. Ma, J. Chem. Eng. Data 56 (2011) 2379–2385.

[41] M.R. Currás, M.M. Mato, P.B. Sánchez, J. García, J. Chem. Thermodyn. 113 (2017) 29–40.

[42] V.S. Rao, M.S. Reddy, K.T.S.S. Raju, B.L. Rani, B.H. Babu, J. Solution Chem. 47 (2018) 430–448.

[43] P. Suneetha, T.S. Krishna, M. Gowrisankar, M.S. Reddy, D. Ramachandran, J. Therm. Anal. Calorim. 134 (2018) 1151–1167.

[44] P.R. Rao, T.S. Krishna, D. Ramachandran, J. Chem. Thermodyn. 141 (2020) 105906.

[45] F. Qi, H. Wang, J. Chem. Thermodyn. 41 (2009) 265–272.

[46] W.L.F. Armarego, C.L.L. Chai, Purification of laboratory chemicals.(7thedn) (2013).

[47] E. Scholz, Karl Fischer Titration, Springer-Verlag, Berlin, 1984.

[48] M.B. Vraneš, S. Dožić, V. Djerić, S.B. Gadžurić, J. Chem. Eng. Data 58 (2013) 1092–1102.

[49] M.S. Reddy, S.M. Nayeem, K. Raju, B.H. Babu, J. Therm. Anal. Calorim. 124 (2016) 959–971.

[50] M.S. Reddy, K.T.S.S.S. Raju, S.M. Nayeem, I. Khan, K.B.M.M. Krishana, B.H. Babu, J. Solution Chem. 45 (2016) 675–701.

[51] S. Reddy, M.N. Sk, K. Raju, J. Mol. Liq. 218 (2016) 83–94.

[52] M.S. Reddy, I. Khan, K.T.S.S. Raju, P. Suresh, B.H. Babu, J. Chem. Thermodyn. 98 (2016) 298–308.

[53] A. Aggarwal, N.L. Lancaster, A.R. Sethi, T. Welton, Green Chem. 4 (2002) 517–520.

[54] V. Znamenskiy, M.N. Kobrak, J. Phys. Chem. B 108 (2004) 1072–1079.

[55] N.R. Dhumal, H.J. Kim, J. Kiefer, J. Phys. Chem. A 115 (2011) 3551–3558.

[56] J.-C. Lassègues, J. Grondin, D. Cavagnat, P. Johansson, J. Phys. Chem. A 113 (2009) 6419–6421.

[57] J.-C. Lassegues, J. Grondin, D. Cavagnat, P. Johansson, J. Phys. Chem. A 114 (2010) 687–688.

[58] E. Vercher, F.J. Llopis, M.V. González-Alfaro, A. Martínez-Andreu, J. Chem. Eng. Data 55 (2010) 1377–1388.

[59] D. Patterson, G. Delmas, Discuss. Faraday Soc. 49 (1970) 98–105.

[60] M.T. Zafarani-Moattar, H. Shekaari, J. Chem. Thermodyn. 38 (2006) 1377–1384.

[61] M. Srinivasa Reddy, K.T.S.S.S. Raju, S. Md Nayeem, K. Bala Murali Krishna, H.B. Bollikolla, Phys. Chem. Liq. 55 (2017) 775–795.

[62] M. SrinivasaReddy, G.S. Rao, S.K.M. Nayeem, K. Raju, B.H. Babu, J. Therm. Anal. Calorim. 132 (2018) 725–739.

[63] R.B. Tôrres, M.I. Ortolan, P.L.O. Volpe, J. Chem. Thermodyn. 40 (2008) 442–459.

[64] P.J. d Flory, J. Am. Chem. Soc. 87 (1965) 1833–1838.

[65] A. Abe, P.J. Flory, J. Am. Chem. Soc. 87 (1965) 1838–1846.

[66] E. Vercher, A.V. Orchilles, P.J. Miguel, A. Martínez-Andreu, J. Chem. Eng. Data 52 (2007) 1468–1482.

[67] A. Kumar, T. Singh, R.L. Gardas, J.A.P. Coutinho, J. Chem. Thermodyn. 40 (2008) 32–39.

[68] Z.S. Vaid, U.U. More, S.B. Oswal, N.I. Malek, Thermochim. Acta 634 (2016) 38–47.

Highlights

- The studied binary systems is {**[Bmim][PF_6]+1-methylpyrrolidone**}
- Density, speed of sound and refractive index are measured at various temperatures
- The interactions in the system are analyzed in terms of excess parameters
- The existing interactions are well explained with the help of IR spectral studies
- Observed experimental results are correlated with PFP theory

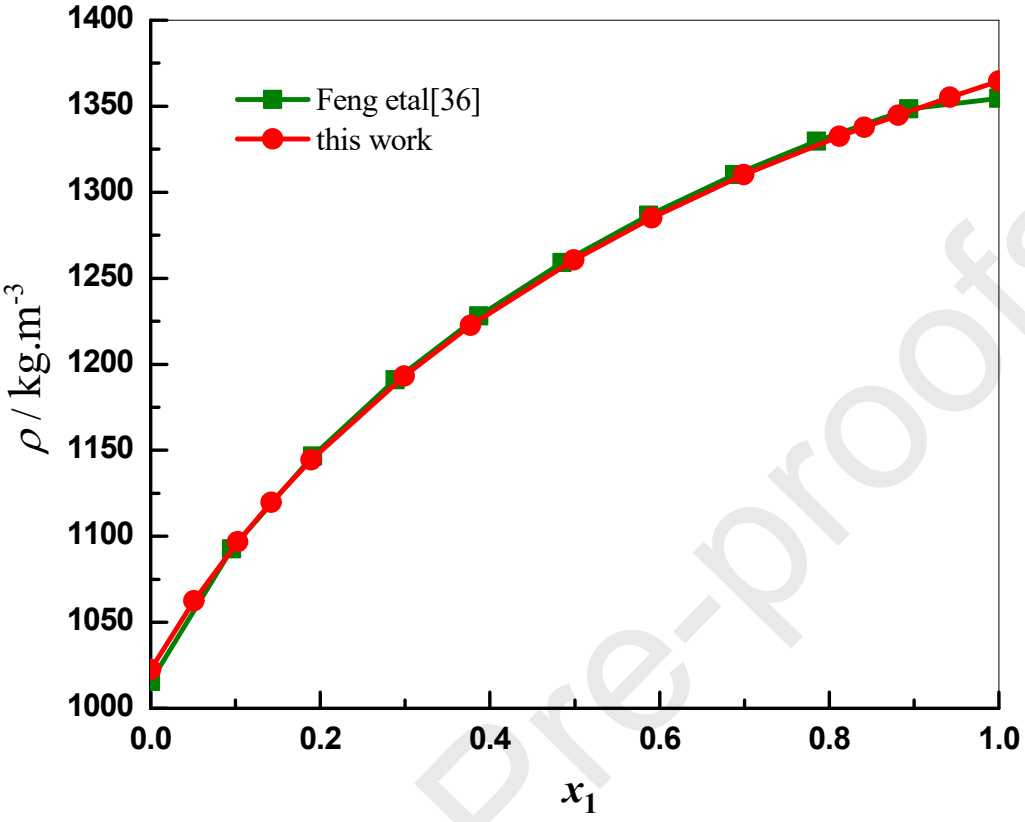

Fig. 1 Plots of experimental densities of Feng etal[36] and this work of the binary mixtures of [Bmim][PF_6] with NMP against mole fraction of [Bmim][PF_6] at 303.15 K.

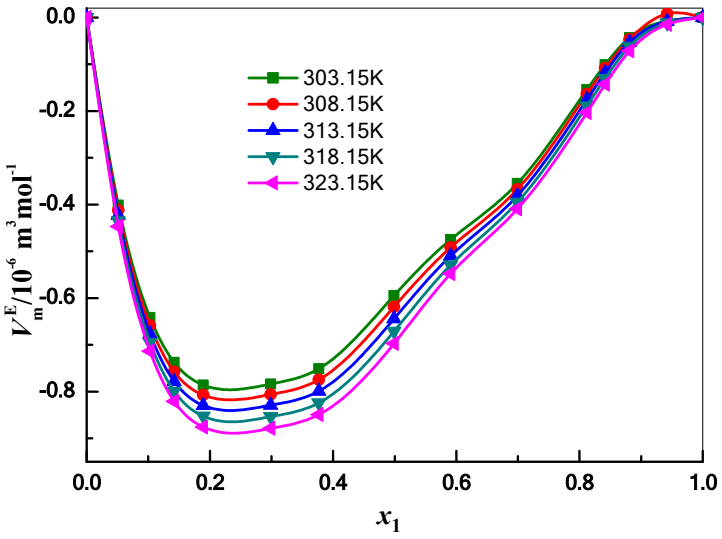

Fig. 2 Plots of excess molar volume (V_m^E) against mole fraction of [Bmim][PF_6] in the mixture with NMP at different temperatures**.**

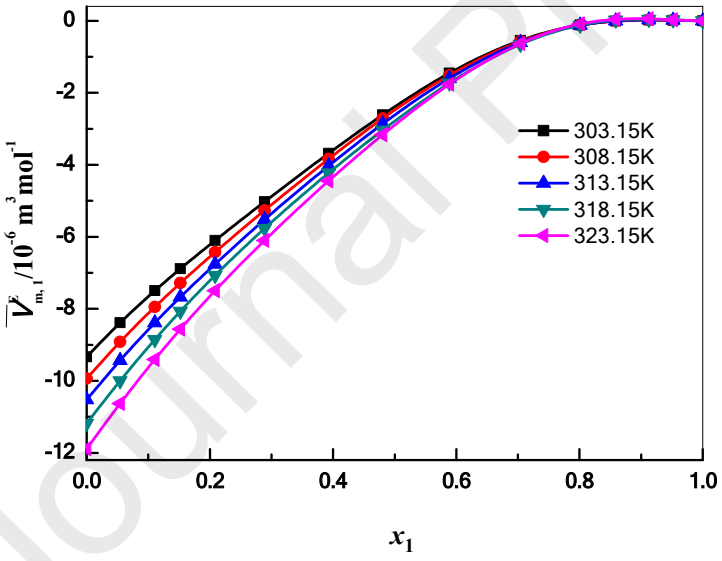

Fig. 3 Plots of excess partial molar volume ($\overline{V}_{m,1}^E$) against mole fraction of [Bmim][PF_6] in the mixture with NMP at different temperatures.

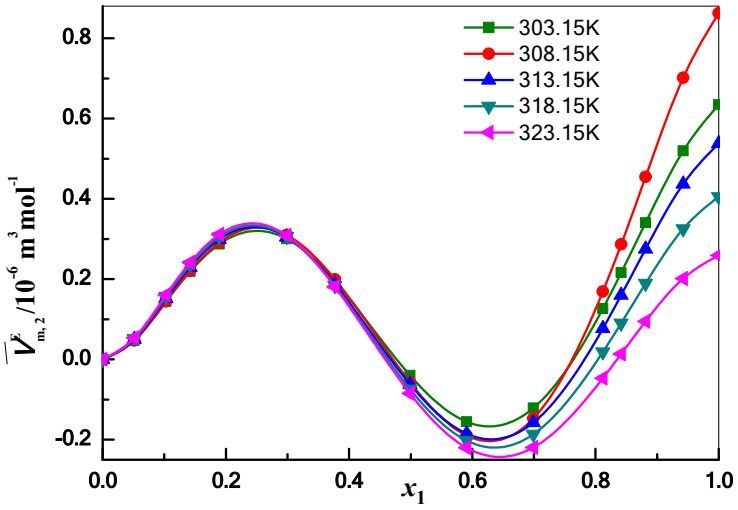

Fig. 4 Plots of excess partial molar volume ($\overline{V}^{E}_{m,2}$) against mole fraction of [Bmim][PF_6] in the mixture with NMP at different temperatures.

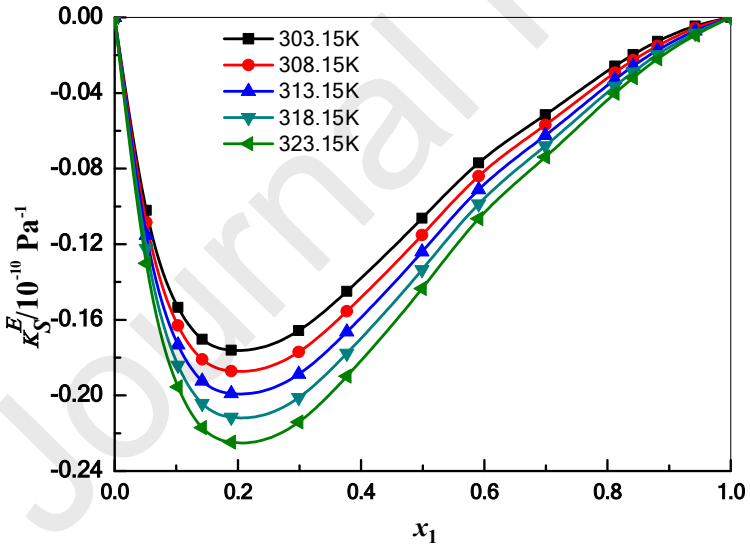

Fig. 5 Plots of excess isentropic compressibility (κ^{E}_{S}) against mole fraction of [Bmim][PF_6] in the mixture with NMP at different temperatures.

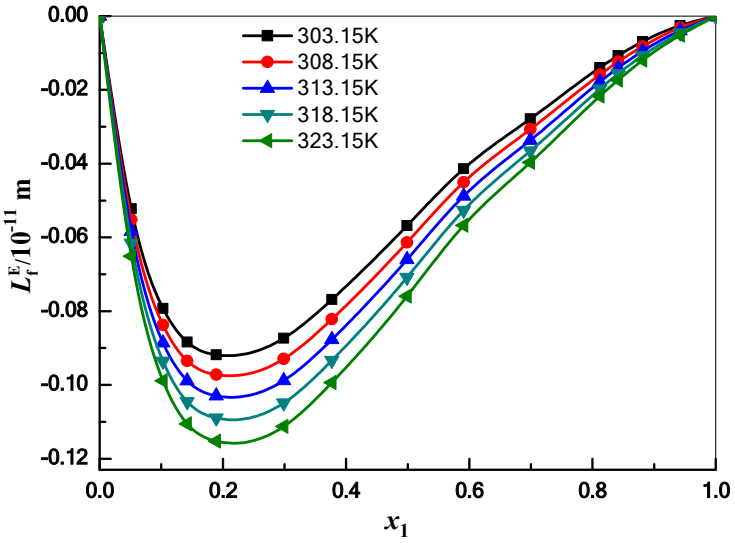

Fig. 6 Plots of excess free length (L_f^E) against mole fraction of [Bmim][PF_6] in the mixture with NMP at different temperatures.

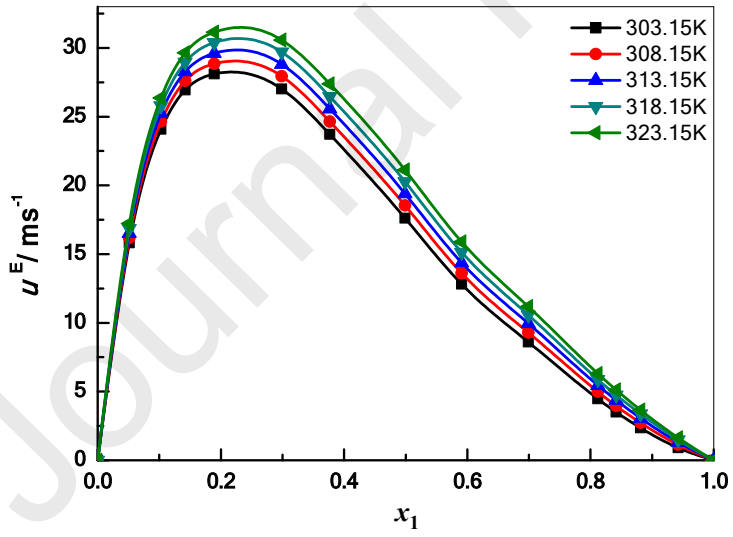

Fig.7 Plots of Excess ultrasonic speed of sounds (u^E) against mole fraction of [Bmim][PF_6] in the mixture with NMP at different temperatures.

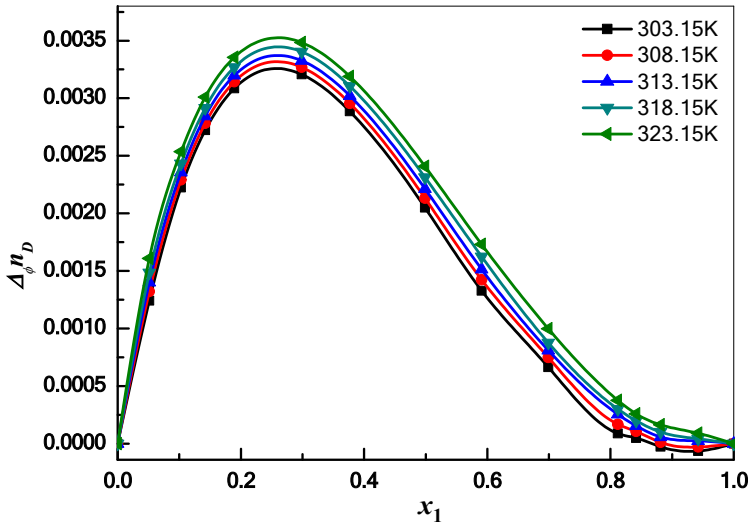

Fig. 8 Plots of deviation in refractive index ($\Delta_\emptyset n_D$) against mole fraction of [Bmim][PF_6] in the mixture with NMP at different temperatures.

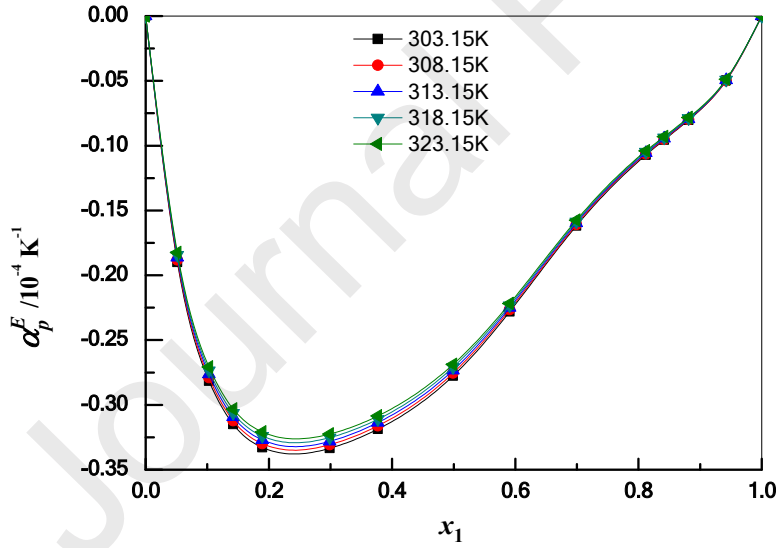

Fig. 9 Plots of Excess isobaric thermal expansion coefficient (α_P^E) against mole fraction of [Bmim][PF_6] in the mixture with NMP at different temperatures.

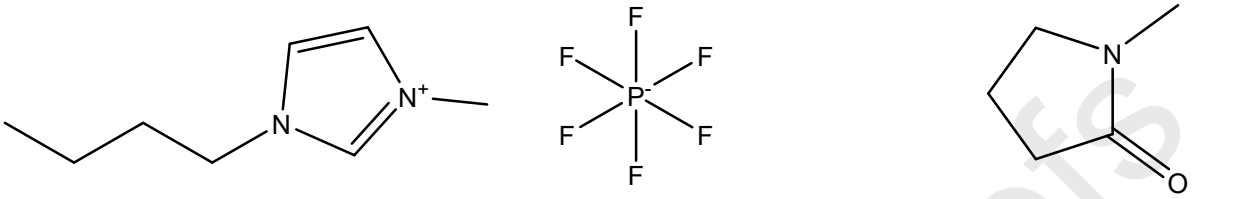

1-butyl-3-methylimidazolium hexafluorophosphate

1-methyl-2-pyrrolidone

Fig.10 Chemical Structures of [Bmim][PF_6] and NMP.

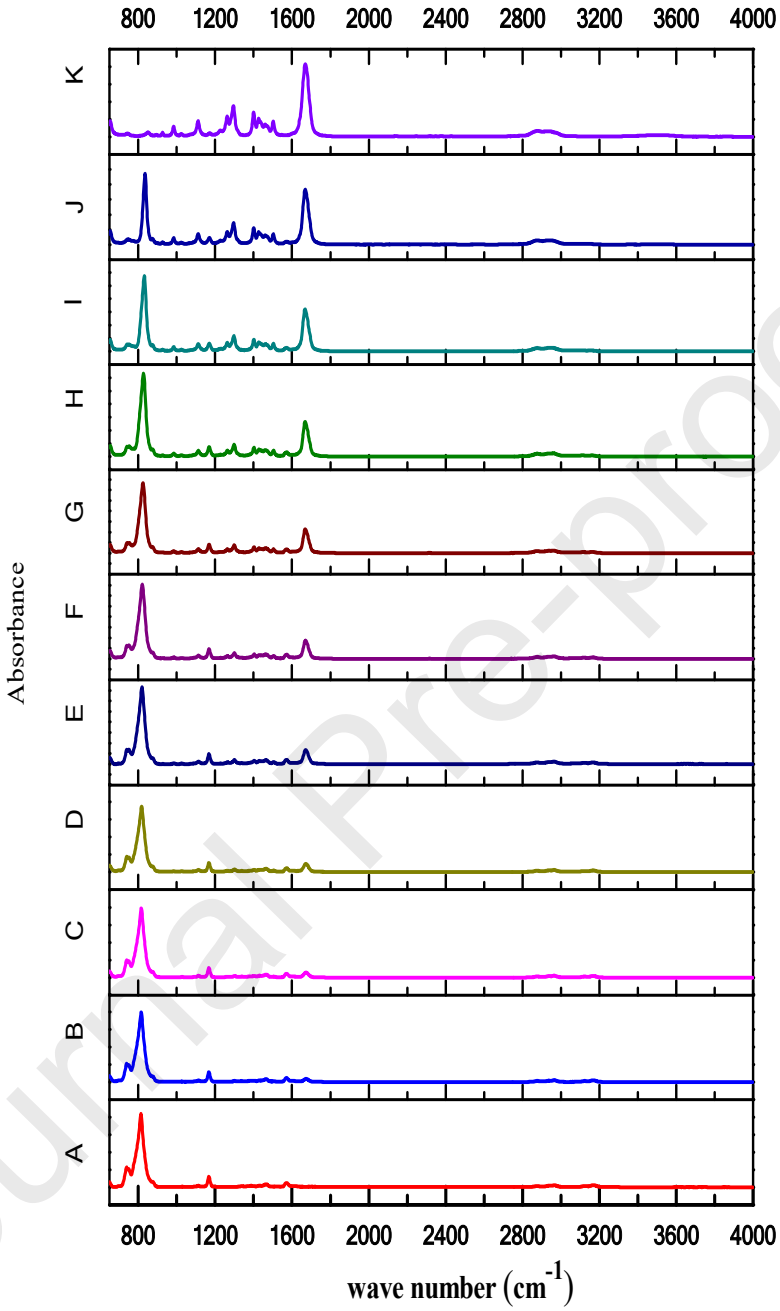

Fig.11 Infrared spectra (650 cm^{-1}-4000 cm^{-1}) of (A) Pure IL [Bmim][PF_6],(B) 0.8812; (C) 0.8120; (D) 0.6991; (E) 0.5910; (F0.4990; (G) 0.3771; (H) 0.2988; (I) 0.1894; (J) 0.1028 and (K) Pure NMP. (B), (C), (D), (E), (F), (G), (H), (I), (J) represents mole fraction of [Bmim][PF_6] in the mixture with NMP.

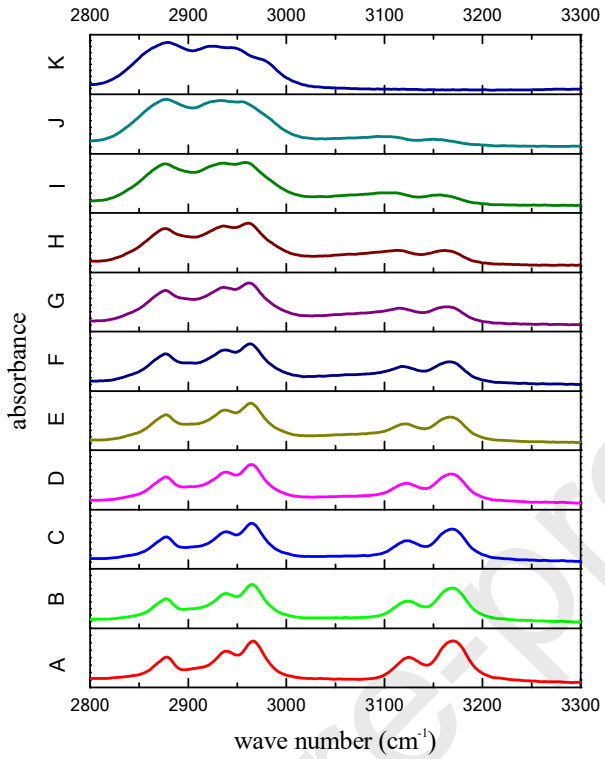

Fig.12 Infrared spectra (2800 cm^{-1}-3300 cm^{-1}) of (A) Pure IL [Bmim][PF_6];(B) 0.8812; (C) 0.8120; (D) 0.6991; (E) 0.5910; (F0.4990; (G) 0.3771; (H) 0.2988; (I) 0.1894; (J) 0.1028 and (K) Pure NMP. (B), (C), (D), (E), (F), (G), (H), (I), (J) represents mole fraction of [Bmim][PF_6] in the mixture with NMP.

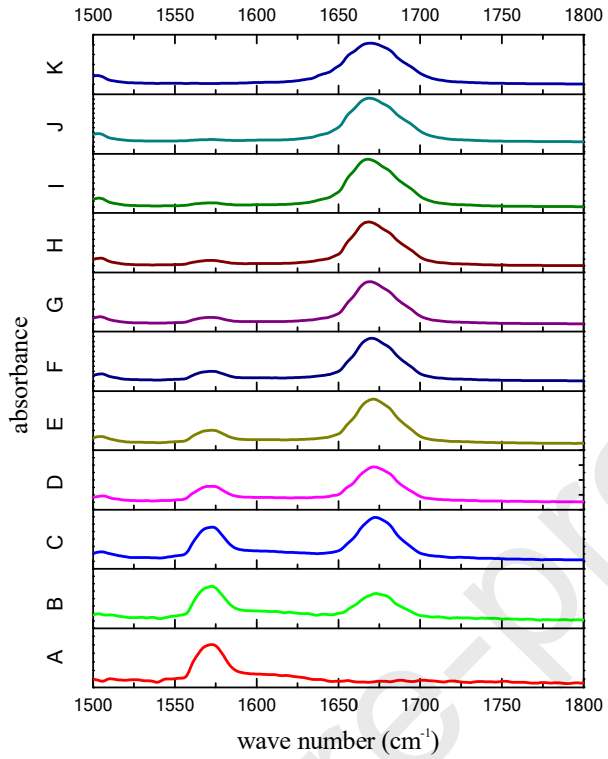

Fig.13 Infrared spectra (1500 cm^{-1}-1800 cm^{-1}) of (A) Pure IL [Bmim][PF_6];(B) 0.8812; (C) 0.8120; (D) 0.6991; (E) 0.5910; (F0.4990; (G) 0.3771; (H) 0.2988; (I) 0.1894; (J) 0.1028 and (K) Pure NMP. (B), (C), (D), (E), (F), (G), (H), (I), (J) represents mole fraction of [Bmim][PF_6] in the mixture with NMP.

Table 1 Comparison of experimental values of density, ρ, speed of sound, u, refractive index, n_D, and specific heat, C_p, of pure liquids with the corresponding literature values at different temperatures and at atmospheric pressure P = 101.3 kPa.

Liquid	Temp / (K)	ρ /(kg m^{-3})		u/(m s^{-1})		n_D		C_p/(J K^{-1} mol^{-1})
		Expt.	Lit.	Expt.	Lit.	Expt.	Lit.	Lit.
[Bmim][PF_6]	303.15	1364.6	1363.277 [25] 1363.08[26]	1431.7	1430.6 [29] 1431.9[2	1.4082 3	1.40746 [30] 1.40812[2	410.33 [31]

			1363.2[27] 1362.36[28]		6]		7] 1.4080[28]	
	308.15	1360.4	1359.191 [25] 1358.91[26] 1359.0[27]	1419.8	1419.0 [29] 1420.1[26]	1.40691	1.40585 [30] 1.40679[27]	413.14 [31]
	313.15	1356.2	1355.087 [25] 1354.74[26] 1354.9[27] 1353.99[28]	1408.2	1406.4 [29] 1408.5[26]	1.40556	1.40468 [30] 1.40546[27] 1.4055[28]	415.98 [31]
	318.15	1352.1	1350.980 [25] 1350.58[26] 1350.8[27]	1396.8	1395.0 [29] 1397.1[26]	1.40414	1.40352 [30] 1.40413[27]	418.91 [31]
	323.15	1348.0	1346.874 [25] 1346.41[26] 1346.8[27] 1345.70[28]	1385.6	1385.15 [29] 1385.9[26]	1.40276	1.40243 [30] 1.4030[28]	421.88 [31]
1-Methyl-2-pyrrolidinone	303.15	1022.6	1022.64 [32] 1023.95[33] 1023.925[34] 1023.70[35]	1524.3	1524.32 [32] 1526.5[33]	1.46638	1.46626 [32] 1.4664[33] 1.46520[34]	166 [36]
	308.15	1018.2	1018.18 [32] 1019.462[34]	1505.0	1504.96 [32]	1.46428	1.46412 [32] 1.46306[34]	167 [36]
	313.15	1013.7	1013.72 [32] 1015.03[33] 1015.000[34] 1014.78[35]	1485.7	1485.74 [32] 1487.8[33]	1.46219	1.46199 [32] 1.4621[33] 1.46095[34]	168 [36]
	318.15	1009.3	1009.25 [32] 1010.533[34]	1466.7	1466.67 [32]	1.46008	1.45983 [32] 1.45891[34]	169 [36]
	323.15	1004.8	1004.78 [32] 1006.10[33]	1447.8	1447.76 [32] 1450.2[3	1.45796	1.45571 [32] 1.4576[33]	170 [36]

	1006.061[34] 1005.85[35]	3]	1.45680[34]

Standard uncertainties u are: $u(\rho)$ = 1.0 kg ·m^{-3},$u(u)$ = 0.5 ms^{-1}, $u(n_D)$ = 0.0005,u (I) = 0.01 K and $u(P)$=0.5kPa

Table 2 Experimental density (ρ), speed of sound (u), refractive index (n_D), molar volume (V_m),Isentropic compressibility(κ_S),free length (L_f)and isobaric thermal expansion coefficient (α_p) with mole fraction (x_1) of [Bmim][PF_6] in the binary liquid mixture of {[Bmim][PF_6]+ 1-Methyl-2-pyrrolidinone} from T/K = 303.15 to 323.15 at pressure P = 101.3 kPa.

x_1	ρ / (kg m^{-3})	u / (m s^{-1})	n_D	V_m/ (10^{-6}m^3 mol^{-1})	κ_S / (10^{-10}Pa^{-1})	L_f /(10^{-11}m)	α_p /10^{-4} K^{-1}
303.15 K							
0.0000	1022.6	1524.3	1.46638	96.94	4.21	4.258	8.73
0.0513	1062.4	1522.2	1.46171	102.24	4.06	4.183	8.27

0.1028	1096.7	1516.1	1.45724	107.74	3.97	4.134	7.93
0.1422	1119.8	1510.0	1.45396	112.03	3.92	4.108	7.72
0.1894	1144.5	1502.2	1.45018	117.23	3.87	4.084	7.52
0.2988	1193.2	1485.8	1.44196	129.41	3.80	4.044	7.14
0.3771	1222.6	1474.9	1.43656	138.17	3.76	4.025	6.92
0.4990	1260.6	1460.7	1.42898	151.89	3.72	4.002	6.66
0.5910	1285.0	1451.8	1.42391	162.25	3.69	3.988	6.51
0.6991	1310.2	1444.3	1.41867	174.41	3.66	3.970	6.37
0.8120	1332.4	1437.9	1.41403	187.18	3.63	3.954	6.25
0.8415	1337.7	1436.6	1.41296	190.51	3.62	3.950	6.21
0.8812	1344.7	1434.9	1.41161	194.99	3.61	3.945	6.17
0.9423	1355.2	1432.9	1.40974	201.83	3.59	3.935	6.12
1.0000	1364.6	1431.7	1.40823	208.26	3.58	3.925	6.10
308.15 K							
0.0000	1018.2	1505.0	1.46428	97.36	4.34	4.361	8.77
0.0513	1058.0	1503.9	1.45966	102.67	4.18	4.281	8.31
0.1028	1092.3	1498.8	1.45526	108.17	4.08	4.228	7.97
0.1422	1115.4	1493.2	1.45203	112.46	4.02	4.199	7.76
0.1894	1140.2	1486.0	1.44830	117.67	3.97	4.174	7.55
0.2988	1189.0	1470.9	1.44020	129.88	3.89	4.129	7.17
0.3771	1218.3	1460.6	1.43488	138.65	3.85	4.108	6.95
0.4990	1256.4	1447.2	1.42741	152.40	3.80	4.083	6.69
0.5910	1280.8	1438.8	1.42241	162.78	3.77	4.067	6.54
0.6991	1306.0	1431.7	1.41723	174.97	3.74	4.048	6.40
0.8120	1328.2	1425.8	1.41265	187.77	3.70	4.030	6.27
0.8415	1333.5	1424.5	1.41159	191.11	3.70	4.026	6.23
0.8812	1340.5	1423.0	1.41025	195.60	3.68	4.020	6.19
0.9423	1350.9	1421.1	1.40840	202.47	3.67	4.010	6.14
1.0000	1360.4	1419.8	1.40691	208.90	3.65	3.999	6.11
313.15 K							
0.0000	1013.7	1485.7	1.46219	97.79	4.47	4.467	8.81
0.0513	1053.6	1485.8	1.45764	103.10	4.30	4.381	8.34
0.1028	1088.0	1481.6	1.45329	108.60	4.19	4.324	8.01
0.1422	1111.1	1476.6	1.45011	112.90	4.13	4.293	7.80
0.1894	1135.9	1470.0	1.44643	118.12	4.07	4.265	7.59
0.2988	1184.7	1456.0	1.43845	130.35	3.98	4.216	7.20
0.3771	1214.1	1446.4	1.43320	139.14	3.94	4.193	6.98
0.4990	1252.2	1433.9	1.42582	152.91	3.88	4.165	6.71
0.5910	1276.6	1425.9	1.42088	163.32	3.85	4.148	6.56

0.6991	1301.8	1419.4	1.41577	175.54	3.81	4.126	6.42
0.8120	1324.1	1413.8	1.41123	188.36	3.78	4.107	6.29
0.8415	1329.4	1412.6	1.41018	191.71	3.77	4.103	6.26
0.8812	1336.3	1411.2	1.40886	196.21	3.76	4.096	6.21
0.9423	1346.8	1409.4	1.40703	203.09	3.74	4.085	6.16
1.0000	1356.2	1408.2	1.40556	209.54	3.72	4.074	6.13
318.15 K							
0.0000	1009.3	1466.7	1.46008	98.22	4.61	4.575	8.85
0.0513	1049.2	1467.8	1.45559	103.53	4.42	4.484	8.38
0.1028	1083.6	1464.5	1.45130	109.04	4.30	4.422	8.04
0.1422	1106.8	1460.1	1.44816	113.34	4.24	4.389	7.84
0.1894	1131.6	1454.1	1.44453	118.57	4.18	4.358	7.63
0.2988	1180.4	1441.3	1.43666	130.82	4.08	4.305	7.24
0.3771	1209.8	1432.4	1.43148	139.62	4.03	4.279	7.02
0.4990	1248.0	1420.7	1.42419	153.42	3.97	4.248	6.74
0.5910	1272.4	1413.2	1.41931	163.86	3.94	4.229	6.59
0.6991	1297.6	1407.1	1.41426	176.10	3.89	4.206	6.45
0.8120	1319.9	1402.0	1.40977	188.95	3.85	4.185	6.31
0.8415	1325.2	1400.9	1.40873	192.31	3.85	4.180	6.28
0.8812	1332.2	1399.6	1.40742	196.82	3.83	4.173	6.23
0.9423	1342.6	1398.0	1.40561	203.71	3.81	4.162	6.18
1.0000	1352.1	1396.8	1.40414	210.19	3.79	4.150	6.15
323.15 K							
0.0000	1004.8	1447.8	1.45796	98.66	4.75	4.686	8.89
0.0513	1044.8	1450.1	1.45353	103.97	4.55	4.588	8.42
0.1028	1079.3	1447.6	1.44930	109.48	4.42	4.522	8.08
0.1422	1102.5	1443.8	1.44620	113.79	4.35	4.486	7.87
0.1894	1127.3	1438.4	1.44261	119.02	4.29	4.453	7.66
0.2988	1176.1	1426.7	1.43483	131.29	4.18	4.395	7.27
0.3771	1205.6	1418.5	1.42972	140.11	4.12	4.366	7.05
0.4990	1243.9	1407.6	1.42253	153.93	4.06	4.332	6.77
0.5910	1268.2	1400.6	1.41772	164.40	4.02	4.312	6.61
0.6991	1293.4	1395.1	1.41274	176.67	3.97	4.286	6.47
0.8120	1315.8	1390.3	1.40831	189.54	3.93	4.264	6.33
0.8415	1321.1	1389.3	1.40729	192.91	3.92	4.259	6.30
0.8812	1328.1	1388.1	1.40600	197.43	3.91	4.251	6.25
0.9423	1338.5	1386.6	1.40421	204.34	3.89	4.239	6.20
1.0000	1348.0	1385.6	1.40276	210.83	3.86	4.227	6.17

	T/K	A_0	A_1	A_2	A_3	A_4	σ
	303.15	-2.4072	2.2409	-1.5853	2.9412	-0.5551	0.0132

Standard uncertainties u are: u (x_1) = 0.0005, u (ρ) = 1 kg·m^{-3},u (u) = 0.5 m s^{-1}, u (n_D) = 0.0005, u (T) = 0.01 K and u(P)= 0.5 kPa Combined uncertainties (Confidence level, 95%).: U_c (V_m) = ± 0.1 x 10^{-6} m^3 mol^{-1},U_c(κ_S) = ± 0.05 x10^{-10} Pa^{-1},U_c (L_f) = ± 0.05 x10^{-11} m, U_c(α_p) = ± 0.06 x10^{-4} K^{-1}. All the experiments were carried out at atmospheric pressure.

Table 3 Redlich-Kister coefficients of deviation/excess properties and corresponding standard deviations (σ) for the system at different temperatures

V_m^E /(10^{-6}m^{3}mol^{-1})	308.15	-2.4870	2.2507	-1.7358	3.1317	-0.2971	0.0128
	313.15	-2.5847	2.3292	-1.5966	3.0718	-0.6820	0.0132
	318.15	-2.6796	2.3766	-1.6045	3.1027	-0.7898	0.0133
	323.15	-2.7732	2.4264	-1.6244	3.1294	-0.8987	0.0135
κ_s^E /(10^{-10} Pa^{-1})	303.15	-0.4256	0.5814	-0.4516	0.6023	-0.4404	0.0023
	308.15	-0.4604	0.6102	-0.4731	0.6364	-0.4763	0.0025
	313.15	-0.4963	0.6419	-0.4948	0.6713	-0.5205	0.0027
	318.15	-0.5338	0.6758	-0.5187	0.7098	-0.5617	0.0028
	323.15	-0.5733	0.7108	-0.5426	0.7545	-0.6087	0.0031
u^E/ (ms^{-1})	303.15	69.39	-94.57	71.93	-84.42	61.72	0.35
	308.15	73.50	-96.18	72.33	-84.78	64.61	0.36
	313.15	77.42	-97.80	73.48	-85.73	66.46	0.38
	318.15	81.30	-99.62	74.30	-86.60	68.17	0.38
	323.15	85.21	-101.29	74.89	-88.13	70.31	0.39
L_f^E/(10^{-11} m)	303.15	-0.2246	0.3037	-0.2329	0.2979	-0.2098	0.0012
	308.15	-0.2439	0.3184	-0.2434	0.3126	-0.2254	0.0013
	313.15	-0.2439	0.3184	-0.2434	0.3126	-0.2254	0.0013
	318.15	-0.2844	0.3518	-0.2651	0.3436	-0.2628	0.0014
	323.15	-0.3061	0.3694	-0.2764	0.3627	-0.2829	0.0015
α_P^E (10^{-4} K^{-1})	303.15	-1.1080	0.8704	-0.1379	0.8614	-1.8421	0.0024
	308.15	-1.1001	0.8638	-0.1304	0.8454	-1.8364	0.0022
	313.15	-1.0915	0.8551	-0.1325	0.8371	-1.8095	0.0022
	318.15	-1.0830	0.8472	-0.1295	0.8260	-1.7919	0.0022
	323.15	-1.0745	0.8393	-0.1256	0.8142	-1.7745	0.0021
$\Delta_\phi n_D$	303.15	0.00812	-0.01538	0.00680	-0.00016	-0.00190	0.00002
	308.15	0.00812	-0.01538	0.00680	-0.00016	-0.00190	0.00002
	313.15	0.00883	-0.01487	0.00575	-0.00143	0.00144	0.00001
	318.15	0.00925	-0.01472	0.00492	-0.00215	0.00331	0.00001
	323.15	0.00968	-0.01430	0.00443	-0.00344	0.00536	0.00002

Table 4 Partial molar volumes of component-1 ($\overline{V}_{m,1}$) ([Bmim][PF_6])and component-2($\overline{V}_{m,2}$) (1-Methyl-2-pyrrolidinone) with mole fraction (x_1) of [Bmim][PF_6] in the binary liquid mixture from T/K =303.15 to 323.15 at pressure P = 101.3 kPa.

	303.15 K		308.15 K		313.15 K		318.15 K		323.15 K	
x_1	$\overline{V}_{m,1}$	$\overline{V}_{m,2}$	$\overline{V}_{m,1}$	$\overline{V}_{m,2}$	$\overline{V}_{m,1}$	$\overline{V}_{m,2}$	$\overline{V}_{m,1}$	$\overline{V}_{m,2}$	$\overline{V}_{m,1}$	$\overline{V}_{m,2}$
	/ 10^{-6} m^3 mol^{-1}		/ 10^{-6} m^3 mol^{-1}		/ 10^{-6} m^3 mol^{-1}		/ 10^{-6} m^3 mol^{-1}		/ 10^{-6} m^3 mol^{-1}	
0.0000	198.53	96.94	199.00	97.36	199.28	97.79	199.63	98.22	199.98	98.66
0.0513	199.62	96.98	200.10	97.41	200.43	97.84	200.82	98.27	201.21	98.71
0.1028	200.83	97.08	201.31	97.50	201.71	97.94	202.14	98.38	202.56	98.82
0.1422	201.75	97.15	202.24	97.58	202.69	98.02	203.15	98.46	203.61	98.90
0.1894	202.82	97.22	203.31	97.65	203.82	98.09	204.31	98.53	204.80	98.97
0.2988	204.91	97.24	205.45	97.67	206.02	98.09	206.58	98.53	207.13	98.97
0.3771	206.01	97.13	206.58	97.56	207.18	97.98	207.76	98.41	208.34	98.84
0.4990	207.09	96.90	207.71	97.30	208.31	97.73	208.92	98.15	209.52	98.57
0.5910	207.54	96.78	208.17	97.17	208.77	97.60	209.39	98.02	210.01	98.44
0.6991	207.83	96.81	208.46	97.21	209.09	97.63	209.72	98.03	210.36	98.44
0.8120	208.04	97.06	208.67	97.53	209.32	97.87	209.96	98.24	210.60	98.61
0.8415	208.09	97.15	208.72	97.65	209.37	97.95	210.01	98.31	210.66	98.67
0.8812	208.15	97.28	208.78	97.81	209.43	98.06	210.08	98.41	210.72	98.75
0.9423	208.23	97.45	208.87	98.06	209.51	98.23	210.16	98.55	210.80	98.86
1.0000	208.26	97.57	208.90	98.22	209.54	98.33	210.19	98.63	210.83	98.92

Combined uncertainties (Confidence level, 95%):$U(\overline{V}_{m,1}) = \pm 0.1 \times 10^{-6}$ m^3 mol^{-1}, $U(\overline{V}_{m,2}) = \pm 0.1 \times 10^{-6}$ m^3 mol^{-1}

Table 5 Partial molar volumes at infinite dilution ($\overline{V}^{\infty}_{m,1}$, $\overline{V}^{\infty}_{m,2}$) and excess partial molar volumes at infinite dilution ($\overline{V}^{E,\infty}_{m,1}$, $\overline{V}^{E,\infty}_{m,2}$) of [Bmim][PF_6] and 1-Methyl-2-pyrrolidinone T = (303.15, 308.15, 313.15, 318.15 and 323.15) K.

T/ K	$\overline{V}^{\infty}_{m,1}$	$\overline{V}^{E,\infty}_{m,1}$	$\overline{V}^{\infty}_{m,2}$	$\overline{V}^{E,\infty}_{m,2}$
	/(10^{-6} m^3mol^{-1})		/(10^{-6} m^3mol^{-1})	
303.15	198.53	-9.73	97.57	0.63
308.15	199.00	-9.90	98.22	0.86
313.15	199.28	-10.26	98.33	0.54
318.15	199.63	-10.55	98.63	0.41
323.15	199.98	-10.85	98.92	0.26

Standard uncertainties u are: u (x_1) = 0.0002, u (T) = 0.01 K and u(P)=0.5 kPa

Combined uncertainties (Confidence level, 95%):$U(\overline{V}^{E,\infty}_{m,1})$ = ± 0.1 x 10^{-6} m^3 mol^{-1}, $U(\overline{V}^{E,\infty}_{m,2})$ = ± 0.1 x 10^{-6} m^3 mol^{-1}

Table 6 Infrared absorbance wave numbers (cm^{-1}) between 2800 to 3200 of [Bmim][PF_6] in NMP at room temperature and atmospheric pressure P = 101.3 kPa.

Infrared absorbance wave numbers /(cm^{-1})

Mole fraction of [Bmim][PF_6]	Mole fraction of NMP	C_2-H stretching	$C_{4,5}$-H stretching	C=O Stretch
1.0000	0.0000	3124.3	3169.2	-
0.8812	0.1188	3123.3	3168.3	1672.7
0.8120	0.1880	3122.2	3168.2	1672.7
0.6991	0.3009	3121.2	3168.2	1671.7
0.5910	0.4090	3120.2	3167.2	1671.7
0.4990	0.5024	3119.2	3166.2	1670.7
0.3771	0.6229	3116.1	3164.1	1669.7
0.2988	0.7012	3113.3	3161.8	1668.5
0.1894	0.8106	-	-	1667.8
0.1028	0.8972	-	-	1668.9
0.0000	1.0000	-	-	1669.3

Table 7 Characteristic and reduced parameters for the pure components used in PFP theory at various temperatures.

T/(K)	$\tilde{V}$	V_1^* /(10^{-6}m^3.mol^{-1})	P_1^* /(10^6 J.mol^{-1})
[Bmim][PF$_6$]			
303.15	1.1642	178.88	604.01
308.15	1.1671	178.99	606.90
313.15	1.1699	179.11	609.77
318.15	1.1728	179.22	612.62
323.15	1.1757	179.33	615.42
NMP			
303.15	1.2242	79.18	713.79
308.15	1.2282	79.27	712.94
313.15	1.2322	79.36	711.85
318.15	1.2361	79.46	710.53
323.15	1.2401	79.56	708.99

Table 8 PFP interaction parameter, χ_{12}, and calculated values of the three contributions from the PFP theory at equimolar composition for ([Bmim][PF$_6$] + NMP) system at *T*=(303.15-323.15) K

T /K	χ_{12} /(10^6 J m^{-3})	$V_m^E(int)$ /(10^{-6} m^3 mol^{-1})	$V_m^E(fv)$ /(10^{-6} m^3 mol^{-1})	$V_m^E(ip)$ /(10^{-6} m^3 mol^{-1})
303.15	-56.5832	-0.7253	-0.1598	0.2833
308.15	-56.1203	-0.7346	-0.1654	0.2782
313.15	-55.9229	-0.7474	-0.1711	0.2722
318.15	-55.5898	-0.7584	-0.1768	0.2654
323.15	-55.1682	-0.7684	-0.1827	0.2578

Journal of Genetic Engineering and Biotechnology

RESEARCH Open Access

Antioxidant potential and optimization of production of extracellular polysaccharide by *Acinetobacter indicus* M6

Ch. Ravi Teja[1], Abraham P. Karlapudi[2], Neeraja Vallur[3], K. Mamatha[1], D. John Babu[2], T. C. Venkateswarulu[2] and Vidya Prabhakar Kodali[1*]

Abstract

Background: Extracellular polysaccharides (ECPs) produced by biofilm-producing marine bacterium have great applications in biotechnology, pharmaceutical, food engineering, bioremediation, and bio-hydrometallurgy industries. The ECP-producing strain was identified as *Acinetobacter indicus* M6 species by 16S rDNA analysis. The polymer produced by the isolate was quantified and purified and chemically analyzed, and antioxidant activities have been studied. The face-centered central composite design (FCCCD) was used to design the model.

Results: The results have clearly shown that the ECP was found to be endowed with significant antioxidative activities. The ECP showed 59% of hydroxyl radical scavenging activity at a concentration of 500 μg/mL, superoxide radical scavenging activity (72.4%) at a concentration of 300 μg/mL, and DPPH$^{\bullet}$ radical scavenging activity (72.2%) at a concentration of 500 μg/mL, respectively. Further, HPLC and GC-MS results showed that the isolated ECP was a heteropolymer composed of glucose as a major monomer, and mannose and glucosamine were minor monomers. Furthermore, the production of ECP by *Acinetobacter indicus* M6 was increased through optimization of nutritional variables, namely, glucose, yeast extract, and $MgSO_4$ by "Response Surface Methodology". Moreover the production of ECP reached to 2.21 g/L after the optimization of nutritional variables. The designed model is statistically significant and is indicated by the R^2 value of 0.99. The optimized medium improved the production of ECP and is two folds higher in comparison with the basal medium.

Conclusions: *Acinetobacter indicus* M6 bacterium produces a novel and unique extracellular heteropolysaccharide with highly efficient antioxidant activity. GC-MS analyses elucidated the presence of quite uncommon (1→4)-linked glucose, (1→4)-linked mannose, and (→4)-GlcN-(1→) glycosidic linkages in the backbone. The optimized medium improved the production of ECP and is two folds higher in comparison with the basal medium. The newly optimized medium could be used as a promising alternative for the overproduction of ECP.

Keywords: Extracellular polysaccharide, Antioxidant activity, Response surface methodology, Monosaccharide composition

* Correspondence: kodalividyaprabhakar@gmail.com
[1]Department of Biotechnology, Vikrama Simhapuri University, Kakutur, Nellore A.P-524320, India
Full list of author information is available at the end of the article

Background

Acinetobacter species produce medicinally and commercially important diverse group of molecules [1]. Extracellular polysaccharides (ECPs) are one of such important molecules. ECPs are long-chain, high molecular-mass polymers which have been reported to show antiulcer, immunomodulatory, antiviral, antioxidant, and various other biological activities [2, 3]. These ECPs are the alternative class of biothickeners and also proved to have good emulsifying property apart from the texture-promoting property in various foods [4]. In some countries of the European Union (EU) and the United States of America (USA), where addition of synthetic texture-promoting agents in food and dairy products is prohibited, ECPs can successfully be used as food additives to enhance texture [5]. The ECPs are economically important because they can impart functional effects to foods. Depending on the monosaccharide composition, ECPs can be classified into homo (HoPSs) and heteropolysaccharides (HePSs). HoPSs consist of only one type of monosaccharide.

Recently, studies have been focused on antioxidant polysaccharides that can find potential applications in food industries [6]. Free radicals such as superoxide radical anion ($O_2^{\cdot-}$), hydroxyl radical (OH·), and other reactive oxygen species (ROS) are considered to be highly potent oxidants that can react with all biomacromolecules in living cells, and they may associate with carcinogenesis and mutagenesis [7]. ECPs were reported to have free radical scavenging activities [8]. Bacterial polysaccharides isolated from *Pantoea agglomerans* and *Microbacterium terregens* [9] showed pronounced antioxidant activities.

Considering the antioxidant activity and other therapeutic importance of the ECP, it is important to characterize the ECP structurally. Therefore, the monomeric composition of the ECP was identified by HPLC, and glycosidic linkages of the ECP were determined by GC-MS. HPLC is frequently used for both the qualitative and quantitative analysis of liberated monosaccharides after acid hydrolysis. HPLC with an ultraviolet (UV) detector or refractive index (RI) is an alternative method for quantitative determination of saccharides. Due to low sensitivity and inapplicability to gradient elution, HPLC with RI detector is less commonly used [10]. The alternative approach is HPLC with UV detector, which is highly sensitive and widely used for analysis and quantification of monomers. GC attached to a mass spectrometer is an efficient and widely applicable method for linkage analysis of methylated polysaccharides. Methylation analysis is an essential step for studying the linkage pattern of sugar residues. Depending on the mass spectra obtained, the glycosidic linkages are analyzed [11, 12].

The production of polymers is highly influenced by different factors such as nutritional variables and physical variables of the process, namely, temperature, pH, RPM, dissolved oxygen concentration, and RPM [9]. Studies also reported that the growth and development of film formation depend on surface area, smoothness, flow velocity, and nutrients [13]. Very few reports are available on design fermentation medium through response surface methodology (RSM) optimization studies for production of ECPs [13]. Therefore, the present study aimed to design the low-cost fermentation medium for enhanced production of the ECP using RSM.

Considering the tremendous reported therapeutic and commercial potentials, the ECP molecule may be developed as a potential drug molecule in the near future. Establishing the structure-function relationship of the ECP molecule by elucidating its complete molecular structure on further chemical derivatizations and enzymatic digestions (with glucosidases) will enable to identify the right fragments of the large ECP molecule, responsible for important bioactive properties of therapeutic and commercial interests. This would also help to use the small fragments for specific therapeutic purposes, instead of using the whole molecule.

Methods

Extraction, purification, and quantification of extracellular polysaccharide

ECP-producing organism was isolated and identified as mentioned previously [14]. Ten milliliters of overnight culture was centrifuged, and 30 mL alcohol (95%) was added to the supernatant. The mixture was shaken thoroughly and kept at 4 °C for overnight. The precipitated polymer was separated by centrifugation and dried to get crude ECP. The dried and crude powder (10 mg) was dissolved in 1 mL 0.2 M NaCl buffer to a concentration of 10 g/L and was filtered through a 0.22-μm membrane filter, loaded onto a Sephadex G-100 column (Sigma Aldrich, St Louis, USA-50 × 1.5 cm). The column was eluted with the same buffer at a flow rate of 0.5 mL/min, and 0.5 mL of fractions was collected. Total carbohydrate content of the fractions was determined by phenol-sulfuric acid method, and the carbohydrate content was measured by phenol sulfuric acid method [15].

Antioxidant activity of the ECP

The antioxidant potential of ECP was studied by superoxide radical scavenging assay by phenazine methosulfate (PMS)-nicotinamide adenine dinucleotide (NADH)-Nitroblue tetrazolium chloride (NBT) system, 1,1-diphenyl-2-picrylhydrazyl (DPPH) radical scavenging activity [16]. Vitamin C was used as a positive control.

Hydroxyl radical scavenging activity of the ECP

The hydroxyl radical scavenging activity of ECP was measured according to Liu et al. and Ren et al. [17, 18]. The hydroxyl radicals were generated in the L-ascorbic acid-$CuSO_4$ system by reduction of Cu^{2+} and were assayed by the oxidation of cytochrome C. In this experiment, hydroxyl radicals were generated in 3 mL of 0.15 mM sodium phosphate buffer (pH 7.4), which included 100 μM L-ascorbic acid, 100 μM $CuSO_4$, 12 μM cytochrome C, and the samples to be tested at different concentrations. The mixture was incubated at 25 °C for 90 min. The color change of cytochrome C was measured at 550 nm. Thiourea was used as control, and glucose was used as negative control.

The inhibition rate of hydroxyl radical generation by thiourea was taken as 100%.

The inhibition rate was calculated using the following equation:

$$\text{Inhibition rate } (\%) = \left[\frac{T - T_2}{T - T_1}\right] \text{x}100$$

where T is the transmittance of hydroxyl radical ($OH^{\cdot}$) generation system and T_1 and T_2 are the transmittance of control and test sample systems respectively.

Superoxide ($O_2^{\cdot}$) radical scavenging activity of the ECP

Measurement of superoxide radical scavenging activity was done based on the method described by Ren et al. [18] and Nishimiki et al. [19]. To 1 mL of NBT solution (156 μM NBT in 100 mM phosphate buffer, pH 7.4), 1 mL NADH solution (468 μM in 100 mM phosphate buffer, pH 7.4) and 0.1 ml of ECP in water were added and mixed well. The reaction was started by adding 100 μL of PMS solution (60 μM PMS in 100 mM phosphate buffer, pH 7.4) to the mixture. The reaction mixture was incubated at 25 °C for 5 min, and the absorbance was measured at 560 nm against blank samples using a spectrophotometer, and vitamin C was used as positive control. Decreased absorbance of the reaction mixture indicated increased superoxide anion-scavenging activity.

The scavenging activity of superoxide radical (%) was calculated from the following equation:

$$\text{Superoxide radical scavenging activity } (\%) = \left[1 - \frac{A_{Sample}}{A_{Blank}}\right] \text{x}100$$

where A_{Blank} is the absorbance of the control reaction (containing all reagents except the test compound) and A_{Sample} is the absorbance of the test compound.

DPPH radical scavenging activity

The free radical scavenging activity of ECP was measured by DPPH free radical scavenging assay. To 1 mL of 0.1 mM solution of DPPH in ethanol, 3 ml of ECP in water was added in different concentrations. After 30 min, absorbance was measured at 517 nm against blank. Radical scavenging activity was expressed as percentage inhibition of DPPH and estimated by the following equation [20]:

$$\text{DPPH free radical scavenging activity } (\%) = \left[1 - \frac{A_{Sample}}{A_{Blank}}\right] \text{x}100$$

where A_{Blank} is the absorbance of the control reaction (containing all reagents except the test compound) and A_{Sample} is the absorbance of the test compound. Vitamin C was used as the positive control. All determinations were performed in triplicate. Decrease in the absorbance indicated the antioxidant activity.

Compositional analysis of ECP

HPLC analysis is a commonly used method to determine the monosaccharide composition of polysaccharides. The polysaccharides are hydrolyzed to get individual monomers and then labeled with anthranilic acid to increase the florescence for easy and accurate identification [21]. The sugar composition of the ECP was studied by high-performance liquid chromatography (HPLC) [7]. For specific determination of monosaccharides with high sensitivity, ECP was acid hydrolyzed and then derivatized in a simple step with excess anthranilic acid (2-aminobenzoic acid) in the presence of sodium cyanoborohydride to give highly fluorescent-stable derivatives. The monosaccharide derivatives were completely separated from the excess reagent and from each other by HPLC on a C_{18} reversed-phase column using a butylamine-phosphoric acid-tetrahydrofuran mobile phase [2].

Acid hydrolysis of ECP

ECP isolated from 36 h culture was dissolved in deionized water and dialyzed against deionized water using 12 kDa membrane at 4 °C for 24 h and then lyophilized. Ten milligrams of lyophilized ECP was hydrolyzed with 2 M trifluoroacetic acid (TFA) for 6 h at 100 °C. TFA was removed using rotary vacuum evaporator [22].

Derivatization of monosaccharides with anthranilic acid

The hydrolysates were derivatized by anthranilic acid reagent [21, 22]. Briefly, anthranilic acid reagent was prepared by dissolving anthranilic acid (30 mg) and sodium cyanoborohydride in 1 mL of acetate-boric acid-methanol solution. The ECP hydrolysates were dissolved

Table 1 Carbohydrate and protein contents of crude and pure ECP

S.No	Fraction	Total carbohydrate (%)	Protein (%)
1.	Crude ECP[a]	92 ± 2	0.9 ± 0.3
2.	Purified ECP[b]	98 ± 1	0

[a]Alcohol-precipitated ECP
[b]Purified ECP by gel filtration chromatography

in 100 μL of 1% sodium acetate, and an aliquot of 50 μL was transferred to a new screw-cap freeze vial. Samples were mixed with 100 μL of anthranilic acid and capped tightly. Vials were heated at 80 °C for 60 min. After cooling, the samples were made up to 1 mL with solvent A (2% 1-butylamine, 0.5% phosphoric acid, and 1% tetrahydrofuran) for analysis in HPLC.

HPLC analysis of anthranilic acid-monosaccharide derivatives

Monosaccharide derivatives were analyzed in Agilent 1000 series HPLC (Agilent Technologies, Model No.1100). A reversed-phase C_{18} column (ZORBAX 300 SB-C18, 5 μm, 4.6 × 250 mm, USA) and 1-butylamine-phosphoric acid-tetrahydrofuran mobile phase system consisting of solvents A and B were used for this analysis. Solvent A comprises of 0.2% 1-butylamine, 0.5% phosphoric acid, and 1% tetrahydrofuran in water, and solvent B consisted of equal parts of solvent A and acetonitrile. The separations were carried out at 24 °C using a flow rate of 1 mL/min, and 20 mL of each sample was injected. An UV detector was used to detect the derivatized monosaccharides. The gradient program was used according to [21].

Determination of monosaccharide linkage analysis of the ECP molecule

GC-MS methylation analysis

A solution of ECP (5 mg) in dimethyl sulfoxide (0.5 mL) was permethylated by adding finely powdered NaOH (20 mg) and methyl iodide (0.1 mL). Then, the mixture was sonicated for 15 min. The permethylated ECP was extracted with $CHCl_3$ (1 mL) and H_2O (3 mL). $CHCl_3$ phase was separated and dried under N_2 and hydrolyzed in 2 M TFA at 100 °C for 1 h. The hydrolyzed ECP was reduced with 50 mM $NaBH_4$ at room temperature for 4 h and evaporated three times from a mixture of acetic acid/methanol (1:1) followed by acetylation with 50:50 acetic anhydride/pyridine at 100 °C for 90 min. Alditol acetates of the methylated sugars were analyzed by Shimadzu GCMS-QP2010. The temperature program and other column conditions were used according to Kim et al. [23, 24].

Optimization studies of ECP production

Production of ECP in shake flask

Luria Bertani medium was inoculated with *Acinetobacter indicus* M6, incubated for 48 h at 160 rpm at room temperature. Effect of salt, carbon, and nitrogen source on ECP production has been studied by varying

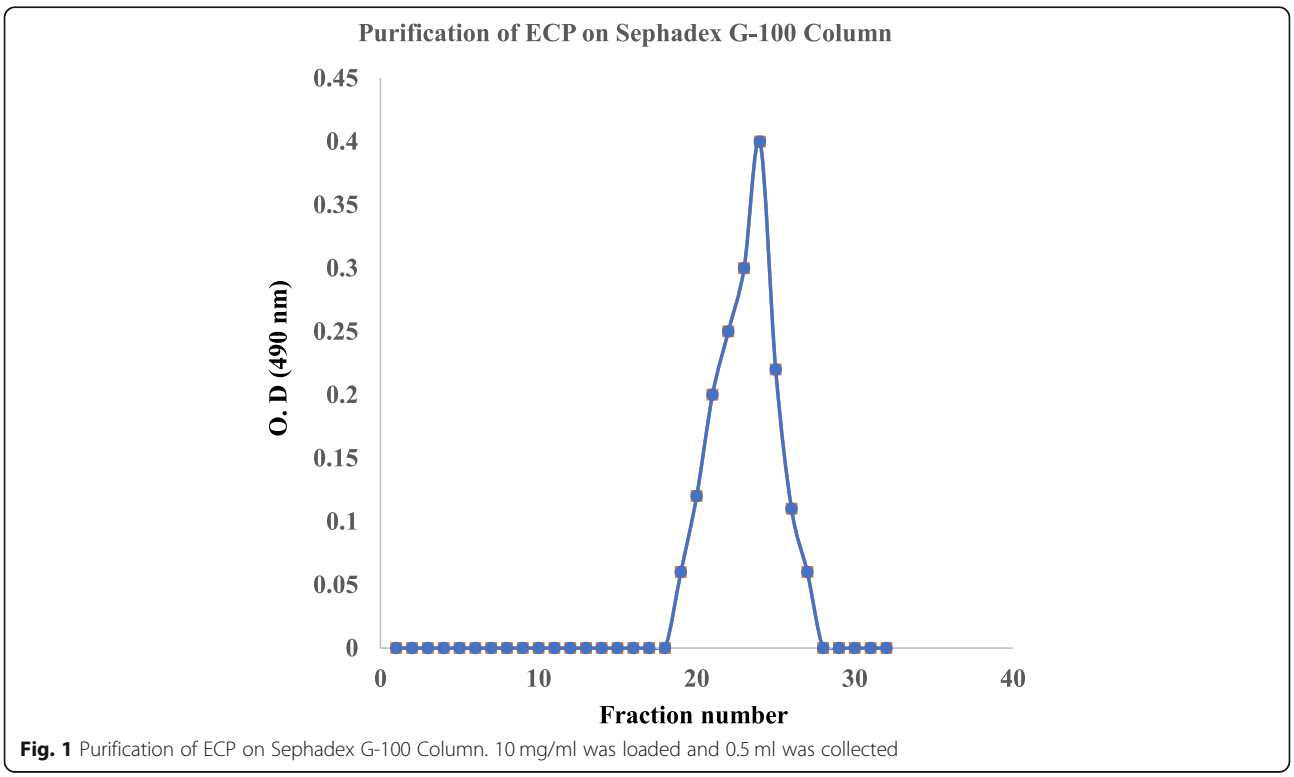

Fig. 1 Purification of ECP on Sephadex G-100 Column. 10 mg/ml was loaded and 0.5 ml was collected

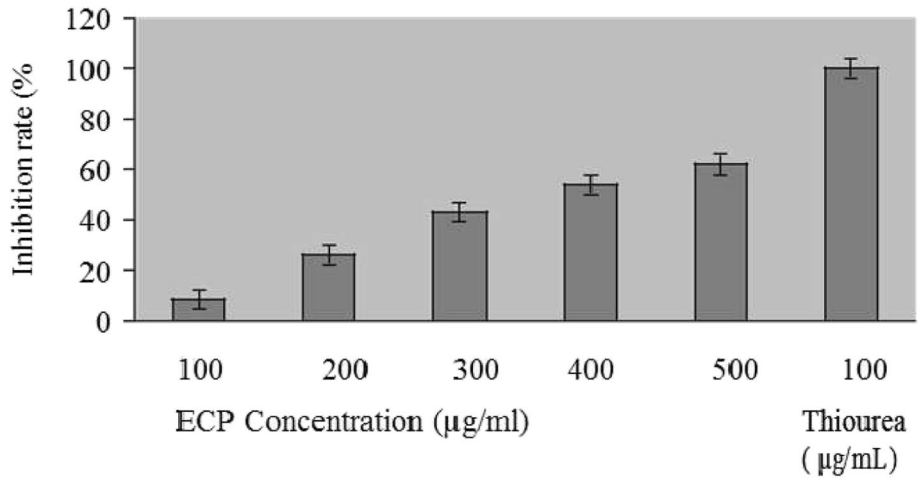

Fig. 2 OH radical scavenging activity of the ECP. Values are means of triplicates ± SD. The rate of inhibition of hydroxyl radical generation by thiourea (100 µg/ml) was taken 100%

concentrations of $MgSO_4$, glucose, and yeast extract. ECP production was expressed in terms of total carbohydrate concentration spectrophotometrically (490 nm) [18]. ECP extraction method was followed as mentioned above.

Optimization of nutritional variables by RSM

Response surface methodology (RSM) is a more convenient tool for designing experiments, plotting models, evaluating the effects of factors, and exploring optimum conditions of factors for significant responses. RSM is also used for optimization of prominent varieties of fermentation media and studying interactions among various bioprocess parameters with the minimum number of experiments [25, 26]. In the present experimentation, production of ECP in shake flask culture with *Acinetobacter indicus* M6 was found to be higher when compared to other bacterial species. Therefore, this strain has been considered as a potential bacterium for ECP production and hence it has been aimed to develop a suitable medium for enhanced production of ECP through optimization of nutrient component concentrations by response surface methodology (RSM). Fermentation medium variables such as glucose (A), yeast extract (B), and $MgSO_4$ (C) were optimized using the Design Expert software (Version 7.0.0, Stat-Ease Inc., Minneapolis, USA). The variables range from low (−1) to high (+ 1) used in the study are presented in Table 1.The impact of nutritional components on production and regression analysis of experimental data was carried out; further, the three-dimensional surface plots were drawn. The model was validated through the conduction of an experiment at predicted variables as suggested by the designed statistical model [27].

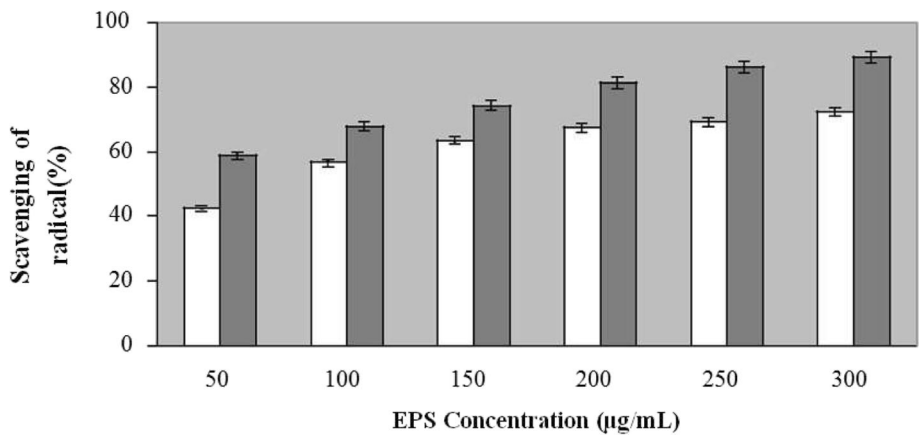

Fig. 3 Scavenging activity of ECP against superoxide radical generated in PMS/NADH system with vitamin C used as positive control. Values are means of triplicates ± SD. White bar indicates ECP, Black bar indicates Vitamin C

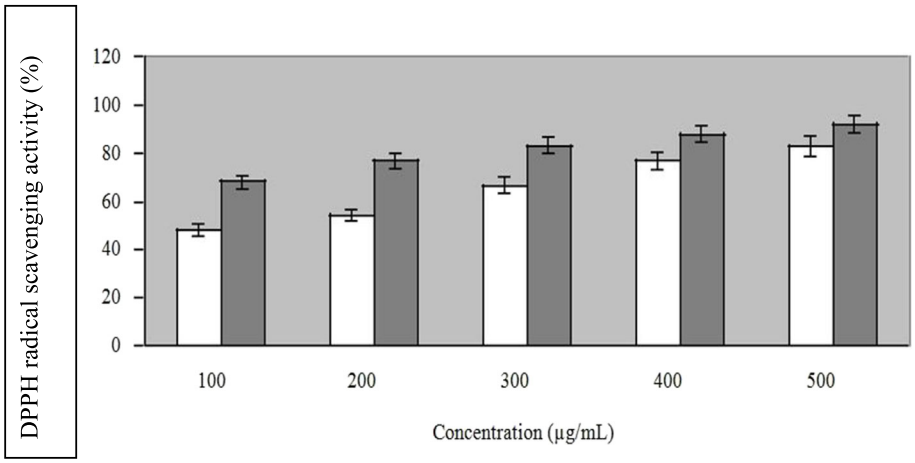

Fig. 4 Scavenging effects of ECP against 1, 1-diphenyl-2-picryl hydrazyl radical with vitamin C used as positive control. Values are means of triplicates ± SD. White bar indicates ECP, Black bar indicates Vitamin C

Results

Extraction, purification, and quantification of the ECP

The ECP produced by *Acinetobacter indicus* M6 was extracted as described previously and then purified. The gel filtration chromatogram (Fig. 1) showed that the elution of the ECP starts at the 18th fraction and ended at the 28th fraction. There was no protein content in polysaccharide fractions, indicating that the ECP had no associated proteins. The carbohydrate and protein contents of the crude and purified ECP are listed in Table 1. While the total sugar content (%, w/w) of the ECP was found to increase by 6% on purification, the % content of the contaminating proteins decreased to zero from a value of 0.9%. The total carbohydrate and protein concentrations were observed to be 380 µg/mL and 150 µg/mL respectively.

Antioxidant activity of the ECP

Hydroxyl radical scavenging assay of the ECP

The hydroxyl radical scavenging activity of ECP (ranging from 100 to 500 µg/mL) by ascorbic acid-Cu^{2+}-cytochrome C system is shown in Fig. 2. The

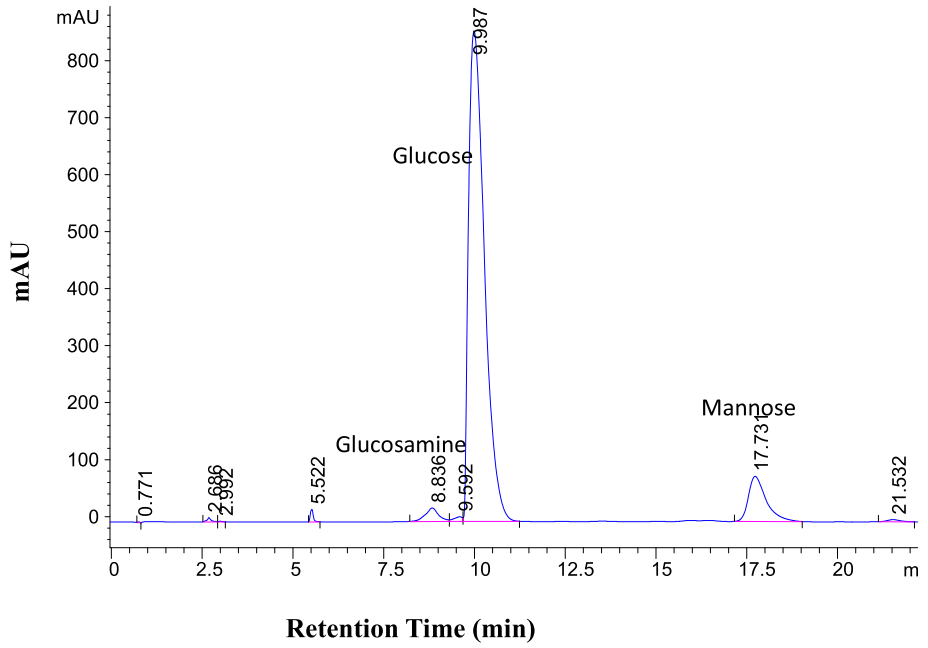

Fig. 5 HPLC analysis of hydrolyzed ECP. (Glucose is a major monomeric unit; mannose and glucosamine are the minor units)

Table 2 Results of the analysis of GC-MS

Fragments[a]	Mode of Linkage
1,2,4-tri-*O*-acetyl-3,6-di-*O*-methyl-D-mannitol	(→1, 2)-Man-(4→
1,4-di-*O*-acetyl-2,4,6-tri-*O*-methyl-D-glucitol	(→1)-Glc-(4→
1,4,6-di-*O*-acetyl-3-mono-*O*-methyl-2-amino-D-glucitol	(→1, 4)-GlcN-(6→

[a]Alditol acetates generated after methylation and reduction of monomers

scavenging activity of the ECP when correlated with its concentration showed that the activity increased till a concentration of 500 μg/mL and remained stable thereafter. ECP showed considerable hydroxyl radical scavenging activity of 59% at the concentration of 500 μg/mL. Here, in these experiments, the rate of inhibition of hydroxyl radical generation by thiourea (as a positive control) at a concentration of 100 μg/mL was taken as 100%, and glucose was used as negative control.

Superoxide ($O_2^{\cdot -}$) radical anion scavenging activity of the ECP

The decrease in absorbance at 560 nm with the addition of ECP indicates the consumption of superoxide radical in the reaction mixture (Fig. 3). The ECP showed noticeable superoxide radical scavenging activity with increasing concentration ranging from 50 to 300 μg/mL. The maximum scavenging activity of the ECP was estimated to be 72.4% where reference compound vitamin C showed 90% at concentration of 300 μg/mL.

DPPH free radical scavenging activity

This method is based on the reduction of methanolic DPPH$^{\cdot}$ solution in the presence of a hydrogen-donating antioxidant, due to the formation of the non-radical form DPPH-H by the reaction. DPPH$^{\cdot}$ is a stable free radical and accepts an electron or hydrogen radical to become a stable diamagnetic molecule [21, 22]. The antioxidant of ECP was determined by DPPH$^{\cdot}$ radical scavenging activity assay. Vitamin C was used as standard. Figure 4 illustrates the DPPH$^{\cdot}$ radical scavenging ability of ECP which increased with increasing concentration of ECP ranging from 100 to 500 μg/mL. Vitamin C and ECP showed 92% and 72.2% DPPH$^{\cdot}$ radical scavenging activity respectively at 500 μg/mL concentration. In terms of this antioxidant activity, the antioxidant activity of the ECP and the standard were comparable.

Compositional analysis of the ECP

The ECP after being hydrolyzed and derivatized with anthranilic acid was analyzed for its sugar composition by HPLC. The HPLC chromatogram (Fig. 5) showed that the ECP was a heteropolysaccharide, composed of glucose and glucosamine [22]. In terms of peak area, glucose (retention time 9.9 min) was the major monosaccharide, whereas glucosamine (retention time 8.8 min), and mannose (retention time 17.7) were the minor ones.

Determination of linkages between the monosaccharide units

The sugar linkages in alditol acetates of the methylated sugars of the ECP were elucidated by GC-MS analysis. Methylation analysis is a widely used method for determining polysaccharide structure [28, 29]. However, reductive cleavage depolymerization has several advantages compared to standard methylation analysis, and it is an effective method for structural characterization of complex carbohydrates, which have different sugar residues [27]. The alditol derivatives were 1,2,4-tri-*O*-acetyl-3,6-tri-*O*-methyl-D-mannitol; 1,4-di-*O*-acetyl-2,4,6-tri-*O*-methyl-D-glucitol; 1,4,6-di-*O*-acetyl-3-mono-*O*-methyl-2-amino-D-glucitol (Tables 2 and 3), revealed that (1→4)-linked glucose, (1→4) linked mannose, (→4)-GlcN-(1→). The linkages between the monosaccharides were predicted according to Bjorndal et al. [12, 27]. Based on the HPLC and GC-MS data, the probable structure of the ECP is given in Figs. 6 and 7.

Optimization studies of ECP production

Central composite design for medium optimization

Response surface methodology (RSM) is a collection of mathematical and statistical techniques widely used to determine the effects of several variables and to optimize different biotechnological processes [26]. The central composite design (CCD) was adopted for optimization of medium components such as glucose, yeast extract, and $MgSO_4$. The experimental results of CCD for enhancing the yield of ECP are shown in Table 4.

The response (Y) fitted with the second-order polynomial equation

Table 3 GC data showing the number of peak traces

Fragments	Mode of linkage	Major mass fragments (m/z) peak traces
1,2,4-tri-*O*-acetyl-3,6-di-*O*-methyl-D-mannitol	(→1, 2)-Man-(4→	104, 113, 129, 147, 161, 181, 191, 197
1,4-di-*O*-acetyl-2,4,6-tri-*O*-methyl-D-glucitol	(→1)-Glc-(4→	103, 119, 130, 151, 177, 193, 196
1,4,6-di-*O*-acetyl-3-mono-*O*-methyl-2-amino-D-glucitol	(→1, 4)-GlcN-(6→	110, 117, 131, 147, 163, 181, 191, 197

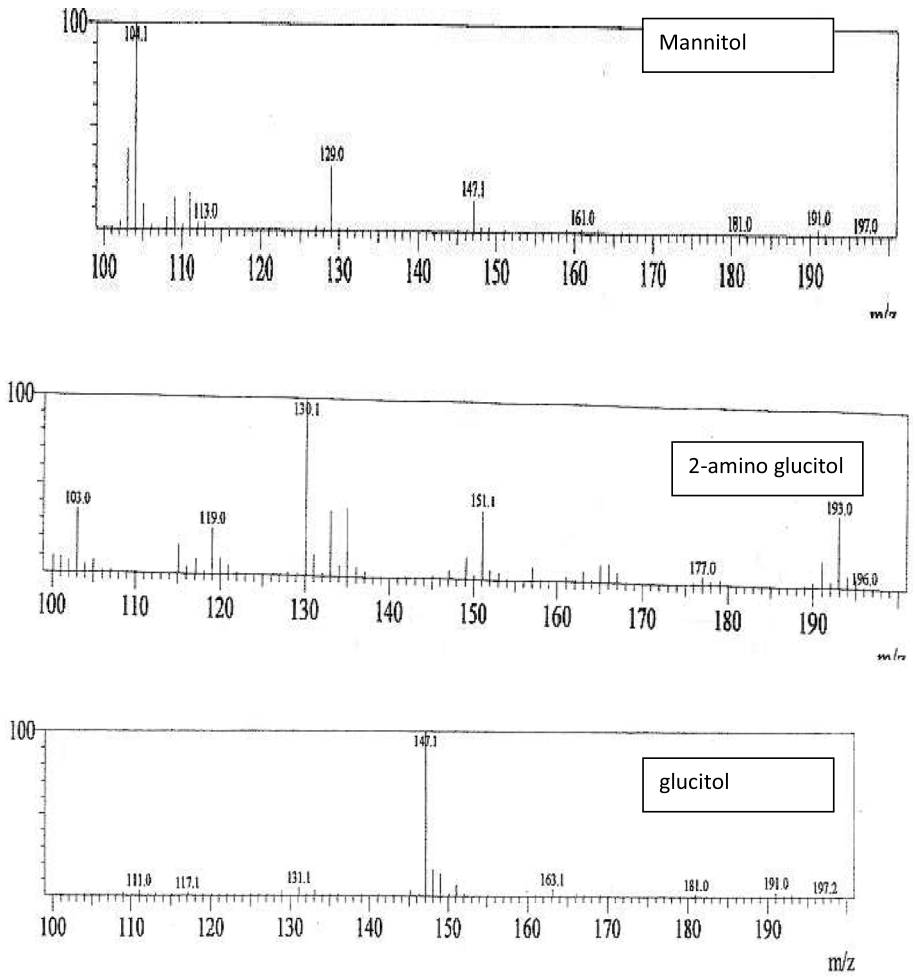

Fig. 6 Mass spectra obtained by GC-MS analysis obtained by Shimadzu GC-MS QP 2010 using ZB-1 column

$$R_1 = +2.54 + 0.14\,A - 0.032B - 0.083\,C + 0.014A\,B - 0.13\,\mathrm{AC} - 0.079\,BC - .59A^2 - 1.23\,B^2 - 0.11C^2$$

R_1 represents the response for ECP production, whereas glucose, yeast extract, and $MgSO_4$ are represented by variables A, B, and C, respectively, and the R^2 coefficient value of 0.99 suggested that predicted model was significant (Table 5). The Model F-value of 154.37 implies the model is significant. In this case, A, C, AC, A^2, and B^2 are significant model terms (Table 6). The combinational effect of

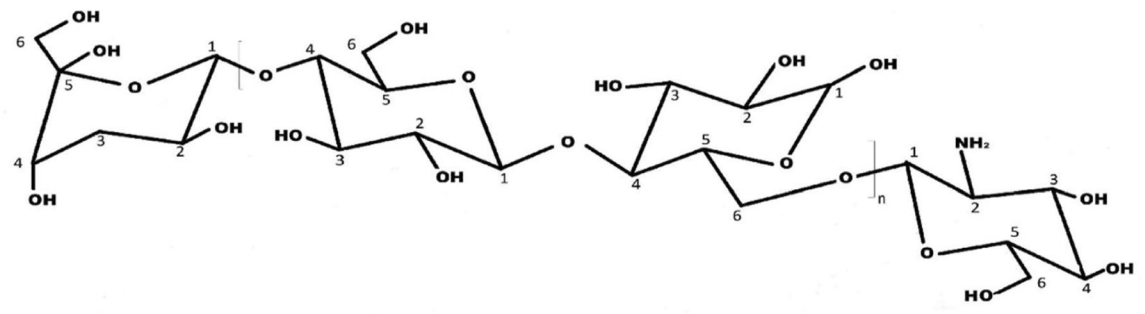

Fig. 7 The probable structure of ECP

Table 4 The nutritional variables selected for optimization study

S.No.	Nutritional variables	[a]Range in g/L
1	Glucose (A)	5–15
2	Yeast extract (B)	5–10
3	$MgSO_4$ (C)	0.2–0.4

[a]Concentration ranges

nutritional variables on the production of ECP was analyzed from the 3-D response surface curves as shown in Fig. 8.

Validation of RSM model

The RSM model is validated by conducting an experiment at best-predicted solution for production of ECP. Under optimized conditions, the ECP yield reached 2.21 g/L from *Acinetobacter indicus* M6, which is almost near to the RSM predicted value (Table 7).

Discussion

Acinetobacter M6 produces ECP in substantial quantities (2.21 g/L). This quantity is considerably higher when compared to other reported bacterial ECPs. As far as our knowledge, there is no report available on ECP from *Acinetobacter indicus* M6 bacterium. ECP from this marine bacterium may be beneficial because few of the ECPs have been reported to have emulsification property which can find potential applications in the reduction of marine water pollution [27, 28]. The purified ECP shows significant antioxidant activities when compared to the standard antioxidant active compound (Vit C). Free radicals such as superoxide radical, hydroxyl radical, and other reactive oxygen species (ROS) are associated with multistage carcinogenesis and mutagenesis [29, 30]. The results of present study have demonstrated that ECP was effective in scavenging superoxide, hydroxyl, and DPPH radicals in a concentration-dependent fashion. There are very few reports available on antioxidant activities of bacterial ECPs. However, this is the first report on antioxidant and free radical scavenging activities of an ECP from *Acinetobacter indicus* M6. Hence, the ECP may be developed as a potential antioxidant molecule after studying various toxicological studies. The monosaccharides in the ECPs are actually potent reductive agents as they have a hidden aldehyde moiety [31]. The antioxidant mechanism of polysaccharides may thus be attributed to the reductive nature of the monosaccharides owing to the presence of –CHO group as these polysaccharides such as ECPs are not proton-donors. The mechanism of free-radical scavenging of polysaccharides is still not fully understood. The results of the present

Table 5 Actual data for design of experiments

S.No.	Glucose	Yeast extract	$MgSO_4$	Production of biosurfactant in g/L	
				Experimental[a]	Predicted[b]
1.	15	10	0.3	1.95	2.1
2.	5	15	0.4	0.36	0.39
3.	10	10	0.3	2.51	2.54
4.	15	15	0.2	1.08	1.03
5.	5	5	0.4	0.63	0.64
6.	10	10	0.3	2.54	2.54
7.	10	10	0.4	2.36	2.34
8.	10	10	0.3	2.63	2.54
9.	10	5	0.3	1.22	1.34
10.	15	5	0.4	0.66	0.63
11.	10	15	0.3	1.25	1.28
12.	5	15	0.2	0.46	0.45
13.	10	10	0.3	2.65	2.54
14.	15	5	0.2	0.98	0.91
15.	10	10	0.3	2.56	2.54
16.	5	10	0.3	1.8	1.81
17.	10	10	0.3	2.65	2.54
18.	5	5	0.2	0.42	0.38
19.	15	15	0.4	0.44	0.44
20.	10	10	0.2	2.34	2.51

[a]Experimental result of biosurfactant production at the mentioned nutrient concentrations
[b]RSM predicted value of biosurfactant production at the mentioned nutrient concentrations

Table 6 ANOVA for response surface quadratic model

Source	Sum of squares	df	Mean square	F-value	*p*-value Prob > *F*	
Model	15.38	9	1.71	154.37	< 0.0001	**Significant**[a]
A-glucose	0.21	1	0.21	18.73	0.0015	
B-yeast extract	0.01	1	0.01	0.92	0.3589	
C-$MgSO_4$	0.07	1	0.07	6.22	0.0318	
AB	0.00	1	0.00	0.14	0.7194	
AC	0.14	1	0.14	12.92	0.0049	
BC	0.05	1	0.05	4.48	0.0604	
A^2	0.95	1	0.95	85.92	< 0.0001	
B^2	4.15	1	4.15	374.61	< 0.0001	
C^2	0.04	1	0.04	3.18	0.1048	
Residual	0.11	10	0.01			
Lack of fit	0.09	5	0.02	4.95	0.0519	**Not significant**
Pure error	0.02	5	0.00			
Cor total	15.50	19				

[a]If *p*-value of a parameter is < 0.05, the effect of that parameter is significant

study have demonstrated that ECP is effective in scavenging superoxide, hydroxyl, and DPPH radicals in a concentration-dependent fashion. There are a very few reports available on antioxidant activities of bacterial ECPs. However, this is the first report on antioxidant and free radical scavenging activities of an ECP from *Acinetobacter indicus* M6. HPLC analysis indicated that ECP was a heteropolymer composed of glucose, mannose, and glucosamine. The presence of these monomers makes the heteropolymer unique, and this monomeric combination was not found in any other reported ECPs. GC-MS data of alditol derivatives revealed that (1→4)-linked glucose, (1→4)-linked mannose, and (→4)-GlcN-(1→) were present in the ECP. Presence of these linkages also makes our ECP unique and novel, and the predicted structure is given in Fig. 7 [32]. ECP from *Acinetobacter indicus* M6 was found to be a structurally complex but novel molecule for its unique

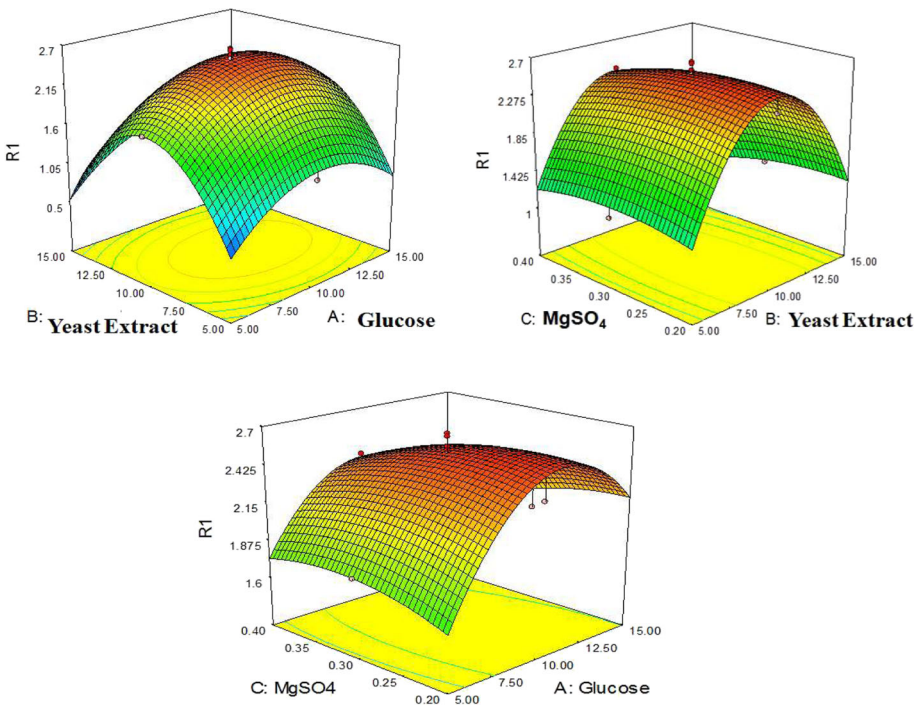

Fig. 8 3D graphs showing the combinational interaction of variables on production of ECP

Table 7 Validation of RSM model for ECP production

S.No.	Glucose (A), g/L	Yeast extract (B), g/L	$MgSO_4$ (C), g/L	ECP production (R_1), g/L	
				RSM model predicted	Experimental
1	15	10.12	0.2	2.19	2.21

monosaccharide composition and the glycosidic linkages between the monomeric units. This unique combination of the monosaccharides and unusual glycosidic linkages between them make our ECP novel. To undertake a holistic approach towards critically establishing the structure-function relationship of the ECP molecule by elucidating its complete molecular structure on further chemical derivatizations and enzymatic digestions (with glucosidases), so as enable us to identify the right fragments of the large ECP molecule, responsible for each of its important bioactive properties of therapeutic and commercial interests [27, 33]. This would also help us to use the small fragments for specific therapeutic purposes, instead of using the whole molecule [34, 35]. However, the complete structural elucidation may be performed by other sophisticated techniques like NMR and ESI-MS which is the scope of the present study. The optimized medium improved the production of ECP and is two folds higher in comparison with the basal medium.

Conclusion

ECP produced by marine bacterium was purified and found to be a heteropolymer composed of glucose as a major monomer, and mannose and glucosamine were minor monomers, and this makes ECP unique in terms of its composition. GC-MS analyses elucidated the presence of quite uncommon (1→4)-linked glucose, (1→4)-linked mannose, and (→4)-GlcN-(1→) glycosidic linkages in the backbone. The purified ECP has shown significant antioxidant activity. The detailed mechanisms of actions of the ECP molecule for its significant antioxidant activities need to be elucidated to develop the whole ECP molecule or the suitable fragments of it into prospective drug candidates. This requires a lot of basic research inputs. The production of ECP reached 2.21 g/L after the optimization of nutritional variables. The designed model is statistically significant and is indicted by the R^2 value of 0.99. The optimized medium improved the production of ECP and is two folds higher in comparison with the basal medium. As a long-term future scope and perspective, it would be prudent to scale the optimal process up to a pilot plant scale for consistent production of this important bioactive ECP molecule in large quantities. Though there are reports available on bacterial ECPs, this is the first report on ECP from *Acinetobacter indicus* M6. Unique monosaccharide composition and the glycosidic linkages between the monomeric units of the ECP markedly differ with the reported ECPs.

Considering the unique monosaccharide composition and significant antioxidant activity, the ECP may be developed as a drug molecule. The ECP is a promising antioxidant, and it can be used as an additive in food, pharmaceutical, and cosmetic preparations. The relationship between structure of ECP and antioxidant activity and also elucidation of its antioxidant mechanism at the molecular level will improve its biological activities by chemical modifications, one of the important implications of this study.

Abbreviations

ECP: Extracellular polysaccharide; DPPH: 1,1-diphenyl-2 picryl hydrazyl; RSM: Response surface methodology

Acknowledgements

Prof. G. Vijay Ananda Kumar Babu, Head, Department of Biotechnology, VSU for providing the facilities.

Authors' contributions

RTCh carried out the isolation and purification of the ECP. APK studied the antioxidant activity of the ECP. NV is involved in the HPLC analysis. VTC and MK helped in GC-MS part of the structural analysis. JBD is involved in optimization studies. VPK is the main author involved in the design and analysis of the whole study. All authors have read and approved the manuscript.

Funding

Department of Biotechnology (DBT), Ministry of Science and Technology, Govt. of India for financial support (F. No. BT/PR/7952/AAQ/3/642/2013) and DST-FIST-LSI-595 (LSI-026) for providing facility.

Availability of data and materials

The data is available and it will be provided to the editor if required.

Declarations

Ethics approval and consent to participate

This work is not involved in animal or human models. Hence, ethical approval is not required.

Consent for publication

Not applicable.

Competing interests

The authors declare no competing interest.

Author details

[1]Department of Biotechnology, Vikrama Simhapuri University, Kakutur, Nellore A.P-524320, India. [2]Department of Biotechnology, VFSTR University, Vadlamudi, Guntur A.P-522213, India. [3]SRR and CVR Government Degree College, Machavaram, Vijayawada A.P-520010, India.

Received: 23 July 2020 Accepted: 16 February 2021
Published online: 12 March 2021

References

1. Shabtai Y (1990) Production of exopolysaccharides by *Acinetobacter* strains in a controlled fed-batch fermentation process using soap stock oil (SSO) as carbon source. Int J Biol Macromol 12(2):145–152
2. Welman AD, Maddox IS (2003) Exopolysaccharides from lactic acid bacteria: perspectives and challenges. Trends Biotechnol 21(6):269–274
3. Naidu AS, Bidlack WR, Clemens RA (1999) Probiotic spectra of lactic acid bacteria (LAB). Crit Rev Food Sci Nutr 39(1):13–126
4. Ashtaputre AA, Shah AK (1995) Emulsifying property of a viscous exopolysaccharide from *Sphingomonas paucimobilis*. World J Microbiol Biotechnol 11:219–222
5. De Vuyst L, Bart D (1999) Heteropolysaccharides from lactic acid bacteria. FEMS Microbiol Rev 23:153–177
6. Kishk YFM, Al-Sayed HMA (2007) Free-radical scavenging and antioxidative activities of some polysaccharides in emulsions. LWT Food Sci Technol 40: 270–277
7. Sun C, Wang JW, Fang L, Gao XD (2004) Free radical scavenging and antioxidant activities of EPS2, an exopolysaccharide produced by a marine filamentous fungus *Keissleriella sp.YS* 4108. Life Sci 75:1063–1073
8. Halliwell B, Gutteridge JMC (1986) Oxygen free radicals and iron in relation to biology and medicine: some problems and concepts. Arch Biochem Biophys 246:501–514
9. Reddy AR, Peele KA, Krupanidhi S, Kodali VP, Venkateswarulu TC (2018) Production of polyhydroxybutyrate from *Acinetobacter nosocomialis* RR20 strain using modified mineral salt medium: a statistical approach. Int J Environ Sci Technol 16(3):6447–6452
10. Wang QJ, Fang YZ (2004) Analysis of sugars in traditional Chinese drugs. J Chromatogr B 812:309–324
11. Donlan RM, Costerton JW (2002) Biofilms: survival mechanisms of clinically relevant microorganisms. Clin Microbiol Rev 15(2):167–193
12. Bjorndal H, Hellerqvist CG, Lindberg B, Svensson SA (1970) Gas-liquid chromatography and mass spectrometry in methylation analysis of polysaccharides. Chem Int 9(8):610–618
13. Gruter M, Leeflang BR, Kuiper J, Kamerling JP, Vliegenthart JF (1993) Structural characterisation of the exopolysaccharide produced by *Lactobacillus delbrückii* subspecies bulgaricus rr grown in skimmed milk. Carbohydr Res 239:209–226
14. Peele KA, Ch VRT, Kodali VP (2016) Emulsifying activity of a biosurfactant produced by a marine bacterium. 3Biotech 6(2):177–180
15. Dubois M, Gilles KA, Hamilton JK, Pebers PA, Smith F (1956) Calorimetric method for determination of sugars and related substances. Anal Chem 28: 350–356
16. Wang H, Dong X, Zhou GC, Cai L, Yao WB (2008) In vitro and in vivo antioxidant activity of aqueous extract from *Choerospondias axillaris* fruit. Food Chem 106:888–895
17. Liu F, Ng TB (2000) Antioxidative and free radical scavenging activities of selected medicinal herbs. Life Sci 66:725–735
18. Ren D, Jiao Y, Yang X, Yuan L, Guo J, Zhao Y (2015) Antioxidant and antitumor effects of polysaccharides from the fungus *Pleurotus abalonus*. Chem Biol Interact 237:166–174
19. Nishimiki M, Rao NA, Yagi K (1972) The occurrence of superoxide anion in the reaction of reduced phenazine methosulfate and molecular oxygen. Biochem Biophys Res Commun 46:849–853
20. Sokmena M, Angelovab M, Krumovab E, Pashovab S (2005) In vitro antioxidant activity of polyphenol extracts with antiviral properties from Geranium sanguineum L. Life Sci 76:2981–2993
21. Anumula KR (1994) Quantitative determination of monosaccharides in glycoproteins by high-performance liquid chromatography with highly sensitive fluorescence detection. Anal Biochem 220(2):275–283
22. Anumula KR, Dhume ST (1998) High resolution and high sensitivity methods for oligosaccharide mapping and characterization by normal phase high performance liquid chromatography following derivatization with highly fluorescent anthranilic acid. Glycobiol 8(7):685–694
23. Kim SJ, Kim BG, Parka HU, Yim JH (2016) Cryoprotective properties and preliminary characterization of exopolysaccharide (P-Arcpo 15) produced by the Arctic bacterium *Pseudoalteromonas elyakovii* Arcpo 15. Prep Biochem Biotechnol 46:261–266
24. Maheswari P, Mahendran S, Sankaralingam S, Sivakumar N (2019) In vitro antioxidant activity of exopolysaccharide extracted from marine sediment soil bacteria. Res J Pharm Tech 12(9)
25. Bomfim VB, Neto JHL, Leite KS, Vieira EA (2020) Partial characterization and antioxidant activity of exopolysaccharides produced by Lactobacillus plantarum CNPC003. Food Sci Tech 127:109349
26. Lin SM, Baek CY, Jung JH, Kim WS, Song HY, Lee JH, Ji HJ, Zhi Y, Kang BS, Bahn YS, Seo HS, Lim S (2020) Antioxidant activities of an exopolysaccharide (DeinoPol) produced by the extreme radiation-resistant bacterium *Deinococcus radiodurans*. Nat Sci Rep 63(10):55
27. Yasuda T, Inaba A, Ohmori M, Endo T (2000) Urinary metabolites of gallic acid in rats and their radical scavenging effect on DPPH. J Nat Prod 63: 1444–1446
28. Cheng BH, Chan JYW, Chan BCL (2014) Structural characterization and immunomodulatory effect of a polysaccharide HCP-2 from *Houttuynia cordata*. Carbohydr Polym 103:244–249
29. Venkateswarulu TC, Kodali VP, Kumar RB (2017) Optimization of nutritional components of medium by response surface methodology for enhanced production of lactase. 3 Biotech 7(3):202
30. Soares JR, Dins TCP, Cunha AP, Ameida LM (1997) Antioxidant activity of some extracts of *Thymus zygis*. Free Radic Res 26:469–478
31. Haschemie KK, Renger A, Steinhart H (1996) A comparison between reductive-cleavage and standard methylation analysis for determining structural features of galactomannans. Carbohydr Polym 30(1):31–35
32. Knight J (1998) Free radicals: their history and current status in aging and disease. Ann Clin Lab Sci 28:331–346
33. Sun T, Powers JR, Tang J (2007) Evaluation of the antioxidant activity of asparagus, broccoli and their juices. Food Chem 105:101–106
34. Kodali VP, Das S, Sen R (2009) An exopolysaccharide from a probiotic: biosynthesis dynamics, composition and emulsifying activity. Food Res Int 42:695–699
35. Venkateswarulu TC, Prabhakar KV, Kumar RB, Krupanidhi S (2017) Modeling and optimization of fermentation variables for enhanced production of lactase by isolated *Bacillus subtilis* strain VUVD001 using artificial neural networking and response surface methodology. 3 Biotech 7(3):1–9

Publisher's Note

Nature Environment and Pollution Technology
An International Quarterly Scientific Journal

p-ISSN: 0972-6268
(Print copies up to 2016)
e-ISSN: 2395-3454

Vol. 19 | No. 5 (Suppl) | pp. 1821-1829 | 2020

Original Research Paper

https://doi.org/10.46488/NEPT.2020.v19i05.005

Open Access Journal

Biochemical Changes Induced by Cartap Hydrochloride (50% SP), Carbamate Insecticide in Freshwater Fish *Cirrhinus mrigala* (Hamilton, 1822)

G. Vani*†, K. Veeraiah, M. Vijaya Kumar*, Sk. Parveen* and G.D.V. Prasad Rao*****

*Department of Zoology, SRR & CVR Government Degree College (A), Vijayawada, Andhra Pradesh, India

**Department of Zoology and Aquaculture, Acharya Nagarjuna University, Nagarjunanagar-522 510, Guntur, Andhra Pradesh, India

***Department of Zoology SGS College, Jaggaiahpet, Andhra Pradesh, India

†Corresponding author: G. Vani; gandhamvanipradeep@gmail.com

Nat. Env. & Poll. Tech.
Website: www.neptjournal.com

Received: 08-11-2019
Revised: 25-11-2019
Accepted: 03-01-2020

Key Words:
Cartap hydrochloride
Cirrhinus mrigala
LC_{50}
Glycogen
Total proteins
Nucleic acids

ABSTRACT

The freshwater fish *Cirrhinus mrigala* was exposed to Cartap hydrochloride (50% SP) for 24, 48, 72 and 96 h. The LC_{50} values were found to be 0.436, 0.419, 0.394 and 0.376 mg^{-1} in static method and 0.399, 0.371, 0.361 and 0.339 $mg.L^{-1}$ in continuous flow-through system. The static LC_{50} values are higher than the continuous flow-through method. The LC_{50} values showed a decreasing trend with an increase in time of exposure in both the methods. The decrease was more in a continuous flow-through method than in the static method. The fish were exposed to sub-lethal ($1/10^{th}$ of 96 h LC_{50} value 0.0376 $mg.L^{-1}$) and lethal (96 h LC_{50} value 0.376 $mg.L^{-1}$) concentrations of the pesticide for 24 and 96 hours to study the alterations in glycogen, total proteins and nucleic acids (DNA & RNA) contents of various tissues viz., gill, brain, liver, kidney and muscle. Glycogen, total proteins and nucleic acids (DNA & RNA) content values decreased in all the tissues of exposed fish and the per cent decrease is more apparent in lethal concentrations than in sub-lethal concentrations. From the present study, it can be concluded that Cartap hydrochloride caused a decline in the glycogen, total protein and nucleic acids (DNA, RNA) content in *Cirrhinus mrigala* and the changes are more pronounced in lethal exposure than in sub-lethal exposure.

INTRODUCTION

Indiscriminate use of pesticides is one of the main reasons for the pollution of aquatic ecosystems. These toxic pesticides are causing deleterious effects on aquatic organisms. They are causing stress to aquatic organisms which are reflected as biochemical changes in their body (Mayers 1977). Fish acts as a bioindicator species and can be used for monitoring of water pollution as they accumulate the contaminants from polluted water and diet (Chaudary & Jabeen 2011, Kafilzadeh et al. 2012). Fish accumulate these pollutants directly or indirectly from polluted waters and food chain (Jabeen et al. 2016, Chaudary & Jabeen 2011). Carbamates are extensively used water-soluble pesticides in agricultural practices. In India, Cartap hydrochloride is a Carbamate pesticide which is considered as nereistoxin analog is extensively used in rice and sugarcane crops to control pests. The present investigation is aimed to study the toxic effects of Cartap hydrochloride in sub-lethal and lethal concentrations at 24 and 96 hours of exposure period on glycogen, total protein, DNA and RNA contents of freshwater fish *Cirrhinus mrigala* (Hamilton 1822).

MATERIALS AND METHODS

The fingerlings of the test fish *Cirrhinus mrigala* size 6-8 ± ½ cm and weight 6-7 ± ½ g were procured from local fish hatcheries of Nandivelugu, Tenali Mandal, Guntur district, Andhra Pradesh. The fish were acclimated at (28 ± 2°C)) in the laboratory conditions for two weeks. All the precautions laid down by APHA et al. (1998) were followed. During the acclimation period, the fish were fed with rice bran and groundnut cake. One day before the experimentation feeding was stopped. Cartap hydrochloride (50% SP) commercial grade was purchased from Mangalagiri, Guntur District. The stock solution was prepared with water as a solvent. The acclimatized fish were exposed to static sub-lethal (0.376 $mg.L^{-1}$) and lethal concentrations (3.76 $mg.L^{-1}$) of Cartap hydrochloride (50% SP) for 24 and 96 h. The hydrographical properties of water were estimated by the modified method followed by Golterman & Claimo (1969) method. Finney's probit analysis (Finney 1971) as reported by Roberts % Boyce (1972) was followed to calculate the LC_{50} value. The 95% confidence limits of the LC_{50} values for each test were also calculated for different time periods

by using SPSS software. At the end of the exposure periods, the tissues like gill, brain, liver, kidney and muscle were taken out from exposed and control fish and processed for the estimation of glycogen, total proteins and nucleic acids (DNA & RNA). Glycogen was estimated by the method of Kemp et al. (1954), total protein by Lowry et al. (1951) and DNA and RNA by the methods of Searchy & Maclinnis (1970a & 1970b).

The data obtained in the present work were expressed as means of four observations ± SD (standard deviation) and were statistically analysed using student "t" test (Pillai & Sinha 1968) to compare means of treated data against their controls and the result was considered significant at ($P < 0.05$) level.

RESULTS AND DISCUSSION

Glycogen, total proteins and nucleic acids (DNA & RNA) decreased in various tissues, viz. gill, brain, liver, kidney and muscle of *Cirrhinus mrigala* exposed to sub-lethal and lethal concentrations of cartap hydrochloride for 24 and 96 hours were graphically represented in Fig. 1 to Fig. 8. In exposed fish per cent decrease is more apparent in lethal concentrations than at sub-lethal concentrations.

Glycogen

The changes in glycogen content observed in the various tissues of *Cirrhinus mrigala* after the Cartap hydrochloride exposure along with the control are graphically represented in Fig .1 and Fig. 2.

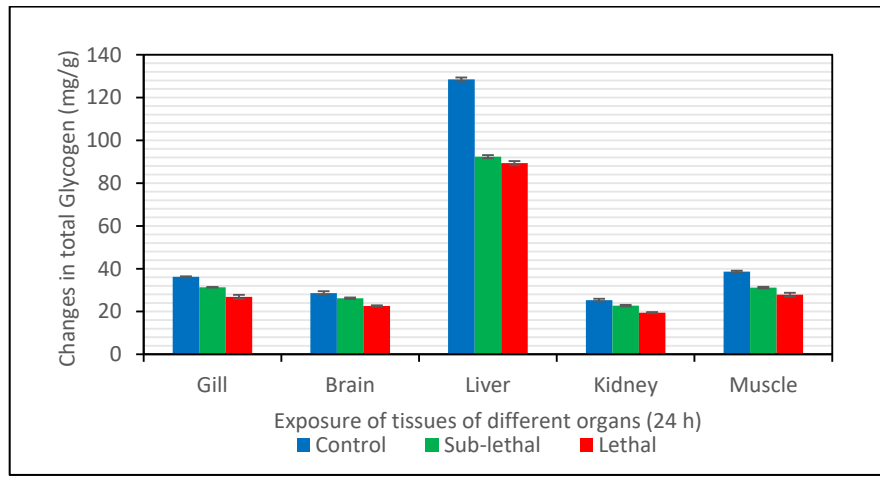

Fig.1: Changes in the glycogen content (mg/g wet weight of the tissue) in the tissue of fish *Cirrhinus mrigala* on exposure to sub-lethal and lethal concentration of Cartap hydrochloride (50%SP) for 24 hours.

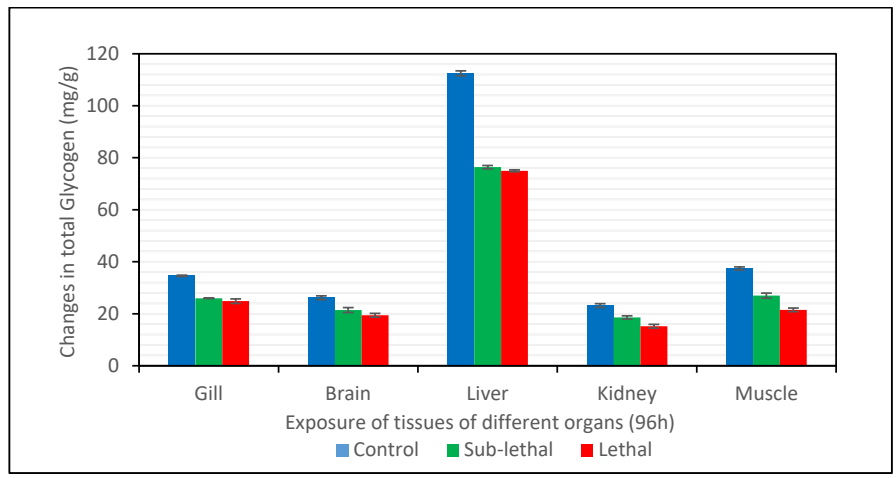

Fig. 2: Changes in the glycogen content (mg/g wet weight of the tissue) in the tissue of fish *Cirrhinus mrigala* on exposure to sub-lethal and lethal concentration of Cartap hydrochloride (50% SP) for 96 hours.

In the tissues of control fish, *Cirrhinus mrigala* glycogen content was in the order of:

Liver > Muscle > Gill > Brain > Kidney

Under exposure to sub-lethal and lethal concentrations of Cartap hydrochloride for 24 and 96 hours, the amount of glycogen was found to decrease in all the tissue of *Cirrhinus mrigala*. The lyotropic gradation series in terms of per cent decrement at 24 h and 96 h exposure was:

Sub-lethal -24 h: Liver > Muscle > Gill > Kidney > Brain

Lethal -24 h: Liver > Muscle > Gill > Kidney > Brain

Sub-lethal 96 h: Liver > Muscle > Gill > Kidney > Brain

Lethal-96 h: Muscle > Kidney > Liver > Gill > Brain

Exposure of *Cirrhinus mrigala* to Cartap hydrochloride for 24 hours caused a maximum decrease of glycogen in the liver (sub-lethal 28.117, lethal 30.453). For 96 h maximum decrease was found in the liver (sub-lethal 32.073) and muscle (lethal 42.570). In the present study under Cartap hydrochloride 24 h sub-lethal and lethal exposure minimum percentage of depletion was in the brain (8.595) and (20.96). For 96 h exposure minimum depletion was found in the brain (sub-lethal 18.056, lethal 25.707).

Srivastava & Singh (2013) observed reduction in glycogen content in different tissues of freshwater fish *Clarius batrachus* exposed to 80% of LC_{50} (22.87 $mg.L^{-1}$) of Mancozeb at different time intervals of 24 and 96 h. Sastry et al. (1982) reported decreased glycogen content of liver and muscles decreased when *Channa punctatus was exposed to* sub-lethal concentration of the carbamate pesticide, Sevin (1.05 $mg.L^{-1}$) for 15, 30 and 60 days. Veeraiah et al. (2013a) observed that exposure to sub-lethal and lethal concentrations of cadmium chloride in the fish *Cirrhinus mrigala* for 96 h caused changes in the total glycogen level which may be attributed to toxic stress, resulting in the disruption of enzymes associated with carbohydrate metabolism. Bantu & Rathnamma (2013) reported that there is a decrease in the amount of glycogen in the fish *Labeo rohita* exposed to sub-lethal and lethal concentrations of Dimethoate for 8 days. Priya et al. (2013) observed depletion of glycogen in the liver of freshwater teleost *Channa punctatus* (Bloch) when exposed to various concentrations of Imidacloprid (0.002 ppm, 0.00 ppm, 0.006 ppm, 0.008 ppm and 0.01 ppm) for 96 h suggesting the possibility of an alter from aerobic to anaerobic mode of energy metabolism of the liver. Dhanalakshmi (2013) noticed decrement in the tissue glycogen concentration in fish *Cirrhinus mrigala* when exposed to 0.25 ppm concentration of the metal chromium sulphate for 24, 48, 72 h and 10, 20 and 30 days which may be due to its enhanced utilization, since glycogen forms the immediate source of energy to meet energy demands under metallic stress caused by test toxicant.

Tataji & Kumar (2016) reported a decline in glycogen content of freshwater fish *Channa punctatus* exposed for 8 days to 1/5th of LC_{50} 96 hours of both Butachlor technical grade and Machete (50% EC), i.e. 32 ppb and 71.2 ppb for both technical and 50% EC respectively. Reduction in glycogen content was also noticed by Naik et al. (2016) in all the tissues of *Labeo rohita* when exposed to sub-lethal concentrations of cypermethrin for 1, 2 and 3 weeks. Exposure of sub-lethal doses (40% and 80 % of LC_{50} of 24 h) of glyphosate for 24 or 96 h against the freshwater non-target fish *Channa punctatus* caused significant ($P < 0.05$) alteration in biochemical parameters in liver and muscle tissues of the fish *Channa punctatus* (Bloch) was reported by Singh et al. (2017). Veeraiah et al. (2018) observed that exposure to lethal and sub-lethal concentrations of cyhalothrin 2.5% EC, in the fish *Ctenopharyngdon idellus* for 24 and 96 hours caused a decrease in glycogen content in all tissues.

According to Dezwaan & Zandee (1973) depletion of glycogen in tissues may be due to direct utilization of the compound for energy generation, a demand caused by pesticide-induced hypoxia. Under hypoxia condition, the fish derives its energy from anaerobic breakdown of glucose which is available to the cell by increased glycogenolysis (Chandravathy & Reddy 1996, Rajamannar & Manohar 1998, Rajamanickam 1992). Reduction in glycogen is probably due to its more rapid break down for energy requirement of fish (Muley et al.1996).

Liver suggested as an organ for detoxification. During exposure to Cartap hydrochloride exposure fishes came under stress condition and need more energy to cope with the toxicants. glycogen serves as reserve material. It is utilized when the body came under stress condition. Depletion of glycogen in liver and tissues may be due to increment in the glycolysis pathway. During stress conditions, the glycogen reserves depleted to meet energy demand (Rawat et al. 2002). Fall in glycogen levels indicates its rapid utilization to meet the enhanced energy demands intoxicant treated animals through glycolysis or hexose monophosphate pathway as observed by Cappon & Nicholas (1975). The above findings support the alterations of glycogen in the present study.

Proteins

The changes in protein content observed in the various tissues of *Cirrhinus mrigala* after Cartap hydrochloride exposure along with the control was graphically represented in Fig. 3 and Fig. 4.

The Protein content in different tissues in control fish *Cirrhinus mrigala* was in the order of:

Muscle > Liver > Brain > Kidney > Gill

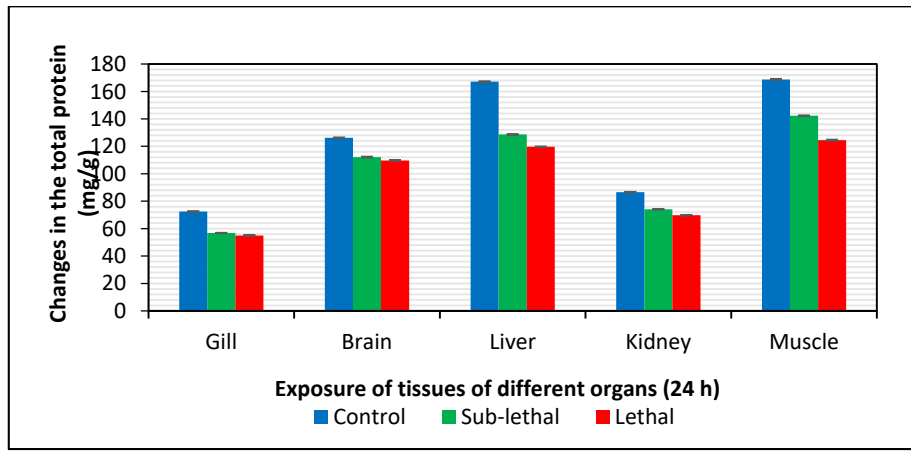

Fig. 3: *Changes* in protein content (mg/g wet wt of the tissue) in different tissues of fish *Cirrhinus mrigala* (Hamilton) on exposure to sub-lethal and lethal concentration of Cartap hydrochloride (50% SP) for 24 hours.

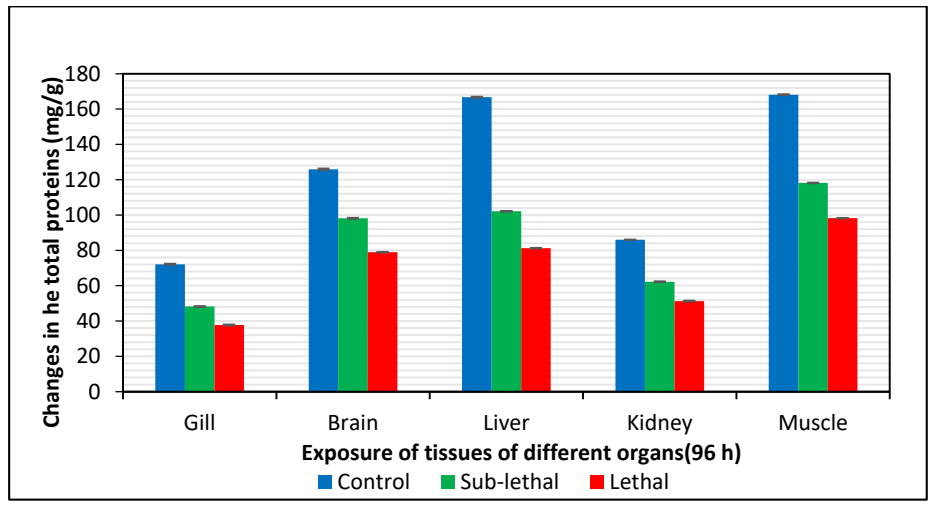

Fig. 4: Changes in protein content (mg/g wet wt of the tissue) in different tissues of fish *Cirrhinus mrigala* (Hamilton) on exposure to sub-lethal and lethal concentration of Cartap hydrochloride (50% SP) for 96hours.

Under exposure of sub-lethal and lethal concentrations of Cartap hydrochloride for 24 h, the amount of protein was found to decrease in all the tissue of *Cirrhinus mrigala.*

The lyotropic gradation series in terms of per cent decrement at 24 h and 96 h exposure was:

Sub-lethal -24 h: Liver > Gill > Muscle > Kidney > Brain

Lethal-24 h- Liver > Muscle > Gill > Kidney > Brain

Sub-lethal -96 h: Liver > Gill > Muscle > Kidney > Brain

Lethal-96 h: Liver > Gill > Muscle > Kidney > Brain

For 24 h exposure maximum per cent of the decrease in total protein was observed in the liver (sub-lethal 23.05, lethal 28.33). For 24 h exposure minimum percentage of depletion of total protein was found in the brain (sub-lethal 11.18, lethal 13.13). For 96 h the percentage of decrease was maximum in the liver (sub-lethal 38.72, lethal 51.27). Similarly, for 96 h minimum percentage of decrease was noticed in the brain (sub-lethal 22.06, lethal 37.30).

Protein is the most primary biochemical ingredient present in large quantities in the body of fish. Liver is rich in protein and centre for various metabolism of the fish. In the present study maximum decrease of total protein in the liver is due to the increased rate of proteolytic activity or repeated break down of protein to yield energy due to stress caused due to pesticide exposure. Anitha & Rathnamma (2016) noticed decreased protein levels in all the tissues like liver, kidney, brain, gill and muscle of *Labeo rohita* exposed to lethal and sub-lethal concentrations of Pyraclostrobin 20%

WG (carbamate) for 24 h and sub-lethal concentrations for 5 and 10 days. A decline in the protein content was noticed by Kumari et al. (2014) in the liver of *Clarias batrachus* when exposed to sub-lethal concentrations (2 and 4 $mg.L^{-1}$) of the Carbaryl for 96 h. A decrease in protein may be due to the impairment of protein synthesis or an increase in the rate of its degradation to amino acids. Exposure to Carbryl for 4 and 24 days, decreased protein content in liver and muscle of fish *Mugil cephalus*, when exposed to the lethal and sub-lethal concentration of Carbaryl for 4 days and 21 days respectively was reported by Shivanagouda et al. (2013). Kumar et al. (2017) reported a reduction in proteins in the liver and kidney of freshwater fish, *Channa punctatus* exposed to different sub-lethal concentrations of pesticide Carbaryl for a period of 15, 30, 45, 60, 75 and up to 90 days. Muddassir (2015) observed significant decrease value in Total protein in the liver of *Channa punctatus* was treated with 0.1 mL Carbofuran and 0.09 mL Malathion pesticides at different time intervals 7, 14, 21 and 28 days. The decrement of total protein may be due to the inhibition of RNA synthesis disturbing the protein metabolism or this may be due to liver damage where most protein synthesis usually occurs, these results agreed with that of Singh & Sharma (1998). The depletion of protein might also be attributed to spontaneous utilization of amino acids in various catabolic reactions inside the organism to combat the stress condition (Borah & Yadav 1996). Wankhedkar & Bhavsar (2015) found that total protein content significantly decreased in foot and hepatopancreas in land snail *C. moussonianus* when treated with Cartap hydrochloride and Imidacloprid at lowest concentration i.e. LC_{50} 0.41ppm and LC_{50} 0.54 ppm respectively. Veeraiah et al. (2018) observed a decrease in protein content in all tissues exposed to lethal and sub-lethal concentrations of cyhalothrin 2.5% EC, in the fish *Ctenopharyngdon idellus* for 24 and 96 h.

Proteins are important organic constituents of the animal cells. Understanding the protein components of the cell becomes necessary in the light of the radical changes taking place in protein profiles during pesticide intoxication (Anitha & Rathnamma 2016). The decreased trend of the protein content as observed in the present study in most of the fish tissues may be due to metabolic utilization of the ketoacids through gluconeogenesis pathway for the synthesis of glucose or due to the directing of free amino acids for the synthesis of necessary proteins, or for the maintenance of osmotic and ionic regulation (Schmidt Neilson 1975).

Nucleic Acids (DNA & RNA)

The changes in DNA content observed in the various tissues of *Cirrhinus mrigala* after the Cartap hydrochloride exposure along with the control was graphically represented in Fig. 5 and Fig. 6.

In control fish, DNA content present in different organs was in the order of:

Muscle > Gill > Brain > Liver > Kidney.

Under exposure to sub-lethal and lethal concentrations of Cartap hydrochloride, for 24 h the amount of DNA was found to decrease in all the tissue of *Cirrhinus mrigala.* The lyotropic gradation series in terms of per cent decrement at 24 h and 96 h exposure was:

Sub-lethal -24 h: Gill > Liver > Muscle > Brain > Kidney

Lethal-24 h-Gill > Liver > Muscle > Brain > Kidney

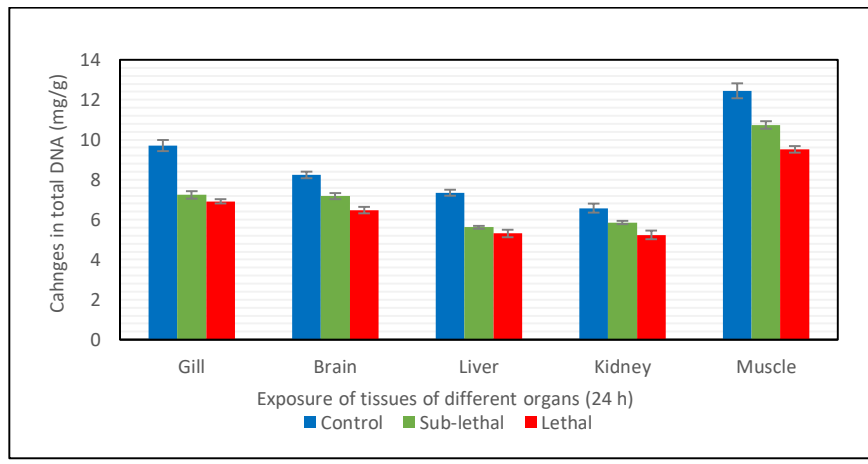

Fig. 5: Changes in the amount of deoxyribonucleic acid (DNA) (mg/g wet weight of the tissue) in different tissues of the fish, *Cirrhinus mrigala* on exposure to sub-lethal and lethal concentration of Cartap hydrochloride (50% SP) for 24 h.

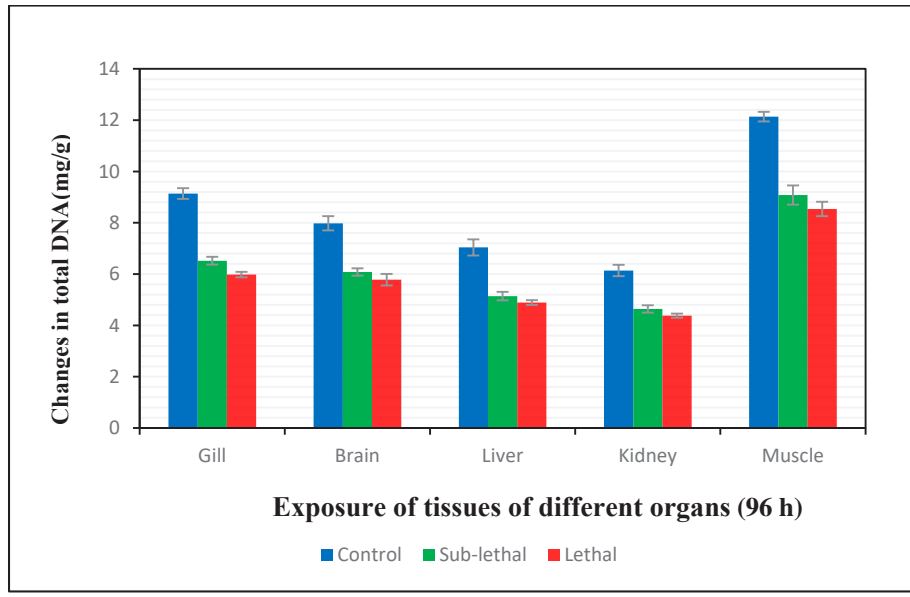

Fig. 6: Changes in the amount of deoxyribonucleic acid (DNA) (mg/g wet wt of the tissue) in different tissues of the fish *Cirrhinus mrigala* on exposure to sub-lethal and lethal concentration of Cartap hydrochloride (50% SP) for 96 h.

Sub-lethal-96 h: Gill > Liver > Muscle > Kidney > Brain

Lethal-96 h: Gill > Liver > Muscle > Kidney > Brain

In the present study under Cartap hydrochloride exposure for 24 h, maximum percentage of depletion in amount of DNA was noticed in Gill (sub-lethal 25.44, lethal 28.74). Minimum percentage of depletion was exhibited in the Kidney (sub-lethal 10.95, lethal 20.37). Under exposure to sub-lethal and lethal concentrations of Cartap hydrochloride for 96 h, maximum percentage of depletion was seen in Gill (sub-lethal 28.67, lethal 34.58) and minimum percentage of depletion was noticed in the brain (sub-lethal 23.81, lethal 27.57).

The changes in RNA content observed in the various tissues of *Cirrhinus mrigala* after Cartap hydrochloride exposure along with the control was graphically represented in Fig. 7 and Fig. 8.

The RNA content in different tissues in control fish *Cirrhinus mrigala* was in the order of:

Muscle > Brain > Gill > Liver > Kidney.

Under exposure to lethal and sub-lethal concentrations of Cartap hydrochloride, for 24 and 96 h, the amount of RNA was found to decrease in all the tissues. The lyotropic gradation series in terms of per cent decrement at 24 h and 96 h exposure was:

Sub-lethal -24h: Muscle > Gill > Kidney > Brain > Liver

Lethal-24h: Muscle > Gill > Kidney > Liver > Brain

Sub-lethal -96h: Gill > Muscle > Kidney > Liver > Brain

Lethal-96h: Gil l > Muscle > Liver > Kidney > Brain

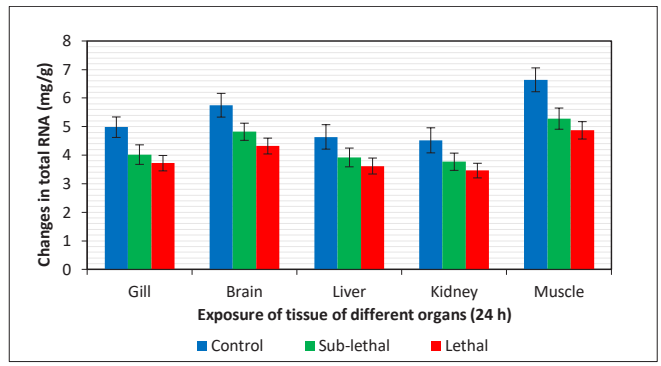

Fig. 7: Changes in the amount of ribonucleic acid (RNA) (mg/g wet wt of the tissue) in different tissues of the fish, *Cirrhinus mrigala* on exposure to sub-lethal and lethal concentration of Cartap hydrochloride (50% SP) for 24 h.

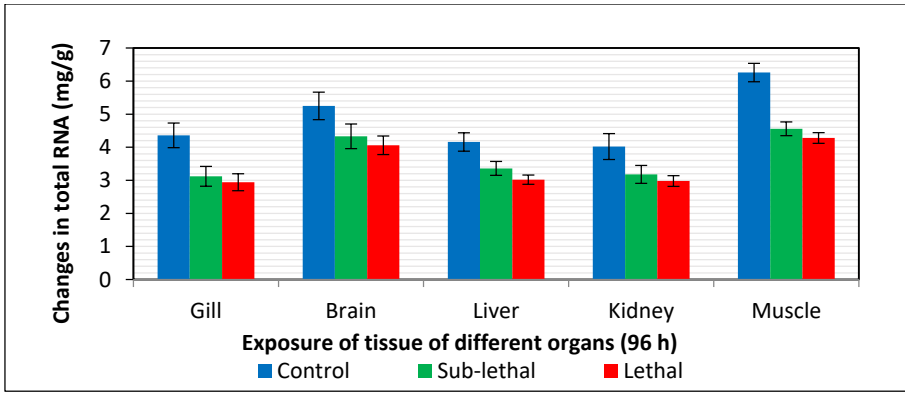

Fig. 8: Changes in the amount of ribonucleic acid (RNA) (mg/gm wet wt of the tissue) in different tissues of the fish, *Cirrhinus mrigala* on exposure to sub-lethal and lethal concentration of Cartap hydrochloride (50% SP) for 96 h.

After 24 h of exposure maximum percentage of decrease in the amount of RNA was found in muscle (sub-lethal 20.48, lethal 26.65). Minimum per cent of the decrease in RNA was found in the liver (15.51) in sub-lethal concentration and brain (19.65) in lethal concentration. After 96h of exposure maximum percentage of decrease in the amount of RNA was found in Gill (sub-lethal 28.44, lethal 32.56). Minimum percentage of decrease in RNA was found in brain(sub-lethal 17.52, lethal 22.66).

The results indicated that the DNA and RNA content in all the tissues of test fish were decreased compared to controls and the decreasing trend was more pronounced in lethal concentrations than in sub-lethal concentrations. In maintaining the physiological configuration of the fish Nucleic acids play a vital role. As Nucleic acid and protein play the main role in regulating different activities of cells they are regarded as important biomarkers of the metabolic potential of cells (Veeriah et al 2013a).

The decrease in nucleic acid content in the present study was in accordance with Vivek (2015) in fingerlings of *Labeo rohita* exposed to sub-lethal concentrations of Cartap hydrochloride for 24, 48, 72 and 96 h. Similar results were also found by Dasu (2014) in fingerlings of *Labeo rohita* were exposed to Thiocarb (Larvin 75% WP) a thiocarbamate pesticide. Anitha & Rathnamma (2016) noticed decreased DNA and RNA levels in all the tissues like liver, kidney, brain, gill and muscle of *Labeo rohita* exposed to lethal and sub-lethal concentrations of Pyraclostrobin 20%WG (carbamate) for 24 h and sub-lethal concentrations for 5 and 10 days.

Tilak et al. (2009) noticed a decreased level of DNA and RNA content in Alachlor treated freshwater fish, *Channa punctatus* (Bloch). The decrease of RNA may be due to inhibiting the function of RNA polymerase or due to interference in the incorporation of precursor in the nucleic acid synthesis. The alterations in DNA levels may be due to disturbances in DNA synthesis and its turnover rate besides degenerative changes caused by pesticides.

From the present study, it can be concluded that exposure of *Cirrhinus mrigala* to Cartap hydrochloride caused a decline in the glycogen, total protein and Nucleic acids (DNA, RNA) content which is more pronounced in lethal exposure than in sub-lethal exposure. The alterations caused during pesticide exposure may be due to the decreased catabolism of the biomolecules to meet the energy demand of test organism under stress or their reduced synthesis due to impaired tissue function. Therefore, the results of this study suggest a serious concern towards the potential danger of Cartap hydrochloride for the aquatic environment and organisms suggesting judicious and careful use of this pesticide in the agricultural area.

ACKNOWLEDGEMENTS

The authors are thankful to the UGC SAP-DRS-III for extending the infrastructure facilities to carry out the present work in the Laboratories of the Deptt. of Zoology & Aquaculture and thank the Head, Department of Zoology and Aquaculture for permitting to do the work.

REFERENCES

Anitha, A. and Rathnamma, V.V. 2016. Toxicity Evaluation and Protein Levels of Fish Labeo rohita Exposed to Pyraclostrobin 20% Wg (Carbamate). International Journal of Advanced Research, 4(3): 967-974.

APHA 1998. Standard Method for the Examination of Water and Wastewater, A.D. Eaton, L.S. Clesceri and A.E. Greenberg (Eds.), 20th edition. American Public Health Association, AWWA and WEF, Washington D.C.

Bantu, N. and Rathnamma Vakita 2013. Effect of dimethoate on mortality and biochemical changes of freshwater fish *Labeo rohita* (Hamilton). Journal of Biology and Today's World, 2(10): 456-470.

Borah, S. and Yadav, R.N.S. 1996. Effect of Rogor (30% w/w dimethoate) on the activity of lactate dehydrogenase, acid and alkaline phosphatase in muscle and gill of a freshwater fish, *Heteropneustes fossilis*. Journal of Environmental Biology, 17(4): 279-283.

Cappon, I.D. and Nicholls, D.M. 1975. Factors involved in increased protein synthesis in liver Microsomes after administration of DDT. Pestic. Biochem. Physiol., 5: 109-118.

Chandravathy, V.M. and Reddy, S.L.N. 1996. Lead nitrate exposure changes in carbohydrate metabolism of freshwater fish. Journal of Environmental Biology, 17: 75-79.

Chaudhry, A.S. and Jabeen, F. 2011. Assessing metal, protein, and DNA profiles in *Labeo rohita* from the Indus River in Mianwali, Pakistan. Environ. Monit. Assess., 174(1-4): 665-679.

Dasu, P.M. 2014. Thiocarb 75 % wp a carbamate insecticide induced toxicity biochemical and histopathological changes in the freshwater Indian major carp *Labeo rohita* Hamilton, Ph.D. Thesis, Acharya Nagarjuna University, Nagarjuna Nagar, Guntur, A.P, India

Dezwaan, A. and Zandee, D.I. 1973. Body distribution and seasonal changes in glycogen content of the common sea mussel, *Mytilus edulis*. Comp. Biochem. Physiol., 43: 53-55.

Dhanalakshmi, B. 2013. Acute and chronic toxicity of chromium on biochemical composition of the freshwater major carp *Cirrhinus mrigala* (Hamilton). Asian J. Sci. Technol., 4: 021-026.

Finney, D.J. 1971. Probit Analysis, 3rd edition. Cambridge University Press.

Golterman, H. and Claimo, R.S. 1969. Methods for Chemical Analysis of Freshwater. Blackwell Sci. Pub., 166 pp.

Jabeen, F., Chaudhry, A.S., Manzoor, S. and Shaheen, T. 2016. Carbamates and neonicotenoids in fish, water and sediments from the Indus River for potential health risks. Environ. Monit. Assess., 187(2): 29.

Kafilzadeh, F., Shiva, A.H., Malekpour, R. and Azad, H.N. 2012. Determination of organochlorine pesticide residues in water, sediments and fish from Lake Parishan, Iran. World J. Fish. Mar. Sci., 4(2): 150-154.

Kemp, A. and and Van Heijningen, A.J.K. 1954. A colorimetric method for the determination of glycogen in tissues. Bio. Chem. J., 56: 646-648.

Kumar, A., Singh, S. and Sharma, H.N. 2017. Changes in total protein in Liver and Kidney of freshwater fish, *Channa punctatus* (Bloch.) after intoxication of Carbaryl. Journal of Advanced Laboratory Research in Biology, 8(2): 41-43.

Kumari, A., Srivastava, A. and Jha, M.M. 2014. Carbaryl Induced alteration in histology and certain biochemical parameter in liver of *Clarias batrachus*. Global Journal of Bioscience and Biotechnology, 3(3): 259-263.

Lowry, O.H., Rosebrough, N.J., Farr, A.L. and Randall, R.J.1951. Protein measurement with the Folin Phenol Reagent. J. boil. Chem., 193: 265-275

Mayers, P. A. 1977. In: Review of Physiological Chemistry, 16th edition. Eds: Harper H A. Rodwell U V and Mayers P.A. Large Medical Publications, California.

Muddassir, A.T. 2015. Comparative study of biochemical alterations induced by carbofuran and malathion on *Channa punctatus* (Bloch.). International Research Journal of Biological Sciences, 4(9): 61-65.

Muley, D.V., Kamble, G.B. and Gaikwad, P.T. 1996. Endosulfan toxicity in the freshwater fish *Tilapia mossambica*. Journal of Aquatic Biology, 11: 61-66.

Naik, B. R., Rao, G. N. and Neelima, P. 2016. Sub-lethal toxicity of cyperkill (a synthetic pyrethroid pesticide) on glycogen content in the tissues of *Labeo rohita.* Int. J. Curr. Res. Aca. Rev., 4(12): 127-134.

Pillai, S.K. and Sinha, H.C.1968. Statistical Methods for Biological Works. Ramprasad and Sons, Agra.

Prasada Rao, G. D. V., Veeraiah, K., Krishna, Ch., Rajeswari, A. and Sindhoori, E. 2018. Cyhalothrin induced bio-chemical alterations in the grass carp *Ctenopharyngodon idellus* (Valenciennes). European Journal of Biomedical and Pharmaceutical Sciences, 5(9): 525-536.

Priya, B.P. and Maruthi, Y.A. 2013. Imidacloprid toxicity on biochemical constituents in liver tissue of fresh water teleost *Channa punctatus*. International Journal of Pharma and Bio Sciences, 4(4b): 50-54.

Rajamanickam, C. 1992. Effects of Heavy Metal Copper on the Biochemical Contents, Bioaccumulation and Histology of the Selected Organs in the Freshwater Fish, *Mystus Vittatus* (Bloch). Ph.D. Thesis, Annamalai University, India.

Rajamannar, K. and Manohar, L. 1998. Sublethal toxicity of certain pesticides on carbohydrates, proteins and amino acids in *Labeo rohita*. J. Ecobiol., 10(3): 185-191.

Rawat, D.K., Bais, V.S. and Agrawal, N.C. 2002. A correlative study on liver glycogen and endosulfan toxicity in *Heterpneustes fossilis*. J. Environ. Biol., 23: 205-207.

Roberts, M. and Boyce, C.B.C. 1972. In Methods in Microbiology. 7-A Edition. (eds: J.R. Norris and D.W. Ribbows). Academic Press, New York, pp 479.

Sastry, K.V. and Abad A Siddiqui. 1982. Chronic toxic effects of the carbamate pesticide Sevin on carbohydrate metabolism in a freshwater snakehead fish, *Channa punctatus*. Toxicology Letters, 14(1-2): 123-130.

Schmidt Nielson, B. 1975. Osmoregulation: Effect of salinity and heavy metal. Fed. Proc., 33: 2137-2146.

Searchy, D.G. and MacLennis, A.J. 1970a. Determination of DNA by the Barton Diphenylanine technique. In: Experiments and Techniques in Parasitology. (eds: A.J. Mac Lnnis and M. Voge) W.H. Freeman and Co, San-Franscisco, 190-191 pp.

Searchy, D.G. and MacLennis, A.J. 1970b. Determination of RNA by Dische orcinol technique. In: Experiments and Techniques in Parasitology. (eds: A.J. Mac Lennis and M. Voge). W.H. Freeman and Co, San-Francisco, pp. 189-190.

Shivanagouda, N., Sanagoudra and Bhat, U.G. 2013. Carbaryl induced changes in the protein and cholesterol contents in the liver and muscle of marine benthic fish, *Mugil cephalus*. American Journal of Biochemistry, 3(2): 29-33.

Singh, A. and Singh, A. 2017. Studies on toxicity stress, behavioural alterations and biochemical changes induced by glyphosate herbicide on the freshwater fish, *Channa punctatus* (Bloch). Int. J. Food Agricul. Veter. Sci., 7(3): 39-48.

Singh, R.K. and Sharma B. 1998. Carbofuran induced biochemical changes in *Clarias batrachus*. J. Pestic. Sci., 53: 285-290.

Srivastava, P. and Singh, A. 2013. In vivo study of effects of dithiocarbamates fungicide (mancozeb) and its metabolite ethylene thiourea (ETU) on freshwater fish *Clarius batrachus*. Journal of Biology and Earth Sciences, 3(2): B228-B235.

Tataji, P.B. and Kumar, M.V. 2016. Biochemical changes induced by Butachlor and Machete 50% EC to the freshwater fish *Channa punctata* (Bloch). International Journal of Science and Research, 5: 2048-2052.

Tilak, K.S., Raju, P.W. and Butchiram, M.S. 2009. Effects of alachlor on biochemical parameters of the freshwater fish, *Channa punctatus* (Bloch). J. Environ. Biol., 30(3): 421-426.

Veeraiah, K., Venkatrao, G., Vivek, Ch. and Hymaranjani, G. 2013a. Heavy metal, cadmium chloride induced biochemical changes in the Indian major *Cirrhinus mrigala* (Hamilton). Int. J. Bioassays, 2(07): 1028-1033.

Veeraiah, K., Vivek, Ch., Srinivas Rao, P. and Venkatrao, G. 2013b. Biochemical changes induced by Cypermethrin (10% EC), a pyrethroid compound in sub-lethal and lethal concentrations to the freshwater fish

Cirrhinus mrigala (Hamilton). J. Atoms and Molecules, 3(6): 625-634.
Vivek, Ch. 2015. Impact of Cartap Hydrochloride (50% SP) on Biochemical, Haematological and Enzymatic Activities of the Freshwater Fish, *Labeo Rohita* (Hamilton). Ph.D. Thesis submitted to Acharya Nagarjuna University, Nagarjuna Nagar, Guntur, A.P, India.
Wankhedkar, P. T. and Bhavsar, S.S. 2015. Effect of Cartap hydrochloride and Imidacloprid on biochemical parameters of *Cerastus moussonianus*. Biolife, 3(1): 125-131.

Eco. Env. & Cons. 26 (August Suppl. Issue) : 2020; pp. (S127-S131)

ISSN 0971–765X

Effect of Cartap hydrochloride (50% SP) insecticide on gill histology of the fish, *Cirrhinus mrigala* (Hamilton)

G. Vani[1]*, K. Veeraiah [2], M. Vijaya Kumar[1] and S.K. Parveen[1]

[1]Department of Zoology, SRR & CVR Government Degree College (A), Vijayawada 520 004, Krishna District, A.P., India
[2]Department of Zoology and Aquaculture, Acharya Nagarjuna University, Nagarjunanagar 522 510, Guntur, A.P., India

Received 26 October, 2019; accepted 3 February, 2020)

ABSTRACT

The fish, *Cirrhinus mrigala,* Indian major carp was exposed to Cartap hydrochloride and the static LC_{50}values for 24,48,72 and 96 hours were found to be 0.436, 0.419, 0.394 and 0.376 mg^{-1} and 0.399, 0.371, 0.361 and 0.339 mg^{-1} in Continuous flow-through system. The gills which are the primary organs to get exposed to foreign contaminants and pesticides were studied for histological changes. The following histological changes like epithelial lifting, degeneration of primary and secondary gill lamellae, curling of secondary gill filaments, atrophy of secondary gill lamellae, congestion of secondary lamellae, fusion of secondary gill filaments were observed. The results obtained were discussed at length with the available literature. By studying the histological deformities, it was concluded that the pesticide caused enough damage to the gills of the fish and can influence on the survival of the fish

Key words : *Cartap hydrochloride, Cirrhinus mrigala, Gill histopathology*

Introduction

Indiscriminate and extensive use of pesticides in modern agricultural practices globally for achieving increased food production is one of the major sources of water pollution. Presence of pesticide in aquatic bodies is largely due to outfall from pesticide manufacturing factories and the runoff from agricultural fields (Ganeshwade, 2012). Pesticides are not highly selective but are generally toxic to macrophytes, non-target organisms such as fish (Ayoola, 2008 and Franklin *et al*., 2010).

Fish accumulate these pollutants directly or indirectly from polluted waters and food chain (Jabeen *et al*., 2016). In India, Cartap hydrochloride, a carbamate pesticide is extensively used in rice, sugarcane cabbage and cauliflower crops to control pests. In fish, the gill is the major organ for respiration, excretion and osmotic regulation. Gills are appropriate for the assessment of environmental impact as they are considered as a good tissue indicator of the water quality (Fanta, 2003). Histopathological analysis is a very sensitive parameter and is helpful in determining cellular damage that may occur in target organs (Altinok and Capkin, 2007). In this viewpoint an attempt was made to study the effect of sublethal and lethal concentrations of Cartap hydrochloride on gill histopathology of freshwater fish, *Cirrhinus mrigala* exposed for 24 and 96 hours.

Materials and Methods

The fingerlings of the test fish *Cirrhinus mrigala* of size 6-8 ± ½ cm and weight 6-7 ± ½ gm were pro-

cured from local fish hatcheries of Nandivelugu, Tenali mandal, Guntur district, Andhra Pradesh. The fish were acclimated at (28±2°C)) in the laboratory conditions for two weeks. All the precautions laid down on recommendations of the toxicity tests to aquatic organisms were followed (Annon, 1975). Fish were regularly fed with rice bran and one day prior to the experimentation feeding was stopped. Fingerlings were exposed to sub-lethal ($1/10^{th}$ of 96 h LC_{50} value 0.0376 mg^{-1}) and lethal (96 hours LC_{50} value 0.376 mg^{-1}) concentrations of Cartap hydrochloride for 24 and 96 hrs.

Gills were processed in laboratory for routine histological characterization by the double staining method using Haematoxylene and Eosin. All samples were fixed in 10% phosphate- buffered formalin for about 24 hrs. The specimens were dehydrated in a series of graded ethanol (50%, 70% and 90%) and then after embedded in paraffin. Five-micron sections were cut using an ultramicrotome (Leica, Japan) and deparaffinized by means of xylol. The sections were dehydrated in 90%, 70% and 50% ethanol followed by a 10 min wash in water and further stained with Hematoxylin and Eosin (HE). Sections were observed in digital microscope (Intel Play QX3) at 400 x magnification.

Results

The transverse section of gill tissue of normal fish shows branches from the central axis called the primary gill lamellae. Each of the primary gill lamella further divides into secondary gill lamellae or filaments. Within each division of the gills are the adjacent afferent vessels and efferent vessels with hemocytes. A thin septum separates the primary and secondary gill filaments. The secondary non branching filament lamella possesses epithelial pillar cells separated by large lacunae Fig. 1.

Cartap hydrochloride has induced marked pathological changes in gills of fish *Cirrhinus mrigala*. In the current study, it was observed that with the increase in the time of exposure the histopathological alterations increased in the gills of fish, *Cirrhinus mrigala*.

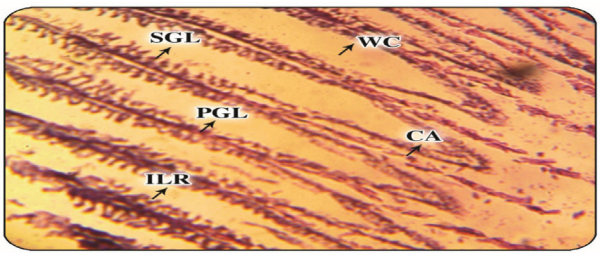

Fig. 1. Normal Gill tissue of *Cirrhinus mrigala*, H.E x 400

CA-Central Axis, PGL-Primary gill lamellae, SGL-Secondary gill lamellae, ILR-Inter lamellar space, WC-Water channel, FSG-Fusion of secondary lamellae, CSG-Curling of secondary lamellae, DPGL-Degenerated primary gill lamellae, DSGL-Degenerated secondary gill lamellae, BC-Blood congestion, EL-Epithelial lifting, LF-Lamellar fusion, ASL-Atrophy of secondary lamellae.

In the control group, no pathological changes were observed in the gills (Fig.1). After treatment with cartap hydrochloride for 24hrs at sublethal concentrationsepithelial lifting,curling of secondary gill filaments,fusion of secondary lamellae and degeneration of secondary gill lamellaestarted to appear (Fig. 2). Degenerative changes like lamellar fusion, epithelial lifting, degenerative secondary gill lamellae and curling of secondary gill filaments were observed after exposure to lethal concentration for 24hrs (Fig. 3). Similar more pronounced degenerative changes like curling of secondary gill filaments, epithelial lifting, degenerative primary and secondary gill lamellae, blood congestion, atrophy of secondary lamellae, mucous secretionwere no-

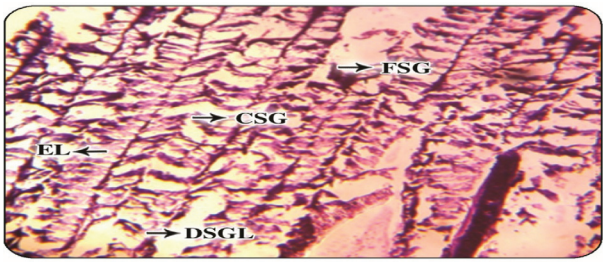

Fig. 2. Gill tissue of *Cirrhinus mrigala*exposed to sublethal concentration of Cartap hydrochloride for 24 hours, H.E x 400

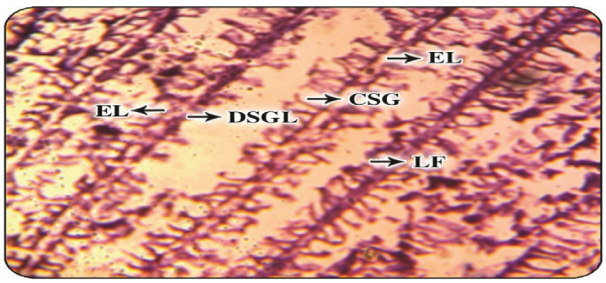

Fig. 3. Gill tissue of *Cirrhinus mrigala* exposed to lethal concentration of Cartap hydrochloride for 24 hours, H.E x 400

ticed in gill exposed to sublethal concentration of cartap hydrochloride for 96 hrs (Fig. 4). Damage in the gills exposed to lethal concentration of cartap hydrochloride for 96 hrs was much extensive with severe degeneration in primary and secondary gill lamellae, hemorrhage between gill filaments, separation of epithelial cells from the basement membrane, collapsed pillar cell, fusion of secondary gill lamellae, lamellar disorganization, atrophy of secondary lamellae, necrosis, blood congestion, mucous secretion, hyperplasia and epithelial lifting (Fig. 5). Thus, the lethal concentration of Cartap hydrochloride has produced significant histopathological changes in comparison to sublethal concentration in *Cirrhinus mrigala*.

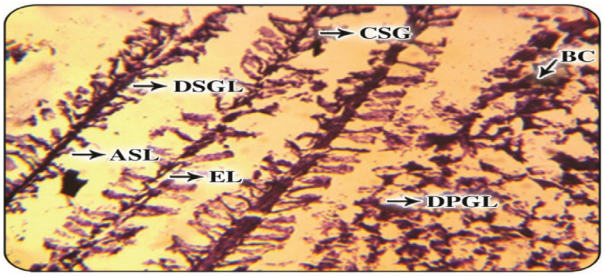

Fig. 4. Gill tissue of *Cirrhinus mrigala* exposed to sublethal concentration of cartap hydrochloride for 96 hours, H.E x 400

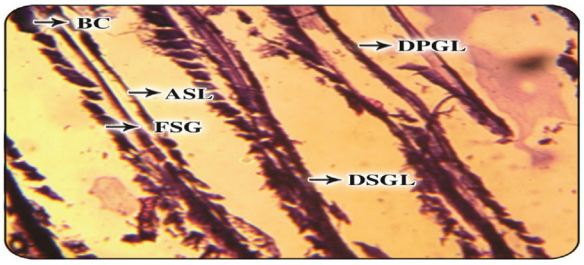

Fig. 5. Gill tissue of *Cirrhinus mrigala* exposed to lethal concentration of cartap hydrochloride for 96 hours, H.E x 400

Discussion

Several authors observed similar degenerative changes in gill when exposed to carbamate pesticides. Vivek *et al.*, (2016) observed fusion of primary and secondary lamellae, epithelial hyperplasia, curling of secondary lamellae, degeneration of lamellae in gills of *Labeo rohita* exposed to sublethal concentrations of cartap hydrochloride for 24,48,72 and 96hrs. Mariya dasu (2014) observed bulging of tips of primary gill filaments, curling of secondary gill filaments, necrosis, fusion of secondary gill lamellae, hyperplasia, hypertrophy of nuclei, pyknotic nuclei, lifting of epithelium in *Labeo rohita* exposed to Thiocarb, a thiocarbamate pesticide in both sublethal and lethal concentrations. Anitha (2015) observed necrosis, curling and fusion of secondary gill filaments, atrophy, degeneration of primary and secondary gill lamella, blood conjunction, epithelial hyperplasia, lamellar telangiectesis, in gills of *Labeo rohita* exposed to sublethal concentrations of Pyraclostrobin for 24 hrs, 5 days and 10 days and to lethal concentration for 24 hrs. Ali Taheri Mirghaed *et al*., (2018) noticed edema, lamellar curling, hyperplasia, lamellar fusion in the gill of *Cyprinus carpio* treated with 0.75 mg/L, 1.5 mg/L, and 3 mg/Lof indoxacarb for 7, 14 and 21 days. The histopathological changes observed in the present study were in accordance with the above studies.

Similar histopathological changes in gills were reported in *Channa punctatus* exposed to Imidacloprid (Pawara *et al.,* 2019), in *Labeo rohita* exposed to phenol (Butchiram *et al.,* 2013), in *Labeo rohita* exposed to cadmium (Saravanan *et al*., 2019), in *Oreochromis niloticus*exposed to heavy metals (Shameem Rani, 2018), in *Labeo rohita* exposed to tannery industrial effluent (Diana Handa and Gurinder Kaur Walia, 2019), in *Puntius sophore* treated with Acephate (Gavit and Patil, 2019), *in Cirrhinus mrigala* exposed to cement factory effluent (Juginu and Sujila, 2019) in *Cirrhinus mrigala*exposed to lead arsenate (Vanitha *et al.,* 2017), in *Labeo rohita* exposed to dimethoate (Dey and Saha, 2014), In *Cirrhinus mrigala* exposed to cypermythrin (Sree Veni and Veeraiah, 2014).

In fish, gill is the major organ for respiration, excretion and osmotic regulation. Gills are appropriate for the assessment of environmental impact as they are considered as a good tissue indicator of the water quality (Fanta, 2003). The lifting of lamellar epithelium in the present studymay be induced by the incidence of severe Oedema (Pane *et al.,* 2004). Swelling in gill epithelium leads to decreased efficiency of gases exchange and oxygen consumption. (Sudhasaravanan and Binukumari, 2015).

The first line of defense to metal/ toxicant exposure in the gills is mucus secretion and by fusion of lamellae it can temporarily protect the underlying epithelium from injury (Handy and Maunder, 2009). Pronounced secretion of mucus layer over the gill lamellae curtails the diffusion of oxygen (David *et al.*, 2002 and Rudragouda Marigoudar *et al*., 2009) which may ultimately reduce the oxygen consump-

tion by the animal (Kalavathy *et al*., 2001). All metabolic pathways depend upon the efficiency of the gills for their energy supply as gills are the major respiratory organs and damage to these vital organs lead to respiratory distress. The present histological studies clearly indicate that the damage in gills of *Cirrhinus mrigala* decreases the uptake of oxygen which results in histotoxic anoxia. Due to this the gill tissue suffers from oxygen debt and losses the capacity to remove CO_2 from blood which is in accordance with (Sathivel *et al*., 1991).

In the present study the observed alterations such as partial fusion of secondary lamellae, lifting of epithelial cells and proliferation of the epithelial cells, act as defense mechanisms towards toxicants. These alterations increase the distance between the external environment and the blood in the gills which serves as a barrier for the entry of contaminants. (Fernandes and Mazon, 2003 and Mallatt, 1985). When any type of toxicants meets gills, lamellar fusion in gills occur which is a protective measure as it diminishes the amount of vulnerable gill surface area in fish (Mallatt, 1985). when gills come in contact withany types of toxicants oedema appears to be a common feature of the gill pathology. Due to disturbance in branchial Na+, K+-ATPase pump by toxicants, solute accumulation in the epithelial cells occur and disturb the osmotic influx of water. This exchange protects the lamellar epithelial cells and prevents the entry of waterborne pollutants into the bloodstream (Arellano *et al*., 1999).

Conclusion

The results of the present study suggest that the changes in gill histomorphology of *Cirrhinus mrigala* may serve as a rapid biological 7monitor to assess the impact of Cartap hydrochloride on other biotic communities in the water body. The results of the present study also stress on the diligent usage of the pesticide product to prevent the environmental pollution.

Acknowledgements

The authors are thankful to the UGC SAP-DRS-III for extending the infrastructure facilities to carry out the present work in the Laboratories of the Dept. of Zoology & Aquaculture. They also thank the Head, Department of Zoology and Aquaculture for permitting to do the work.

References

Ali Taheri Mirghaed., Melika Ghelichpour., Seyed Saeed Mirzargar., Hamidreza Joshaghani. and Hoseinali Ebrahimzadeh Mousavi, 2018. Toxic effects of indoxacarb on gill and kidney histopathology and biochemical indicators in common carp (*Cyprinus carpio*). *Aquaculture Research*. 49(4) : 616-1627.

Altinok, I. and Capkin, E. 2007. Histopathology of rainbow trout exposed to sublethal concentrations of methiocarb or endosulfan. *Toxicol Pathol*. 35 : 405–10.

Anitha, A. 2015. *Pyraclostrobin (20%WG) induced toxicity and biochemical aspects of freshwater fish Labeo rohita* (Hamilton) Ph.D. Acharya Nagarjuna University. Nagarjuna Nagar, Guntur, A.P, India.

Annon, 1975. Committee on methods of toxicity tests with fish macro invertebrates and amphibians. EPA. Oregon: 61.

Arellano, J. M., Storch, V. and Sarasquete, C. 1999. Histological changes and copper accumulation in liver and gills of the *Senegales sole, Solea senegalensis. Ecotoxicology and Environmental Safety*. 44 : 62-72.

Ayoola, S.O. 2008. Toxicity of glyphosate herbicide on Nile tilapia (*Oreochromis niloticus*) juvenile. *Afr. J. Agric. Res*. 3 (12): 825-834.

Butchiram, M.S., Vijaya Kumar, M. and Tilak, K.S. 2013. Studies on the histopathological changes in selected tissues of fish *Labeo rohita* exposed to phenol. *Journal of Environmental Biology*. 34: 247-51.

David, M., Mushigari, S. B. and Prashanth, M. S. 2002. Toxicity of fenvalerate to the freshwater fish. *Labeo rohita. Geobios*. 29 : 25-28.

Dey Chandrimaand Saha Samir Kumar, 2014. Dimethoate (30% EC) induced toxicities on the tissues of the Indian major carp: *Labeo rohita* (Hamilton). *International Journal of Fisheries and Aquatic Studies*. 1(6) : 232-236.

Diana Handa. and Gurinder Kaur Walia. 2019.Quantitative and Semi-quantitative analysis on Gills of a freshwater fish, *Labeo rohita* (Hamilton-Buchanan, 1822) exposed to Tannery industrial effluent using histopathology as biomarker. *IJRAR*. 6(1): 980-981.

Fanta, E., Rios, F.S., Romao, S., Vianna, A.C.C. and Freiberger, S. 2003. Histopathology of the fish *Corydoras paleatus* contaminated with sublethal levels of organophosphorus in water and food. *Ecotoxicology and Environmental Safety*. 54(2) : 119-130.

Fernandes, M.N. and Mazon, A.F. 2003. Environmental Pollution and Fish Gill Morphology. In: Val, A.L. and Kapoor, B.G., Eds., Fish Adaptation. Science Publishers, Enfield: 203-231.

Franklin R. K., Loo, H. S. and Osumanu, H. A. 2010.Incorporation of Bentazone with Exserohilumrostratum for Controlling *Cyperusiria. Am. J. Agri. Biol. Sci*. 5: 210-214.

Gavit, P. J. and Patil, R. D. 2019. Effect of Acephate (Organophosphate) on Gill Histology of the Fresh Water Fish *Puntius sophore* (Hamilton). *IJRAR*. 6(1): 338-342.

Ganeshwade, R.M. 2012. Histopathological changes in the gills of *Puntius Ticto* (Ham) under dimethoate toxicity. *The BioScan*.7(3) : 423-426.

Handy, R. D. and Maunder, R. J. 2009. The biological roles of mucus: Importance for osmoregulation and osmoregulatory disorders of fish health. In: *Osmoregulation and Ion Transport: Integrating Physiological, Molecular and Environmental Aspects*. Society for Experimental Biology Press, London. I: 203- 235.

Jabeen, F., Chaudhry, A.S., Manzoor, S. and Shaheen, T. 2016. Carbamates and neonicotenoids in Fish, water and sediments from the Indus River for potential health risks. *Environ. Monit. Assess*. 187 (2) : 29.

Juginu, M. S. and Sujila, T. 2019. Histopathological responses of gill, liver and kidney in the freshwater fish, *Cyrrhinus mrigala* exposed to cement factory effluent. *Wjpps*. 8 (8) : 1511-1530.

Kalavathy, K., Siva Kumar, A.A. and Chandran, R. 2001. Toxic effects of the pesticide dimethoate on the fish, *Sarotherodon mossambicus*. *J. Ecol. Res Bio*. 2 : 27-32.

Mallatt, J. 1985. Fish gill structural changes induced by toxicants and other irritants: a statistical review. *Canadian Journal of Fisheries and Aquatic Science*. 42(4): 630-648.

Mariya Dasu, P. 2014. *Thiocarb 75 percentage WP a carbamate insecticide induced toxicity biochemical and histopathological changes in the freshwater Indian major carp Labeo rohita* Hamilton, Ph.D. Thesis, Acharya Nagarjuna University, Nagarjuna Nagar, Guntur, A.P, India.

Pane, E.F., Haque, A. and Wood, C.M. 2004. Mechanistic analysis of acute, induced respiratory toxicity in the rainbow trout, *Oncorhynchus mykiss*: an exclusively branchial phenomenon. *Aquatic Toxicology*. 69 : 11-24.

Pawara., Ravindra, H., Patel Nisar, G. and Sarvade Raju, C. 2019.Study on the effect of Imidacloprid on gill tissue of the fish *Channa punctatus* (Perciformes: Channidae) (Bloch.). *IJRAR*. 6 (1): 372-378.

Rudragouda Marigoudar, S., Nazeer Ahmed, R. and David, M. 2009. Cypermethrin induced respiratory and behavioral responses of the freshwater teleost, *Labeo rohita* (Hamilton). *Veterinarski Arhive*. 79(6): 583-590.

Sakthivel., Sampath, K. and Pandian, T.J. 1991. Sublethal effects of textile dye stuff effluent on selected oxidative enzymes and tissue respiration of *Cyprinus carpio* (Linn). *Indian J. Expt. Biol*. 29 : 979-981.

Saravanan, K., Mohanambal, R. and Iyyappan, A. 2019. Effect of cadmium on the histology of gill, liver and hepatopancreas of freshwater fish *Labeo rohita* (Hamilton, 1822). *IJRAR*. 6 (1) : 1255-1263.

Shameem Rani, K. 2018. Histological studies and heavy metal accumulation in the gills and muscles of tilapia fish from Vellar estuary, South East Coast of India, Tamilnadu. *IJRAR*. 5(3) : 298-304.

Sree Veni, S.M. and Veeraiah, K. 2014. Effect of Cypermethrin (10%EC) on Oxygen Consumption and Histopathology of Freshwater Fish *Cirrhinus mrigala*(Hamilton). *IOSR J. Environ. Sci., Toxicol. Food Technol*. 8(10) : 12–20.

Sudhasaravanan, R. and Binukumari, S. 2015. Effects of different concentartions of detergent on dissolved oxygen consumption in *Lepidocephalichythyes thermalis*. *World Journal of Pharmaceutical Research.* (2): 940-945.

Vanitha, S., Amsath,A., Shanthi,P. and Muthukumaravel, K. 2017. Sublethal effects of lead Arsenate on histology of selected organs of freshwater fish, *Cirrhinus mrigala*. *International Journal of Zoology and Applied Biosciences*. 2(5): 250-257.

Vivek, Ch., Veeraiah, K., Padmavathi, P. Dhilleswara Rao, H. and Bramhachari, P.V. 2016. Acute toxicity and residue analysis of cartap hydrochloride pesticide: Toxicological implications on the fingerlings of freshwater fish *Labeo rohita*. *Biocatalysis and Agricultural Biotechnology*. 7 : 193-201.

Eco. Env. & Cons. 27 (November Suppl. Issue) : 2021; pp. (S218-S225)
Copyright@ EM International
ISSN 0971–765X

Acute toxicity and effect of Flubendiamide (39.35% SC) on the oxygen consumption of the Fish, *Catla catla* (Hamilton)

S.K. Parveen*[1], K. Veeraiah[2], G. Vani[1] and M. Vijaya Kumar[1]

[1]Department of Zoology, SRR & CVR Government Degree College (A), Vijayawada 520 004, Krishna District, A.P., India
[2]Department of Zoology and Aquaculture, Acharya Nagarjuna University, Nagarjunanagar 522 510, Guntur, A.P., India

(Received 10 March, 2021; Accepted 18 May, 2021)

ABSTRACT

The fish *Catla catla* fingerlings were exposed to the test toxicant an insecticide Flubendiamide for 24, 48, 72 and 96 hrs and the LC_{50} values were calculated and were reported to be 3.566, 3.456, 3.0221 and 2.892 mg5^{-1} respectively for 24, 48, 72 and 96 hrs. After determination of LC_{50} values the fish were exposed to sub-lethal concentration ($1/10^{th}$ of 96 hrs LC_{50} value i.e., 0.289 mg5′¹) for 24, 48, 72, 96 hrs and 8 days and the changes in oxygen uptake of the Indian major carp *Catla catla* was studied. Fingerlings were exposed to sub-lethal (0.289 mg5^{-1}) and lethal (2.892 mg5′¹) concentrations of flubendiamide for 24 hrs, 48 hrs, 96 hrs and only to the sub-lethal concentration exposed for 8 days. In both sub-lethal and lethal concentrations for all exposed periods *Catla catla* showed an increase in oxygen consumption during the initial time of exposure and a gradual decrease during the subsequent periods of exposures. This initial increase was from 0-6 hours in 24, 48 and 96 hrs where as in 8 days exposed fish the initial increase is only up to 0-4 hours. Alterations in oxygen consumption may be due to respiratory distress as a consequence of impaired oxidative metabolism. In the present study it was observed that flubendiamide has altered respiratory metabolism in the test fish *Catla catla* which can be used as a bio-indicator for assessing pesticide induced alterations in the uptake of oxygen in the fish. Fish in the sub-lethal concentration were found under stress, but that was not fatal. The results obtained in all were discussed with the available literature.

Key words: *Flubendiamide, Catla catla, LC_{50} Values, and Oxygen consumption.*

Introduction

After green revolution during sixties especially in India, pesticides emerged as knight armours for crops (Srivastava and Singh, 2014). Pesticides has credited with economic potential to enhance production of food and fibre and ameliorated in vector-borne diseases, the long-term use has caused effects on human health and the environment including aquatic ecosystem that evolved new branch of aquatic toxicology (Igbedioh, 1991; Forget, 1993; Aktar *et al.*, 2009). Pesticides have been found to be highly toxic not only to fish but also to the other organisms which constitute the food chain. Agricultural run-off from near water bodies is the major cause of deposition of pesticides in aquatic ecosystem. The qualitative and quantitative chemical usage is of great concern ecologically. The discriminate use of chemicals is for the control of insect pests by elimination of target species whereas indiscrimi-

nate usage posed the problem on non-target organisms including man.

Wide and indiscriminate use of pesticides in modern agricultural practices throughout the world has indirectly created problem of pollution of aquatic ecosystems (Ganeshwade, 2012). These chemicals impair water quality which becomes unsuitable for all aquatic organisms due to their toxicity, persistence, bioaccumulation, and biomagnifications in food chain and ecological balance (Subramani Lavanya *et al.*, 2011). Fish accumulate these pollutants directly or indirectly from polluted waters and food chain (Jabeen *et al*., 2016).

Mass mortality of fish due to pesticide exposure is rare, and results only from accidents or direct spraying of the water bodies. Fish are the most often tested aquatic organisms because they are the most conspicuous as predominant and are economically important to man because they are linked in the food chain. Evaluation of LC_{50} is the pioneer step in toxicological assessment of any chemical. It helps to select sub-lethal concentrations to carry out several toxicity tests. Therefore, this knowledge is essential for exploring impacts of any chemical on physical and physiological status of exposed organisms.

In India, flubendiamide, a rynoid pesticide is extensively used in rice and pulse crops to control pests. The excess pesticides used in the farms reach the water bodies by the surface run off and are known to cause ill effects on aquatic organisms. One of the indicators of the health status of a fish is its total oxygen consumption. It helps in evaluating the susceptibility or resistance potential useful to assess the physiological condition of an organism and to correlate the behaviour of the animal, which ultimately serve as predictors of functional disruptions of population. Hence, the analysis of total oxygen consumption can be used as a tool of bio-indicator system to evaluate the basic damage caused to the animal which could either decrease or increase the oxygen uptake (Maharajan *et al.,* 2013). In this viewpoint an attempt was made to study the effect of sub-lethal and lethal concentrations of flubendiamide on oxygen consumption of freshwater fish, *Catla catla* exposed for 24, 48, 96 hrs, and only sub-lethal concentration for 8 days.

Materials and Methods

The fingerlings of the test fish *Catla catla* of size 6-8 ± ½ cm and weight 6-7 ± ½ gm were procured from local fish hatcheries of Nandivelugu, Tenali mandal, Guntur district, Andhra Pradesh. The fish were acclimated at (28±2°C) in the laboratory conditions for two weeks. All the precautions laid down on recommendations of the toxicity tests to aquatic organisms were followed (Annon, 1975). Fish were regularly fed with rice bran and one day prior to the experimentation feeding was stopped. Experiments on the oxygen consumption of the fish *Catla catla* was carried out in a respiratory apparatus developed by Job (1955). Fish were exposed to sub-lethal ($1/10^{th}$ of 96 hrs LC_{50} value 0.289 $mg5^{\sim 1}$) and lethal (96 hrs LC_{50} value 2.892 $mg5^{\sim 1}$) concentrations of Flubendiamide for 24, 48, 72 and 96 hrs and only for sub-lethal concentration for 8 days. The samples for estimation of oxygen, consumption were taken from the respiratory chamber, at alternate hours of intervals for 24 hrs. The amount of dissolved oxygen consumption was calculated per gram body weight per hour. The dissolved oxygen content was estimated by modified Winkler's method as described by Golterman and Clymo (1969). The difference in the dissolved oxygen content between initial and final water samples represents the amount of oxygen consumed by the fish. Students, "t-test" was employed to calculate the significance of the differences between control and experimental means. P values of 0.05 or less were considered statistically significant (Fisher, 1950).

Results

Toxicity

The calculated LC_{50} values for 24, 48, 72 and 96 hrs to the test fish *Catla catla* were presented in Table 1 and graphically represented in Figure 1. The LC_{50} values obtained were 3.566, 3.456, 3.0221 and 2.892 $mg5^{\sim 1}$ respectively for 24, 48, 72 and 96 hrs. The LC_{50} values decreased with the increase in the period of exposure.

The toxicity may be influenced by exposure conditions, source and size of fish, formulation, and water quality. The ground water used for acclimatization of fish and experimental purpose was clear and unchlorinated. The hydrographical properties of water were estimated by the modified methods of Golterman and Clymo, (1969).

Oxygen Consumption

Determination of oxygen consumption by the fish is

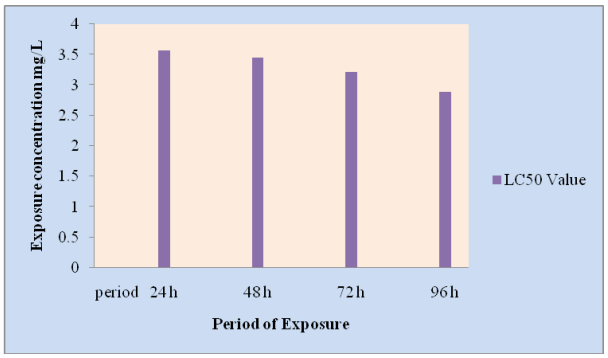

Fig. 1. Calculated LC_{50} values for flubendiamide to the fish *Catla catla* under static exposure for 24, 48, 72 and 96 hrs.

an important indicator which reflects physiological state of animal and is useful for assessment of lethal effects (Tilak *et al.*, 2007). One of the indicators of the health status of a fish is its total oxygen consumption. It helps in evaluating the susceptibility or resistance potential useful to assess the physiological condition of an organism and to correlate the behavior of the animal, which ultimately serves as predictors of functional disruptions of population (Maharajan *et al.*, 2013). Oxygen consumption is an important physiological parameter which can be used as a useful measure of toxic effects of pesticides in sub-lethal and lethal concentrations because energy processes are indicators of overall physiological state of organism. Changes in the respiratory activity in fish have been used by several investigators as indicator of response to environmental stress (Ram Nayan Singh, 2014; Sudhasaravanan and Binukumari, 2015; Neelima *et al.*, 2016; Adnan Amin *et al.*, 2017).

Exposure to sub-lethal concentrations of toxicant is reported to increase respiratory activity, leading to increased ventilation and hence increased uptake of the toxicant. The comparative data of the whole animal oxygen consumption in control and experimental fish, *Catla catla* calculated per gram body weight per hour in sub-lethal and lethal concentrations of flubendiamide for 24, 48, and 96 hrs and 8 days were given in the Tables 2 and 3 and graphically represented in Figures 2 and 3.

The results of the experimental and control fish values are graphically represented in Figures 2 and 3 by taking hours of exposure on X axis and the amount of oxygen consumed per gram body weight per hour on Y axis. In sub-lethal concentrations of flubendiamide, it was observed that the fish showed increase in oxygen consumption during the initial time of exposure i.e., 0-6 hours in 24 and 48 hrs treated fish and 0-4 hours in 96 hrs and 8 days exposed fish and thereafter a gradual decrease was observed in the subsequent periods of exposure. The

Table. 1. Calculated LC_{50} values of flubendiamide to the fish *Catla catla* under static exposure for 24, 48, 72 and 96 hrs

S. No.	Test Fish	Exposure period	Concentration in mg/L	Log Conc.	No. of fish exposed	Percent mortality	Probit Mortality	LC_{50} Value
1	*Catla catla*	24 h	3.20	0.51	10	20	4.16	3.566
2			3.40	0.53	10	30	4.48	
3			3.60	0.56	10	60	5.25	
4			3.80	0.58	10	70	5.52	
5			4.00	0.60	10	80	5.84	
6		48 h	3.00	0.48	10	20	4.16	3.456
7			3.20	0.51	10	30	4.48	
8			3.40	0.53	10	50	5.00	
9			3.60	0.56	10	60	5.25	
10			3.80	0.58	10	70	5.52	
11		72 h	2.80	0.45	10	10	3.72	3.221
12			3.00	0.48	10	30	4.48	
13			3.20	0.51	10	50	5.00	
14			3.40	0.53	10	70	5.52	
15			3.60	0.56	10	80	5.84	
16		96 h	2.60	0.41	10	20	4.16	2.892
17			2.80	0.45	10	40	4.75	
18			3.00	0.48	10	60	5.25	
19			3.20	0.51	10	80	5.84	
20			3.40	0.53	10	90	6.28	

Table 2. Changes in oxygen consumption of the fish *Catla catla* under exposure to lethal and sub-lethal concentrations of flubendiamide for 24 and 48 hrs.

Hours	Control	24 Sub-lethal	24 Lethal	48 Sub-lethal	48 Lethal
0	0.795±0.0032	0.886±0.0038	0.874±0.0042	0.83±0.0040	0.846±0.0026
2	0.781±0.0045	1.436±0.0036	1.482±0.0046	1.428±0.0038	1.576±0.0048
4	0.770±0.0035	1.424±0.0042	1.454±0.0042	1.454±0.0042	1.592±0.0042
6	0.761±0.0041	1.406±0.0044	1.436±0.0040	1.474±0.0046	1.602±0.0044
8	0.754±0.0045	0.988±0.0044	0.922±0.0046	0.988±0.0046	0.932±0.0042
10	0.742±0.0043	0.83±0.0036	0.864±0.0044	0.892±0.0038	0.856±0.0038
12	0.736±0.0040	0.678±0.0040	0.688±0.0046	0.658±0.0036	0.626±0.0042
14	0.734±0.0044	0.548±0.0038	0.444±0.0038	0.454±0.0038	0.396±0.0038
16	0.732±0.0036	0.534±0.0036	0.42±0.0040	0.436±0.0044	0.364±0.0044
18	0.730±0.0042	0.515±0.0042	0.398±0.0042	0.388±0.0044	0.326±0.0046
20	0.725±0.0034	0.488±0.0034	0.378±0.0034	0.368±0.0046	0.292±0.0036
22	0.720±0.0044	0.466±0.0044	0.356±0.0044	0.356±0.0044	0.266±0.0044

Results are mean values of four observations
Standard Deviation is indicated as (±)
Values are significant at $p < 0.05$

Table 3. Changes in oxygen consumption of the fish *Catla catla* under exposure to lethal and sub-lethal concentrations of flubendiamide for 96 hrs and only for sub-lethal concentration for 8 days.

Hours	Control	96 h Sub -lethal	96 Lethal	8 d Sub-lethal
0	0.757±0.0032	0.829±0.0048	0.846±0.0026	0.456±0.0040
2	0.782±0.0046	0.846±0.0038	0.788±0.0046	0.460±0.0038
4	0.770±0.0035	0.857±0.0049	0.850±0.0042	0.388±0.0042
6	0.761±0.0041	0.634±0.0046	0.606±0.0040	0.407±0.0046
8	0.753±0.0046	0.784±0.0048	0.726±0.0046	0.394±0.0046
10	0.741±0.0044	0.594±0.0036	0.556±0.0034	0.386±0.0038
12	0.736±0.0042	0.564±0.0040	0.526±0.0036	0.401±0.0036
14	0.735±0.0045	0.456±0.0038	0.398±0.0038	0.378±0.0038
16	0.733±0.0034	0.439±0.0046	0.366±0.0040	0.356±0.0044
18	0.730±0.0042	0.288±0.0042	0.284±0.0042	0.309±0.0044
20	0.725±0.0034	0.266±0.0046	0.290±0.0034	0.298±0.0046
22	0.719±0.0044	0.256±0.0044	0.256±0.0044	0.276±0.0044

Results are mean values of four observations
Standard Deviation is indicated as (±)
Values are significant at $p < 0.05$

presence of sub-lethal concentration of toxicant is aquatic environment is inevitable. The toxicant stress on oxygen consumption along with depletion in oxygen in aquaculture practices makes fish less fit and reduces their growth due to lack of proper metabolism (Hyma Ranjani, 2015 and Bantu *et al*., 2017). In lethal concentrations of flubendiamide, it was observed that a gradual increase in oxygen consumption during the initial time of exposure i.e., 0 to 6 hours in 24 and 48 hrs treated fish and 0 to 4 hours in 96 hrs and 8 days exposed fish and a gradual decline is observed during the later periods of exposure. In control fish the rate of oxygen consumption gradually decreased and this might be due to starved conditions and the reduced metabolic rates of the starved fish (Anitha, 2015). From the present study it is clear that the flubendiamide affected oxygen consumption of *Catla catla* under all hours of exposure in both sub-lethal and lethal concentrations.

Discussion

Several authors have reported the effect of Rynoid pesticides on the oxygen consumption in fish. Mariya Dasu (2014) observed initial increase in oxy-

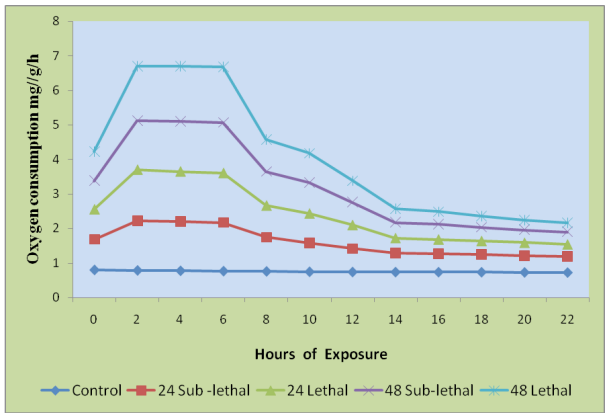

Fig. 2. Changes in oxygen consumption of the fish *Catla catla* under exposure to lethal and sub-lethal concentrations of flubendiamide for 24 and 48 hrs.

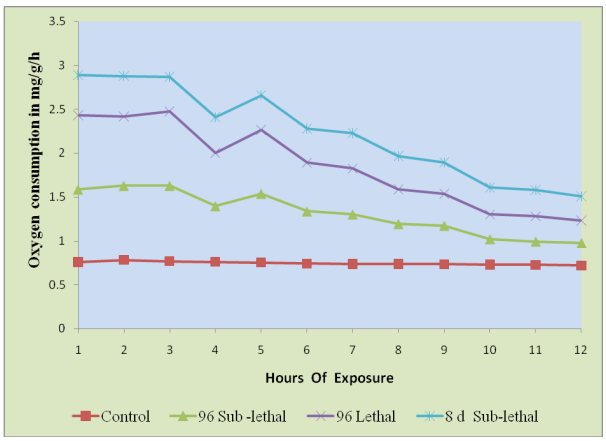

Fig. 3. Changes in oxygen consumption of the fish *Catla catla* under exposure to lethal and sub-lethal concentrations of flubendiamide for 96 hrs and sub-lethal concentration for 8 days.

gen consumption in *Labeo rohita* exposed to Thiocarb. Anitha (2015) also observed increase in oxygen consumption during the initial time of exposures, i.e. 1 to 6 hours and a gradual decrease was observed during the subsequent period of study in *Labeo rohita* exposed to Pyraclostrobin. In lethal concentrations the rate of oxygen consumption showed a decreasing trend from the beginning to the end. Bantu *et al.*, (2017) observed increase in oxygen consumption during the initial time of exposures i.e., 1 to 4 hours and a gradual decrease during the subsequent period in *Labeo rohita* exposed to sublethal concentrations of Indoxacarb for 24 hrs and 8 days. Oxygen consumption decreased in *Labeo* during exposure to lethal concentrations of indoxacarb for 24 hrs.

The initial increase in oxygen consumption in the present study is in agreement with Neelima *et al.*, (2016) in *Cyprinus carpio* exposed to cypermethrin. Jothinarendiran (2012) in *Channa punctatus* exposed to dimethoate, Bantu *et al.*, (2017) in *Labeo rohita* exposed Indoxacarb, Tilak and Vijaya Kumar (2009) in *Channa punctatus* exposed to Quinaphos, Veeraiah (2001) in *Labeo rohita* exposed to Cypermethrin, Hyma Ranjani (2015) in *Catla catla* exposed to Glyphosate. The present work coincides with the reports of the same. The initial increase in oxygen uptake in sub-lethal concentration might be the reflection of an augmented physiological activity for elimination acting the chemical stress (Tilak and Vijaya kumar, 2009). Due to stress, muscular activity increases which results in an increased demand for oxygen. The increase in activity might boost up oxidative metabolism which results in increased supply of energy to combat the chemical stress (David *et al.*, 2003). Sree Veni and Veeraiah (2014) reported that due to stress there is increased respiratory activity resulting in increased ventilation and increased uptake of the toxicant in *Cirrhinus mrigala* exposed to cypermethrin. Several authors (Veenethkumar and David, 2008; Shereena *et al.*, 2009; Logaswamy and Remia, 2009) reported that alteration in whole animal oxygen consumption is due to the disturbance in oxidative metabolism in different species of fish exposed to pesticides. During the initial hours of exposure elevation in the rate of respiration could be explained in terms of acceleration of oxidative metabolism, as a result of sudden response to the toxic stimulus of the pesticide. With the onset of symptoms of poisoning, probably due to acclimatization to the chemical environment the rate decreased in the later periods of exposure. Similar observations were also made by Neelima *et al.* (2016) and Jothinarendiran (2012). Vani *et al.* (2020) also reported that their is an initial increase in oxygen consumption of fish *Cirrhinus mrigala* (Hamilton) with the effect of carbamate Cartap hydrochloride (50% SP) and gradually decreased. The results of the present study agree with above findings.

As the pesticides stimulate the peripheral nervous system, the activity of fish increases which requires more oxygen to fulfill the energy demand. This could be the reason for initial elevation in the rate of oxygen consumption (Rao, 1989). In sub lethal medium, in the subsequent period of exposure the respiration rate of fish decreased which might be

due to acclimatization of the fish in the chemical environment (Rao, 1989 and Neelima *et al.,* 2016). Under toxic conditions, the oxygen in take decreases and a number of poisons become more toxic, so the amount of poison being exposed to the animal also increases. Fish breath more rapidly and the amplitude of respiratory movements will increase (Vakita Venkata Rathnamma and Nagaraju Bantu, 2014). By triggering the process of detoxification, the fish might have overcome the pesticide toxicity. In the later period the decrease in oxygen consumption appears to be a protective measure to ensure that there is low intake of the toxic substances which agrees with the findings of Tilak and Vijaya Kumar (2009). Subsequent decrease in oxygen consumption may be due to increased entry of flubendiamide molecules or their accumulation in the body of fish as a function of time. In sub-lethal concentrations of the flubendiamide the decrease in oxygen consumption appears to be mainly due to lowering down of energy requirements which can be considered as adaptive and even strategic this is in accordance with findings of Tilak and Vardhan, (2002). Depletion in the oxygen consumption is due to disorganization of the respiratory action caused by rupture in the respiratory epithelium of the gill tissue and also secretion of mucus over the gill curtails the diffusion of oxygen (Neelima *et al*., 2016).

Decreased oxygen consumption was observed by Maharajan *et al.,* (2013) in *Catla catla* exposed to Profenofos, by Vakita Venkata Rathnamma and Nagaraju Bantu (2014) in *Labeo rohita* exposed to Chlorantraniliprole, by Jipsa *et al.,* (2014) in *Tilapia mossambica* exposed to Cypermethrin, by Anthony Reddy (2015) in *Labeo rohita* exposed to Spinosad. Joshi and Kulkarni (2007) reported that *Garra mullya* (Skyes) when exposed to Cypermethrin and Fenvalerate, oxygen consumption increased in the initial period in both lethal and sub lethal concentrations and thereafter decreased. They concluded that alteration in oxygen consumption increased and later decreased which is a bio-indicator for assessing the pesticide toxicity, which can be correlated with the present study.

Mucus secretion in fish forms a barrier between the body irritating effects, or to eliminate it through epidermal mucus. Similar observations were made by Rao *et al*. (2003) and Parma De Croux *et al.* (2002) in *Prochilodus lineatus* under monocrotophos stress. Opercular movements increased initially in all exposure periods but decreased later steadily in lethal compared to sub lethal exposure periods. The increased opercular gill movements observed initially may possibly compensate for increased physiological activity under stressful conditions (Shivakumar and David, 2004). Gulping of air at the surface, swimming on the water surface, disrupted shoaling behaviour and easy predation was seen on the first day itself in lethal and sub-lethal exposure periods and continued the same more intensely, which is in accordance with the observations made by Ural and Simsek (2006). Gulping of air may help to avoid contact with the toxic medium. Surfacing phenomenon i.e., significant preference of upper layers the exposure period (Katja *et al.,* 2005). Finally fish sank to the bottom with the least opercular movements and died with their mouths open.

Under sub-lethal exposure, the fish bodies became lean towards the abdomen position compared to the control fish and they were found to be under stress, but this was not fatal. Leanness in fish indicates a reduced amount of dietary protein consumed by the fish under pesticide stress which is immediately utilized and not stored as body mass (Kalavathy *et al.,* 2001).

From the above results and discussion, it can be concluded that decrease in oxygen consumption in fish in response to the toxic stress is the cumulative effect of several stages at which the toxicant act. From the results obtained, it is clearly evident that flubendiamide affect the oxygen consumption of *Catla catla* in all exposed concentrations.

Conclusion

In conclusion, the analysis of data from the present investigation demonstrated that flubendiamide had a profound impact on respiration in *Catla catla* in both sub-lethal and lethal concentrations. Variation in the oxygen consumption in flubendiamide exposed fish was probably due to impaired oxidative metabolism and pesticide induced stress. Changes in gill architecture under flubendiamide stress would alter the diffusing capacity of gill with consequent hypoxic or anoxic conditions thus respiration may become a problematic task for the fish. These results suggest that the altered rates of respiration in *Catla catla* may also serve as a rapid biological monitor to assess the impact of pesticides such as flubendiamide on other biotic communities in the water body. This study also stresses the diligent use of pesticides to prevent environmental pollution.

Acknowledgements

The authors are thankful to the UGC for extending the infrastructure facilities to carry out the present work in the laboratories of the Dept. of Zoology & Aquaculture under UGC SAP DRS Phase-III and also thankful to the Head, Department of Zoology and Aquaculture for permitting to do the work.

References

Adnan Amin, Ramachandra Naik, A.T., Nilma Priyadarshini, Harsha Nayak and Sruthi Sree, C. 2017. Toxic effect of heavy metal lead on oxygen consumption of rohu (*Labeo rohita*) fingerlings. *Biochem. Cell. Arc,*. 17(1) : 225-228.

Aktar, W., Sengupta, D. and Chowdhury, A. 2009. Impact of pesticides use in agriculture their benefits and hazards. Interdiscip. *Toxicol.* 2 : 1-12.

Anon, 1975. Committee on methods of toxicity tests with fish macro invertebrates and amphibians. *EPA, Oregon.* 61.

Anitha, A. 2015. *Pyraclostrobin (20% WG) induced toxicity and biochemical aspects of freshwater fish Labeo rohita* (Hamilton). *Ph.D. Thesis,* submitted to Acharya Nagarjuna University. Nagarjuna Nagar, Guntur, A.P, India.

Anthony Reddy, P. 2015. *Impact of Spinosad (45% SC, Tracer) a biopesticide compound on freshwater fish, Labeo rohita* (Hamilton) *Ph.D. Thesis*, submitted to Acharya Nagarjuna University, Nagarjuna Nagar, Guntur, A.P, India.

Bantu, N., Hagos, Z. and Krishna, C., Gopla Krishnan; Abaynew; Rathnamma and Ravibabu. 2017. Acute toxicity and respiratory responses in freshwater fish, *Labeo rohita* exposed to an agrochemical Indoxacarb. *Algerian Journal of Environmental Science and Technology.* 3(3-B) : 595-603.

David, M., Shivakumar, H.B., Shivakumar, R. Mushigeri, S.B. and Ganti, B.H. 2003. Toxicity evaluation of cypermethrin and its effect on oxygen consumption of the freshwater fish , *Tilapia mossambica. Indian J. of Environ. Toxicol.* 13 : 99-102.

Fisher, R.A. 1950. *Statistical Methods for Research Workers.* 11th edition, Edinburgh UK: Oliver and Boyd Ltd.

Forget, G. 1993. Balancing the need for pesticides with the risk to human health. In: *Impact of Pesticide Use on Health in Developing Countries* (eds. Forget G, Goodman T and De Villiers A.): 2-16. IDRC, Ottawa.

Ganeshwade, R.M. 2012. Histopathological changes in the gills of *Puntius Ticto* (Ham) under dimethoate toxicity. *The Bio Scan.* 7(3) : 423–426.

Golterman, H. and Clymo. 1969. Methods for Chemical Analysis of Fresh Water. *Black well Scientific Publication.* 166.

Hyma Ranjani, G. 2015. *Glyphosate (Glycil 41% SL) a systemic herbicide impact on biochemical and histopathological changes in the freshwater fish Catla catla* (Hamilton). *Ph.D Thesis,* submitted to Acharya Nagarjuna University. Nagarjuna Nagar, Guntur, A.P, India.

Igbedioh, S.O. 1991. Effects of agricultural pesticides on humans, animals and higher plants in developing countries. Arch. *Environ. Hlth.* 46 : 218-224.

Jabeen, F., Chaudhry, A.S., Manzoor, S. and Shaheen, T. 2016. Carbamates and neonicotenoids in fish, water and sediments from the Indus River for potential health risks. *Environ. Monit. Assess.* 187 (2): 29.

Jipsa, J.R., Kalavathi, R., Dhanya, P.Y., and Logaswamy, S. 2014. Studies on the impact of a Cypermethrin insecticide on oxygen consumption and certain biochemical constituents of a fish *Tilapia mossambica*. *International Journal of Fisheries and Aquatic Studies.* 1(5) : 93-97.

Job, S.V. 1955. The oxygen consumption of *Salvelinus fontinalis*. *Univ. Toronto Biol. Ser*. No. 61; Ont. Fish. Res. Lab. Publ. 73 : 1-39.

Joshi, P.P. and Kulkarni, G.K. 2007. Change in the oxygen consumption of a freshwater fish *Garra mulya* (Sykes) exposed to cypermethrin and fenvalerate. *Himalayan J. Environ. Zool*. 21(1): 7–13.

Jothinarendiran, N. 2012. Effect of dimethoate pesticide on oxygen consumption and gill histology of the fish, *Channa punctatus* (Hamilton). *Current Biotica*. 5 (4) : 500-507.

Kalavathy, K., Siva Kumar, A.A. and Chandran, R. 2001. Toxic effect of the pesticide Dimethoate on the fish *Sarotherodon mossambicus*. *J. Ecol. Res. Bioconserv.* 2(1-2): 27-32.

Katja, S., Georg, B.O.S., Stephan, P. and Christian, E.W.S. 2005. Impact of PCB mixture (Aroclor 1254) and TBT and a mixture of both on swimming behavior, body growth and enzymatic biotransformation activities (GST) of young carp ,*Cyprinus carpio*. *Aqua. Toxicol*. 71: 49-59.

Logaswamy, S. and Remia. K.M. 2009. Impact of Cypermethrin and Ekalux on respiratory and some biochemical activities of a freshwater fish. *Tilapia Mossambica*. *Current Biotica*. 3 : 65-73.

Maharajan, A., Usha, R., Paru Ruckmani, P.S., Vijaykumar, B.S., Ganapiriya, V. and Kumarasamy, P. 2013. Sublethal effect of Profenofos on oxygen consumption and gill histopathology of the Indian major carp, *Catla catla* (Hamilton). *Int. J. Pure Appl. Zool.* 1 (1) : 196-204.

Mariya Dasu, P. 2014. *Thiodicarb 75 percentage wp a carbamate insecticide induced toxicity biochemical and histopathological changes in the freshwater Indian major carp Labeo rohita* (Hamilton). *Ph.D Thesis*, submitted to Acharya Nagarjuna University, Nagarjuna Nagar, Guntur, A.P, India.

Neelima, P., Gopala Rao, N., Srinivasa Rao, G. and Chandra Sekhara Rao, J. 2016. A study on oxygen consumption in a freshwater fish *Cyprinus carpio* exposed to lethal and sublethal concentrations of cypermethrin (25% EC). *Int. J. Curr. Microbiol. App. Sci.* 5 (4) : 338-346.

Parma de Croux, M.J., Loteste, A. and Cazenave, J. 2002. Inhibition of plasma cholinesterase and acute toxicity of monocrotophos in Neotropical fish, *Prochilodus lineatus* (Pisces, Curimatidae). *Bull. Environ. Contam. Toxicol.* 69 : 356-362.

Ram Nayan Singh. 2014. Effects of Dimethoate (EC 30%) on Gill Morphology, Oxygen Consumption and Serum Electrolyte Levels of Common Carp, *Cyprinus Carpio* (Linn). *International Journal of Scientific Research in Environmental Sciences*. 2(6) : 192-198.

Rao, D.M.R. 1989. Studies on the relative toxicity of Endosulphan to the Indian major carp *Catla catla* with special reference to some biochemical changes induced by the pesticide. *Pest. Biol. Phy*. 33 : 220-229.

Rao, J.V. 2003. Rani, C.H.S., Kavitha, P., Rao, R.N. and Madhavendra, S.S.Toxicity of chlorpyrifos to the fish, *Oreochromis mossambicus*. *Bull. Environ. Contam. Toxicol.* 70 : 985-992.

Sree Veni, S.M. and Veeraiah, K. 2014. Effect of Cypermethrin (10%EC) on Oxygen Consumption and Histopathology of Freshwater Fish *Cirrhinus mrigala* (Hamilton). *IOSR J. Environ. Sci., Toxicol. Food Technol.* 8(10): 12–20.

Srivastava, P. and Singh, A .2014. Fate of fungicides on fish, *Clarias batrachus*- a complete study. *LAP LAMBERT Academic Publishing*, Germany. 134 p

Shereena, K.M., Logaswamy, S. and Sunitha, P. 2009. Effect of an organo phosphorous pesticides (Dimethoate) on oxygen consumption of the fish *Tilapia Mossambica*. *Recent Res. Sci. Technol*. 1: 4-7.

Shivakumar, R. and David, M. 2004. Toxicity of endosulfan to the freshwater fish, *Cyprinus carpio*. *Indian J. Ecol*. 31 : 27–29.

Subramani Lavanya, Mathan Ramesh, Chokkalingam Kavitha, and Annamalai Malarvizhi, 2011. Haematological, biochemical and ion regulatory responses of Indian major carp *Catla catla* during chronic sub-lethal exposure to inorganic arsenic. *Chemosphere*. 82 : 977-985.

Sudhasaravanan, R. and Binukumari, S. 2015. Effects of different concentartions of detergent on dissolved oxygen consumption in *Lepidocephalichythyes thermalis*. *World Journal of Pharmaceutical Research*. (2): 940-945.

Tilak, K.S. and Vardhan, S.K. 2002. Effect of fenvalerate on oxygen consumption and haematological parameters in the fish. *Channa punctatus* (Bloch). *J. Aquatic Biol*. 17 : 81–86.

Tilak, K. S., Veeraiah, K., Bhaskara Thathaji, P. and Butchiram, M. S. 2007. Toxicity studies of butachlor to the freshwater fish *Channa punctatus* (Bloch). *Journal of Environmental Biology*. 28 (2) : 485-487.

Tilak, K. S. and Vijaya Kumar, M. 2009. Effect of Quinaphos technical grade and commercial grade (25%EC) formulations on oxygen consumption in freshwater fish *Channa punctatus* (Bloch). *ANU Journal of Natural Sciences*. 39-45.

Ural, M. S. and Simsek, K. S. 2006. Acute toxicity of dichlorvos on fingerling of European catfish, *Silurus glanis*. *Bulletin of Environmental Contamination and Toxicology*. 76 : 871-876.

Vakita Venkata Rathnamma and Nagaraju Bantu, 2014. The effect of Chlorantraniliprole on the oxygen consumption of the freshwater fish *Labeo rohita* (Hamilton). *Frontiers of Biological and Life Sciences*. 5-7.

Vani, G., Veeraiah, K., Vijaya Kumar, M. and Parveen, S.K. 2020. Effect of Cartap hydrochloride (50%) on oxygen consumption of freshwater, *Cirrhinus mrigala*. (Hamilton). *Poll. Res.* 39 (2) : 368-372.

Veeraiah, K. and Durga Prasad, M. K. 2001. Studies on ventilatory patterns of fish under normal and stressed conditions using indigenously designed electronic recording instrument. *Proc. Intern. Conf. ICIPACT* -2001.

Vineetkumar, K. Patil and David, M. 2008. Behavior and respiratory dysfunction as an index of Malathion toxicity in the freshwater fish *Labeo rohita*. (Hamilton). *Turkish Journal of Fisheries and Aquatic Sciences.* 8 : 233-237.

Journal of Molecular Structure 1243 (2021) 130784

Contents lists available at ScienceDirect

Journal of Molecular Structure

journal homepage: www.elsevier.com/locate/molstr

Luminescence investigations on Dy^{3+} doped CdO-PbF_2 phosphate glass-ceramics

Ch. Nageswara Rao[a,g], P. Vasudeva Rao[a,g], R. Kameswari[b], R. Ramesh Raju[c], G. Chandana[d], K. Samatha[d], M.V.V.K. Srinivas Prasad[e], M. Venkateswarlu[e], A. Naveen[e,f], G.G. Dhar[g,*]

[a] Department of Physics, Acharya Nagarjuna University, Guntur, A.P., India
[b] Department of Physics, SRR & CVR Government Degree college (Autonomous), Vijayawada, A.P., India
[c] Department of Chemistry, Acharya Nagarjuna University, Guntur, A.P., India
[d] Department of Physics, Andhra University, Visakhapatnam, A.P., India
[e] Department of Physics, Koneru Lakshmaiah Education Foundation, Vaddeswaram, Guntur, A.P., India
[f] Department of Physics and Electronics, Chaitanya Deemed to be University, Hanamkonda, Telangana, India
[g] Department of Nanotechnology, Acharya Nagarjuna University, Guntur, A.P., India

ARTICLE INFO

Article history:
Received 18 December 2020
Revised 24 May 2021
Accepted 25 May 2021
Available online 31 May 2021

Keywords:
Phosphate glass
Glass ceramics
Nanocrystals
Luminescence

ABSTRACT

This paper reports the structural and photoluminescence investigations on Dy^{3+} doped transparent CdO-PbF_2 phosphate glass/glass ceramics with SrO. Upon heat treatment, the nanocrystals occurred in glass ceramics are spherical in shape in the sizes of 10nm to 20nm. The luminescence intensities were strongly dependent on nanocrystallinity and showing the same kinetics as efficient luminescent hosts. In the present host, well incorporation of Dy^{3+} ions in nanocrystals and low energy transfer to Dy^{3+} ions due to existence of other crystalline phases, both the mechanisms occurred. The consequent variations in luminescence intensities also observed.

1. Introduction

Search for new optical materials has always had considerable interest to cater to the requirements in telecommunication, solid-state lasers, optical amplifiers as well as up-conversion fibers [1]. Controlled nucleation and growth of crystalline phase cause the glass ceramic formation which has a polycrystalline structure [2]. These glass-ceramics are useful in many current applications like liquid crystal displays, photonic devices and solar concentrator cells [3]. In glass-ceramics, nanocrystals can enhance luminescence efficiency by conquering a decrease in absorption coefficient [4–8].

In recent years, many researchers are working on glass ceramics based on the glass transition temperatures to achieve both transparence and improvement in luminescence properties of rare-earth ions in glass ceramics [9–12]. Studies on Na_2O-CaF_2-P_2O_5 glasses/glass ceramics reported the dependence of optical properties on structural arrangement upon heat treatment in the glass network [13]. In glass ceramics, the formed nanocrystals will improve the local field around the rare-earth ions and result in an enhancement in absorption cross section and luminescent intensity [14–16]. Therefore, to understand the luminescence enhancement mechanism, a thorough study is required on the interactions between doped activators and formed nanocrystals in the glass ceramics.

Among Rare Earth(RE) ions, trivalent dysprosium (Dy^{+3}) is useful for white light emission in both glass and glass-ceramics [17–22]. Dy^{3+} ion shows intense emission bands at blue (at 486 nm, $^4F_{9/2} \rightarrow {}^6H_{15/2}$) and yellow (at 575 nm, $^4F_{9/2} \rightarrow {}^6H_{13/2}$) regions upon suitable excitation. Here, in the yellow region, $^4F_{9/2} \rightarrow {}^6H_{13/2}$ the transition of Dy^{3+} is hypersensitive and its intensity strongly depends on the host [23–25]. The transition $^4F_{9/2} \rightarrow {}^6H_{15/2}$ in the blue region is a magnetic dipole allowed transition and is less sensitive to the host matrix. Therefore, the intensity ratio of these transitions (Yellow/Blue) determines the generation of white light in the host matrix. Besides that, lead content in the glasses leads to high transparency and shows more stability over atmospheric moisture [26]. PbF_2 content in glasses can increase the refractive index and can be useful as a core material in optical fibers [27]. Rare-earth doped glasses with PbF_2 content reported high luminescence emission with large radiative transition probabilities. Further, a high refractive index leads to an increase in the local field on dopant ions [28–30]. Further, one of the effective ways to improve the chemical durability of phosphate glasses is the addition

* Corresponding author.
E-mail address: drggiridhar@rediffmail.com (G.G. Dhar).

https://doi.org/10.1016/j.molstruc.2021.130784
0022-2860/

of various oxides to phosphate glasses. Here, SrO addition to the host improves the strength of the phosphate network by decreasing the non-bridging oxygens. Sr^{2+} has higher field strength than other alkali earth ions like Ca^{2+} and Mg^{2+} results an improvement in the glass network strength [31–34].

Previous reports on Dy^{3+} ions doped hosts for high performance white light generation explained through various aspects like concentration variation of activator, co-doped, tri-doped and energy transfer mechanisms [11,19,35–46]. Besides, activator behavior in the host, an additional structural information is also required in well establishment of luminescence efficiency. In view of that, we made an attempt in the present phosphate glass matrix.

The aim of the present study is to find out the growth of lead fluoride nanocrystals in Dy^{3+} doped cadmium phosphate glass upon heat treatment and their effect on structural, luminescence properties for a wide variety of lighting applications. Variations in luminescence intensities observed due to the existence of multiple nanocrystalline phases. Further, Glass-ceramics showed higher emission intensity over glass whereas GC5 (5h annealed) had a higher emission than all other glass and glass-ceramics.

2. Experimental

The basic composition of the present glass matrix (as-melted) used in this study was 49.5 P_2O_5 – 20 CdO – 25 PbF_2 -5 SrO – 0.5 Dy_2O_3. The raw materials used were obtained from Loba Chemicals pvt ltd in high purity. Glass was prepared by using the well known melt quenching technique. All the chemicals were mixed in a mortar and thoroughly grinded for 1 hour. The resultant mixture was taken into a porcelain crucible and kept in an electrical furnace at 200 °C for 1h to remove the excess gasses. This was further heated at 950 °C for 1.5h. At that stage, the mixture was in melt form and was poured on a pre heated brass plate, then immediately placed in high temperature furnace at 250 °C to overcome the cracks due to thermal strain. The resultant samples were cut and polished into the glass samples with a thickness of ~1.5 mm and was denoted as GS. To obtain glass ceramics, the samples were annealed at slightly above the glass transition (T_g) point 380 ± 5°C for a duration of 2h, 5h and 10h continuously and thereafter were cooled to room temperature. Attained samples were denoted as GC2, GC5 and GC10 respectively.

Physical properties of the current glasses were measured as per our previous reports [47] in different methods. Shimadzu DTG-60H was used for DTA (Differential Thermal Analysis) measurement. The sample was taken in powder form in aluminium crucible and experiment done at a rate of 10 °C/min in air. BRUKER FTIR spectrometer was used and recorded the FTIR spectra of KBr associated samples in the frequency range 400±1400 cm^{-1} at room temperature with 2 cm^{-1} resolution.

Thermo scientific spectrophotometer was used to study the emission and excitation properties. Lifetime measurements were carried out by using Edinburgh Instruments FLSP 920 system to study the decay mechanism. All the spectral recordings were done at room temperature only.

3. Results and discussion

3.1. TG-DTA analysis

Fig. 1 shows the differential thermal analysis curves for the CdO-PbF2 phosphate glass and glass-ceramics. From the DTA curves, both glass transition temperatures (T_g – 380 °C) and an exothermic peak or crystallization peak at temperatures (T_c – 470 °C) of the glass sample was estimated. The samples were annealed at slightly above the T_g as partial and controlled crystallization gives glass ceramic. At this point, one can get the glass ceramics with good mechanical stability due to less internal mechanical stress. This heat treatment was done for the duration of 2h, 5h and 10h continuously for resultant glass ceramic samples containing fluoride nanophase. A Small increase in both T_g and T_c takes

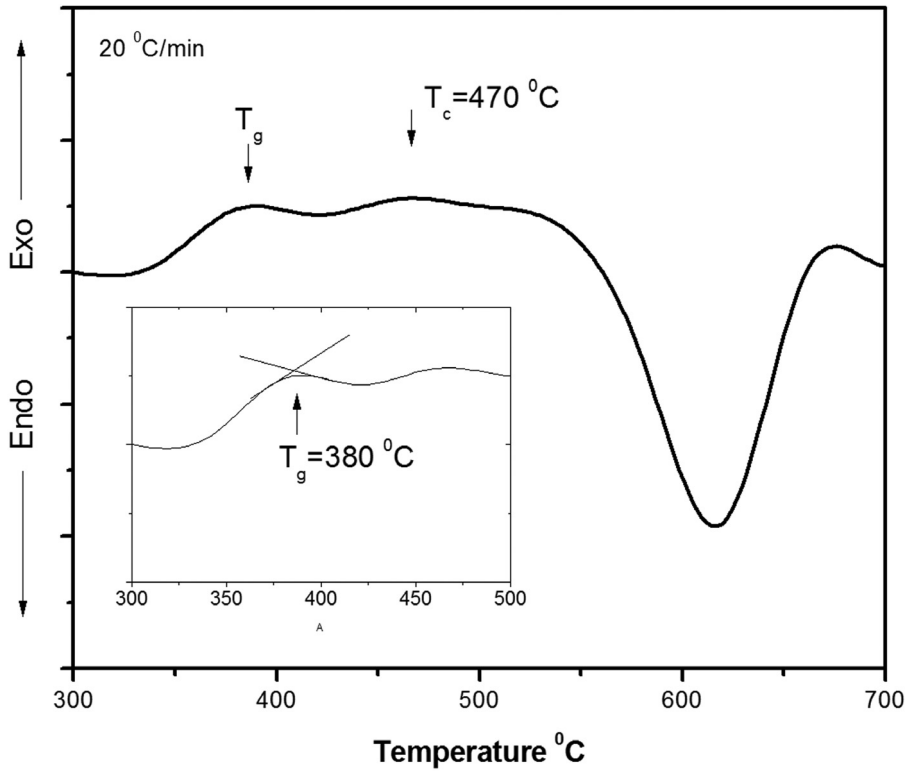

Fig. 1. T_g-DTA graph of GS sample

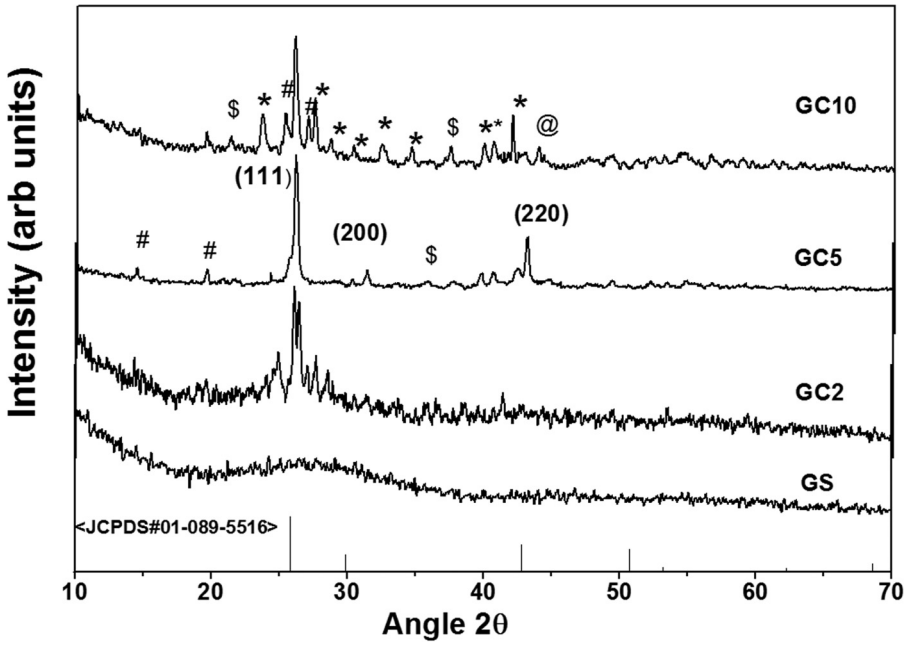

Fig. 2. XRD spectra of CdO-P2O5 glass and Glass Ceramics

place as annealing time increases from 2h to 10h. This is because of becoming strong network connectivity on heat treatment.

3.2. X-Ray diffraction studies

The X-ray diffraction (XRD) spectra of the cadmium phosphate glass and glass-ceramics (GS-GC10) have been recorded in the range of $10° \leq \theta \leq 80°$ to bring the proper understanding of the effect of heat treatment on structural evolution.

The resultant diffraction spectra did not show a sharp peak except for widespread scattering at low angles. This confirms the amorphous nature of the base glass. Glass ceramic samples (GC2, GC5 and GC10) are showing considerable peaks indicating the crystalline phases. Both glass and glass ceramics XRD spectra are shown in Fig. 2.

These diffraction peaks are matched with the standard powder diffraction data and reveal the formation of PbF_2 and metal phosphate crystals. Besides, existence of other phosphate phases and the enhancement in peak intensity was observed. Grain size was calculated by using Scherrer's formula,

$$D_{hkl} = \frac{k}{\beta cos\theta}$$

where D_{hkl} is the grain size at the vertical direction of (h k l), λ, θ and β are the wavelength of X-ray, angle of diffraction and the full-width half-maximum of the diffraction peak, respectively. Here the shape factor and/or proportionality constant is k = 0.90 as most of the grains are in spherical in shape. The evaluated average grain size is 25-38 nm. Further, upon increasing annealing time, the crystallization process is stabilized and nearly similar grain sizes observed in GC10 glass-ceramic. Other cadmium phosphate phases were raised as annealing time increased(*-$Cd_3(PO4)_2$ #-$Cd(PO_3)_2$ $-$Sr(PO_3)_2$ and @-$Cd_2P_6O_{17}$).

3.3. TEM analysis

Fig. 3 (a-GS; b- GC5 c-GC10) shows the transmission electron micrograph of GC10 sample only. No dark crystallites were observed in the glassy matrix to represent any kind of crystal nature. In case of 10 hours heat treated sample (c1 and c2), one can clearly distinguish dark crystallites and the light background of the glassy matrix, which resembles the homogeneous distribution of crystallites. These images are processed by Image J software and particle size estimated by using the formula

$$d_i = \sqrt{\frac{4}{\pi}A_i}$$

where Ai area of each particle, d_i an average diameter [48].

The crystallite size distribution of GC10 is shown in Fig. 4. 50 crystallites are analyzed and found that the mean diameter is (7.3 ± 0.1) nm, which shows a narrow crystallite size with polydispersity or the degree of non-uniformity, is only 2%. This is near and supports the calculated crystallite size from XRD spectra by using Scherrer's formula.

3.4. FTIR- analysis

Fourier Transform Infrared (FTIR) spectra of present CdO-PbF_2 phosphate glass and glass ceramics are shown in Fig. 5. P_2O_5 glass contains extended network of the [PO_4] tetrahedral; each tetrahedral shares three corners. The sharing will be through P-O-P linkage. Here the unshared oxygen ion has a double bond with phosphorous ion due to its pentavalence [49–51]. The vibrational bands depend on the concentration of network former. In the present glass system, the major building units are Q_2 and Q_3 because of higher P_2O_5 concentration. The remaining metal oxides can be positioned with phosphorus linkage.

FTIR spectra show nearly twelve bands as characteristics of the phosphorus–oxygen networks in the present glass and glass ceramics.

The asymmetric and symmetric stretching of O-P-O band is observed at ~ 1261 cm^{-1} and ~ 1058 cm^{-1}respectively. It indicates the formation of Q_2 phosphate tetrahedral long chain along with asymmetric stretching of P-O-P mode vibration observed at ~ 910 cm^{-1} [52–55].

The band at ~ 749 cm^{-1} is attributed to symmetric stretching of P-O-P groups [56]. The remaining bands observed in the range 600-400 cm^{-1} are P-O-P bending and P-O-P stretching modes [57,58]. Here one can observe the peak shifts with in this range

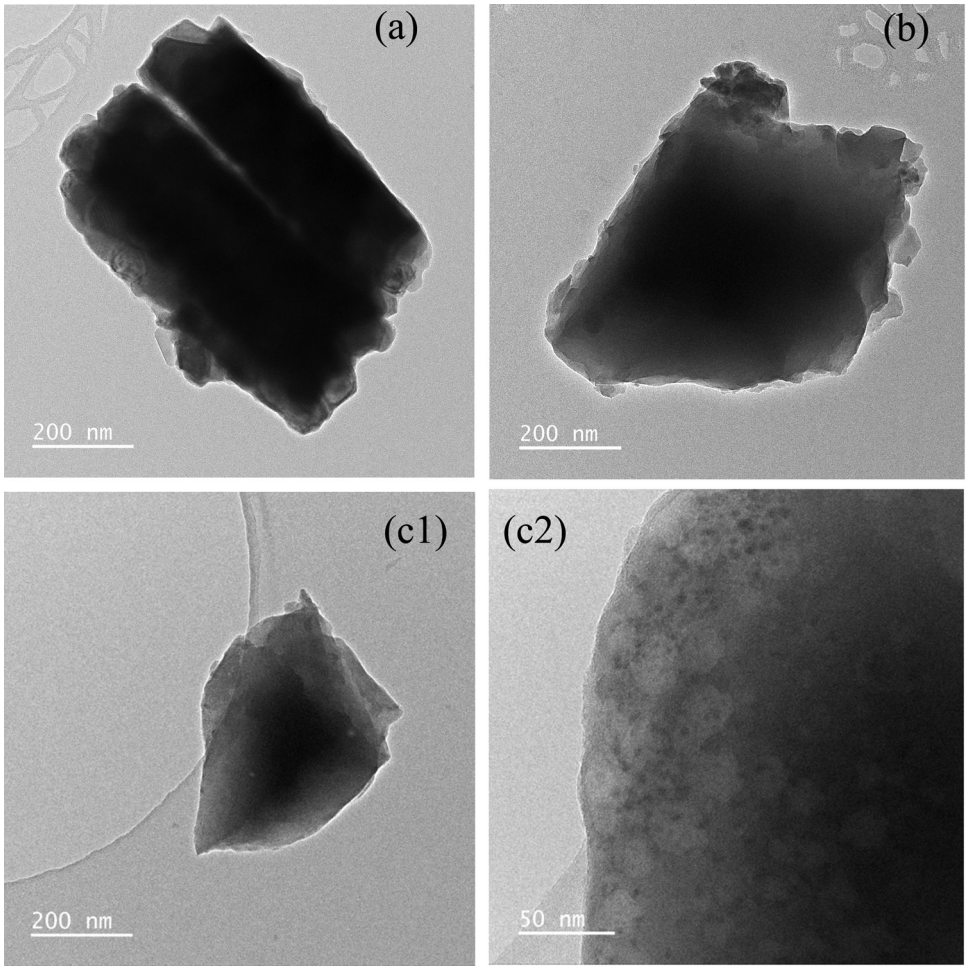

Fig. 3. TEM images of GC10

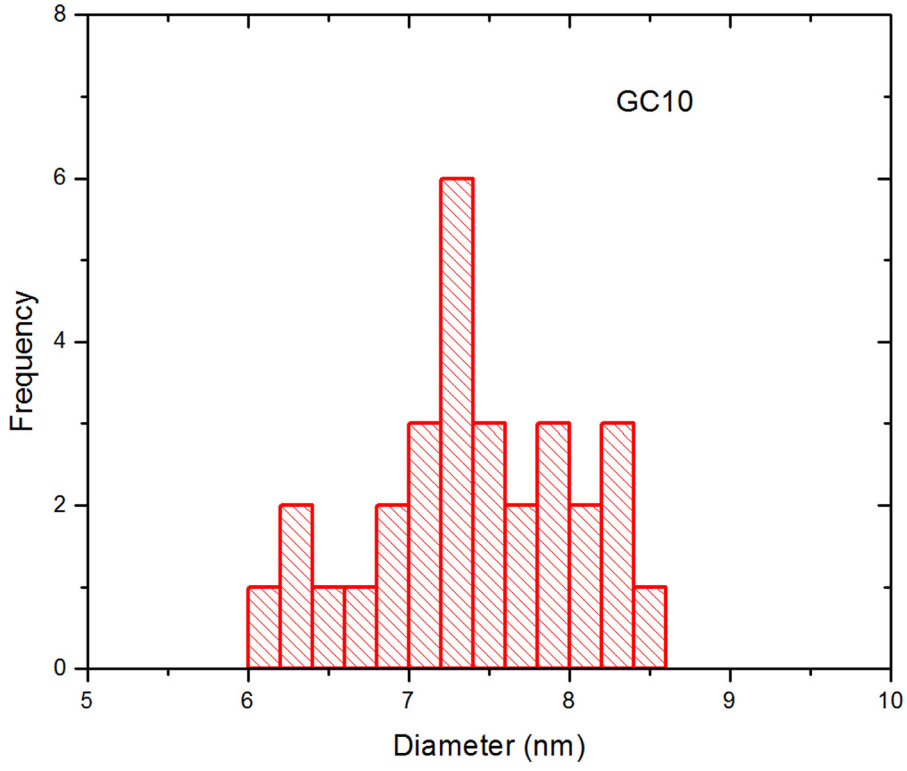

Fig. 4. Crystallite size distribution of GC10 sample (10h heat treated)

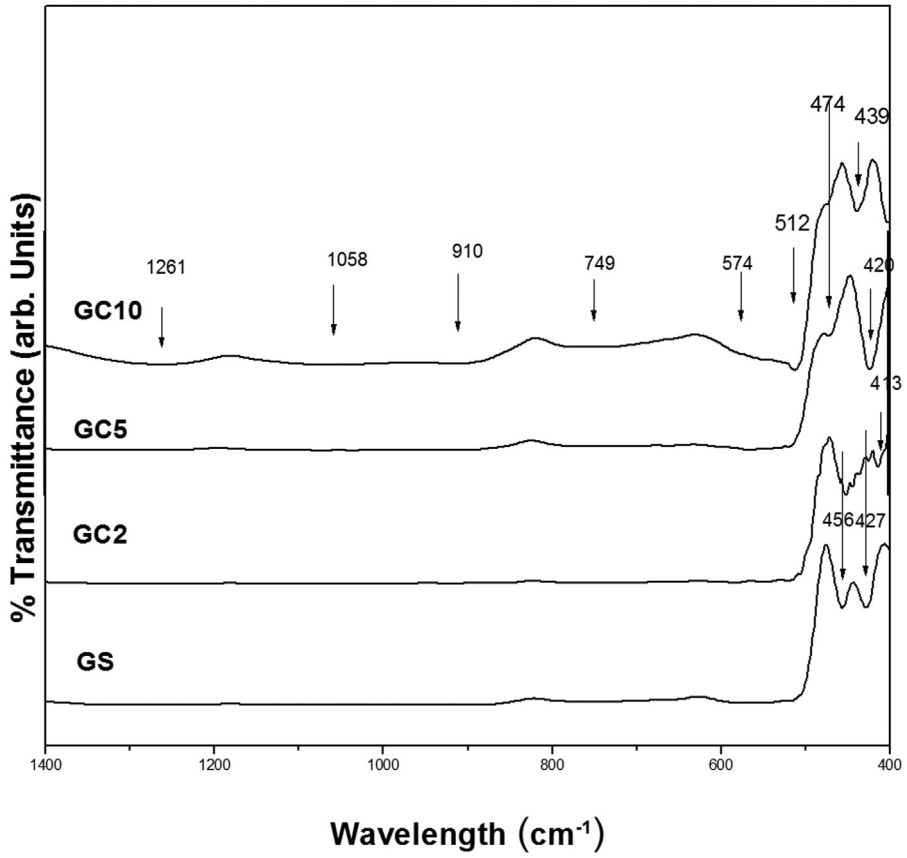

Fig. 5. FTIR spectra of Cadmium Phosphate glass and glass ceramics

when compared to glass (GS) with glass ceramics samples (GC2, GC5 and GC10). Because of the heat treatment, it is clear that prominent changes occurred in PO_4 structural units in terms of position, bandwidth and intensity. Therefore upon heat treatment, more other ions coupled with P-O bonds [59]. The existence of other crystalline phases in the heat treated samples evidenced that Cd-O-P or Sr-O-P type bonds formed in the structure. These structural changes are well connected with X-ray diffraction studies as it shows the other crystalline phases upon heat treatment.

3.5. Emission and excitation

Fig 6 (a,b) shows the excitation and emission spectra of the precursor glass and glass ceramic under respective emission and excitation wavelengths. In all the spectra, spectral shape look alike but in case of glass ceramics, the luminescence intensity is strong and higher in order than the base glass.

Fig 6a illustrates the excitation spectrum of GC10 glass ceramic in the range of 320–500 nm with λ_{em} = 574nm ($^4F_{9/2}\rightarrow{}^6H_{13/2}$ transition) recorded at room temperature. Nearly seven intense peaks were identified and assigned to the transitions from $^6H_{15/2}$ -the ground state to different excited states of Dy^{3+} ions. At 322 nm, 348 nm, 363nm, 385 nm, 424 nm, 451 nm and 472 nm bands were assigned to $^6H_{15/2}\rightarrow{}^4K_{15/2}+(^4D,^4G)_{5/2}$, $^6H_{15/2}\rightarrow{}^6P_{7/2}+(^4M,^4I)_{15/2}$, $^6H_{15/2}\rightarrow{}^6P_{5/2}+{}^4I_{11/2}$, $^6H_{15/2}\rightarrow{}^4M_{21/2}+{}^4K_{17/2}+{}^4M_{11/2}+(^4P,^4D)_{3/2}$, $^6H_{15/2}\rightarrow{}^4G_{11/2}+{}^4F_{7/2}+{}^4I_{13/2}$, $^6H_{15/2}\rightarrow{}^4I_{15/2}$ and $^6H_{15/2}\rightarrow{}^4F_{9/2}$ transitions respectively [12,60,61].

The emission spectra were recorded for present glass, glass ceramics with selected high intense excitation wavelength 348 nm in the spectral region 450–700 nm. The resultant spectra (shown in Fig 6b) reveals that the emitted peaks at 482 and 574 nm are very strong and at 663 nm is feeble and were assigned to $^4F_{9/2}\rightarrow{}^6H_{15/2}$ (blue) and $^4F_{9/2}\rightarrow{}^6H_{13/2}$ (yellow-hypersensitive) and $^4F_{9/2}\rightarrow{}^6H_{11/2}$ (red) transitions in visible region respectively.

Further, it is observed that emission intensities were varied upon heat treatment. To analyze the change in the intensities one can estimate the asymmetric intensity ratio (AIR) which is the ratio between the electric dipole and the magnetic dipole transitions. But in case of Dy^{3+} ions, estimation of the Yellow to Blue (Y/B) ratio is appropriate as relative fluorescence intensity and it is inversely proportional to local ion symmetry. That is the degree of distortion from the inversion symmetry of the local environment of Dy^{3+} in the lattice [39,62,63]. Therefore to estimate the Y/B ratio, the intense electric dipole transition (in yellow region- 574nm) and the magnetic dipole transitions (in blue region-472nm) were taken into account and the values are 1.08, 1.18, 1.05 and 1.22 for GS, GC2, GC5 and GC10 respectively. The variation in the intensity ratio values reflects the substitution of Dy^{3+}, in place of the element with same valence, minute variation; or in place of the element with different valence, considerable variation due to formation of defects in the host matrix. So, Y/B ratio is dependent on site asymmetry or environmental variations in the vicinity of the Dy^{3+} ion [18].

However, the yellow emission is more prominent than blue which suggests that there is no centre of symmetry around the Dy^{3+} ions due to the charge separation [64,65] in both the glass and glass ceramics. In GC10, higher the Y/B ratio may be due to higher degree of covalancy between Dy-O than others.

Here the change in Y/B ratio strongly influenced by the local environment of the rare earth ions. Therefore the varied values of Y/B ratio in glass ceramics than glass, clearly represents the structural

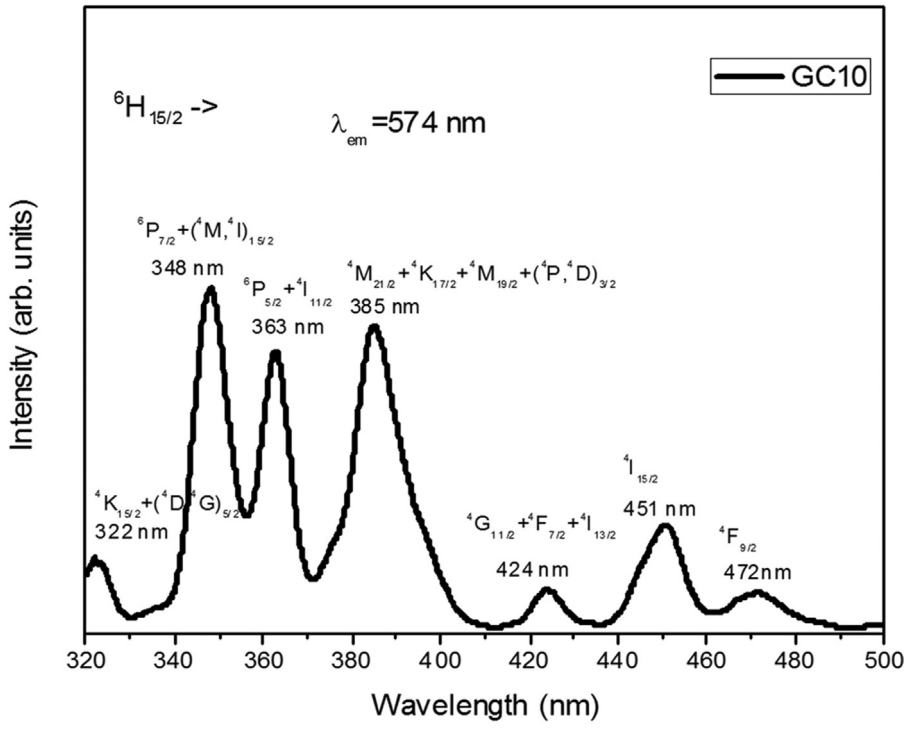

Fig. 6. a Excitation spectrum of GC10 sample. b Emission spectra of CdO-P2O5 glasses

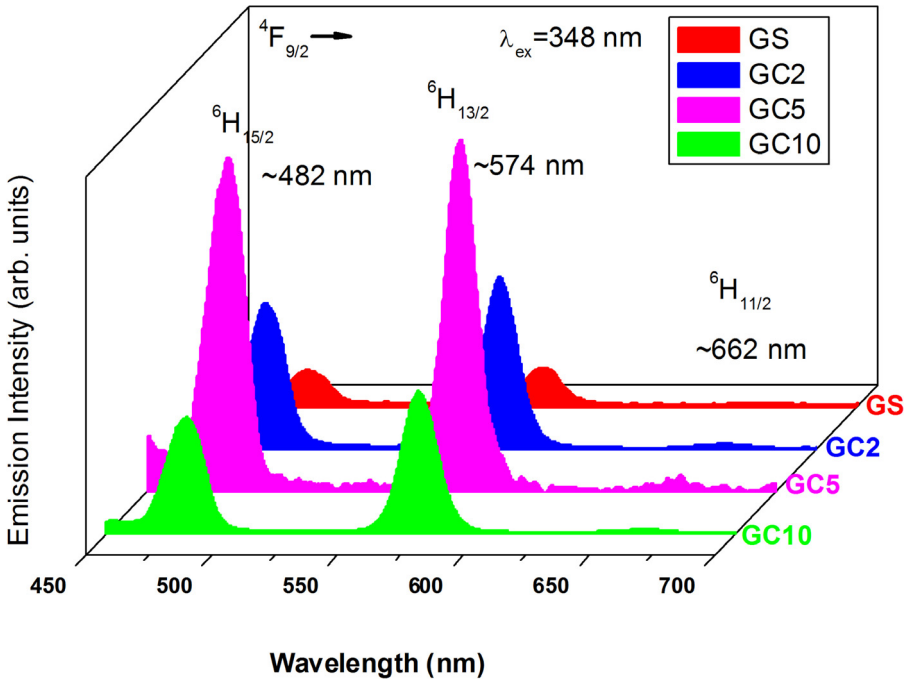

Fig. 6. Continued

changes as Dy^{3+} ions incorporated into PbF_2 nanocrystals. In other words changes in the local environment around the Dy^{3+} ions can control the white light emission.

The yellow band at 574 nm is more intense than the blue band (Fig. 4b), suggests that the Dy^{3+} ion is in lower symmetry local site [24]. Further, heat treatment gives enhancement in emission intensities in present glass ceramics under study from GC2 to GC5.

The GC5 shows 10 times more enhancement in emission intensity when compared untreated glass (GS glass). In addition, there was an increase in intensity from GS to GC5 as Dy^{3+} ions are well incorporated in PbF_2 nanocrystals; it is to note that the fluoride nanocrystals have low phonon energies than oxide. In case of GC10, intensity decreased. It suggests that, after 10h heat treatment, there are considerable structural changes in the host. In spite of the fact that Dy^{3+} ions are incorporated in PbF_2 nanocrystals, due to superimposition of other cadmium phases, excitation energy was fully not transferred to Dy^{3+} ions from PbF_2 crystallites [17,18].

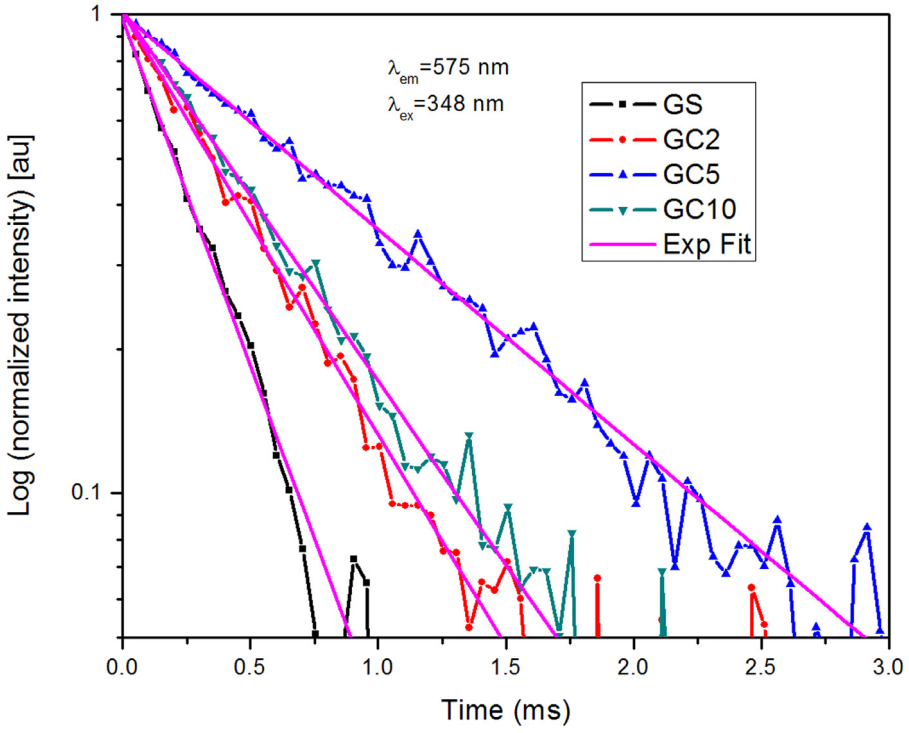

Fig. 7. Decay profiles of CdO-PbF_2 phosphate glass and Glass-Ceramics for $^4F_{9/2}$

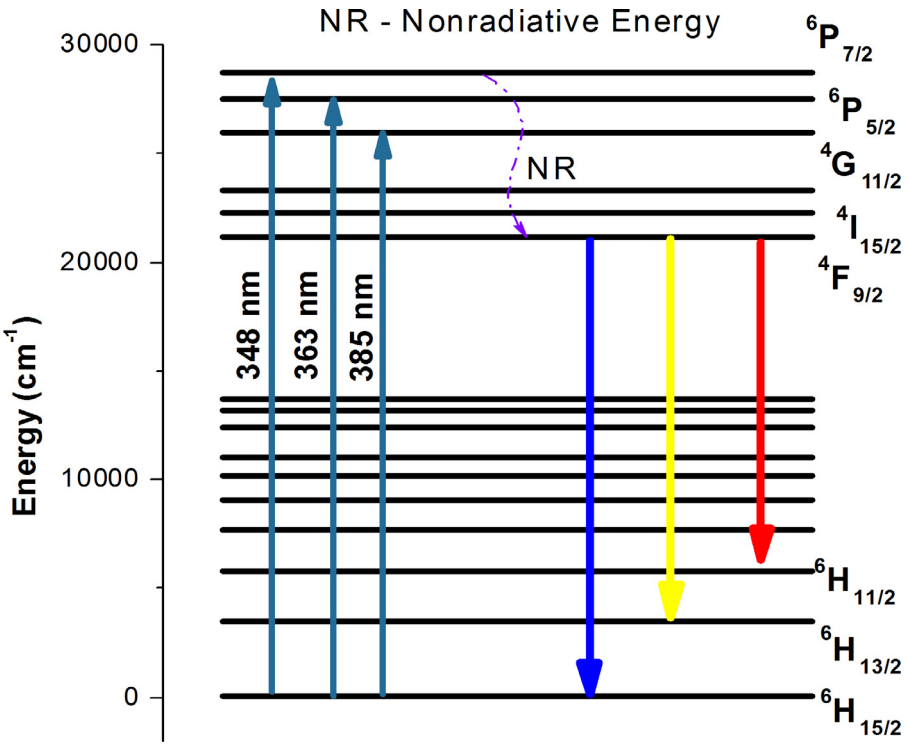

Fig. 8. Energy Level diagram representing excitation and emission mechanisms

The decay curves of CdO-PbF_2 phosphate glass and Glass-Ceramics doped with Dy^{3+} were measured and fitted by single exponential curves (Fig. 7). The measured lifetimes (in mille seconds) are 0.37 ms, 0.53 ms, 0.86 ms and 0.59 ms for GS, GC2, GC5 and GC10 respectively. An Energy level diagram for Dy^{3+} ions in the present glass host matrix is shown in Fig. 8. It illustrates the excitation and emission processes pertaining to radiative and non-radiative transitions in the present phosphate glasses.

Colorcalculator v.7.77 was used to analyze the experimental emission data of CdO-PbF2 phosphate glass, glass ceramics in terms of CIE 1931 (Commission Internationale de l'Eclairage) colour coordinates to characterize the colour rendering. The obtained values were presented in Table 1 with correlated color temperatures (CCT) values and shown in Fig. 9.

The coordinates were well placed in the white light region. The CCT values indicate that these materials were emitting cool white

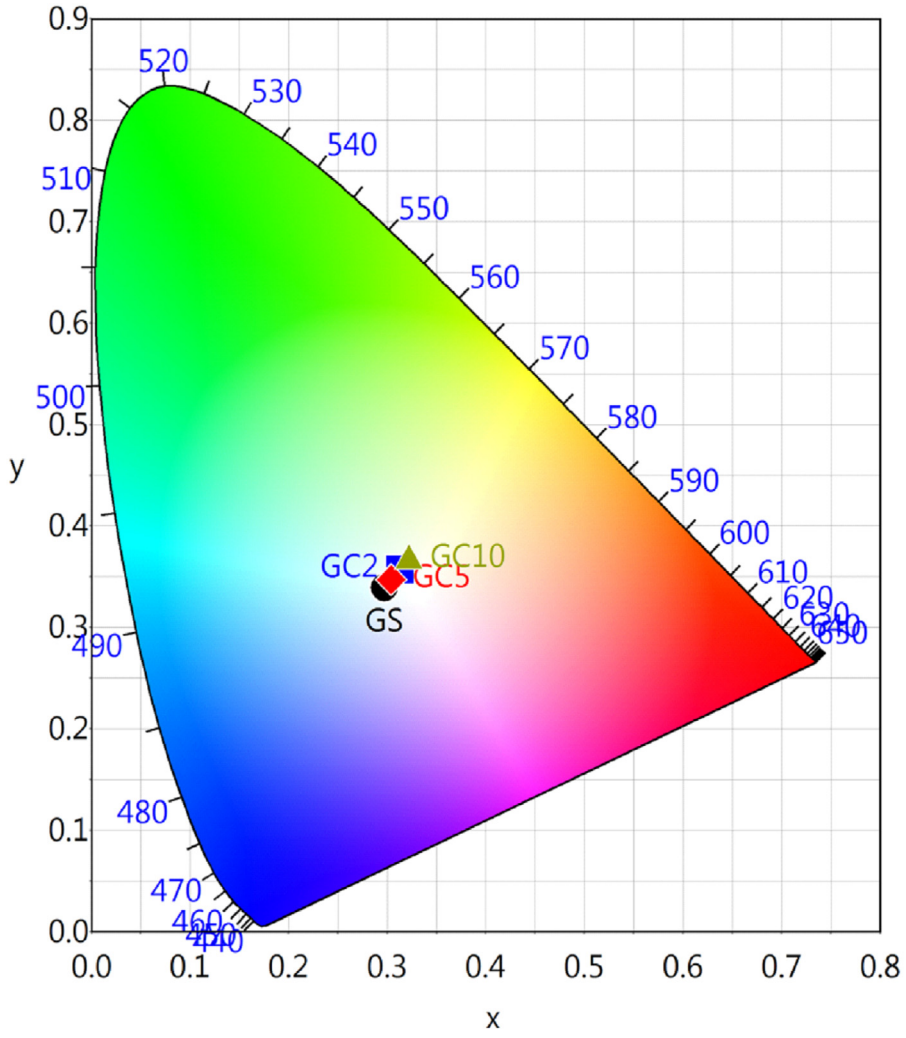

Fig. 9. CIE diagram for CdO-PbF2 phosphate glass and glass ceramics

Table 1
CIE co-ordinates and CCT values for CdO-PbF2 phosphate glass and glass ceramics

Glass/Glass Ceramic sample	x	y	CCT (K)
GS	0.297	0.339	7258
GC2	0.313	0.357	6317
GC5	0.304	0.347	6805
GC10	0.322	0.367	5908

light and can be useful for security lights, offices and/or retail locations. Therefore, these prepared glass and glass ceramics with PbF_2 nanocrystals are efficient and useful to cater the needs of efficient white light generating device applications.

4. Conclusion

CdO-PbF_2 phosphate glass, glass-ceramics doped with Dy^{3+} ion were prepared by using most familiar melt quenching method. Glass transition temperature was obtained from DTA measurement. At slightly above (+5 °C) the T_g, samples were annealed and obtained glass ceramics. Structural information was confirmed as polycrystalline from X-Ray diffraction spectra. The diffraction pattern confirmed the existence of PbF_2 and other crystalline phases in glass ceramics together with other cadmium phosphate phases in GC10 (maximum annealing time of 10h). The crystallite size distribution in the glass ceramic (GC10) is homogeneous with an average size of 7.3 ± 0.1 nm. The enhancement in Dy^{3+} characteristic luminescent emission intensity upon excitation was obtained in host glass ceramics than glass. Such enhancement was due to the well placement of Dy^{3+} ions into PbF_2 nanocrystals in GC2 and GC5. But in case of 10h annealed GC10 glass ceramic the emission intensity was decreased. This is due to the superimposition of other cadmium phosphate phases. So, sufficient excitation energy was not transferred from PbF_2 crystallites to Dy^{3+} ions. Therefore, structural feasibility is also an important element for efficient light emission. FTIR spectra show the distinct changes in phosphate structural units of Glass and glass-ceramics. So, the results of the present glass, glass ceramics are clearly indicating that, excess heat treatment undeniably influences emission intensity with the inducement of other crystallite phases. The CIE co-ordinates were well placed in the cool white light region. Hence, these glass/glass ceramics are useful in light emission and as well as promising candidates for white light emission devices.

Declaration of Competing Interest

The authors declare that they have no known competing financial interests or personal relationships that could have appeared to influence the work reported in this paper.

CRediT authorship contribution statement

Ch. Nageswara Rao: Data curation, Methodology, Writing - original draft, Writing - review & editing. **P. Vasudeva Rao:** Data curation, Methodology, Writing - original draft, Writing - review & editing. **R. Kameswari:** Data curation, Methodology, Writing - review & editing. **R. Ramesh Raju:** Methodology, Writing - original draft, Writing - review & editing. **G. Chandana:** Data curation, Methodology, Writing - original draft, Writing - review & editing. **K. Samatha:** Methodology, Writing - original draft, Writing - review & editing. **M.V.V.K. Srinivas Prasad:** Data curation, Methodology, Writing - original draft, Writing - review & editing. **M. Venkateswarlu:** Data curation, Methodology, Writing - review & editing. **A. Naveen:** Methodology, Writing - original draft, Writing - review & editing. **G.G. Dhar:** Conceptualization, Data curation, Methodology, Writing - original draft, Writing - review & editing.

References

[1] K.A. Bashar, G. Lakshminarayana, S.O. Baki, A.-B. Mohammed, U. Caldiño, A.N. Meza-Rocha, V. Singh, I.V Kityk, M.A. Mahdi, Tunable white-light emission from Pr3+/Dy3+ co-doped B2O3-TeO2 PbO-ZnO Li2O-Na2O glasses, Opt. Mater. (Amst). 88 (2019) 558–569.

[2] R. Narro-García, H. Desirena, T. López-Luke, J. Guerrero-Contreras, C.K. Jayasankar, R. Quintero-Torres, E. De la Rosa, Spectroscopic properties of Eu3+/Nd3+ co-doped phosphate glasses and opaque glass–ceramics, Opt. Mater. (Amst). 46 (2015) 34–39.

[3] K.V. Krishnaiah, Y. Ledemi, C. Genevois, E. Veron, X. Sauvage, S. Morency, E.S. de Lima Filho, G. Nemova, M. Allix, Y. Messaddeq, Ytterbium-doped oxyfluoride nano-glass-ceramic fibers for laser cooling, Opt. Mater. Express. 7 (2017) 1980–1994.

[4] S.P. Singh, B. Karmakar, Photoluminescence enhancement of Eu 3+ by energy transfer from Bi 2+ to Eu 3+ in bismuth glass nanocomposites, RSC Adv. 1 (2011) 751–754.

[5] J. Qian, Q. Luo, D. Zhao, S. Cui, X. Qiao, X. Fan, X. Zhang, Preparation and photoluminescence properties of fluorosilicate glass ceramics containing CeOF: Dy3+ nanocrystals, Opt. Mater. (Amst). 34 (2012) 700–704.

[6] A. Antuzevics, M. Kemere, G. Krieke, R. Ignatans, Electron paramagnetic resonance and photoluminescence investigation of europium local structure in oxyfluoride glass ceramics containing SrF2 nanocrystals, Opt. Mater. (Amst). 72 (2017) 749–755.

[7] B. Ghaemi, G. Zhao, G. Jie, H. Xi, X. Li, J. Wang, G. Han, A study of formation and photoluminescence properties of ZnO quantum dot doped zinc-alumino-silicate glass ceramic, Opt. Mater. (Amst). 33 (2011) 827–830.

[8] A. Tarafder, A.R. Molla, S. Mukhopadhyay, B. Karmakar, Fabrication and enhanced photoluminescence properties of Sm3+-doped ZnO–Al2O3–B2O3–SiO2 glass derived willemite glass–ceramic nanocomposites, Opt. Mater. (Amst). 36 (2014) 1463–1470.

[9] Y. Chen, G.H. Chen, X.Y. Liu, T. Yang, Enhanced up-conversion luminescence and optical thermometry characteristics of Er3+/Yb3+ co-doped transparent phosphate glass-ceramics, J. Lumin. 195 (2018) 314–320.

[10] D. Chen, Y. Wang, K. Zheng, T. Guo, Y. Yu, P. Huang, Bright upconversion white light emission in transparent glass ceramic embedding Tm 3+/ Er 3+/ Yb 3+: β-YF 3 nanocrystals, Appl. Phys. Lett. 91 (2007) 251903.

[11] M. Kemere, U. Rogulis, J. Sperga, Luminescence and energy transfer in Dy3+/Eu3+ co-doped aluminosilicate oxyfluoride glasses and glass-ceramics, J. Alloys Compd. 735 (2018) 1253–1261.

[12] S. Kaur, O.P. Pandey, C.K. Jayasankar, N. Chopra, Spectroscopic, thermal and structural investigations of Dy3+ activated zinc borotellurite glasses and nano-glass-ceramics for white light generation, J. Non. Cryst. Solids. 521 (2019) 119472, doi:10.1016/j.jnoncrysol.2019.119472.

[13] M.A. Marzouk, N.A. Ghoneim, Gamma irradiation and crystallization effects on the photoluminescence properties of soda lime fluorophosphates host glass activated with Ce4+, Dy3+ or Pr3+ ions, Radiat. Phys. Chem. (2020) 108893, doi:10.1016/j.radphyschem.2020.108893.

[14] A.A. Cabral, R. Balda, J. Fernández, G. Gorni, J.J. Velázquez, L. Pascual, A. Durán, M.J. Pascual, Phase evolution of KLaF 4 nanocrystals and their effects on the photoluminescence of Nd 3+ doped transparent oxyfluoride glass-ceramics, CrystEngComm 20 (2018) 5760–5771.

[15] G. Lakshminarayana, R. Yang, M. Mao, J. Qiu, I.V Kityk, Photoluminescence of Sm3+, Dy3+, and Tm3+-doped transparent glass ceramics containing CaF2 nanocrystals, J. Non. Cryst. Solids. 355 (2009) 2668–2673.

[16] N. Pawlik, B. Szpikowska-Sroka, T. Goryczka, W.A. Pisarski, Photoluminescence investigation of sol-gel glass-ceramic materials containing SrF2: Eu3+ nanocrystals, J. Alloys Compd. 810 (2019) 151935.

[17] J. Pisarska, R. Lisiecki, W. Ryba-Romanowski, T. Goryczka, W.A. Pisarski, Unusual luminescence behavior of Dy3+-doped lead borate glass after heat treatment, Chem. Phys. Lett. 489 (2010) 198–201.

[18] J. Pisarska, L. Żur, W.A. Pisarski, Optical spectroscopy of Dy3+ ions in heavy metal lead-based glasses and glass–ceramics, J. Mol. Struct. 993 (2011) 160–166.

[19] L.L. Martin, P. Haro-González, I.R. Martín, Optical properties of transparent Dy3+ doped Ba2TiSi2O8 glass ceramic, Opt. Mater. (Amst). 33 (2011) 738–741.

[20] K. Swapna, S. Mahamuda, A.S. Rao, M. Jayasimhadri, T. Sasikala, L.R. Moorthy, Visible fluorescence characteristics of Dy3+ doped zinc alumino bismuth borate glasses for optoelectronic devices, Ceram. Int. 39 (2013) 8459–8465.

[21] L. Wang, Z. Guo, S. Wang, H. Zhang, H. Lv, T. Wang, C. Su, Luminescence properties of Dy3+ doped glass ceramics containing Na3Gd (PO4) 2, J. Non. Cryst. Solids. 543 (2020) 120091.

[22] K. Linganna, C.S. Rao, C.K. Jayasankar, Optical properties and generation of white light in Dy3+-doped lead phosphate glasses, J. Quant. Spectrosc. Radiat. Transf. 118 (2013) 40–48.

[23] S. Damodaraiah, V. Reddy Prasad, Y.C. Ratnakaram, Structural and luminescence properties of Sm3+-doped bismuth phosphate glass for orange-red photonic applications, Luminescence 33 (2018) 594–603, doi:10.1002/bio.3451.

[24] M. Vijayakumar, K. Viswanathan, K. Marimuthu, Structural and optical studies on Dy3+:Tb3+ co-doped zinc leadfluoro-borophosphate glasses for white light applications, J. Alloys Compd. 745 (2018) 306–318, doi:10.1016/j.jallcom.2018.02.211.

[25] N. Chanthima, Y. Tariwong, T. Sareein, J. Kaewkhao, N.W. Sangwaranatee, Investigation of Luminescence Properties of Dy3+ Doped Alkaline Earth Oxides Barium Phosphate Glasses, Appl. Mech. Mater., Trans Tech Publ (2018) 27–31.

[26] K. Jha, M. Jayasimhadri, Spectroscopic investigation on thermally stable Dy3+ doped zinc phosphate glasses for white light emitting diodes, J. Alloys Compd. 688 (2016) 833–840.

[27] M. Braglia, J. Kraus, S. Mosso, Core/clad compositions with high numerical aperture for single-mode fluoride fibres, J. Non. Cryst. Solids. 201 (1996) 237–245.

[28] S. Todoroki, K. Hirao, N. Soga, Local structure around rare-earth ions in indium-and lead-based fluoride glasses with high upconversion efficiency, J. Non. Cryst. Solids. 143 (1992) 46–51.

[29] L. Niu, A.R. Kortan, N. Kopylov, P.H. Citrin, Local structural study of Pb-induced instability in ZBLAN glass, J. Non. Cryst. Solids. 213 (1997) 358–362.

[30] G. Chandana, C.N. Rao, P.V. Rao, M.J.S. Al-Musawi, K. Samatha, G.G. Dhar, Luminescent properties of Sm3+ doped metal fluoro phosphate glasses, Optik (Stuttg) (2019) 163909.

[31] A. Moguš-Milanković, A. Šantić, A. Gajović, D.E. Day, Spectroscopic investigation of MoO3–Fe2O3–P2O5 and SrO–Fe2O3–P2O5 glasses. Part I, J. Non. Cryst. Solids. 325 (2003) 76–84, doi:10.1016/S0022-3093(03)00362-4.

[32] S. Li, H. Liu, F. Wu, Z. Chang, Y. Yue, Effects of alkaline-earth metal oxides on structure and properties of iron phosphate glasses, J. Non. Cryst. Solids. 434 (2016) 108–114, doi:10.1016/j.jnoncrysol.2015.12.004.

[33] E.A. Abou Neel, W. Chrzanowski, D.M. Pickup, L.A. O'Dell, N.J. Mordan, R.J. Newport, M.E. Smith, J.C. Knowles, Structure and properties of strontium–doped phosphate-based glasses, J. R. Soc. Interface. 6 (2009) 435–446.

[34] P.-Y. Shih, H.-M. Shiu, Properties and structural investigations of UV-transmitting vitreous strontium zinc metaphosphate, Mater. Chem. Phys. 106 (2007) 222–226.

[35] E.F. Huerta, A.N. Meza-Rocha, R. Lozada-Morales, A. Speghini, S. Bordignon, U. Caldiño, White, yellow and reddish-orange light generation in lithium-aluminum-zinc phosphate glasses co-doped with Dy3+/Tb3+ and tri-doped with Dy3+/Tb3+/Eu3+, J. Lumin. 219 (2020) 116882.

[36] B.H. Babu, V.V.R.K. Kumar, Warm white light generation in γ-irradiated Dy3+, Eu3+ codoped sodium aluminoborate glasses, J. Lumin. 169 (2016) 16–23.

[37] L.Q. Yao, G.H. Chen, H.J. Zhong, S.C. Cui, F. Li, J.Y. Gan, Enhanced Luminescent Properties in Tm3+/Dy3+ Co-doped Transparent Phosphate Glass Ceramic, in: MATEC Web Conf, EDP Sciences, 2016, p. 4005.

[38] D. Valiev, S. Stepanov, O. Khasanov, E. Dvilis, E. Polisadova, V. Paygin, Synthesis and optical properties of Tb3+ or Dy3+-doped MgAl2O4 transparent ceramics, Opt. Mater. (Amst). 91 (2019) 396–400.

[39] P.R. Rani, M. Venkateswarlu, S. Mahamuda, K. Swapna, N. Deopa, A.S. Rao, Spectroscopic studies of Dy3+ ions doped barium lead alumino fluoro borate glasses, J. Alloys Compd. 787 (2019) 503–518.

[40] G.V. Prakash, Absorption spectral studies of rare earth ions (Pr3+, Nd3+, Sm3+, Dy3+, Ho3+ and Er3+) doped in NASICON type phosphate glass, Na4AlZnP3O12, Mater. Lett. 46 (2000) 15–20.

[41] U. Caldiño, A. Lira, A.N. Meza-Rocha, I. Camarillo, R. Lozada-Morales, Development of sodium-zinc phosphate glasses doped with Dy3+, Eu3+ and Dy3+/Eu3+ for yellow laser medium, reddish-orange and white phosphor applications, J. Lumin. 194 (2018) 231–239.

[42] J. An, Z. Zhang, Y. Qiu, Z. Fu, Y. Zhou, F. Zeng, Luminescence properties of borosilicate glass doped with Ce3+/Dy3+/Eu3+ under ultraviolet excitation for white LED, J. Non. Cryst. Solids. 503 (2019) 208–213.

[43] C. Ming, F. Song, Y. Qin, X. Ren, L. An, M (Tm3+, Tb3+, Ho3+, Dy3+, Mn2+)-doped transparent fluorophosphate glasses for white light-emitting–diodes, Opt. Commun. 321 (2014) 195–197.

[44] Y. Liu, G. Liu, J. Wang, X. Dong, W. Yu, Single-component and warm-white-emitting phosphor NaGd (WO4) 2: Tm3+, Dy3+, Eu3+: synthesis, luminescence, energy transfer, and tunable color, Inorg. Chem. 53 (2014) 11457–11466.

[45] N.P. Rajesh, G. Subalakshmi, C.K. Jayasankar, Investigations on energy transfer and tunable luminescence spectra for single, co-doped and tri-doped RE3+ (RE3+= Dy3+, Sm3+ and Eu3+) activated Sr1. 99Bi0. 01CeO4 phosphors, Opt. Mater. (Amst). 85 (2018) 464–473.

[46] Y. Yu, F. Song, C. Ming, J. Liu, W. Li, Y. Liu, H. Zhao, Color-tunable emission and energy transfer in Tm3+/Dy3+/Sm3+ tri-doped phosphate glass for white light emitting diodes, Opt. Commun. 303 (2013) 62–66.

[47] V.R. Kumar, G. Giridhar, V. Sudarsan, N. Veeraiah, Influence of red lead on the intensity of green and orange emissions of Sm3+ and Ho3+ co-doped ZnO–SrO–P2O5 glass system, J. Alloys Compd. 695 (2017) 668–681.
[48] C. Bocker, S. Bhattacharyya, T. Höche, C. Rüssel, Size distribution of BaF2 nanocrystallites in transparent glass ceramics, Acta Mater 57 (2009) 5956–5963, doi:10.1016/j.actamat.2009.08.021.
[49] Y.M. Moustafa, K. El-Egili, Infrared spectra of sodium phosphate glasses, J. Non. Cryst. Solids. 240 (1998) 144–153.
[50] A.H. Hammad, A.M. Abdelghany, Optical and structural investigations of zinc phosphate glasses containing vanadium ions, J. Non. Cryst. Solids. 433 (2016) 14–19.
[51] J. Wong, C.A. Angell, Glass: structure by spectroscopy, M. Dekker New York, 1976.
[52] A. Shaim, M. Et-Tabirou, Role of titanium in sodium titanophosphate glasses and a model of structural units, Mater. Chem. Phys. 80 (2003) 63–67.
[53] G.Le Saout, P. Simon, F. Fayon, A. Blin, Y. Vaills, Raman and infrared study of (PbO) x (P2O5)(1−glasses, J. Raman Spectrosc. 33 (2002) 740–746.
[54] P.K. Jha, O.P. Pandey, K. Singh, FTIR spectral analysis and mechanical properties of sodium phosphate glass-ceramics, J. Mol. Struct. 1083 (2015) 278–285, doi:10.1016/j.molstruc.2014.11.027.
[55] M. Karabulut, A. Popa, G. Borodi, R. Stefan, An FTIR and ESR study of iron doped calcium borophosphate glass-ceramics, J. Mol. Struct. 1101 (2015) 170–175, doi:10.1016/j.molstruc.2015.08.004.
[56] A. Chahine, M. Et-Tabirou, J.L. Pascal, FTIR and Raman spectra of the Na2O–CuO–Bi2O3–P2O5 glasses, Mater. Lett. 58 (2004) 2776–2780.
[57] A.M. Abdelghany, G. El-Damrawi, A.H. Oraby, M.A. Madshal, Optical and FTIR structural studies on CoO-doped strontium phosphate glasses, J. Non. Cryst. Solids. 499 (2018) 153–158, doi:10.1016/j.jnoncrysol.2018.07.022.
[58] A. Okasha, A.M. Abdelghany, S.K. Mohamed, S.Y. Marzouk, H.A. El-Batal, M.S. Gaafar, Gamma ray interactions with samarium doped strontium phosphate glasses, J. Mater. Sci. Mater. Electron. 29 (2018) 20907–20913, doi:10.1007/s10854-018-0234-3.
[59] S. Rada, E. Culea, FTIR spectroscopic and DFT theoretical study on structure of europium-phosphate-tellurate glasses and glass ceramics, J. Mol. Struct. 929 (2009) 141–148, doi:10.1016/j.molstruc.2009.04.021.
[60] W.T. Carnall, P.R. Fields, K. Rajnak, Electronic energy levels in the trivalent lanthanide aquo ions. I. Pr3+, Nd3+, Pm3+, Sm3+, Dy3+, Ho3+, Er3+, and Tm3+, J. Chem. Phys. 49 (1968) 4424–4442.
[61] I.I. Pm, W.T. Carnall, P.R. Fields, K. Rajnak, Spectral Intensities of the Trivalent Lanthanides and Actinides in Solution. II. Pm3+, Sm3+, Eu3+, Gd3+, Tb3+, Dy3+, and Ho3+, 4412 (1968). doi:10.1063/1.1669892.
[62] M. Kaur, A. Singh, V. Thakur, L. Singh, Thermal, optical and structural properties of Dy3+ doped sodium aluminophosphate glasses, Opt. Mater. (Amst). 53 (2016) 181–189.
[63] D.V. Rao, C.M. Kumar, G. Srinivas, R. Manepalli, R.R. Raju, G. Giridhar, Spectroscopic properties of Dy3+ doped MgO-LiF-CdO-P2O5 glasses, Optoelectron. Adv. Mater. Commun. 11 (2017) 691–696.
[64] K. Anilkumar, S. Damodaraiah, S. Babu, V.R. Prasad, Y.C. Ratnakaram, Emission spectra and energy transfer studies in Dy3+ and Dy3+/Eu3+ co-doped potassium fluorophosphate glasses for white light applications, J. Lumin. 205 (2019) 190–196.
[65] T.R. Raman, Y.C. Ratnakaram, Concentration dependent Dy3+ activated LiPbB5O9 phosphor: Structure and luminescence studies for white LED applications, Opt. Mater. (Amst). 99 (2020) 109515.

Volume 65, Issue 3, 2021
Journal of Scientific Research
Institute of Science,
Banaras Hindu University, Varanasi, India.

Glomerulotubular Injury and Phenotypic Switch of Kidney Cells in Diabetic Nephropathy

Syed Vaziha Tahaseen[1,2], Manga Motrapu[3], Rajkishor Nishad[3] and Kiranmayi Peddi[*2]

[1]Department of Biochemistry, SRR & CVR College, Vijayawada-520004, India. vazeehatahaseensuraj@gmail.com
[2]Department of Biochemistry, Acharya Nagarjuna University, Guntur-522510, India. kiranmayi.kodali@rediffmail.com*
[3]Department of Biochemistry, University of Hyderabad, Hyderabad- 500046, India. biochemistry1520@gmail.com

Abstract: **The increased prevalence of diabetes mellitus (T2DM), and one of the complications, diabetic nephropathy (DN), constitutes a significant health care burden worldwide. Nephron, the kidney's structural and functional unit, includes two principal regions: glomerulus and tubule. Glomerular dysfunction and podocyte injury are significant factors in the development and progression of DN. Nevertheless, emerging evidence suggests that kidney tubular damage also contributes significantly to the pathogenesis of DN. To assess the contribution of both glomerular and tubular damage in DN's pathogenesis, we evaluated the functional and histochemical parameters and immunohistochemistry of the kidney biopsy specimens for EMT and fibrosis markers from 11 patients with confirmed diabetic nephropathy. Histopathological analysis revealed that besides significant glomerulosclerosis, kidneys are presented with tubular injury. These patients' glomeruli showed decreased epithelial markers' expression while expressing a more considerable number of mesenchymal markers. On the other hand, the tubular region displays an enhanced expression of the fibroblastic marker. Pathogenesis and proteinuria in DN patients could be contributed by the morphometric transformation of podocytes into mesenchymal form, tubular epithelial cells into fibroblasts. Our observations are significantly relevant for identifying novel therapeutics for both diagnosing and treating DN.**

Index Terms: **Diabetes, EMT, Fibroblast, Glomerulus, Nephropathy, Podocytes.**

I. INTRODUCTION

Vertebrate kidneys contribute to the body's homeostasis by regulating electrolyte, acid-base, and water balance with millions of nephrons' collective effort. The glomerulus and tubule are two regions of the nephron, while the former responsible for permselectivity, latter ensures selective reabsorption. Thus, the collective effort of the glomerulus and tubule determines the final composition of urine. The kidney's potential to excrete ultrafiltrated urine devoid of large molecules, including protein, is primarily determined by a three-layered glomerular filtration barrier (GFB). The three layers of GFB are the fenestrated endothelium of glomerular capillaries, glomerular basement membrane (GBM), and glomerular podocytes.

Podocytes are considered highly imperative for the normal function of GFB over the other components. Podocytes are visceral epithelial cells of the glomerulus, presented with a giant cell body and characteristic primary and secondary foot processes. With the help of foot processes, podocytes provide epithelial coverage to the capillaries. Podocytes injury is expected to impair the efficiency of glomerular permselectivity and is manifested by sclerosis and varying degree of albuminuria. Simultaneously, the kidney tubule is a layer of elongated tubular epithelial cells connected with the kidney capsule wall. The kidney tubular epithelial cells constitute the tubule's outer layer that plays a crucial role in absorbing glucose, amino acids, and primary urine proteins. At the same time, tubular cells elicit several essential functions such as regulating water, electrolyte, acid, and alkali balance. Injury to the kidney cells, including podocytes and tubular epithelial cells, during clinical conditions such as diabetic nephropathy (DN), compromise both kidney architecture and function.

DN is one of the most common complications in diabetic patients and the primary cause of end-stage kidney failure (ESKD) and is associated with increased mortality. 30-40% of diabetic patients (both type 1 and type2) develop DN, whereas a significant proportion of DN cases progresses to end-stage kidney disease (ESKD).

Although early stages of DN are asymptomatic, end-stage is being treated by either dialysis or kidney transplantation. DN'spathophysiological features include glomerulosclerosis, interstitial and tubular fibrosis, inflammation, thickening of GBM, decreased glomerular filtration rate (GFR), and overt proteinuria. Progressive proteinuria is a hallmark of DN, whereas patients initially show microalbuminuria (30-300 mg/24 hr) for an extended period (5-10 years), followed by

* Corresponding Author

DOI: 10.37398/JSR.2021.650313

macroalbuminuria (≥300 mg/ 24 hr). A proteinuric condition during DN suggests both impaired glomerular permselectivity and tubular reabsorption. Despite microalbuminuria or proteinuria, diabetic patients might have a standard glomerular structure with or without tubulointerstitial and arteriolar abnormalities (Rockwell,1994) .The clinical manifestations of DN are strongly related to the degree of mesangial expansion. Microscopic morphometric analysis has described both structural changes and the structural-functional relationships of DN. These structural changes may include injury to both podocytes and tubular epithelial cells. Podocytes (visceral epithelial cells) may undergo phenotypic conversion to mesenchymal cells and become motile and detach from GBM. Alternatively, tubular epithelial cells may transform into fibroblasts due to various noxious stimuli in the T2DM. Nevertheless, the simultaneous occurrence of both events was not demonstrated earlier in the glomeruli from DN subjects.

Since podocyte contributes to the glomerular permselectivity and integrity of GBM, any insult to podocytes could contribute to altered glomerular morphology and proteinuria. Simultaneously, tubular injury and impaired reabsorption could also be anticipated during damage to tubular cells. This study demonstrated the phenotypic switch of podocytes (glomerular regions) and tubular epithelial cells (kidney tubule) in biopsy sections from T2DM patients.

II. METHODOLOGY

A. *Enrollment of Patients:*

We enrolled 11 patients with T2DM undergoing biopsy as recommended by the nephrologist. Inclusion criteria are diabetes with more than 15 years, persistently inadequate glycemic control, and proteinuria above 300 mg/24 hr. Exclusion criteria were hematuria, clinical and laboratory findings suggestive of non-diabetic glomerulopathy, and secondary renal damage due to hypertension. For the enrolled patients, 24 hours of urine and early morning spot urine were collected, and proteinuria was determined. Kidney biopsies of these 11 DN patients were collected and performed histopathological analysis. Biopsy specimens from kidney cancer patients who underwent nephrectomy for a localized kidney tumor were considered non-diabetic. The non-affected part of the kidney tissue was utilized for histopathological examinations. The kidney biopsy serial sections (4 μm) from paraffin-embedded tissues were prepared to perform morphometric analysis. The Institutional Review Board approved the study of GunturMedical College, Guntur, Andhra Pradesh, India (#GMC/IEC/120/2018). Our studies abide by the Declaration of Helsinki principle.

B. *Clinical Examination:*

Anthropometric measurements were recorded for the patients; Body mass index (BMI) was calculated using the formula: weight in kg and height in m^2. Blood pressure (BP) was checked thrice by a digital oscillometer (Omron Healthcare Co. Ltd.). Fasting blood glucose (FBG) was assessed in the whole blood using a glucometer (Accu-Chek Aviva, Roche *Diagnostics GmbH, Germany). HbA1c was estimated in whole blood using a bio-rad D-10 analyzer. Urinary albumin (number COD11573) and creatinine (number COD11502) levels were estimated using existing assay kits (Biosystems).*

C. *Morphometric analysis:*

For histological analysis, kidney cortical samples were fixed with 4% neutral buffered paraformaldehyde before embedding in paraffin. Paraffin-embedded tissues were sliced longitudinally into four μm thick sections, subjected to staining with haematoxylin and eosin for general evaluation of the cellular structure, periodic acid–Schiff (PAS) staining applied to provides excellent definitions for glomerular basement membrane, tubular basement membrane, and mesangium. Masson's trichrome staining is used to observe the extracellular mesangial volume, interstitial fibrosis percentage, and tubular atrophy (IFTA). At least 15 glomeruli per stained biopsy had to be counted for the measurement to be considered valid. The diagnosis and histological scoring for kidney damage were evaluated based on Tervaert et al.(2010). At least six glomeruli were captured for each biopsy sample and quantified for histopathological changes. We took images with a BX51 light microscope (Olympus, Tokyo) with appropriate filters. Histological positive staining intensity was quantified using software (Image J 1.44, NIH, USA) (Nishad et al., 2019; Kudose et al., 2018; Meyer, 2003).

D. *Nephroseq analysis:*

To validate the observations found in biopsy specimens holds with the existing database generated with data from human, we analysed the expression of the same set of genes Nephroseq database (https://nephroseq.org). The source for Nephroseq database is the University of Michigan O'Brien Renal Centre, Michigan, Ann Arbor, MI.

E. *Statistical analysis*:

Data are presented as mean±SD. For the statistical difference between the two groups of the data, Student's t-test was used to generate the P-values ($p \leq 0.05$). Statistical analyses were performed using GraphPad Prism V.6.0.

III. RESULTS

A. *Impaired renal function in diabetic subjects:*

Mean age of 11 diabetic patients was 61±5 years, BMI 29.7 ± 5.6, and HbA1c 9.1 ± 2%. Fasting glucose of diabetic patients significantly high (Fig.1A). Similarly, urinary albumin (302±71.87mg/24hrs.) and serum creatinine (3.87± 2.52 mg/dL)), and eGFR values (34.9±11.9ml/min/1.73m^2) suggests kidney functional parameters were in the progressive DN pathological range (Fig.1B-D). High fasting and postprandial

glucose levels and HbA1c (%) indicate poor glycemic control in these patients. These patients have ~15 yrs of diabetic history, and they are high overt proteinuria, suggesting that kidney function has been compromised and suffering from progressive DN.

Figure 1

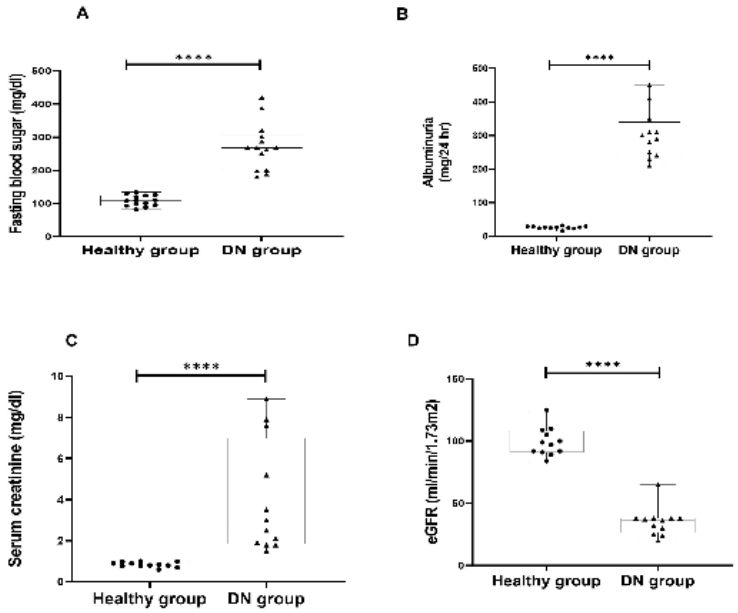

Figure 1: The kidney functional parameters in patients enrolled in the study:(A) Fasting blood glucose levels of healthy volunteers and patients with DN. (B) Albumin levels were measured in healthy volunteers and DN patients. (B) Creatinine levels were estimated in serum. (C) Glomerular filtration rate (GFR) was calculated in healthy volunteers and DN patients. Data from the DN group is significantly different from the Healthy group. ($p < 0.001$).

Figure 2

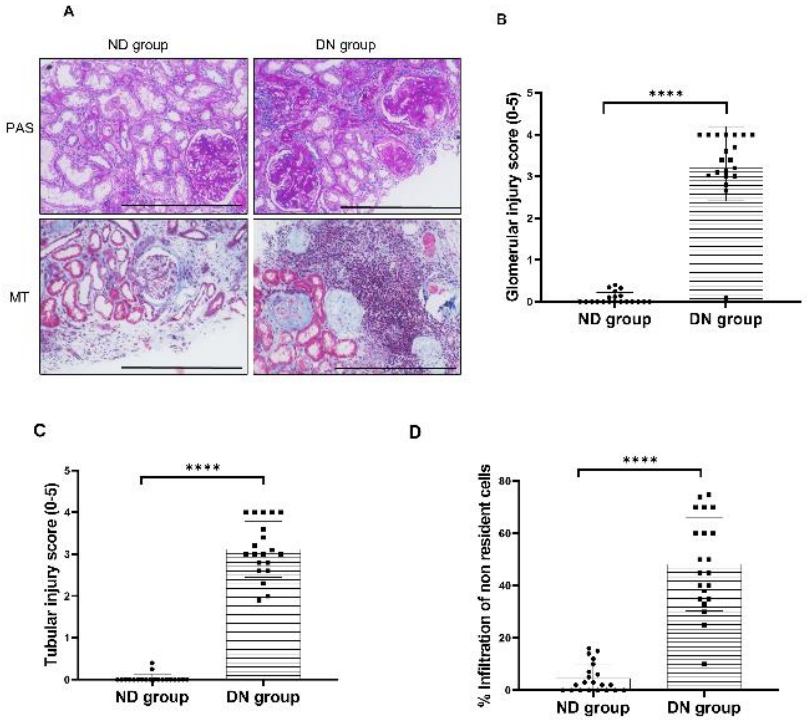

Figure 2: Quantification of kidney injury in DN patients. (A) Representative images of periodic acid Schiff's stain and Mason's trichrome staining of kidney sections from non-diabetic (ND) and diabetic nephropathy (DN) subjects. Glomerular injury score (B) and tubular injury score (C) were quantified in biopsy sections (n= 20). (D) % of infiltrated cells was quantified in ND and DN patients' specimens. Data from DN is significantly different from ND subjects ($p < 0.001$).

Figure 3

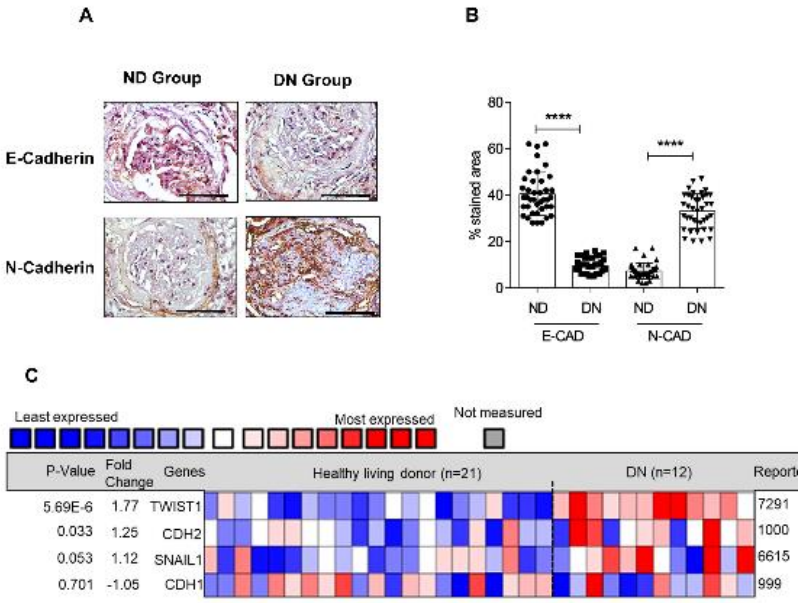

Figure 3: Quantification of epithelial-mesenchymal markers in glomerulus from DN patients, A) Staining for E-cadherin (epithelial marker) and N-cadherin (mesenchymal marker) in the glomerular region of non-diabetic (ND) and diabetic nephropathy (DN) subjects. (B) Staining intensity for E-cad and N-cad was quantified using Image-J (NIH, USA) and presented as a bar diagram (n= ~40 sections) (p <0.001). (C) Expression of EMT markers in glomeruli from healthy living donors vs. DN patents (Data mining in the Nephroseq database (University of Michigan O'Brien renal center, Ann Arbor, USA).

Figure 4

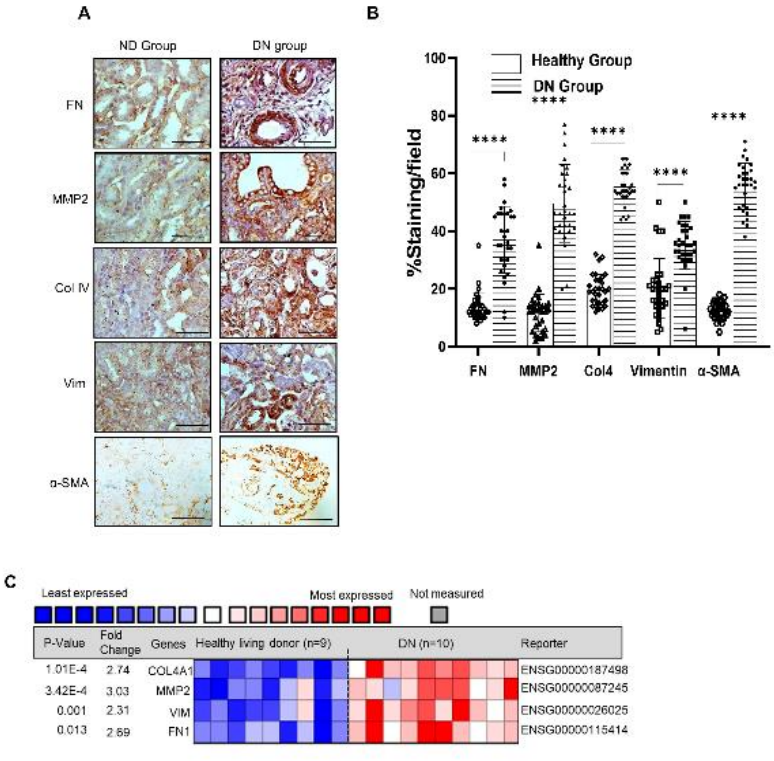

Figure 4*:* Quantification of fibroblast markers in the tubular region from DN patients**.** (A), (B), Representative images of staining for fibronectin (FN), MMP2, Collagen IV (Col IV), Vimentin (Vim), and α-Smooth Muscle Actin (SMA) in a tubular region of non-diabetic (ND) and diabetic nephropathy (DN) subjects. Staining intensity was quantified using Image-J (NIH, USA) and presented as a bar diagram (n= ~40 sections) (p <0.001). (C) Expression of fibroblastic markers from healthy living donors vs. DN patents (Data mining in the Nephroseq database, U of Michigan O'Brien renal center, Ann Arbor, USA).

B. Severe glomerular and tubular injury in DN patients:

Since diabetic patients showed macroalbuminuria, we wanted to perform a histological examination to assess nephropathy intensity. We performed PAS and Mason's trichrome stainings (Fig.2A) and evaluated both glomerular and tubular injury in these patients. One of the characteristic features of DN is the infiltration of non-resident cells into glomeruli. Therefore, we

counted % of in filtered cells into the glomeruli of these patients and found that ~50% of glomerular cells are non-resident cells compared with ~5% of non-resident cells in non-diabetic individuals (Fig.2D)

C. Attenuated expression of epithelial markers in glomerular regions in DN patients:

As discussed in the introduction, the appearance of protein in the urine indicates a structural and functional artifact, particularly in the glomerular area. Podocytes are the primary cell type and account for ~40% of all glomerular cells. In response to injury, Podocytes undergo a morphologic switch known as epithelial to mesenchymal transition (EMT), during which they attain an embryonic form by shedding their epithelial features. It is conceivable that podocytes, undergone EMT, abandon their complex architecture and relinquish their specialized functions, leading to proteinuria. Since we observed proteinuria in these patients and few resident cells in the glomerulus, we suspect that podocytes might have undergone EMT. When we stained for E-cadherin, a putative epithelial marker, we observed decreased staining (Fig.3A).

On the other hand, N-cadherin (a mesenchymal marker) expression enhanced, suggesting loss of epithelial features and gain of mesenchymal features (Fig.3A&B). We also performed a meta-analysis of the Nephroseq database for EMT markers. Nephroseq analysis (Fig.3C) reveals a marginally decreased expression of E-cadherin (CDH1; -1.05) but an enhanced expression of N-cadherin (CDH2; 1.25), SNAIL1 (1.12), and TWIST. (1.77). Together Nephroseq analysis and histochemical data suggest podocytes undergo EMT in DN patients.

D. Elevated fibrotic markers in tubular regions in diabetic patients:

Recent studies suggest that increased glomerular leakage and impaired tubular reabsorption are accountable for albuminuria in the early DN(Zeni et al., 2017). Further, tubulocentric pathology and treatment for DN were proposed(Zeni et al., 2017). Since we observed tubular injury in these patients (Fig2C), we investigated whether tubular cells have undergone any phenotypic transformation. Interestingly, we observed enhanced expression of fibrotic markers such as fibronectin (FN), MMP2, collagen IV, vimentin, and α-SMA in both proximal and distal tubules (Fig.4A&B). Thesignificantinduction of these markers suggests that the transformation of tubular cells to fibroblasts. We also performed a meta-analysis using the Nephroseq database for fibroblasts markers. Nephroseq analysis (Fig.4C) reveals the significant induction of the above-mentioned fibrotic markers suggesting our biopsy data correlates with data mined from the database (Fig.4B vs. Fig.4C). Together our data suggest tubular cells from DN patients could transform into fibroblasts.

DISCUSSION

Diabetes is presented with high morbidity and often progresses to chronic kidney disease and accounts for significant ESKD and dialysis cases. With the increasing prevalence of T2DM, its complications DN impose a tremendous burden on individuals, families, and the health care sector. Although there is extensive information on diagnosis and biomarkers of diabetic kidney diseases, it is still increasingly clear whether the glomerulus or tubules are more critical in DN's development and progression. Glomerulosclerosis was considered a primary event of the pathogenesis in DN. Other glomerular changes such as thickening of the basement membrane and mesangial expansion, and podocytopathy are prominent manifestations during DN.Although glomerular centric pathological events undoubtedly contribute to DN's pathology, there is growing evidence to suggest a significant role for the proximal tubules as drivers of proteinuria and other clinical manifestations of DN. In the present, we noticed that DN patients showed both glomerular and tubular injury, as evidenced by PAS and Mason's trichrome staining. Indeed, we saw the loss of epithelial markers and mesenchymal markers in glomerular cells and fibrotic markers in tubular cells. This evidence of both glomerular cells and tubular cells' transition to mesenchymal and fibrotic phenotype, respectively, provides a new perspective on the pathophysiology of DN. This novel observation provides new diagnosis and therapeutic approaches by targeting both glomerular epithelial cells and tubular cells in DN.

Both glomerular filtration barrier (consist of podocytes, basement membrane, and endothelium) and tubular epithelium work in concert to ensure the ultrafiltration of plasma and reabsorption of primary urine, respectively, from becoming urine. Thus, both glomerulus and tubule regulate the final composition of urine. Besides being a part of the filtration apparatus, glomerular podocytes elicit several functions to maintain the glomerular function's integrity. Podocytes provide epithelial coverage to the glomerular capillaries and oppose hydrostatic pressure to facilitate glomerular filtration and are thus indispensable to renal filtration. However, podocytes are exposed to a myriad of hematological agents and noxious stimuli due to diabetes. A body of experimental data demonstrated high glucose, glucose-derived advanced glycation end-products (AGEs), activation of sorbitol, RAAS, Growth hormone (GH), and TGF-β, etc., were contributed to the altered signaling events thus pathology of DN. Accumulating evidence suggests that glomerular podocytes undergo EMT during various insults such as high glucose, AGEs, GH, and TGF-β (Anil Kumar et al., 2014). Podocytes

might majorly contribute to the EMT phenomenon; we observed glomeruli from DN patients as they are the glomerulus' predominant epithelial cells. EMT of podocytes might compromise their ability to offer epithelial coverage to the capillaries and oppose hydrostatic pressure, resulting in impaired glomerular filtration.EMT of podocytes could be a reason for podocytes' appearance in urine from patients with advanced DN (Reidy & Susztak, 2009). The two parts of the kidney tubule, proximal and distal, have specialized functions. The proximal part is concerned with the reabsorption of several primary urine components to maintain homeostasis; in contrast, the distal tubule is associated with complete water, electrolyte, and acid-base balance regulation. Recent studies suggest that in addition to increased glomerular leakage, impaired tubular reabsorption is also accountable for DN's albuminuria(Zeni et al., 2017). DN's tubular manifestations include tubular atrophy, interstitial fibrosis, and thickening of the tubular basement membrane, correlated with kidney dysfunction and proteinuria. It is noteworthy that the proximal tubule injury can trigger glomerular dysfunction and such retrograde trafficking has implications in the progression of DN(Hasegawa et al., 2013).Glomerular podocytes and proximal tubular cells work in association with complementing each other's biology. Hasegawa et al. demonstrated that proximal tubules communicate with podocytes by releasing nicotinamide mononucleotide(Hasegawa et al., 2013).Proximal tubule-specific Sirt1 helps maintain glomerular NMN concentrations, thus preserving the glomerular podocyte function and offering protection against diabetic kidney disease(Hasegawa et al., 2013). These observations suggest that the injury to tubular cells significantly affects the glomerular function and promotes DN progression.

Additionally, the injured proximal tubule epithelium triggers the inflammatory response, which leads to tubulointerstitial fibrosis, tubular atrophy that, in turn, promotes secondary glomerulosclerosis(Lee et al., 2012). Therefore, the observed tubular and glomerular injury in DN patients from our study reveals that DN's pathological evaluation needs to be comprehensive and evaluate the tubular injury and not only glomerulus. In summary, our study provides evidence for significant tubular damage in addition to glomerular injury. It suggests a need for diagnostic evaluation and therapeutic advances in DN towards both glomerulus and tubule.

ACKNOWLEDGMENTS

Authors thank Guntur Medical College and Dr. Srilatha .V, nephrologist, NRI hospital, patients, and their families, for their support during this study.

REFERENCES

Anil Kumar, P., Welsh, G.I., Saleem, M.A., Menon, R.K. (2014) Molecular and cellular events mediating glomerular podocyte dysfunction and depletion in diabetes mellitus. *Front Endocrinol (Lausanne)*, 5(SEP),1-10.

Hasegawa, K., Wakino, S., Simic, P., et al. (2013) Renal tubular sirt1 attenuates diabetic albuminuria by epigenetically suppressing claudin-1 overexpression in podocytes. *Nat Med*, 19(11), 1496-1504.

Kudose, S., Hoshi, M., Jain, S., Gaut, J,P. (2018) Renal Histopathologic Findings Associated with Severity of Clinical Acute Kidney Injury. *Am J Surg Pathol*, 42(5), 625-635.

Lee, P.T., Chou, K.J., Fang, H.C. (2012) Are tubular cells not only victims but also perpetrators in renal fibrosis. *Kidney Int*, 82(2), 128-130.

Meyer, T.W. (2003) Tubular injury in glomerular disease. *Kidney Int*, 63(2), 774-787.

Nishad, R., Mukhi, D, Tahaseen, S.V., Mungamuri, S.K., Pasupulati, A.K. (2019) Growth hormone induces Notch1 signaling in podocytes and contributes to proteinuria in diabetic nephropathy. *J Biol Chem*, 294(44), 16109-16122.

Reidy, K., Susztak, K. (2009) Epithelial-Mesenchymal Transition and Podocyte Loss in Diabetic Kidney Disease. *Am J Kidney Dis*, 54(4), 590-593.

Rockwell, R. (1994) Interview with the Executive Director. *ICPSR Bull*, 15(2), 1-6.

Tervaert, T,W,C., Mooyaart, AL., Amann, K., et al. (2010) Pathologic classification of diabetic nephropathy. *J Am Soc Nephrol*, 21(4), 556-563.

Zeni, L., Norden, A.G.W., Cancarini, G., Unwin, R.J. (2017) A more tubulocentric view of diabetic kidney disease. *J Nephrol*, 30(6), 701-717.

***

Original Article

Prediction and Risk Factor Analysis of Obesity-related Proteinuria among Individuals with Metabolic Syndrome

Syed Vaziha Tahaseen, P. Kiranmayi[1], Marni Rakshmitha[2], Bezawada Anusha[3]

Department of Biochemistry, SRR & CVR Govt. Degree College (A), Vijayawada, [1]Department of Biochemistry, Acharya Nagarjuna University, Guntur, [2]Department of Biochemistry, Gitam University, Visakhapatnam, [3]Department of Biotechnology, Acharya Nagarjuna University, Guntur, Andhra Pradesh, India

Abstract

Objective: In the present modern era of time, poor and frantic lifestyle has led to an enumerate increase in the number of people with obesity and metabolic syndrome (MS). Epidemiological studies have shown the incidence of chronic kidney disease (CKD) risk factors in individuals with obesity and MS; despite the nonclear evidence on the existing potential risk factors, it became important to reassess existing potential risk factors that are involved in disease progression and its further complications. The strongest risk factor of CKD, albumin-to-creatinine ratio (ACR) recognized as a marker of MS and obesity. This study was carried out to identify the association of obesity (body mass index [BMI]) as a risk factor for albuminuria and to observe the dependence and association with albuminuria of each critical and basic factor of MS. **Design:** We conducted the potential risk factor analysis on 913 subjects, including 398 females and 515 males, from various diabetic hospitals of Vijayawada, Andhra Pradesh from early 2013 to June 2015. The medical records of the patients followed up; the anthropometric measurements and clinical parameters were retrospectively collected. The total subjects were categorized as subjects with and without MS as per National Cholesterol Education Program Adult Treatment Panel (NCEP-ATPIII) and the subjects with BMI more than 30 kg/m^2 were defined as obese according to WHO classification. **Results:** Student's *t* test analysis indicates a significant difference for ACR with mean values of 39.5 ± 44.8 and 18.4 ± 24.3 ($P < 0.0001$) in subjects with MS and without MS, 43.4 ± 48.3 and 36.7 ± 42.5 ($P < 0.02$) in obese and nonobese subjects, respectively. Chi-square analysis showed a significant association ($P < 0.05$) between MS and ACR and correlation analysis manifested significant association ($P < 0.01$) between ACR and FBS, TG, B.P, and Age in subjects with MS. The subjects with high prevalence of albuminuria exhibited significant association with an odds ratio (OR) of 1 (referent) 1.9 (95% CI, 1.34–2.58, $P = 0.0002$), 1.5 (95% CI, 1.11–1.96, $P = 0.0082$) for FBS >110 mg/dL, and TG > 150 mg/dL, respectively. Although the subjects with obesity showed no correlation with albuminuria, the risk for albuminuria was 1.5 times (95%CI 1.03–2.40, $P = 0.03$) higher among obese male subjects compared to obese female subjects. **Conclusion:** Our study strongly supports that albuminuria is highly prevalent among the subjects, with MS showing a significant positive association between obesity (BMI) with albuminuria in males only.

Keywords: ACR, BMI, chronic kidney disease, FBS, HDL, metabolic syndrome, TG

Introduction

Chronic kidney disease (CKD) has become a major global health problem with an estimated worldwide affected population of 2 million. In this context, early detection of CKD is crucial to prevent the progression of CKD to end-stage renal disease (ESRD). The presence of persistently elevated albuminuria is an early clinical marker of CKD and a predictor for cardiovascular diseases (CVD) and mortality. The clinical manifestation of CKD includes albuminuria/proteinuria as an important diagnostic tool for primary treatment[1-3] and also considered in the definition of the metabolic syndrome (MS) by the World Health Organization.[4] The MS is defined as a

Received: 22-May-2020, **Revised:** 08-June-2020, **Accepted:** 09-June-2020, **Published:** 31-March-2021

Access this article online

Quick Response Code:

Website: www.journalofdiabetology.org

DOI: 10.4103/jod.jod_37_20

Address for correspondence: Dr. P. Kiranmayi, Department of Biochemistry, Acharya Nagarjuna University, Nagarjuna Nagar, Guntur 522510, Andhra Pradesh, India. E-mail: Kiranmayi.kodali@rediffmail.com

How to cite this article: Tahaseen SV, Kiranmayi P, Rakshmitha M, Anusha B. Prediction and risk factor analysis of obesity-related proteinuria among individuals with metabolic syndrome. J Diabetol 2021;12:140-5.

constellation of risk factors including obesity, impaired fasting glucose (FBS >110 mg/dL), increased triglycerides (TG>150 mg/dL), associated with insulin resistance, hypertension (systolic >140 mm Hg), low levels of high-density lipoprotein cholesterol (HDL< 40 mg/dL)[5] and chronic inflammation,[6] leads to composite metabolic derangements that contribute to CKD and coronary artery disease. As per the prior investigations, the relationship between albuminuria, and MS risk factors percentage of prevalence being reported to be 10%-42% in persons with type II diabetes, 11%-40% in people with hypertension and 5%-10% in those without diabetes, hypertension or cardiovascular disease.[7-9] Obesity has been pointed out as one of the critical factors of MS, and the body mass index (BMI) estimate of more than 30 kg/m^2 indicates obesity, and people with MS are at higher risk of many chronic diseases with reduced life expectancy. One of the molecular mechanisms underlying obesity-related CKD is the abnormal or excessive accumulation of fat, characterized by adipocytes hypertrophy. This phenomenon induces hypoxia,[10] promoting inflammation and secretion of adipokines such as leptin, which specifically binds to the receptors on glomerulus and show a direct effect on kidney by promoting excessive production of pro-fibrotic transforming growth factor beta (TGF-β) which further enhance the production of extracellular matrix (ECM) components leading to fibrosis.[11,12] In obesity, increased adipose storage or inflammation of adipocytes brings about insulin resistance conversely insulin sensitivity reduction by several intracellular mechanisms causing the onset of hyperglycemia facilitating renal fibrosis.[13]

In the studies with obesity, the possible existence of a relationship between the roles of obesity executed as BMI in routine clinical practice with kidney dysfunction remains controversial. Weisinger *et al.*[14] first reported that massive proteinuria is associated with obesity. Similarly, limited studies have systematically addressed the association between microalbuminuria with obesity or central obesity irrespective of gender and other predisposing conditions. Hoffmann *et al.* [15] conversely found that there is no difference in albuminuria levels in lean and obese glucose-tolerant subject's studies.[16] However, very fewer studies focused on microalbuminuria, especially in obese nondiabetic, no hypertensive subjects. Our study focused to predict the risk factors of CKD in obesity-associated albuminuria in the south Asian population having unique anthropometric body measurements and to substantiate the clinical practices in most of the hospitals where BMI usually considered as the only clinical parameter to determine obesity.

Materials and Methods

Study area and population

This study is a cross-sectional analysis carried out in Vijayawada, Krishna District, Andhra Pradesh, India, among subjects aged between 20 and 84 years. The study was conducted on 913 subjects including 398 females (43.6%) and 515 (56.4%) males during their hospital visit who underwent medical screening at various diabetic hospitals of Vijayawada from early 2013 to June 2015 and have undergone diagnosis. Majority of them had MS. The exclusion criteria of the study were pregnant women with MS and the patients who had other CKDs. The clinical diagnosis reports and anthropometric measurements regarding height and weight were collected with patient consent.

Sample size (n) was calculated as follows = z^2 p $(1–p)/d^2$. In this study, the sample size for obesity was calculated using prevalence P = 6.5%[17] and confidence level of 95% and the precision of 0.05, by adding 10% nonresponsive rate.The total sample size was n = 103. The sample size for obese was 258. Among them, 112 were males and 146 were females. For MS, the sample size was calculated using a 95% confidence level with the margin of error 0.05 and prevalence P = 20%[18] by adding 10% non-responsive rate, the total sample size should be n = 270, but a total number of 874 MS subjects included in the study.

Sampling technique and procedure

Laboratory findings

According to the "III Adult Treatment Panel" of the "National Cholesterol Education Program" (NCEP-ATPIII of 2001) principles, MS includes the evaluation of the following risk factors: (1) fasting serum glucose (FBS), (2) TG (triglycerides), and (3) HDL (high-density lipoproteins) with consideration of BMI >30 kg/m^2 and with systolic pressure > 130 mm Hg and diastolic pressure > 90 mm Hg. According to the National Kidney Foundation (NKF) guidelines (Joint National Committee on Prevention, Detection, Evaluation, and Treatment of High Blood Pressure, 1997),[19] the urinary albumin (μg/mL) to creatinine (mg/mL) ratios in an untimed urine specimen is a convenient way to assess albumin excretion. Albuminuria is classified based on severity as normal healthy category ACR <30 μg/mg and unhealthy albuminuria category ACR >30 μg/mg. Among the 913 subjects, 402 (44%) are unhealthy albuminuria subjects and 511 (56%) are healthy albuminuria subjects.

Physical examination and clinical data

The anthropometric measurements were carried out as per the hospital standard operating procedures, the height was measured using calibrated height meters with subjects standing bare-footed in erect position placing the feet together and weight measured with the calibrated weighing machine. BMI was calculated as weight in kilograms divided by a square of height in meters. Blood pressure (BP) was measure by trained nurses employing a standard mercury sphygmomanometer, while the subject sit in a chair with feet on the floor and arm reinforced elbow is at around heart level. The average of two readings was used

for the analysis. All participants' clinical data related to routine laboratory findings were collected from medical records of the respective hospitals.

Statistical analysis

We performed statistical analysis using the SPSS software package. The results summarized as percentages and as the mean ± standard deviation (SD). The Pearson chi-square test and Student's *t* test were used to compare the differences between categorical variables. An appropriate condition among each parameter tested using Spearman's correlation coefficient. A value of $P < 0.05$ was considered a statistically significant difference. We calculated odds ratios using a 2×2 table.

Ethical consideration

We conducted this study with the ethical consideration approval got from the institutional review board of Guntur Medical College and Government General Hospital, Guntur, Andhra Pradesh, India and approved by the Helsinki Declaration. (Application number GMC/IEC/120/2018).

Results

This cross-sectional study performed on 913 randomly selected individuals with the majority (874) participants having MS. Irrespective of their metabolic condition we categorized the total subjects into three different categories. Each time in this study, the total subjects were categorized individually following presence/absence of MS as with MS (95.7%) and without MS (4.3%), similarly with obesity (28%) and without obesity (72%) and with healthy albuminuria (56%) and unhealthy albuminuria (44%). The mean and SD values of the following risk factors such as anthropometric, BP, lipid profile, and blood

Table 1: Comparison of baseline characteristics in, without MS and with MS groups, without MA and with MA groups and without obesity and with obesity groups using Student's *t* test

	Metabolic syndrome (MS)				
	Without MS ($n = 39$)		With MS ($n = 874$)		
Risk factor	Mean	SD	Mean	SD	*P* Value
BMI	25.57	2.08	28.23	4.64	<0.0001*
FBS	91.00	5.69	147.73	50.79	<0.0001*
ACR	18.43	24.27	39.48	44.76	<0.0001*
TGs	112.72	29.74	174.70	89.91	<0.0001*
HDL	39.28	5.32	40.84	5.65	0.07
BP	125.00	16.37	128.26	17.77	0.22
Age	50.56	13.89	50.38	10.48	0.94
	Microalbumin (MA)				
	Without MA (albumin < 30) ($n = 402$)		With MA (albumin > 30) ($n = 511$)		
Risk factor	Mean	SD	Mean	SD	*P* Value
BMI	27.88	4.31	28.42	4.91	0.07
FBS	138.17	46.76	154.39	54.69	<0.0001*
ACR	12.21	7.86	72.09	48.67	<0.0001*
TGs	169.26	89.32	175.61	88.72	0.28
HDL	40.77	5.69	40.79	5.58	0.95
BP	126.75	16.36	129.87	19.18	<0.0001*
Age	50.17	10.25	50.66	11.12	0.48
	Obesity				
	Without obesity BMI < 30) $n = 655$		With obesity (BMI > 30) $n = 258$		
Risk factor	Mean	SD	Mean	SD	*P* Value
BMI	25.87	2.58	33.80	3.55	<0.0001*
FBS	145.62	52.21	144.52	47.95	0.76
ACR	36.68	42.47	43.38	38.58	0.02*
T. Gs	173.65	89.52	168.00	87.92	0.10
HDL	41.00	5.70	40.21	5.45	0.056
B. P	127.45	18.15	129.84	16.48	0.06
Age	50.33	10.92	50.55	9.90	0.77

SD = standard deviation, BMI = body mass index, FBS = fasting blood sugar, ACR= albumin creatinine ratio, HDL = high-density lipoproteins, BP = blood pressure

**P* value significant at <0.05

glucose measures are compared and ascertained [Table 1], similarly correlated with each parameter [Table 2].

Among all baseline characteristics, a significant difference was observed between the mean values of BMI, FBS, ACR, and TG in subjects with the prevalence and absence of MS [Tables 1 and 2] and in subjects with MS, albuminuria (ACR) is highly correlated with the incidence of FBS, TG, BP, and age ($P < 0.01$) [Table 2]. However, the frequency albuminuria is high with the FBS, BP, and TG in the study population and seems to be less associated with obesity [Tables 1 and 2] suggesting the least association between albuminuria and overweight. But we found a significant correlation between ACR with obesity in males ($P < 0.05$) [Tables 3 and 4] emphasizing the sexual dimorphism in adipose tissue distribution and associated comorbidities.

Discussion

The occurrence and severity of MS are followed by the association of the sum of critical risk factors that include obesity, hypertension, insulin resistance, dyslipidemia, and albuminuria. According to CJKN studies and NCEP ATP III, the relationship between kidney damage and MS is complex. It is also in debate whether the collective existence of all the risk factors of MS improves CKD beyond that afforded by individual risk factors. However, very fewer studies have been undertaken to incorporate the coexistence of risk factors associated with MS and CKD. The present study results targeted to recognize and correlate the strong integrated relationship of fasting blood glucose, hyper-triglyceridemia, and high systolic BP the three of the five risk factors of MS in association with albuminuria than each independent risk factor.

In this cross-sectional study, we observed a significant difference in albuminuria in obese and nonobese subjects [Table 1], but we observed gender difference in the association of BMI with albuminuria; BMI had a greater association with ACR in males, whereas in females BMI is not associated with ACR [Tables 3 and 4]. Many studies show that there is a strong, linear relationship between obesity and hypertension. Chang *et al.*[20] study reported that systolic BP is an independent risk factor of

Table 2: Correlation analysis of each parameter with baseline parameters in subjects with metabolic syndrome ($n = 874$), with unhealthy ACR ($n = 402$), and with obesity ($n = 258$)

With metabolic syndrome							
Risk factor	**BMI**	**FBS**	**ACR**	**TGs**	**HDL**	**BP**	**Age**
BMI	1.0	0.281	0.104	0.591	0.111	0.087	0.340
FBS	0.281	1.0	0.000*	0.001*	0.051	0.537	0.031*
ACR	0.104	0.000*	1.0	0.008*	0.939	0.001*	0.002*
T.Gs	0.591	0.001*	0.008*	1.00	0.000*	0.468	0.094
HDL	0.111	0.051	0.939	0.000*	1.00	0.150	0.037*
B.P	0.087	0.537	0.001*	0.468	0.150	1.00	0.000*
Age	0.340	0.031*	0.002*	0.094	0.037*	0.000*	1.00
With unhealthy ACR							
Risk factor	**BMI**	**FBS**	**ACR**	**TGs**	**HDL**	**BP**	**Age**
BMI	1.0	0.965	0.334	0.472	0.159	0.629	0.459
FBS	0.965	1.0	0.000*	0.010	0.658	0.267	0.189
ACR	0.334	0.000*	1.0	0.002*	0.936	0.020	0.000*
T.Gs	0.472	0.010*	0.002*	1.00	0.000*	0.430	0.080
HDL	0.159	0.658	0.936	0.001*	1.00	0.264	0.422
B.P	0.629	0.267	0.020*	0.430	0.264	1.00	0.000*
Age	0.459	0.189	0.000*	0.080	0.422	0.000*	1.00
With obesity							
Risk factor	**BMI**	**FBS**	**ACR**	**TGs**	**HDL**	**BP**	**Age**
BMI	1.0	0.501	0.232	0.600	0.854	0.130	0.230
FBS	0.501	1.0	0.018*	0.015*	0.767	0.308	0.043*
ACR	0.232	0.018*	1.0	0.003*	0.586	0.711	0.027*
TGs	0.600	0.015*	0.003*	1.00	0.197	0.759	0.820
HDL	0.854	0.767	0.586	0.197	1.00	0.333	0.193
BP	0.130	0.308	0.711	0.759	0.333	1.00	0.002*
Age	0.230	0.043*	0.027*	0.820	0.193	0.002*	1.00

*Correlation is significant at <0.05 level (two tailed)

microalbuminuria in euglycemic normotensive males. Our analysis also confirms this association between obesity and high BP. Yesmin *et al.*[21] report shows that there is no microalbuminuria in obese women without diabetes and/or hypertension suggesting in obese women and lean women; urinary albumin excretion was similar. A recent study on Japanese hypertensive patients showed that there were sex-related differences in the associations of insulin resistance and obesity to left ventricular hypertrophy.[22] Also Foster *et al.*[23] showed that in comparative Framingham heart study microalbuminuria is associated with visceral adipose tissue in men but not in women.

This study reports elucidate that in subjects with MS and unhealthy albuminuria [Table 2], coexistence of three of the five risk factors is strongly associated with the total conditions of the study. Age also shows a positive correlation with albuminuria. With these findings, our data analysis suggests that a gender difference may exist in the association between BMI and albuminuria. The difference might be due to gender-related specifications, such as the role of sex hormones on the inflammatory mechanism that links albuminuria to central obesity or it can be also predicted that the muscle mass in males is more than in females, which can warrant the creatinine levels and gender difference in interpretation.

The gender difference can be partly because of the prevalence of smoking in males, and the absence of smoking in females. In females, there is a highly significant relationship between anthropometric variables and albuminuria due to potential sex-based divergence in fat distribution pattern and renal outcomes for differential steroid hormone levels. The contradiction may be because of higher upper body adiposity and higher visceral fat for a given BMI in the Asian Indians. The study conducted by Wang *et al.*[24] on aboriginal people by receiver operating characteristic (ROC) analysis suggested that measuring body size-related diabetes waist circumference is the best method comparing a few more methods of body size measurement.

Conclusion

This study shows the relationship between obesity and the risk for CKD by gender-specific examination, which was measured clinically in the form of micro/macroalbuminuria that leads to proteinuria. Our findings suggest that BMI has an association with albuminuria in men showing that obesity calculated as BMI is a risk factor for kidney damage in males with a high prevalence of FBS, BP, TG, and age. However the contradictory results with females demonstrate that obesity calculated as BMI is not a high-risk factor for kidney harm in females, due to an account of gender specific variation in distribution of fat indicating men having a relatively more central allocation of fat giving the fact that male obese with hyperglycemia,

Table 3: Pearson chi-square analysis between risk factors and albuminuria

	Status of microalbumin				X^2 (df)	*P*	phi
	Healthy		Unhealthy				
	N	(%)	*N*	(%)			
Metabolic syndrome (MS							
Yes	481	55.0	393	45.0	7.26	0.005*	+0.09
No	30	76.9	9	23.1			
Obesity							
Yes	135	52.3	123	47.6	1.92	0.165	+0.05
No	377	57.4	280	42.6			
Obesity in males							
Yes	54	48.2	58	51.7	4.04	0.04*	+0.09
No	232	58.9	162	41.1			

Computed only for a 2 x 2 table

*Significant at $P < 0.05$

Table 4: Risk factors of microalbuminuria in the study population

Sex	Risk factors	OR (95% CI)	*P* Value*
Males	BMI > 30 kg/m^2	1.51(1.033–2.397)	0.03*
Females	BMI > 30 kg/m^2	0.98(0.65–1.47)	0.93
Both genders	FBS > 110 mg/dL	1.865(1.34–2.58)	0.0002*
Both genders	Triglycerides > 150 mg/dL	1.47(1.105–1.957)	0.0082*
Both genders	HDL < 40 mg/dL	0.99(0.746–1.328)	0.976
Both genders	BP > 130 mm Hg	1.29(0.971–1.71	0.078

OR = odds ratio

*Significant at $P < 0.05$

hypertension and hypertriglyceridemia are at high risk of developing CKD. The major limitation of this study is that it was conducted by not focusing on dietary patterns of the individuals that might influence the relationship between the severity of obesity and microalbuminuria and ignored alternative methods for the calculation of obesity.

Acknowledgement

We express a deep sense of gratitude to Dr. P. Anil Kumar, assistant professor at Department of Biochemistry, School of Life Sciences, University of Hyderabad, for his direction and suggestions in all aspects of my research work.

Financial support and sponsorship

Nil.

Conflicts of interest

There are no conflicts of interest.

References

1. National Kidney Foundation. K/DOQI clinical practice guidelines for chronic kidney disease: Evaluation, classification, and stratification. Am J Kidney Dis 2002;39: S1-S266.
2. Sarnak MJ, Levey AS, Schoolwerth AC, Coresh J, Culleton B, Hamm LL, *et al*.; American Heart Association Councils on Kidney in Cardiovascular Disease, High Blood Pressure Research, Clinical Cardiology, and Epidemiology and Prevention. Kidney disease as a risk factor for development of cardiovascular disease: A statement from the American Heart Association councils on kidney in cardiovascular disease, high blood pressure research, clinical cardiology, and epidemiology and prevention. Circulation 2003;108:2154-69.
3. Diercks GF, van Boven AJ, Hillege JL, de Jong PE, Rouleau JL, van Gilst WH. The importance of microalbuminuria as a cardiovascular risk indicator: A review. Can J Cardiol 2002;18:525-35.
4. Alberti KG, Zimmet PZ. Definition, diagnosis and classification of diabetes mellitus and its complications. Part 1: Diagnosis and classification of diabetes mellitus provisional report of a WHO consultation. Diabet Med 1998;15:539-53.
5. Alberti KG, Eckel RH, Grundy SM, Zimmet PZ, Cleeman JI, Donato KA, *et al*.; International Diabetes Federation Task Force on Epidemiology and Prevention; National Heart, Lung, and Blood Institute; American Heart Association; World Heart Federation; International Atherosclerosis Society; International Association for the Study of Obesity. Harmonizing the metabolic syndrome: A joint interim statement of the international diabetes federation task force on epidemiology and prevention; national heart, lung, and blood institute; American Heart Association; world heart federation; international atherosclerosis society; and international association for the study of obesity. Circulation 2009;120:1640-5.
6. Ramkumar N, Cheung AK, Pappas LM, Roberts WL, Beddhu S. Association of obesity with inflammation in chronic kidney disease: A cross-sectional study. J Ren Nutr 2004;14:201-7.
7. Deferrari G, Repetto M, Calvi C, Ciabattoni M, Rossi C, Robaudo C. Diabetic nephropathy: From micro- to macroalbuminuria. Nephrol Dial Transplant 1998;13:11-5.
8. Rosa TT, Palatini P. Clinical value of microalbuminuria in hypertension. J Hypertens 2000;18:645-54.
9. Jones CA, Francis ME, Eberhardt MS, Chavers B, Coresh J, Engelgau M, *et al*. Microalbuminuria in the US population: Third national health and nutrition examination survey. Am J Kidney Dis 2002;39:445-59.
10. Sun K, Kusminski CM, Scherer PE, Sun K, Kusminski CM, Scherer PE. Adipose tissue remodeling and obesity find the latest version : Review series Adipose tissue remodeling and obesity. J Clin Invest 2011;121:2094-101.
11. Tang J, Yan H, Zhuang S. Inflammation and oxidative stress in obesity-related glomerulopathy. Int J Nephrol 2012;2012:1-11.
12. Wolf G, Chen S, Han DC, Ziyadeh FN. Leptin and renal disease. Am J Kidney Dis 2002;39:1-11.
13. Anil Kumar P, Swathi Chitra P, Bhanuprakash Reddy G. Metabolic syndrome and associated chronic kidney diseases: Nutritional interventions. Rev Endocr Metab Disord 2013;14:273-86.
14. Weisinger JR, Kempson RL, Eldridge FL, Swenson RS. The nephrotic syndrome: A complication of massive obesity. Ann Intern Med 1974;81:440-7.
15. Hoffmann IS, Jimenez E, Cubeddu LX. Urinary albumin excretion in lean, overweight and obese glucose tolerant individuals: Its relationship with dyslipidaemia, hyperinsulinaemia and blood pressure. J Hum Hypertens 2001;15:407-12.
16. Nielsen S, Jensen MD. Relationship between urinary albumin e x c retion, body composition, and hyperinsulinemia in normotensive glucose - tolerant adults. Diabetes Care 1999;22:1728-33.
17. Schwartz GL, Sheps SG. A review of the sixth report of the joint national committee on prevention, detection, evaluation, and treatment of high blood pressure. Curr Opin Cardiol 1999;14:161-8.
18. Fouad M, Ismail MI, Gaballah A, Reyad E, ELdeeb S. Prevalence of obesity and risk of chronic kidney disease among young adults in Egypt. Indian J Nephrol 2016;26:413-8.
19. Singh AK, Kari JA. Metabolic syndrome and chronic kidney disease. Curr Opin Nephrol Hypertens 2013;22:198-203.
20. Chang Y, Yoo T, Ryu S, Huh BY, Cho BL, Sung E, *et al*. Abdominal obesity, systolic blood pressure, and microalbuminuria in normotensive and euglycemic Korean men. Int J Obes (Lond) 2006;30:800-4.
21. Yesim TE, Ugurlu S, Caglar E, Balci H, Ucgul A, Sarkis C, *et al*. Investigation of microalbuminuria in nondiabetic, normotensive obese women. Intern Med 2007;46:1963-5.
22. Shigematsu Y, Norimatsu S, Ogimoto A, Ohtsuka T, Okayama H, Higaki J. The influence of insulin resistance and obesity on left atrial size in Japanese hypertensive patients. Hypertens Res 2009;32:500-4.
23. Foster MC, Hwang SJ, Massaro JM, Hoffmann U, DeBoer IH, Robins SJ, *et al*. Association of subcutaneous and visceral adiposity with albuminuria: The Framingham heart study. Obesity (Silver Spring) 2011;19:1284-9.
24. Wang Z, Hoy WE. Body size measurements as predictors of type 2 diabetes in aboriginal people. Int J Obes Relat Metab Disord 2004;28:1580-4.

Antioxidant Activity Evaluation of Methanolic Leaf Extracts of Krishna Estuary Mangroves, Andhra Pradesh., India

P Suneeta*[1], Nageswara Rao Naik B[2], D Jyothi[3], Z Vishnuvardhan[4]

1. *Department of Microbiology, Government College (Autonomous), Rajahmundry, Andhra Pradesh.*
2. *Department of Environmental sciences, Acharya Nagarjuna University, Guntur, Andhra Pradesh.*
3. *Department of Botany SRR & CVR Govt.college Vijayawada Andhra Pradesh.*
4. *Department of Botany and Microbiology, Acharya Nagarjuna University, Guntur, Andhra Pradesh.*

Abstract: *Antioxidants are vital substances that protect the body from damages caused by free radical-induced oxidative stress. A variety of natural antioxidants are found in plants. The present study is aimed at assessment of relative antioxidative potential of methanolic leaf extracts of eight mangrove species. Four different assays have been used to determine the best mangrove with superior antioxidant capacity. B. gymnorrhiza is adjudged as the best species. E. agallocha, A. marina, A. officinalis and A. rotundifolia exhibited moderate activity, where as less antioxidant activity is recorded in A. corniculatum, R. apiculata and B. cylindrica.*

Key words: *Krishna Estuary mangroves, phenolic content, Reducing power, Oxidative stress, Antioxidants.*

1. INTRODUCTION

Free radicals/oxidants are being produced with enhanced rate during oxidative stress in organisms. The family of free radicals generated from the oxygen is known as 'Reactive Oxygen Species (ROS) and responsible for many diseases. Antioxidants are important since they offer protection to organisms from damage caused by free radical ROS. The antioxidants present in plants offer considerable resistance to oxidative damage caused by ROS. Mangrove plants are rich in phytochemicals capable of removing free radicals before they cause damage. Therefore the present study is aimed at evaluation of antioxidant potential of eight mangrove species. Antioxidant potential of mangrove species is assessed through four different assays evaluation of viz., i) DPPH free radical scavenging ii) reducing power iii) total phenolic content and iv) total antioxidant activity.

2. Materials and Methods

Eight mangrove species were collected from Krishna estuary, Nagayalanka, Andhra Pradesh, India which is located between latitude $15^{0}15^{1}$ - $15^{0}55$N and $80^{0}45^{1}$-81^{1}00E longitude. The plant material were identified to their species level with the help of available flora. The plant specimens were preserved in the dept. of Botany & Microbiology, Acharya Nagarjuna University. Methanolic leaf extracts of eight mangrove species constitute the materials for the present study.

Preparation of plant extract

Leaves of eight mangroves were air dried at room temperature to constant weights. The dried plant materials were ground separately to powder. 100 gms of each ground plant materials were shaken separately in methanol for 48 hrs on an orbital shaker. Extracts were filtered using a

whatman No. 1 filter paper. Each filtrate was concentrated by soxhlet apparatus and each extract was resuspended in methanol to make 100 mg/ml stock solution.

DPPH free radical activity

Diphenyl Picryl Hydrozyl radical scavenging assay was determined by Bamionuri *et al*., 2010. Briefly, 5 ml of DPPH solution (0.004%) in methanol was added to 50 µl of plant extract. After 30 minutes of incubation period at room temperature, the absorbance was read against a blank containing sample and methanol at 517 nm. Control containing the buffer and reagent was carried out. Similarly positive controls were treated in the same way as test sample replaced by positive control. Butyl Hydroxyl Touline (BHT) used as positive control. Inhibition (I) of Diphenyl Picryl Hydroxyl radical was calculated in the following way.

$$\text{Percentage of inhibition (I)} = \frac{\text{Absorbance of control} - \text{Absorbance of test}}{\text{Absorbance of control}} \times 100$$

Total Phenolic compounds estimation

The total phenolic contents in the extract, was determined by Bomaniri *et al*., 2010 with minor modifications, including gallic acid as standard and Folincioculteau reagent. To 2.5 ml of 10% Folincioculteau reagent 2 ml of Na_2CO_3 (2%, w/v) was added to 0.1 ml of each sample (3 replicates) of plant extract solution (1 mg/ml). The resulting mixture was incubated at 45^0C with shaking for 15 minutes. The absorbance of the sample was measured at 765 nm using Uv/visible light. Results were expressed as mgs of Gallic acid (20-100 µg/ml) dissolved in water.

Reducing Power assay (RP)

The reducing power of the extracts was determined according to the method of Oyaizu (1986). Extracts (100 ml) of mangrove plant parts were mixed with phosphate buffer (2.5ml, 0.2M, pH 6.6) and 1% Potassium Ferricyanide (2.5 ml). The mixture was incubated at 50^0C for 20 minutes. Aliquots of 10% trichloroacetic acid (2.5 ml) were added to the mixture, which was then centrifuged at 3000 rpm for 10 minutes. The upper layer of the solution (2.5 ml) was mixed with distilled water (2.5 ml) and freshly prepared ferric chloride solution (0.5 ml, 0.1%). The absorbance was measured to 700 nm. Reducing power in given in ascorbic acid equivalent (AAE) in milligram per gram of dry material.

Total Antioxidant activity

It is determined by the conjugated diene method of Lingnert *et al* (1979). The extract is mixed with 2 ml of 10 mN linoleie acid emulsion in 0.2 M sodium phosphate buffer (P^H 6.6) and kept in dark at $37^{0C.}$ After 15 hrs of incubation, 0.1 ml from each tube is mixed with 7.0 ml of 80% methanol. The absorbance is read at 234 nm against blank in spectrophotometer. Antioxidant activity (%) = $\frac{AO-A1}{AO} \times 100$ where AO is the absorbance of control-A1 is the absorbance of test. Phenol is the positive control.

3. Results and Discussion

Total phenolic content and total antioxidant activity of methanolic leaf extracts of eight mangrove species are presented in table1. Leaf extract concentrations raging from 100µg to 500 µg were subjected to above assessment. 100 µg methanolic extract of *B. cylindrica* contained less

amount of phenolic substances (34.26 µg) and it was proportionately increased with an increase in extract concentration up to 500 µg in all the species. 500 µg leaf extract of *B. gymnorrhiza* contained the maximum quantity (95.62 µg) of phenolics followed by *E. agalloch* (84 µg), *A. marina* (82.78 µg), *A. rotundifolia* (82.62 µg), *A. officinalis* (79.09 µg), *A. corniculatum* (63.03 µg) *R. apiculata* (62.32 µg) and *B. cylindrica* (52.97 µg).

Total antioxidant activity of 500 µg extract of *B. gymnorrhiza* was found be maximum (93.24%) and it was minimum in *B. cylindrica* extract (52.87%). The other species viz., *E. agallocha, A. rotundifolia* and *A. marina* were rated next to *B. gymnorrhiza* with the range of antioxidant activity between 79.42 to 84.48%.

The DPPH free radical scavenging activity of eight mangroves is presented in table 2. Free radical inhibition percent of mangrove extracts was increased steadly with an increase in extract concentration of mangroves from 100 µg to 500 µg. The free radical scavenging activity of *B. gymnorrhiza* 500 µg extract of excelled other species with 93.15% inhibition *A. corniculatum* extract (500µg) showed the minimum inhibition (62.97%) of DPPH radical while the other six species manifested the DPPH radical scavenging in the range from 72.09% to 75.3%.

Reducing power of the mangroves extracts was presented in the table2. 500µg extract of *A. corniculatum* has the lowest percent (65.82) of reducing power, where as *B. gymnorrhiza* expressed the highest percent (89.71%) of reducing power. The remaining six mangroves exhibited moderate reducing power rangining between 80.41% and 86.48%.

Discussion

Plants serve as a reservoir of effective chemotherapentants. Organisms are equipped with antioxidant system via many natural compounds and enzymes. In addition to the inherent mechanisms, exist in organisms, they must be sometimes supplemented through diet. In this context natural antioxidants from plants appear to be the solution to mitigate the effects of oxidative stress. Hence, there is growing demand for antioxidants from plants. The plant based antioxidants belong to different classes ranging from carotenoids, flavonoids, polyphenols, galic acid derivatives, tannins and catechins.

According to Miles *et al* (1998) mangroves have been considered as great source for chemical compounds of potential value. The flavonoids and polyphenolic compounds are powerful antioxidants due to the presence of C_4-C_7 hydroxyl groups that act as hydrogen donors. The phenolic compounds and flavonoids have positive correlation with free radical scavenging activity (Cushnie &Andrew 2005; Bandini *et al* 2006; Deepanjan *et al* 2008).

The results of present study comprehensively revealed that *B. gymnorrhiza* possess greater antioxidant potential since its extract contain the highest DPPH free radical scavenging activity, reducing power, phenolic content and total antioxidants. Mldadulal Haq *et al* (2011) and Kiran Kumar & Sitaram (2013) also found the highest antioxidant activity in *B. gymnorrhiza.* Moderate antioxidant activity was found in *E. agalloch, A. marina*, *A. officinalis* and *A. rotundifolia*. Relatively less antioxidant activity was recorded in *A. corniculatum*, *R. apiculata* and *B. cylindrica.* In the mangroves of present study Suneeta (2020) reported the presence of flvonoids, terpenoids and hydrocarbons (alkanes and alkenes). Hence, the compounds may be responsible for the antioxidant activity of eight mangrove species in the present study.

Table 1: Total phenolic content and Antioxidant activity of methanolic leaf extracts of eight mangrove species

S.No	Name of the Mangrove species	PHENOLIC CONTENT (µg)					TOTAL ANTIOXIDANT ACTIVITY (%)				
		Extract conc. in µg					Extract conc. in µg				
		100	200	300	400	500	100	200	300	400	500
1	***A.corniculatum***	49.20	54.16	56.92	60.91	63.03	48.09	54.90	59.72	62.27	63.23
2	***A. Marina***	42.76	51.37	68.78	73.23	82.78	33.06	45.21	54.31	76.09	79.42
3	***A. officinalis***	44.02	64.21	65.62	68.78	79.09	23.53	34.06	57.71	59.23	64.34
4	***A. rotundifolia***	51.32	66.42	67.53	73.09	82.62	32.05	49.62	52.23	71.64	82.32
5	***B. cylindrica***	34.26	38.04	49.82	50.20	52.97	33.09	42.32	48.08	51.03	52.87
6	***B. gymnorrhiza***	42.03	73.92	77.62	81.93	95.62	15.87	32.34	50.27	71.14	93.24
7	***E. agallocha***	41.05	57.42	73.92	78.09	84.00	26.52	38.32	59.15	72.62	84.48
8	***R. apiculata***	42.26	54.31	56.42	59.51	62.32	35.57	39.61	42.62	57.43	62.21

Table. 2 : DPPH free radical scavenging and Reducing Power (RP) activity of methanolic leaf extracts of eight mangrove species.

S.No	Name of the Mangrove species	DPPH (%)					REDUCING POWER (%)				
		Extract conc. in µg					Extract conc. in µg				
		100	200	300	400	500	100	200	300	400	500
1	***A. corniculatum***	12.50	21.03	35.01	54.19	62.97	43.23	56.32	58.78	59.04	65.82
2	***A. Marina***	10.90	21.23	34.20	49.52	73.12	42.34	56.28	69.31	74.71	80.41
3	***A. officinalis***	15.25	29.36	46.97	61.06	72.80	42.26	58.29	73.34	78.62	86.48
4	***A. rotundifolia***	13.23	19.31	34.90	47.73	75.30	43.03	50.52	66.25	79.62	82.02
5	***B. cylindrica***	11.08	23.32	35.03	52.13	69.16	46.56	59.23	62.31	71.52	72.09
6	***B. gymnorrhiza***	15.76	32.73	50.35	71.92	93.15	32.98	55.73	62.35	74.82	89.71
7	***E. agallocha***	12.90	26.23	38.20	51.00	75.12	44.06	74.12	74.51	81.32	84.41
8	***R. apiculata***	9.27	20.00	35.23	43.41	72.09	50.62	62.59	74.26	76.31	85.23

References

[1] Bamoniri A, Ebrahimabadi AH, Mazochi A, Behpour M, Kashi FJ and Batooli H (2010). Antioxidant and Antimicrobial activity evaluation and essential oil analysis of Semenovia tragioides Bioss. From Iran. *Food Chem*. 122 ; 553-8.

[2] Bandini A and Cerrestanil Pizolante L (2006). Phenol content related to Antimicrobial and antioxidant activity of *Passiflora* species Extracts. *European Food Research Technology* 223: 102-109.

[3] Cushnie TPT and Andrew JL (2005). Antimicrobial activity of flavonoids. *International Journal of antimicrobial agents* 26: 343-356.

[4] Deepanjan Banerjee, Shrabana Chakrabarti, Alok K Hazra, Shivaji Banerjee, Jharna Ray and Biswapati Mukherjee(2008). Antioxidant activity and total phenolics of some mangroves in Sundarbans. *African Journal of Biotechnology Vol.* 7(6): pp. 805-810.

[5] Kiran Kumar, Mundla and Sitaram, B (2013). Comparative Study of Phytochemical, Antimicrobial, Cytotoxic and antioxidant Activities in *Blepharis genus* plant Seeds. *IJSIT*. 2(1): 07-20.

[6] Miles DH, Kokpal U, Chittawong V, Tip-Pyang S, Tunsuwan K and Nguyen C (1998). Mangrove forests – The importance of conservation as a bioresource for ecosystem diversity and utilization as a source of chemical constituents with potential medicinal and agricultural value. *IUPAC* 70 (11): 1-9.

[7] Mldadul Haq, Wirakarnain Sani, Hossain ABMS, Rosna Mat Taha and Monneruzzaman KM (2011). Total phenolic contents, antioxidant and antimicrobial activities of *Bruguiera gymnorrhiza. Journal of Medicinal Plants Research* Vol. 5(17): 4112-4118.

[8] Suneeta .P (2010).Ph. D Thesis entitled Antibacterial, Antioxidant and phytochemical studies of certain mangroves of Krishna district, Andhra Pradesh.

SRR & CVR GOVERNMENT DEGREE COLLEGE(A) VIJAYAWADA

DEPARTMENT OF POLITICAL SCIENCE & PUBLIC ADMINISTRATION

WORKSHOP ON IMPLEMENTATION OF RTI ACT 2005

7th March 2021

The Department of Political Science & Public Administration conducted one day workshop to create awareness on the Right To Information Act 2005 (RTI 2005) and changes brought recently. The council for citizen's rights, civil and human rights protection Non-Government Organisation has also participated to air their views and issues.

The AP Chief Information Officer Rtd. Sri Ramesh Kumar IAS and AP Information Officer Sri Srinivasu attended the workshop and addressed the RTI activists of 13 districts across Andhra Pradesh. Activists of 126 from 13 districts participated enthusiastically and expressed their own experiences. Dr.Illa Ravi, principal of the college spoke on the awareness and importance campaign on the Right to Information.

Dr.DSVS.Balasubrahmanyam, Associate Professor of the Political science department welcomed the dignitaries and spoke about the importance of the RTI Act with examples of his own experience. The Right to Information Act, simply known as RTI, is a revolutionary act that aims to promote transparency in government institutions in India. The Act came into existence in 2005, after sustained efforts of anti-corruption activists. RTI or Right to Information Act is a fundamental right and is an aspect of Article 19 (1)(a) of the Indian Constitution.

Right to Information replaced the Freedom of Information Act, 2002. Grounds for Rejection of RTI There are only three possible grounds on which information can be denied: The organisation is not a Public authority - eg. a Cooperative Society, or a Private corporate or Institution, not substantially financed or controlled by the Government.

The AP Chief Information Officer Rtd. Sri Ramesh Kumar IAS addressed the workshop. He informed the various provisions and sections of RTI Act sub-section (1) of section 4, sub-sections (1) and (2) of section 5, sections 12, 13, 15,16, 24, 27 and 28 shall come into force at once, and the remaining provisions of this Act shall come into force on the one hundred and twentieth day of its enactment. Issue of Enforceability as he said the Act does not give adequate authority to the Information Commissions to enforce their decisions. Information commissions can give directions to public authorities to take the steps necessary to comply with the Act but are not empowered to take any action if such directions are ignored. Situations for filing First Appeals and prescribed Time Limits. 1. PIO did not respond within 30 days from receipt of RTI Application in his office. After 30 (+7 days for postal transit time) but within 60 days from the date of receipt of RTI Application at PIO's Office. You may only ask for specific information under the RTI Act, 2005 rather than questioning the action of public authority. ' The RTI act does not state that queries must not be answered, nor does it stipulate that prefixes such as 'why, what, when and whether' cannot be used.

స.హ.చట్టాన్ని వినియోగించుకోవాలి

మధురానగర్(విజయవాడ సెంట్రల్): సమాచార హక్కు చట్టాన్ని సమాజ హితం, సమాజ అభివృద్ధి కోసం వినియోగించుకోవాలని రాష్ట్ర ముఖ్య సమాచార కమిషనర్ పీ రమేష్‌కుమార్ సూచించారు. స్థానిక మాచవరం ఎస్ఆర్ఆర్ అండ్ సీవీఆర్ ప్రభుత్వ డిగ్రీ కళాశాలలో కౌన్సిల్ ఫర్ సిటిజన్ రైట్స్ పౌర, మానవ హక్కుల స్వచ్ఛంద సంస్థ సహకారంతో సమాచార హక్కు చట్టంపై అవగాన సదస్సు శనివారం నిర్వహించారు. కార్యక్రమంలో ఆయన ముఖ్య అతిథిగా పాల్గొని సమాచార హక్కు చట్టం గురించి వివరించారు. ఆర్‌టీఐ యాక్ట్ ప్రకారం ఐఏఎస్, ఐపీఎస్ తరహాలో రికార్డులు తనిఖీ చేయవచ్చని, గ్రామ పరిధి నుంచి రాష్ట్ర కేంద్ర స్థాయి వరకు సహ చట్టాన్ని వినియోగించి సమాచారం తీసుకోవచ్చని తెలిపారు. ఏపీ సమాచార కమిషనర్ రేపాల శ్రీనివాస్, ఎన్.హరినాథ్, మంచికట్ల అనిల్‌కుమార్, కళాశాల ప్రిన్సిపాల్ డాక్టర్ ఇళ్ల రవి మాట్లాడారు. కార్యక్రమాన్ని రాజనీతి శాస్త్ర విభాగం అధ్యాపకులు డాక్టర్ డీఎస్‌వీఎస్ బాలసుబ్రహ్మణ్యం, అధ్యాపకులు పర్యవేక్షించారు.

అవగాహన సదస్సులో వక్తలు

సాక్షి Sun, 07 March 2021
https://epaper.sakshi.com/c/58923625

The RTI act influence on people and impact on Indian Administration in greater Transparency in functioning of public authorities: disclosure of information regarding government rules, regulations and decisions, every public authority is mandated to 'maintain all records duly catalogued and indexed. “Improving Transparency and Accountability in Government through effective implementation of Right to Information

It was published in the paper that the CIO stressed that the RTI Act was promulgated in October 2005 to ensure transparency and good governance in the country. Based on content analysis and depth interviews with a few bureaucrats and activists, the paper indicates that RTI Act has succeeded in reducing information asymmetries and exposing corruption.

In the last 15 years, at least 86 people who had filed RTI applications have been killed while 175 others have been attacked. At least seven applicants committed suicide while 184 applicants reported being harassed.

అవినీతి రహిత భారతదేశానికి ఆర్టిఐ యాక్ట్ ఓ ఆయుధం

(వార్తామండలి ప్రతినిధి)

విజయవాడ: రాష్ట్రంకానీ దేశంకానీ అవినీతి రహితంగా నిలబడడానికి ఆర్టిఐ యాక్ట్ ఆయుధంగా ఉపయోగపడుతుందని రాష్ట్ర ముఖ్య సమాచార కమిషనర్ విశ్రాంత ఐ ఏ ఎస్ అధికారి పి. రమేష్ కుమార్ అన్నారు. కౌన్సిల్ ఫర్ సిటిజెన్ రైట్స్ ఆధ్వర్యంలో విజయవాడ నగరంలోని ఎస్ ఆర్ ఆర్ అండ్ సివిఆర్ కళాశాలలో అవగాహన సదస్సు సి సి ఆర్ అధికార ప్రతినిధి వ్యవస్థాపకులు మాచి కట్ల అనిల్ కుమార్ అధ్యక్షతన జరిగింది. ముఖ్య అతిథి రమేష్ కుమార్ మాట్లాడుతూ కళాశాల ప్రిన్సిపాల్ అధ్యాపక ఉపాధ్యాయులు ఆర్ టి ఐ యోధులను తయారుచేయడం అభినందనీయమన్నారు. ఆర్టిఐ యాక్ట్ సద్వినియోగం వలన ఎన్నో ఫలితాలు ఉంటాయన్నారు. అదే ఆర్టిఐ యాక్ట్ ను దుర్వినియోగం చేస్తే ఆర్టిఐ యాక్ట్ నిర్వీర్యం అవుతుందన్నారు.ఆర్ టి ఐ అవగాహన సదస్సు విజయవంతం అవడం అభినందనీయ మన్నారు. మరో ముఖ్య అతిథి రేపాక శ్రీనివాసరావు, ఎన్ హరినాథ్ ఆర్టిఐ చట్టం విధివిధానాలను అవగాహన సదస్సులో వివరించారు, ఈ కార్యక్రమంలో కళాశాల ప్రిన్సిపాల్ డాక్టర్ రవిని జ్ఞాపికతో సన్మానించారు. అవగాహన సదస్సుకు వచ్చిన అతిథులకు షీల్డులు బహుకరించారు. ఆర్టిఐ కార్యకర్తలకు సర్టిఫికెట్లు ప్రధానోత్సవం చేశారు. అవగాహన సదస్సులో హైకోర్టు అడ్వకేట్, సి సి ఆర్ లీగల్ అడ్వైజర్ అనిల్ వైద్య ప్రసంగించారు. కెట్టీ రామకృష్ణ, పావులూరి కోటేశ్వరరావు, ఇ లక్ష్మీ ప్రశాంత్, బి మహేష్, శ్రీనివాస రావు సభా నిర్వాహకులుగా వ్యవహరించారు. ఈ కార్యక్రమంలో విద్యార్థినీ విద్యార్థులు ఉపాధ్యాయులు తదితరులు పాల్గొన్నారు.

SRR & CVR GOVERNMENT DEGREE COLLEGE(A) VIJAYAWADA

DEPARTMENT OF POLITICAL SCIENCE & PUBLIC ADMINISTRATION

WORKSHOP ON IMPLEMENTATION OF RTI ACT 2005

7th March 2021

The department of Political Science & Public Administration conducted one day workshop to create awareness on the Right To Information Act 2005 (RTI 2005) and changes brought recently. The council for citizen's rights, civil and human rights protection Non-Government Organisation has also participated to air their views and issues.

The AP Chief Information Officer Rtd. Sri Ramesh Kumar IAS and AP Information Officer Sri Srinivasu attended the workshop and addressed the RTI activists of 13 districts across Andhra Pradesh. Activists of 126 from 13 districts participated enthusiastically and expressed their own experiences. Dr.Illa Ravi, principal of the college spoke on the awareness and importance campaign on the Right to Information.

Dr.DSVS.Balasubrahmanyam, Associate Professor of the Political science department welcomed the dignitaries and spoke about the importance of the RTI Act with examples of his own experience. The Right to Information Act, simply known as RTI, is a revolutionary Act that aims to promote transparency in government institutions in India. The Act came into existence in 2005, after sustained efforts of anti-corruption activists. RTI or Right to Information Act is a fundamental right and is an aspect of Article 19 (1)(a) of the Indian Constitution. Right to Information replaced the Freedom of Information Act, 2002. Grounds for Rejection of RTI There are only three possible grounds on which information can be denied: The organisation is not a Public authority - eg. a Cooperative Society, or a Private corporate or Institution, not substantially financed or controlled by the Government.

The AP Chief Information Officer Rtd. Sri Ramesh Kumar IAS addressed the workshop. He informed the various provisions and sections of RTI Act sub-section (1) of section 4, sub-sections (1) and (2) of section 5, sections 12, 13, 15,16, 24, 27 and 28 shall come into force at once, and the remaining provisions of this Act shall come into force on the one hundred and twentieth day of its enactment. Issue of Enforceability as he said the Act does not give adequate authority to the Information Commissions to enforce their decisions. Information commissions can give directions to public authorities to take the steps necessary to comply with the Act, but are not empowered to take any action if such directions are ignored.

Situations for filing First Appeals and prescribed Time Limits. 1. **PIO did not respond within 30 days from receipt of RTI Application in his office**. After 30 (+7 days for postal transit time) but within 60 days from the date of receipt of RTI Application at PIO's Office. You may only ask for **specific information** under RTI Act, 2005 rather than questioning the action of public authority. ' The RTI act does not state that queries must not be answered, nor does it stipulate that prefixes such as 'why, what, when and whether' cannot be used.

స.హ.చట్టాన్ని వినియోగించుకోవాలి

మధురానగర్(విజయవాడ సెంట్రల్): సమాచార హక్కు చట్టాన్ని సమాజ హితం, సమాజ అభివృద్ధి కోసం వినియోగించుకోవాలని రాష్ట్ర ముఖ్య సమాచార కమిషనర్ పీ రమేష్‌కుమార్ సూచించారు. స్థానిక మాచవరం ఎస్‌ఆర్‌ఆర్ అండ్ సీవీఆర్ ప్రభుత్వ డిగ్రీ కళాశాలలో కౌన్సిల్ ఫర్ సిటిజన్ రైట్స్ పౌర, మానవ హక్కుల స్వచ్ఛంద సంస్థ సహకారంతో సమాచార హక్కు చట్టంపై అవగాన సదస్సు శనివారం నిర్వహించారు. కార్యక్రమంలో ఆయన ముఖ్య అతిథిగా పాల్గొని సమాచార హక్కు చట్టం గురించి వివరించారు. ఆర్‌టీఐ యాక్ట్ ప్రకారం ఐఏఎస్, ఐపీఎస్ తరహాలో రికార్డులు తనిఖీ చేయవచ్చని, గ్రామ పరిధి నుంచి రాష్ట్ర కేంద్ర స్థాయి వరకు సహ చట్టాన్ని వినియోగించి సమాచారం తీసుకోవచ్చని తెలిపారు. ఏపీ సమాచార కమిషనర్ రేపాల శ్రీనివాస్, ఎన్‌మారి

అవగాహన సదస్సులో వక్తలు

నాథ్, మంచికట్ల అనిల్‌కుమార్, కళాశాల ప్రిన్సిపాల్ డాక్టర్ ఇళ్ల రవి మాట్లాడారు. కార్యక్రమాన్ని రాజనీతి శాస్త్ర విభాగం అధ్యాపకులు డాక్టర్ డీఎస్‌వీఎస్ బాలసుబ్రహ్మణ్యం, అధ్యాపకులు పర్యవేక్షించారు.

సాక్షి Sun, 07 March 2021
https://epaper.sakshi.com/c/58923625

అవినీతి రహిత భారతదేశానికి ఆర్టిఐ యాక్ట్ ఓ ఆయుధం

(వార్తామండలి ప్రతినిధి)

విజయవాడ: రాష్ట్రంకానీ దేశంకానీ అవినీతి రహితంగా నిలబడడానికి ఆర్టిఐ యాక్ట్ ఆయుధంగా ఉపయోగపడుతుందని రాష్ట్ర ముఖ్య సమాచార కమిషనర్ విక్రాంత్ ఐ ఏ ఎస్ అధికారి పి. రమేష్ కుమార్ అన్నారు. కౌన్సిల్ ఫర్ సిటిజన్ రైట్స్ ఆధ్వర్యంలో విజయవాడ నగరంలోని ఎస్ ఆర్ ఆర్ అండ్ సివిఆర్ కళాశాలలో అవగాహన సదస్సు సి సి ఆర్ అధికార ప్రతినిధి వ్యవస్థాపకులు మాచి కట్ల అనిల్ కుమార్ అధ్యక్షతన జరిగింది. ముఖ్య అతిథి రమేష్ కుమార్ మాట్లాడుతూ కళాశాల ప్రిన్సిపాల్ అధ్యాపక ఉపాధ్యాయులు ఆర్ టి ఐ యోధులను తయారుచేయడం అభినందనీయమన్నారు. ఆర్టిఐ యాక్ట్ సద్వినియోగం వలన ఎన్నో ఫలితాలు ఉంటాయన్నారు. అదే ఆర్టిఐ యాక్ట్ ను దుర్వినియోగం చేస్తే ఆర్టిఐ యాక్ట్ నిర్వీర్యం అవుతుందన్నారు.ఆర్ టి ఐ అవగాహన సదస్సు విజయవంతం అవడం అభినందనీయ మన్నారు. మరో ముఖ్య అతిథి రేపాక క్రీనివాసరావు, ఎన్ హరినాథ్ ఆర్టిఐ చట్టం విధివిధానాలను అవగాహన సదస్సులో వివరించారు, ఈ కార్యక్రమంలో కళాశాల ప్రిన్సిపాల్ డాక్టర్ రవిని జ్ఞాపికతో సన్మానించారు. అవగాహన సదస్సుకు వచ్చిన అతిథులకు పీట్లులు బహుకరించారు. ఆర్టిఐ కార్యకర్తలకు సర్టిఫికెట్లు ప్రధానోత్సవం చేశారు. అవగాహన సదస్సులో హైకోర్టు అడ్వకేట్, సి సి ఆర్ లీగల్ అడ్వైజర్ అనిల్ వైద్య ప్రసంగించారు. శెట్టి రామకృష్ణ, పావులూరి కోటేశ్వరరావు, ఇ లక్ష్మీ ప్రశాంత్, బి మహేష్, శ్రీనివాస రావు సభా నిర్వాహకులుగా వ్యవహరించారు. ఈ కార్యక్రమంలో విద్యార్థినీ విద్యార్థులు ఉపాధ్యాయులు తదితరులు పాల్గొన్నారు.